T.C.
DOKUZ EYLÜL UNIVERSITY
İZMİR INTERNATIONAL
BIOMEDICINE AND GENOME
INSTITUTE

COMPARATIVE ANALYSIS OF THE MOLECULAR MECHANISMS OF BRAIN REGENERATION AND GLIOMA USING ZEBRAFISH MODEL TO DEVELOP THERAPEUTIC APPROACHES FOR GLIOMAS

YELİZ DEMİRCİ

MOLECULAR BIOLOGY AND GENETICS

PhD THESIS

İZMİR-2021

THESIS CODE: DEU.IBG.PhD/2016850025

T.C.
DOKUZ EYLÜL UNIVERSITY
İZMİR INTERNATIONAL
BIOMEDICINE AND GENOME
INSTITUTE

COMPARATIVE ANALYSIS OF THE MOLECULAR MECHANISMS OF BRAIN REGENERATION AND GLIOMA USING ZEBRAFISH MODEL TO DEVELOP THERAPEUTIC APPROACHES FOR GLIOMAS

MOLECULAR BIOLOGY AND GENETICS

PhD THESIS

YELİZ DEMİRCİ

Supervisor: Assoc. Prof. Dr. H. Güneş ÖZHAN

THESIS CODE: DEU.IBG.PhD/2016850025

Yeliz DEMİRCİ, PhD Student at
Dokuz Eylül University Izmir International Biomedicine and Genome Institute,
Department of Genome Sciences and Molecular Biotechnology,
Molecular Biology and Genetics Doctorate Programme,
successfully completed her doctoral thesis entitled
'COMPARATIVE ANALYSIS OF THE MOLECULAR MECHANISMS OF BRAIN REGENERATION AND GLIOMA USING ZEBRAFISH MODEL TO DEVELOP THERAPEUTIC APPROACHES FOR GLIOMAS'
on 28/07/2021.

CHAIR
Assoc. Prof. Dr. H. Güneş ÖZHAN

MEMBER
Assoc. Prof. Dr. Zeynep YÜCE

MEMBER
Assoc. Prof. Dr. Zeynep FIRTINA KARAGONLAR

MEMBER
Asst. Prof. Dr. Ayşe Banu DEMİR

MEMBER
Asst. Prof. Dr. Yavuz OKTAY

Dokuz Eylül Üniversitesi, Izmir Uluslararası Biyotıp ve Genom Enstitüsü,
Genom Bilimleri ve Molekküler Biyoteknoloji Anabilim Dalı,
Moleküler Biyoloji ve Genetik Doktora Programı Doktora öğrencisi Yeliz DEMİRCİ,
"BEYİN REJENERASYONU VE GLİOMA MOLEKÜLER MEKANİZMALARININ GLİOMALAR İÇİN TERAPÖTİK YAKLAŞIMLAR GELİŞTİRMEK ÜZERE ZEBRABALIĞI MODELİ KULLANARAK KARŞILAŞTIRMALI ANALİZİ"
konulu Doktora tezini 28/07/2021 tarihinde başarılı olarak tamamlamıştır.

BAŞKAN
Doç. Dr. H. Güneş ÖZHAN

ÜYE
Doç. Dr. Zeynep YÜCE

ÜYE
Doç. Dr. Zeynep FIRTINA KARAGONLAR

ÜYE
Dr. Öğretim Üyesi Ayşe Banu DEMİR

ÜYE
Dr. Öğretim Üyesi Yavuz OKTAY

ACKNOWLEDGMENT

Firstly, I would like to express my special thanks and gratitude to my supervisor Assoc. Prof. Dr. H. Güneş Özhan for the continuous support of my PhD study and research, for her belief in me, motivation, enthusiasm and immense knowledge.

Besides my supervisor, I would like to thank the rest of my thesis committee: Assoc. Prof. Dr. Zeynep Yüce and Asst. Prof. Dr. Ayşe Banu Demir, for their encouragement, insightful comments, and hard questions.

My sincere thanks also go to Dr. Irene Papatheodorou and Dr. Alvis Brazma from EMBL-EBI, for providing me with fellowship opportunities in their groups and leading my work on diverse exciting projects. I would also like to thank Dr. Suhaib Mohammed and Dr. Pablo Moreno for supervising me during my fellowships.

I would like to express my special thanks to Eng. Guillaume Heger who shared kindly his immense expertise with me about mathematics, statistics, bioinformatics and programming and assisting my research patiently during my studies.

I thank my friends and my labmates in IBG, Gökhan Cucun, Özgün Özalp, Kaan Poyraz, Burcu Akman, Esra Katkat, Yağmur Azbazdar and Gökçen Garanlı for the times we were working together and for all the time we enjoyed in the last four years.

I also thank all the members of Dokuz Eylül University, İzmir Biomedicine and Genome Institute, İzmir Biomedicine and Genome Center and European Molecular Biology Laboratory-European Bioinformatics Institute providing me with a great working environment and kindly hosting me during my research pursuit.

I would like to thank TÜBİTAK (The Scientific and Technological Research Council of Turkey, project number 215Z365) and EMBO (European Molecular Biology Organization Installation Grant Project) for covering all the wet lab expenses of projects that I worked on during my education.

My special thanks and appreciation are also extended to TÜBİTAK and the Council of Higher Education (CoHE) of Turkey (YÖK) for supporting me with two great scholarships which are the National PhD Scholarship Program in the Priority Fields in Science and Technology (2211C) and the 100/2000 PhD Scholarship Program providing me with financial support.

I wish to acknowledge TÜBİTAK (2214A International Research Fellowship Programme for PhD Students), EMBO (EMBO-STF) and Federation of European Biochemical Society (FEBS-STF) for their grants giving me a peerless opportunity to work in one of the most prestigious institutes of bioinformatics.

I would like to thank my sister Yeşim Demirci for supporting me.

Last but not least, I appreciate my parents Hasibe Demirci and Aziz Demirci, for giving birth to me at the first place and spiritually supporting me during my life.

TABLE OF CONTENTS

TABLE OF CONTENTS ..... **I**
LIST OF TABLES ..... **IV**
LIST OF FIGURES ..... **V**
LIST OF ABBREVIATIONS ..... **VII**
ÖZET **1**
ABSTRACT **2**
1. INTRODUCTION **3**
2. GENERAL INFORMATION **7**
2.1. Tissue regeneration **7**
2.2. Zebrafish as a model organism for regeneration studies **8**
2.3. Adult brain regeneration in mammalian and zebrafish **9**
2.4. Glioma mechanisms **15**
2.5. Possible links between regeneration and cancer **16**
3. METHODS **19**
3.1. Fish maintenance **19**
3.2. Stab wound assay and sample collection for RNA experiments **19**
3.3. Histological demonstration of stab lesion **20**
3.3.1. Brain dissection and fixation 20
3.3.2. Embedding of the brains for sectioning 21
3.3.3. Cryosectioning 21
3.3.4. Hematoxylin/Eosin (HE) staining 21
3.4. RNA isolation **22**
3.5. Quantitative and qualitative measurements of isolated RNA samples **22**
3.6. Library construction and RNA-Sequencing (RNA-Seq) **22**
3.7. Obtaining cancer samples from public databases **23**
3.8. Bioinformatics analysis of zebrafish brain regeneration samples and human brain cancer samples **23**
3.8.1. Quality check of raw RNA sequencing (RNA-Seq) data for brain regeneration 25
3.8.2. Mapping of the brain regeneration reads to the zebrafish reference genome 26
3.8.3. Quantitative analysis of mapped reads 27
3.8.4. Quality check results of brain regeneration samples after mapping to the reference genome 28
3.8.5. Batch effect correction of brain regeneration samples 29
3.9. Sample-to-sample distances between brain regeneration samples **29**
3.10. Principal Component Analysis (PCA) of the brain regeneration samples **30**

3.11. Differential gene expression analysis 30
3.12. Ortholog conversion 32
3.13. Functional analysis 32
3.14. Weighted gene co-expression network analysis (WGCNA) 33
3.14.1. Data input, cleaning and pre-processing 33
3.14.2. Choosing the soft-thresholding power with scale free topology - Network construction and module detection (cluster dendrogram) 33
3.15. Ethical committee approval 34
4. RESULTS 35
4.1. Histological demonstration of stab lesioned telencephalon 35
4.2. Quantitative and qualitative measurements of isolated RNA samples 36
4.3. Quality check results of raw samples of brain regeneration samples 38
4.4. Quality check results of brain regeneration samples after mapping to the reference genome 43
4.5. Batch effect correction of brain regeneration samples 52
4.6. Transcriptome profiling of adult zebrafish brain regeneration 54
4.6.1. Differential gene expression and functional gene annotation analyses of early wound healing stage (1 dpl) of brain regeneration 54
4.6.2. Differential gene expression and functional gene annotation analyses of early proliferative stage (3 dpl) of brain regeneration 55
4.6.3. Differential gene expression and functional gene annotation analyses of differentiation stage (14 dpl) of brain regeneration 59
4.7. Functional gene annotation analyses of zebrafish brain regeneration at all stages by using all DEGs 60
4.8. Comparison of DEG sets between regeneration stages 63
4.9. Weighted gene co-expression network analysis of adult zebrafish brain regeneration 68
4.10. Transcriptome profiling of brain cancer datasets 71
4.10.1. Differential gene expression analysis of low-grade glioma 71
4.10.2. Differential gene expression analysis of glioblastoma 71
4.11. Comparison of early wound healing, early proliferative, and differentiation stages of adult zebrafish brain regeneration with low-grade glioma and glioblastoma 73
4.11.1. Comparison of early wound healing stage of brain regeneration with low-grade glioma and glioblastoma 73
4.11.2. Comparison of early proliferative stage of brain regeneration with low-grade glioma and glioblastoma 80
4.11.3. Comparison of differentiation stage of brain regeneration with low-grade glioma and glioblastoma 85
4.12. Comparison of the DEG sets of three different stages of zebrafish brain regeneration and two different human brain cancers 90

5. DISCUSSION.....95
6. CONCLUSIONS AND FUTURE DIRECTIONS 100
7. REFERENCES 101
8. APPENDICES.....126

LIST OF TABLES

Table 1. Forward and reverse primers for zebrafish actb1 gene. 22
Table 2. Qualitative and quantitative measurements of RNA samples used in this study. 36

LIST OF FIGURES

Figure 1. Tissue regeneration 7
Figure 2. Tissue and organ regeneration in zebrafish 9
Figure 3. Neurogenic regions of the zebrafish brain in comparison to mammals 12
Figure 4. Schematic summary of the zebrafish telencephalic progenitor niche 13
Figure 5. The major proliferative cell types in the telencephalon stem cell niche 14
Figure 6. Schematic representation of adult zebrafish telencephalic stab injury 20
Figure 7. Bioinformatics analysis pipeline 24
Figure 8. Statistical analysis of DESeq2 31
Figure 9. Histological demonstration of stab lesion assay in the adult zebrafish telencephalon 35
Figure 10. Integrity check of RNA samples 37
Figure 11. Total number of reads sequenced for each sample 38
Figure 12. Results of the "Mean Quality Scores" and "Per Sequence Quality Scores" modules of MultiQC generated based on FastQC results 40
Figure 13. Results of the "Per Base N Content" and "Adapter Content" modules of MultiQC generated based on FastQC results 41
Figure 14. Results of the "Sequence Counts" and "Sequence Duplication Levels" modules of MultiQC tool generated based on the FastQC results 42
Figure 15. Results of the "PE Alignment Scores" module of MultiQC 46
Figure 16. Overall alignment rates of the samples to the zebrafish reference genome 47
Figure 17. Results of the "HTSeq: Count Assignments" module of MultiQC 48
Figure 18. Visualization of alignments of RNA-Seq reads for 18 brain regeneration samples for whole genome by using Integrative Genomics Viewer (IGV) 49
Figure 19. Visualization of alignment and coverage of RNA-Seq reads for 18 brain regeneration samples for *gfap* gene by using Integrative Genomics Viewer (IGV) 50
Figure 20. Visualization of alignments and coverage of RNA-Seq reads for 18 brain regeneration samples for s100b gene by using Integrative Genomics Viewer (IGV) 51
Figure 21. Heatmap of sample-to-sample distances between expression patterns of three stages of zebrafish brain regeneration and control brain samples 52
Figure 22. Principal component analysis (PCA) of expression patterns for three stages of zebrafish brain regeneration and control brain samples 53
Figure 23. Transcriptome profiling of early wound healing stage (1 dpl) of zebrafish brain regeneration 54
Figure 24. GO terms enriched at early wound healing stage (1 dpl) of brain regeneration by using up- and downregulated genes separately 56
Figure 25. Transcriptome profiling of early proliferative stage (3 dpl) of zebrafish brain regeneration 57
Figure 26. GO terms enriched at early proliferative stage (3 dpl) of brain regeneration by using up- and downregulated genes separately 58
Figure 27. Transcriptome profiling of differentiation stage (14 dpl) of zebrafish brain regeneration 59
Figure 28. GO terms enriched at differentiation stage (14 dpl) of brain regeneration by using up- and downregulated genes separately. 61
Figure 29. GO-BP terms enriched at three different stages of zebrafish brain regeneration by using all DEGs 62
Figure 30. KEGG pathways enriched at three different stages of zebrafish brain regeneration by using all DEGs 63

Figure 31. Heatmaps of all DEGs (9136 genes) across three stages of adult zebrafish brain regeneration 64
Figure 32. UpSet plot showing the comparison of DEG sets between regeneration stages. 65
Figure 33. Heatmaps of log_2 fold changes of selected genes across stages of adult zebrafish brain regeneration 66
Figure 34. Heatmap representing clustering of the regeneration-related selected GO-BP terms enriched at each stage. 68
Figure 35. Network analysis of zebrafish brain regeneration 69
Figure 36. Heatmap and functional annotations of the genes clustered in each module 70
Figure 37 . Transcriptome profiling of LGG-TCGA 71
Figure 38. Transcriptome profiling of GBM-TCGA 72
Figure 39. Comparison of early wound healing stage of brain regeneration with low-grade glioma and glioblastoma. 75
Figure 40. GO terms enriched in comparison of early wound healing stage of brain regeneration with low-grade glioma 76
Figure 41. GO terms enriched in comparison of early wound healing stage of brain regeneration with glioblastoma 77
Figure 42. KEGG pathways performed by using DEGs shared between zebrafish brain regeneration and human brain cancers. 78
Figure 43. KEGG pathways performed by using the DEGs unique to zebrafish brain regeneration 79
Figure 44. Comparison of early proliferative stage of brain regeneration with low-grade glioma and glioblastoma 82
Figure 45. GO terms enriched in comparison of early proliferative stage of brain regeneration with low-grade glioma. 83
Figure 46. GO terms enriched in comparison of early proliferative stage of brain regeneration with glioblastoma 84
Figure 47. Comparison of differentiation stage of brain regeneration with low-grade glioma and glioblastoma 87
Figure 48. GO terms enriched in comparison of differentiation stage of brain regeneration with low-grade glioma 88
Figure 49. GO terms enriched in comparison of differentiation stage of brain regeneration with glioblastoma 89
Figure 50. Heatmaps of the DEGs (3615 genes) across three stages of adult zebrafish brain regeneration and two brain cancers 90
Figure 51. Chord plot shows log_2 fold changes of the genes annotated in selected KEGG pathways (Glioma and Pathways in cancer) for three stages of the zebrafish brain regeneration and two different types of human brain cancers 91
Figure 52. Chord plot shows log_2 fold changes of the genes annotated in selected KEGG pathways (RAS, MAPK, mTOR and PI3K-Akt pathways) for three stages of the zebrafish brain regeneration and two different types of human brain cancers 92
Figure 53. Chord plot shows log_2 fold changes of the genes annotated in selected KEGG pathways (Wnt signaling, p53 signaling, Jak-STAT signaling, Apoptosis and Notch signaling pathways) for three stages of the zebrafish brain regeneration and two different types of human brain cancers 93

LIST OF ABBREVIATIONS

AELEC	Animal experiments local ethics committee
API	Application programming interface
BAI	Indexed BAM file
BAM	Binary alignment map
BP	Biological process
bp	Base pair
BW	Bigwig file
Ce	Cerebellum
CC	Cellular component
cDNA	Complementary DNA
CNS	Central nervous system
Ct	Cycle threshold
DAVID	Database for Annotation, Visualization and Integrated Discovery
DEG	Differentially expressed gene
DG	Dentate gyrus
dH_2O	Distilled water
DNA	Deoxyribonucleic acid
Down	Downregulated
DPL	Day post lesion
DT	Dorsal telencephalon
ECM	Extracellular matrix
EDTA	Ethylene diamine tetra acetic acid
FDR	False discovery rate
GBM	Glioblastoma multiforme
GLM	Generalized linear model
GO	Gene ontology
GSC	Glioblastoma stem cell
GTF	Gene transfer format
HE	Hematoxylin/Eosin
HTML	Hypertext markup language
IBG	Izmir Biomedicine and Genome Center
IGV	Integrative genomics viewer
KEGG	Kyoto Encyclopedia of Genes and Genomes
LGG	Low-grade glioma
MAPK	Mitogen-activated protein kinase
MF	Molecular function
NB	Negative binomial
NS	Not significant
NSC	Neural stem cell
OB	Olfactory bulb
QC	Quality control
OT	Optic tectum
PBS	Phosphate buffer saline
PC	Principal component
PCA	Principal component analysis
PE	Paired end
PFA	Paraformaldehyde

RGC	Radial glial cell
RIN	RNA integrity number
RNA	Ribonucleic acid
RNA-Seq	RNA sequencing
rRNA	ribosomal RNA
RT-PCR	Reverse transcriptase polymerase chain reaction
SAI	Indexed SAM file
SAM	Sequence alignment map
SC	Spinal cord
SVA	Surrogate variable analysis
SVZ	Subventricular zone
TCGA	The Cancer Genome Atlas
UCSC	The University of California, Santa Cruz
Up	Upregulated
vst	variance stabilizing transformation
WGCNA	Weighted gene co-expression network analysis
WT	wild type
qPCR	quantitative polymerase chain reaction

BEYİN REJENERASYONU VE GLİOMA MOLEKÜLER MEKANİZMALARININ ZEBRABALIĞI MODELİ KULLANILARAK GLİOMALARDA TERAPÖTİK YAKLAŞIMLAR GELİŞTİRİLMESİ İÇİN KARŞILAŞTIRMALI OLARAK ANALİZİ

Yeliz Demirci, DEU, İzmir Uluslararası Biyotıp ve Genom Enstitüsü

ÖZET

Araştırmalar, proliferasyon, hücre yenilenmesi ve farklılaşma gibi olayların kanser ve rejenerasyon arasında ortak olduğunu göstermiştir. Ancak bu olaylar rejenerasyonda uygun şekilde sonlandırılırken, kanserde durdurulamazlar ve hücreler sürekli olarak anormal doku bütünlüğü ve anormal doku kütlesi ile sonuçlanan proliferasyona uğrar. Memelilerin aksine, zebrabalığı, beyin dokusunu da içeren birçok organ ve dokularını yenileyebilme kabiliyetine sahiptir. Bu özelliği zebrabalığını vertebralı rejenerasyon çalışmaları için elverişli bir organizma haline getirmiştir. Bu çalışma, telensefalon dokusunda erken yara iyileşmesi, erken proliferasyon ve farklılaşma evrelerinde rejenerasyonda rol alan mekanizmaları tüm transkriptom düzeyinde araştırmayı ve verilerin kanser veritabanlarından elde edilen insan beyin kanseri verileriyle kıyaslayarak beyin dokusunda rejenerasyon ve kanser arasındaki ilişkiyi aydınlatmayı hedeflemektedir.

Bu çalışmada, mikro-manipülasyon teknikleri, histolojik teknikler, qPCR ve transkriptom dizileme gibi çeşitli moleküler biyoloji teknikleri kullanılmıştır. Transkriptom dizilemesi sonuçlarını analiz etmek için, kalite analizleri, okumaların referans genoma haritalanması ve sayısal olarak hesaplanması, diferansiyel olarak eksprese olan genlerin tespiti ve sonuçların kanser veritabanlarından elde edilen kanser verileriyle karşılaştırılmasını içeren biyoenformatik analizler yapılmıştır.

Sonuç olarak, (i) beyin rejenerasyonunun üç evresi birbirinden farklı karakteristikte transkriptoma sahiptir; (ii) erken yara iyileşmesi evresi, beyin kanserlerine protein translasyonu, hücre gelişimi, nörogenez ve sinaptik sinyal yolakları açısından; (iii) erken hücre çoğalması evresi ile beyin kanserleri hücre bölünmesi ve DNA replikasyonu açısından; (iv) beyin rejenerasyonunun farklılaşma evresi ile beyin kanserleri sinir sistemi gelişimi, damar gelişimi ve organ morfogenezi açısından benzerlik göstermektedir. Bu çalışma, ilk defa telensefalon yenilenmesinin üç farklı evresi ile iki farklı beyin kanserini tüm transkriptom düzeyinde araştıran bir kaynak niteliğindedir. Sonuçlar, beyin kanserlerinin, nörodejeneratif hastalıkların ve beyin hasarının tedavisinde yeni yaklaşımların geliştirilmesi için literatüre katkı sağlamaktadır.

Anahtar sözcükler: beyin, glioma, rejenerasyon, telensefalon, kanser, zebrabalığı, transkriptom, RNA-dizileme, biyoenformatik

COMPARATIVE ANALYSIS OF THE MOLECULAR MECHANISMS OF BRAIN REGENERATION AND GLIOMA USING ZEBRAFISH MODEL TO DEVELOP THERAPEUTIC APPROACHES FOR GLIOMAS

Yeliz Demirci, DEU, İzmir International Biomedicine and Genome Institute

ABSTRACT

Studies have shown that events such as proliferation, renewal of cells and differentiation are shared between cancer and regeneration. However, while these events are terminated properly in regeneration, they cannot be halted in cancer and the cells undergo proliferation consistently resulting with abnormal tissue integrity and abnormal tissue mass. Unlike mammals, zebrafish has the ability to regenerate many organs and tissues, including brain tissue. This feature has made zebrafish a suitable model organism for vertebral regeneration studies. This study aims to investigate the mechanisms involved in regeneration in early wound healing, early proliferation and differentiation stages in telencephalon tissue at the whole transcriptome level and to elucidate the relationship between cancer and regeneration in brain tissue by comparing these results with human brain cancers obtained from cancer databases.

In this study, various molecular biology techniques such as micro-manipulation techniques, histological techniques, qPCR and RNA-sequencing were used. Bioinformatics analyses, including quality control, mapping to the reference genome, read counting, detection of differentially expressed genes, and comparison of results with cancer data from cancer databases were performed to analyse RNA-sequencing data.

As a result, (i) the transcriptome of three phases of brain regeneration shows different characteristics; (ii) early wound healing stage is similar to the brain cancers in terms of protein translation, cell development, neurogenesis and synaptic signaling pathways; (iii) early cell proliferation stage and brain cancers are similar each other in terms of cell division and DNA replication; (iv) the differentiation stage and brain cancers resembles each other in terms of nervous system development, vascular development and organ morphogenesis. This study is a resource that investigates three different stages of brain regeneration and two different brain cancers at the whole transcriptome level for the first time. The results will be able to contribute to the literature on the development of new approaches in the treatment of brain cancers, neurodegenerative diseases and brain injury.

Key Words: bioinformatics, brain, cancer, glioma, regeneration, RNA-sequencing (RNA-Seq), transcriptome, zebrafish.

1. INTRODUCTION

Despite decades of research, primary brain tumours are still the most difficult-to-treat and deadliest types of cancer. They can be caused by the uncontrolled proliferation of brain cells including neurons and glial cells. About 240,000 cases of brain and nervous system-related cancers are diagnosed worldwide every year (Boffetta et al., 2014). Among these, gliomas, arising from glial tissue, are the most frequently occurring types of brain cancers of the central nervous system (CNS) which are responsible for 80% of all malignant primary cancers of the brain (Agnihotri et al., 2013; Boffetta et al., 2014; Hanif et al., 2017; Messali et al., 2014; Ostrom et al., 2013; Schwartzbaum et al., 2006). Gliomas are classified into grade I to IV by WHO (World Health Organization) according to their histopathological and immunohistochemical similarity to the putative cell of origin. Whereas grade I gliomas are less aggressive and slow-growing, grades II to IV are more aggressive, highly malignant and invasive (Hanif et al., 2017; Louis et al., 2007, 2016). Grade IV gliomas, also known as Glioblastoma multiforme (GBM), are the most aggressive diffuse forms of all gliomas and account for more than 50% of adults diagnosed with glioma (Louis et al., 2016; Tamimi & Juweid, 2017). Although it can affect children, it is relatively rare when compared with adults and its incidence increases with age (Ansari et al., 2012; Kanti Das & Kumar, 2017).

Although the exact reason for gliomas is still unknown, some factors have been linked to an increased risk such as age, gender, ethnicity, inherited susceptibility, immune factors and radiation (Bondy et al., 2008; Ladomersky et al., 2019; Ostrom et al., 2013; Prasad & Haas-Kogan, 2009; Tamimi & Juweid, 2017). Age is one of the main risk factors for all types of cancers. However, a brain tumour can be seen at any age. While some types of gliomas such as pilocytic astrocytoma are more prevalent in children and young adults, the incidence of meningioma and GBM increases at advanced ageing with the median diagnosis age of 64 (Ladomersky et al., 2019; Merchant et al., 2010). The incidence of GBM is higher in men than in women (Ohgaki & Kleihues, 2005). According to some studies, Blacks show less prevalence than Asians, Latinos and Whites, however, this might be related to socioeconomic inequalities and underreporting of cases rather than a genetic tendency (Iacob & Dinca, 2009). There is also an increased relationship between the incidence of brain tumours and some hereditary cancer predisposition disorders such as Li-Fraumeni syndrome, neurofibromatosis, tuberous sclerosis and Turcot's syndrome, arisen from mutations in a tumour suppressor gene (Hill et al., 2003; Reilly, 2009). Also, individuals who have been exposed to radiation at any stage of their life

are at increased risk of brain tumours. Radiation-induced gliomas can be caused by non-ionizing rediation, such as electromagnetic fields, cell phones, or ionizing radiation such as radiation therapy, and atomic bombs (Bondy et al., 2008; Claus et al., 2005; Ron, 2003; Thompson et al., 1994).

In addition to common mutations of *IDH1*, *IDH2*, and *TERT*, progression of glioma has been associated with alterations in various pathways that are crucial to today's glioma/glioblastoma treatments (Idilli et al., 2017): (i) alterations in the PI3K-PTEN-Akt-mTOR signaling pathway regulated by *EGF* (epidermal growth factor) and its receptor *EGFR* (Xiaoman Li et al., 2016; Zoncu et al., 2011) (ii) mutations of p53 signaling pathway promoting excessive cell cycle and preventing apoptosis (Ohgaki & Kleihues, 2007; Speidel, 2015; Viotti et al., 2014); (iii) mutations of genes affecting RAS/MAPK signaling pathways such as *NF1, BRAF, RAF1, MEK, PDGFR*, and *RTKs* (Nasser & Mehdipour, 2018; Venkatesan et al., 2016); (iv) changes in the genes regulating cell cycle and cell growth such as *pRB* (tumour suppressor retinoblastoma), *CDK4* (cyclin-dependent kinase 4), *CDKN2A* (cyclin-dependent kinase inhibitor 2A, a negative regulator of the proliferation of normal cells) (Idilli et al., 2017; H. Mao et al., 2012; Nasser & Mehdipour, 2018).

Despite the modern therapies, curing brain tumours is still a considerable challenge due to the tumour heterogeneity, the presence of blood-brain barrier (BBB) and the inability to well understand its underlying reasons. Among these brain tumours, GBM remains one of the deadliest cancer types, having a very poor prognosis with a median survival of about 15 months from the diagnosis and only 5% of patients survive 5 years after diagnosis (Fernandes et al., 2017; Ohka et al., 2012; Tamimi & Juweid, 2017; X. Wang et al., 2021). GBM treatment consists of a complex multidisciplinary treatment including maximal surgical resection followed by radiation therapy and chemotherapy. After resection, applying radiotherapy and TMZ (temozolomide) is the most effective combinatorial treatment shown to extend survival. Combinations of conventional therapies and new approaches targeting several molecular events such as triggering of apoptosis and suppression of angiogenesis, can improve the prognosis of patients (Fernandes et al., 2017; Tamimi & Juweid, 2017). However, for over four decades, outcomes of GBM treatment have remained stable, and it requires the rapid development of new approaches and therapies.

Regenerative medicine aims to replace cells, tissues and organs which are lost or damaged by disease, injury, ageing, or innate defects (A. S. Mao & Mooney, 2015) by using stem cells, tissue engineering and artificial organ production techniques. Since regeneration and tumorigenesis have been proposed to be related processes (Oviedo & Beane, 2009), figuring out the link between regeneration and cancer can offer up new treatments in addition to current therapies for cancer patients, in the area of regenerative medicine. Therefore, to better understand its molecular mechanisms, regeneration has been studied in diverse animal groups and their wide range of tissues and organs (Gemberling et al., 2013; Joven et al., 2019; Roy & Gatien, 2008). Furthermore, comparative studies have been conducted, in which zebrafish are used as model organisms for regeneration and different human cancers, and their results have been compared with those of human cancer studies to understand similarities and differences between both phenomena (Hagedorn et al., 2016; I. S. Kim et al., 2017). It has been shown that there is a significant link between melanocyte differentiation during development of blastema (a group of highly proliferating undifferentiated cells that plays role in regeneration) in melanocyte regeneration and dysregulation of melanocyte differentiation programme during melanoma development (Hagedorn et al., 2016; White & Zon, 2008). Based on microarray data, 40% of genes whose expression was upregulated during blastema formation were also highly expressed in human melanoma. Among those genes, there were two extracellular matrix proteins, *TNC* (tenascin C) and *FN1* (fibronectin 1), known to induce melanoma and also *BAMBI* (BMP and active membrane-bound inhibitor homolog), a novel candidate gene important for melanoma formation (Fukunaga-Kalabis et al., 2010; Hagedorn et al., 2016; Kääriäinen et al., 2006).

Contrary to the limited ability of the human brain to regenerate, a non-mammalian vertebrate species, zebrafish can regenerate the CNS during their entire life (Grandel et al., 2006). This capability of the zebrafish brain is maintained by the existence of stem/progenitor cells, and its favourable environment (Kizil, Kaslin, et al., 2012). While mammalian adult neurogenesis is restricted with only two distinct regions of the forebrain, i.e., the subventricular zone (SVZ) of the lateral ventricles in the telencephalon and the subgranular zone (SGZ) of the dentate gyrus in the hippocampus (Alvarez-Buylla et al., 2001; Bonfanti & Peretto, 2011; Kriegstein & Alvarez-Buylla, 2009), zebrafish has 16 distinct proliferative niches located in the ventricular zone and deeper in the brain parenchyma containing self-renewing neural progenitors (Kaslin et al., 2008). This outstanding regeneration capacity of zebrafish makes it

a useful model organism by helping understanding the molecular programmes required for brain regeneration and producing new possible therapies for neurodegenerative diseases and brain cancers.

2. GENERAL INFORMATION

2.1. Tissue regeneration

Tissue regeneration or wound healing is the replacement of lost/damaged tissue and organ parts by newly synthesized tissue of remaining tissue parts. The regeneration process is triggered by several overlapping phases, including tissue homeostasis, inflammatory phase, proliferation and tissue remodelling (Figure 1) (Marques et al., 2019).

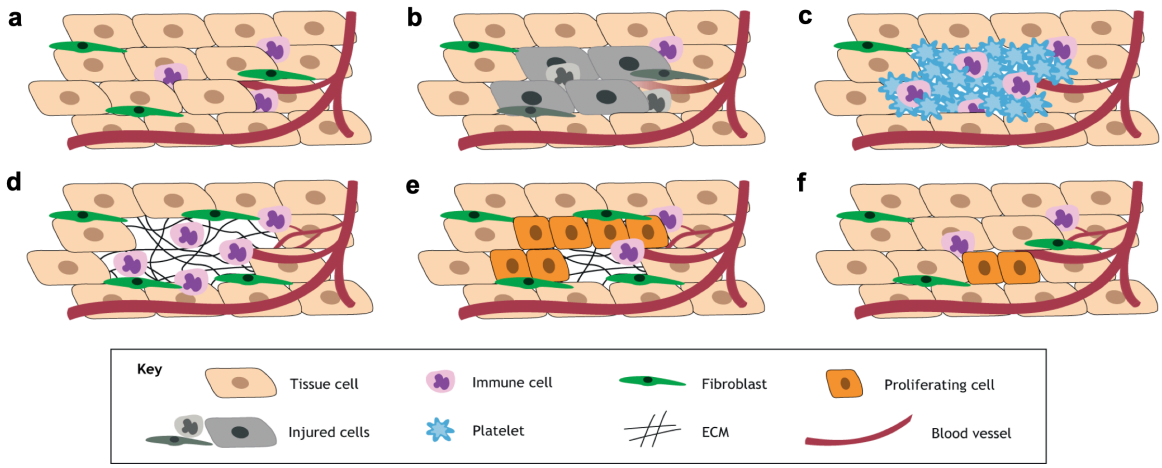

Figure 1. Tissue regeneration. (a) Intact undamaged tissue. **(b)** Injury site is shown in grey, indicating damage. Lighter red colour represents injured blood vessel in the lesion site. **(c)** Platelets (blue) penetrate the injury site to halt bleeding. Immune cells (purple) also penetrate the wounded region. **(d)** Dead cells debris are cleaned by immune cells. Extracellular matrix (ECM) is produced by proliferating fibroblasts (green) to keep the empty area from falling down. Angiogenesis also occurs at this stage. **(e)** As new cells repopulate the area by proliferating cells (orange), ECM begins to disappear. (**f**) The wounded region is repopulated entirely, and the tissue is rebuilt to its normal state. Cells return to their quiescent state and only a few cells continue proliferation. Note: Adapted from "Model systems for regeneration: zebrafish" (Marques et al., 2019). *Development, 2019,* 146 (18): dev167692. doi: 10.1242/dev.167692. Copyright 2019. Published under licence to The Company of Biologists Ltd. This is an Open Access article distributed under the terms of the Creative Commons Attribution License (https://creativecommons.org/licenses/by/4.0), which permits unrestricted use, distribution and reproduction in any medium provided that the original work is properly attributed.

Firstly, injured blood vessels in the damaged area are closed up by a temporary "platelet plug" that stops bleeding to establish tissue homeostasis (Figure 1b, 1c) (LaPelusa & Dave, 2021). The optimum level of immune response is required for an effective response to injury. As a result of the adaptive immune response, immune cells penetrate the lesion site to remove dead cells and tissue debris. This also protects lesion site against infections. Extracellular matrix (ECM) fibres are produced by proliferating fibroblast cells supporting damaged area physically, they also provide a favourable environment for progenitor cells, affecting their proliferation and differentiation (Figure 1c, 1d) (Bonnans et al., 2014; Ma et al., 2020). The imbalance between the accumulation and the degradation processes of ECM can result in permanent fibrotic scars (Silva et al., 2021). Alternatively, proper degradation of ECM can facilitate cell proliferation, and cell migration resulting in tissue regeneration (Figure 1e, 1f).

2.2. Zebrafish as a model organism for regeneration studies

Danio rerio, commonly known as zebrafish, is a scientific model organism for studies including vertebrate developmental genetics, cell biology, toxicology, high-throughput screening of drug libraries and human diseases (Dai et al., 2014; Gemberling et al., 2013; Lessman, 2011; S. Zhao et al., 2015). The evolution of zebrafish to an attractive vertebrate model is due to a variety of essential scientific reasons such as a high degree of sequence and functional homology with mammals, a fully sequenced genome, easy maintenance, large offspring, as well as fast and transparent embryogenesis (Dahm & Geisler, 2006; Howe et al., 2013; Kettleborough et al., 2013).

Regeneration is one of the most important research uses of zebrafish. Undoubtedly, one of the most striking features of zebrafish is its distinctive regeneration capacity upon injury or loss of various tissues and organs, including heart, pancreas, liver, muscle, skin, blood and pigment cells, fins and central nervous system (CNS) (Figure 2), making it an extremely valuable vertebrate model system for studying the body's repair mechanisms against tissue loss and organ damage (Antos & Tanaka, 2010; Hata et al., 2007; H.-T. Huang & Zon, 2008; Keating, 2004; Moss et al., 2009; Poss et al., 2003; Stoick-Cooper et al., 2007; White & Zon, 2008). A comprehensive understanding of regeneration mechanisms in any given system requires detailed identification of the source of all types of cells that are rebuilt after injury. Various genetic fate-mapping studies in zebrafish have clarified the source of regenerated bone, heart, liver and CNS (Bernardos et al., 2007; Choi et al., 2014; Geurtzen et al., 2014; González-

Rosa et al., 2012; He et al., 2014; Jopling et al., 2010; Kikuchi et al., 2010; Knopf et al., 2011; Kroehne et al., 2011; Thummel et al., 2008). Those transgenic approaches relying on tissue-specific protein expression are also extremely useful in regeneration studies to perform spatially and temporally controlled cell ablation (Curado et al., 2007, 2008).

There are several tissue injury models used for regeneration studies in zebrafish, including resection (heart, fin, liver), cryoinjury (heart and fin), chemical ablation (liver, kidney, pancreas), genetic ablation (heart and kidney), light/heat (retina and skin), and stabbing/transection (brain and spinal cord) (Marques et al., 2019).

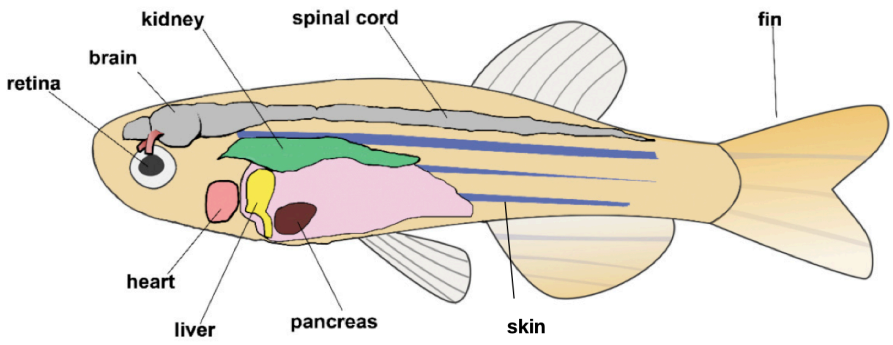

Figure 2. Tissue and organ regeneration in zebrafish. Summary of the adult zebrafish tissues and organs used in regeneration studies. Note: Adapted from "The Diversity of Muscles and Their Regenerative Potential across Animals" (Zullo et al., 2020). Cells, 2020, Sep; 9(9):1925. doi: 10.3390/cells9091925. Copyright 2020. Published under licence to MDPI, Basel, Switzerland. This article is an open access article distributed under the terms and conditions of the Creative Commons Attribution (CC BY) license (http://creativecommons.org/licenses/by/4.0/).

2.3. Adult brain regeneration in mammalian and zebrafish

As an elaborate network of neurons, glial cells and blood vessels, the central nervous system (CNS) has vital roles in numerous biological processes including memory, thinking, perception, control of behaviour, emotions, balance and coordination and endocrine functions. The CNS, composed of the brain and the spinal cord, is the most complex and yet to be fully

understood part of the body. In the 1920s, Cajal reported the brain as a non-regenerating tissue where generation of new neurons was terminated once development ended (Cajal, 1928). However, all adult vertebrate brains studied so far were shown to undergo adult neurogenesis, which is the process of generating new neurons that integrate into existing circuits after foetal and early postnatal development. Adult neurogenesis is achieved via stem/progenitor cells in particular zones that exhibit varying degrees of abundance and neurogenic capacity among vertebrate species, and it correlates with the capacity to regenerate upon damage to neuronal networks caused by injury (Bonfanti & Peretto, 2011; Chapouton et al., 2007; Doetsch & Scharff, 2001; Kaslin et al., 2008). Radial glia or glia-like cells, most of which express glial fibrillary acidic protein (GFAP) and have the characteristics of astrocytes (the star-shaped glial cells in CNS), act as primary neural stem cells (NSCs) that generate new neurons in the adult brain (Dhaliwal & Lagace, 2011; Doetsch et al., 1999; Ming & Song, 2011; Noctor et al., 2001; Seri et al., 2001).

Mammalian adult neurogenesis takes place predominantly via the neural stem cells (NSCs) residing in two specific neurogenic niches of the forebrain, i.e., the subventricular zone (SVZ, also known as the subependymal zone) of the lateral ventricles in the telencephalon and the subgranular zone (SGZ) of the dentate gyrus in the hippocampus (Figure 3a) (Alvarez-Buylla et al., 2001; Bonfanti & Peretto, 2011; Kriegstein & Alvarez-Buylla, 2009). Multipotent neural stem cells in the adult mammalian brain show two main abilities: self-renewal and differentiation to generate new cell types, such as endothelial cells, microglia, astrocytes, and new NSCs (Bond et al., 2015; Gage, 2000). In addition to these two main regions, increasing evidence points that the adult brain includes other potential neurogenic regions harbouring multipotent precursor cells, such as hypothalamus, substantia nigra, cerebellum, and amygdala. Although they contain NSCs, neurogenesis occurs at low levels in these regions (Oyarce et al., 2014). With these stem cell niches, the mammalian brain, amongst the vertebrates, has the most restricted capacity to regenerate. This restriction can be explained partially by different hypotheses, which include the reduction of proliferation zones in mammalian brain during evolution (Lindsey & Tropepe, 2006; Rakic, 2002; Tanaka & Ferretti, 2009), a specific or general resistance against cell proliferation due to the evolution of tight control mechanisms against tumorigenesis (Pearson & Alvarado, 2008) or altered cellular plasticity that affect stem or progenitor cells character (Kizil, Kaslin, et al., 2012; Peng et al., 2002; Shihabuddin et al., 2000). Moreover, the low regenerative capacity of the brain has been questioned with respect

to the presence of a non-permissive environment, which is frequently encountered in mammals that form scar tissues (e.g., in heart, lungs or skin) at the wound site after injury (Ekdahl et al., 2003; Fitch & Silver, 2008; Rolls et al., 2009). In response to a brain injury or a neurological disease, astrocytes are activated and recruited to the site of injury via a process called reactive astrogliosis (Verkhratsky & Butt, 2013). Here, the astrocytes lay an extensive extracellular matrix, which ultimately forms the gliotic scar that has previously been thought to prevent axon regeneration (Faijerson et al., 2006; Rolls et al., 2009; Sofroniew, 2009). Recently, however, an elegant work using genetically targeted loss-of-function manipulations in adult mice has shown that astrocyte scar formation after spinal cord injury (SCI) aids CNS axon regeneration rather than preventing it (Anderson et al., 2016). These findings have important implications for CNS repair strategies by demonstrating that newly generated immature scar-forming astrocytes derived after SCI from endogenous progenitors (Brosius Lutz & Barres, 2014; Wanner et al., 2013) and also potentially from grafted progenitors (Shih et al., 2014), assist axon regrowth and hence may represent critical therapeutic options for axonal regeneration after severe CNS lesions.

In contrast to the limited regenerative ability of the adult mammalian brain, neurogenic activity within the telencephalon is more extensive in reptiles where postnatal/adult neurogenesis is pronounced in all major subdivisions of the telencephalon, including olfactory bulbs and all cortical areas (González-Granero et al., 2011). Adult neurogenesis in zebrafish, however, outscores higher vertebrates by exhibiting the most pronounced and widespread intensity known to date (Kaslin et al., 2008; Kizil, Kaslin, et al., 2012). 16 distinct constitutively proliferative zones, mostly located along the ventricular surface but also deeper in the brain parenchyma, are detected along the entire rostro-caudal axis of the zebrafish brain and contain ventricularly positioned self-renewing neural progenitors (Grandel et al., 2006; Grandel & Brand, 2013; Kaslin et al., 2008). Zebrafish CNS regenerates via proliferation and differentiation of the radial glial and neuroepithelial-like progenitor cells (Fleisch et al., 2011; Ganz et al., 2010; Grandel et al., 2006; Kizil, Kaslin, et al., 2012). The permissive environment that is necessary for these progenitors, upon injury, to get activated and differentiate into functional neurons results most likely from the fact that zebrafish does not form any obvious scar tissue after injury in the CNS (Becker & Becker, 2002; Kroehne et al., 2011). Hence this permissiveness might be a factor granting zebrafish a higher regeneration potential than that of mammals. Due to a high degree of conservation between zebrafish and mammals at the

sequence and proteome level (Howe et al., 2013; Kettleborough et al., 2013), understanding the molecular signals that reprogram stem/progenitor cells in zebrafish brain to generate new neurons rather than forming scar tissue after the injury response is critical to discover what is so special about zebrafish that it can efficiently regenerate the CNS while mammals cannot.

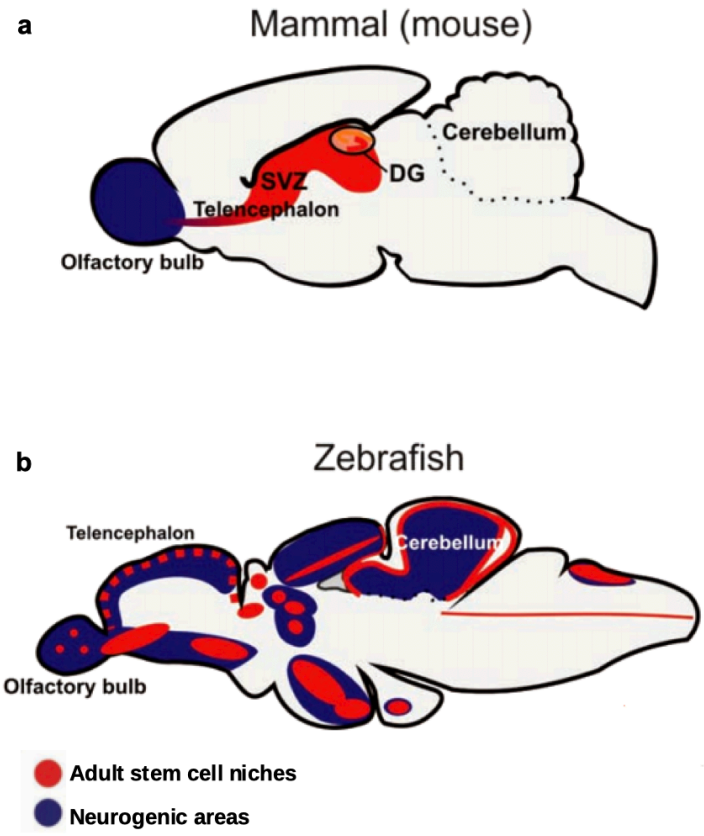

Figure 3. Neurogenic regions of the zebrafish brain in comparison to mammals. (a) Mammalian neurogenesis takes place via the NSCs residing in two specific neurogenic niches in the telencephalon: the subventricular zone (SVZ) of the lateral ventricles in the telencephalon and the subgranular zone (SGZ) of the dentate gyrus in the hippocampus. **(b)** There are 16 stem cell niches located along the rostro-caudal axis of the brain. Note: Adapted with copyright permission from John Wiley and Sons and Copyright Clearance Center from "Adult Neurogenesis and Brain Regeneration in Zebrafish" (Kizil, Kaslin, et al., 2012). *Dev. Neurobiology,* 2012 Mar;72(3):429-61. doi: 10.1002/dneu.20918. Copyright 2011, Wiley Periodicals, Inc.

Among neurogenic niches in zebrafish brain, telencephalic niches are well-studied. These progenitors are located in the ventricular zone of the telencephalon (Kizil, Kaslin, et al., 2012). Progenitor cells of the ventricular zone reveal different characteristics and they are positioned dorsally and ventrally (Grandel et al., 2006; Kizil, Kaslin, et al., 2012). The ventral area harbours mostly proliferating nestin-expressing neuroepithelial progenitors (Ganz et al., 2010) generating HuC-expressing differentiating neurons. The dorsal area includes proliferating and non-proliferating radial glial shaped progenitors which express glial markers such as S100, glial fibrillary acidic protein (GFAP) and Vimentin (Ganz et al., 2010; Grandel et al., 2006). These cells subsequently generate HuC-expressing newborn neurons. Another proliferating cell population that does not express the radial glial cell markers has also been detected in this region. However, the contribution of these cells to neurogenesis is not clear yet (Figure 4) (Kizil, Kaslin, et al., 2012).

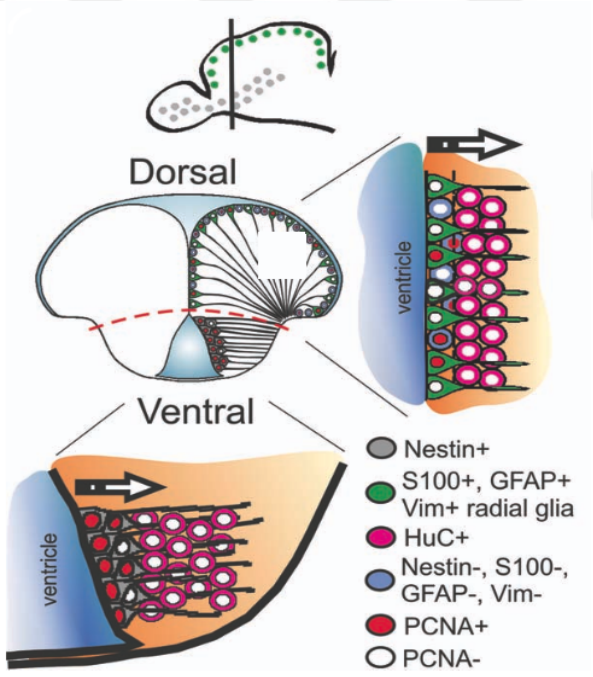

Figure 4. Schematic summary of the zebrafish telencephalic progenitor niche. Arrows show the direction of neurogenesis and migration. Note: Adapted with copyright permission from John Wiley and Sons and Copyright Clearance Center from "Adult Neurogenesis and Brain Regeneration in Zebrafish" (Kizil, Kaslin, et al., 2012). *Dev. Neurobiology*, 2012 Mar;72(3):429-61. doi: 10.1002/dneu.20918. Copyright 2011, Wiley Periodicals, Inc.

Radial glial cells, whose bodies are located in the ventricular zone, have a significant role in adult zebrafish neurogenesis (Schmidt et al., 2013). These cells can proliferate, renew themselves and give rise to new neurons (Rothenaigner et al., 2011). Research suggests that they are also involved in the development of mammalian telencephalon, although they disappear shortly after birth (Alvarez-Buylla et al., 2001; Schmidt et al., 2013). There are two subtypes of radial glial cells that are characterized by proliferation markers (i.e., proliferating cell nuclear antigen, PCNA), or by BrdU incorporation (Schmidt et al., 2013), in addition to the glial cell markers GFAP, S100β, and brain lipid-binding protein (BLBP). While Type I cells, remaining at the quiescent state, are BrdU-, PCNA-, GFAP+, S100β+, and BLBP+, Type II cells, proliferating slowly, are BrdU+, PCNA+, GFAP+, S100β+, and BLBP+ (Figure 5) (Schmidt et al., 2013).

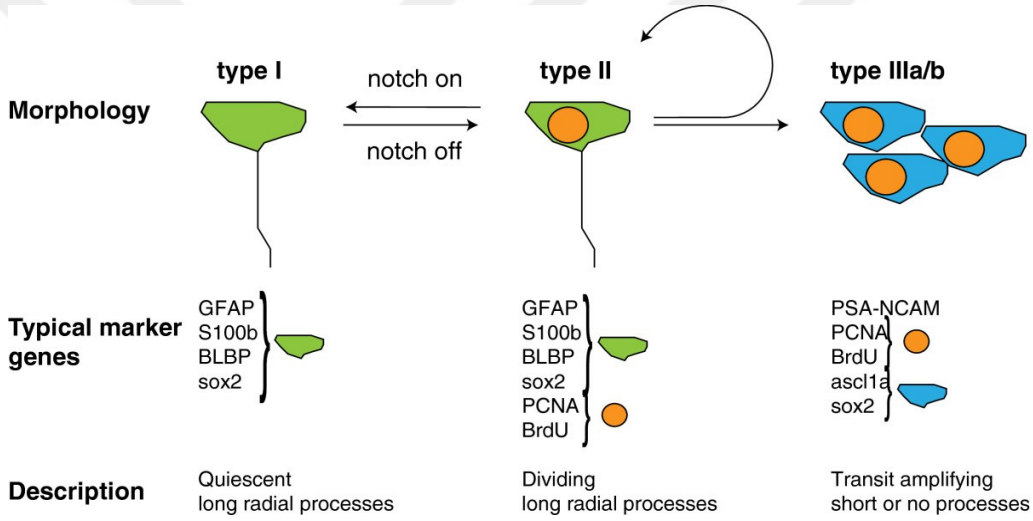

Figure 5. **The major proliferative cell types in the telencephalon stem cell niche.** Type I cells: BrdU-, PCNA-, GFAP+, S100β+, BLBP+; Type II cells: BrdU+, PCNA+, GFAP+, S100β+, BLBP+; Type III cells: PSA-NCAM+, ascl1+. Note: Adapted from "Neurogenesis in zebrafish – from embryo to adult" (Schmidt et al., 2013). *Neural Dev*, 8,3 (2013). https://doi.org/10.1186/1749-8104-8-3. Copyright 2013. Published under licence to BioMed Central Ltd. This is an Open Access article distributed under the terms of the Creative Commons Attribution License (https://creativecommons.org/licenses/by/2.0), which permits unrestricted use, distribution and reproduction in any medium provided that the original work is properly attributed.

Most radial glial cells in the stem cell niches of the telencephalon are Type I cells. In order to maintain the population of stem cells in the niches, Notch signaling can affect the proportion of Type I (quiescent) and Type II (proliferating) cells. With the activation of Notch signaling, stem cells enter the quiescent state (Type I) (Chapouton et al., 2010). If a Type II cell divides symmetrically, a new Type II cell forms. However, asymmetrical division of this cell gives rise to another cell type, Type III, also known as neuroblasts. Neuroblasts are precursor cells that proliferate and express neural and proneural genes, such as *PSA-NCAM* and *ascl1*, respectively (Figure 5) (Schmidt et al., 2013). In addition to these cells, studies suggest that other cell types in the periventricular zone can contribute to neurogenesis directly or indirectly (Lindsey et al., 2012). The cellular structures of the niches are more complicated than depicted on Figure 5.

2.4. Glioma mechanisms

Gliomas are the CNS's most prevalent primary malignant tumours, originating from glial tissue (Ostrom et al., 2014). They are classified by the World Health Organization (WHO) according to their histopathological and molecular properties from grade I to IV. While grade I is slow-growing and less aggressive, grades II to IV are more aggressive and more malignant. Grade IV gliomas, the most common and deadliest form of the glioma subtypes, are also known as glioblastoma multiforme (GBM).

Radial glial cells, which act as primary NSCs for new neurons in the adult CNS of both mammals and zebrafish, also appear to act as a source of gliomas (Lim et al., 2007; Sanai et al., 2005). It has been showed that glial tumours are related with the genes specific to undifferentiated neural cells (Barnett et al., 1998; Dahlstrand et al., 1992; Nakano et al., 2007; Noble & Mayer-Pröschel, 1997). Abnormal NSC-like cells, such as astroglial cells, are also thought to contribute to neoplastic growth of glial tumours (Ignatova et al., 2002). Thus, a glial cell has the ability to give rise to new cell types, but it may also proliferate abnormally and become glioma. Mouse functional models of gliomagenesis have provided a platform to study the cell of origin of gliomas (de Almeida Sassi et al., 2012; Wee et al., 2011). These models mostly used the genetic targets that are mutated in GBM (Louis et al., 2016; Modrek, 2014).

GBMs are more malignant, are the most frequent gliomas and have high proliferation rate, tumour angiogenesis and chemoresistance (Franceschi et al., 2017). IDH1, IDH2 and TERT are

the most frequently occurring mutations in glioma/glioblastoma (Killela et al., 2014). In addition to these mutations, GBM has been characterized with a number of high frequency alterations in tumour suppressors including p53, PTEN and RB as well as proto-oncogenes such as EGFR, PDGFR and Kras (Brennan et al., 2009; Parsons et al., 2008; Verhaak et al., 2010). While expression of oncogenic Kras is often insufficient to induce malignant gliomagenesis in mouse models (Holland et al., 2000), it has recently been demonstrated to be sufficient to initiate glioma formation in transient transgenic situations (Ju et al., 2015).

2.5. Possible links between regeneration and cancer

The ability to regenerate damaged or lost tissues in response to injury or disease varies significantly among animal phyla and between different organs. While the regenerative process can occur through distinct routes such as (i) activation of resident stem cells, (ii) direct proliferation of differentiated cells, (iii) dedifferentiation of mature cells or (iv) transdifferentiation of differentiated cells into another type; they all involve stimulation of cell proliferation. In addition to regeneration, cell proliferation is also tightly associated with embryonic development and cancer. The mechanistic link between these phenomena had first been brought forward by Waddington in the early 1930s, when he hypothesized the existence of "individuation fields" (first recognized by Spemann and Mangold as potent regional cellular and humoral factors in a growing embryo (Spemann & Mangold, 2001)) both as developing regions in which organizers can rearrange tissues to become a complete embryo and as regulators of tissue growth in adult organisms (Stern, 2000; Waddington, 1935). Waddington had proposed the adult individuation fields to be potent sites in organisms with high regenerative potential such as urodeles and larval anurans (Waddington, 1935). The presence of those fields in adult tissues made him argue that tissues escaping from the organizing pattern of the fields could grow into cancer. These observations thus rationalize a potential link between regeneration and cancer. Nowadays, there is growing evidence associating regeneration mechanisms with cancer biology (Beachy et al., 2004; J. Brockes, 1998; Dvorak, 1986; Gurtner et al., 2008; Rose & Wallingford, 1948; Schäfer & Werner, 2008; Tsonis, 1983; White & Zon, 2008).

Under normal conditions, regeneration follows a common route of injury-induced events that include cell proliferation, migration, differentiation and morphogenesis to restore tissue integrity and function. Most importantly, these events are terminated in a controlled manner so

that the regenerating tissue does not transform into a mass of cells that undergo uncontrollable proliferation. If regeneration cannot be processed or terminated properly, the tissue might -as in the case of cancer- undertake continuous proliferation due to chronic injury, hypoxia, and inflammation, and cannot re-establish tissue integrity (Beachy et al., 2004; Coussens & Werb, 2002; Dvorak, 1986; Gurtner et al., 2008; Oviedo & Beane, 2009; Schäfer & Werner, 2008; Seilern-Aspang & Kratochwill, 1965; Verkhratsky & Butt, 2013). From an alternative point of view, regeneration might halt abnormally proliferating cells in cancer and help them recuperate abilities to undergo normal morphogenesis (Cajal, 1928; Rose & Rose, 1952; Rose & Wallingford, 1948; Tsonis, 1983). Hence, regeneration might in fact both contribute to abnormal tissue growth and also provide a means to prevent and correct growth abnormalities (Oviedo & Beane, 2009). The main difference between regeneration and tumorigenesis thus appears to occur not early during the generation of a proliferative response to injury but later when the cells are expected to decelerate proliferation, differentiate, undergo morphogenesis and complete regeneration.

Most of the molecular evidence establishing a link between regeneration and cancer comes from studies performed in urodele amphibians and planarians (Oviedo & Beane, 2009). This is mainly because both groups have an extraordinary capacity to regenerate (Agata & Watanabe, 1999; Alvarado & Tsonis, 2006; J. P. Brockes, 2005; Jeremy P. Brockes, 1997; Jeremy P. Brockes & Kumar, 2008; Odelberg, 2002; Reddien & Alvarado, 2004; Saló, 2006; Sánchez Alvarado, 2000) as well as to develop cancer via chemical induction (Best & Morita, 1982; J. Brockes, 1998; Cajal, 1928; Foster, 1969; Seilern-Aspang & Kratochwill, 1965). Intriguingly, the newt limb, where amputation at the site of induced tumours results in regeneration of a normal limb without any tumour, serves as a unique model showing that regeneration has indeed the capacity to correct malignant transformation (Cajal, 1928; Rose & Rose, 1952; Rose & Wallingford, 1948; Tsonis, 1983). Although both urodeles and planarians undergo extensive regeneration upon tissue injury, their frequencies of tumour development upon carcinogenic exposure differ remarkably, being much lower in urodeles than in planarians (J. Brockes, 1998; Foster, 1963, 1969; González-Granero et al., 2011; Hall et al., 1986; Oviedo & Beane, 2009; Schaeffer, 1993; Tsonis, 1983). Thus, generation of differential responses to carcinogens in two highly regenerative animal groups will bring us back to the question of molecular potential of Waddington's "individuation fields" from where tissue growth can lead to regeneration of tumorigenesis depending on how growth is controlled (Waddington, 1935).

It is therefore particularly intriguing to explore whether these regenerative fields develop an intrinsic resistance to cancer formation.

Due to the cellular similarities between tumour stroma and granulation tissue which forms at the injury site, cancers have long been described as wounds that do not heal (Dvorak, 1986; Haddow, 1972; Schäfer & Werner, 2008). This hypothesis has been supported by a large number of cellular and molecular studies showing that cancer and wound repair share remarkable features in generation of an inflammatory response, activation of angiogenesis and differential expression of genes involved in cell proliferation, survival and migration (Chang et al., 2004; Crusz & Balkwill, 2015; de Visser et al., 2006; DiPietro, 2013, 2016; Karin & Clevers, 2016; Martin & Leibovich, 2005; Pedersen et al., 2003; Riss et al., 2006; Sherwood et al., 1971). On the other hand, tumours differ from healing wounds in various aspects including invasive growth and gene expression leading to continuous cell growth, metastasis and ultimately failure of healing (Pedersen et al., 2003; Schäfer & Werner, 2008). As both phenomena start in a similar vein but diverge later, it would be absolutely exciting to compare transcriptome of a healing wound at a late repair stage with that of a continuously growing/metastasizing tumour. Such a comparison will yield critical insights into the molecular mechanisms that lead to controlled cessation of repair and open new avenues on how tumour growth can be halted, and cancer cells can potentially be directed to a regeneration-like route.

3. METHODS

3.1. Fish maintenance

The AB wild-type 6-10-months-old adult zebrafish were used for brain injury model. Zebrafish were raised and handled in accordance with the guidelines of the Izmir Biomedicine and Genome Center's Animal Care and Use Committee.

3.2. Stab wound assay and sample collection for RNA experiments

Wild-type (WT) AB zebrafish were used for brain regeneration model. Before generating lesion, fish were anaesthetized with 0.02% (w/v) of tricaine (Supelco, A5040, Pennsylvania, United States) (Schmidt et al., 2014). Stab injury was performed in 6–10-months-old fish as previously described (Baumgart et al., 2012; Kroehne et al., 2011). A 30-gauge needle was inserted through the left nostril until the caudal end of the telencephalon (Figure 6). Afterwards, the fish were transferred into a tank with freshwater. At 1 day post-lesion (dpl), 3 dpl or 14 dpl of stab injury, zebrafish were re-anaesthetized with 0.02% (w/v) of tricaine solution (Supelco, A5040, Pennsylvania, United States) and euthanized by putting them into ice water for 5 minutes (Schmidt et al., 2014). After removing the whole telencephalon tissue, lesioned (left) hemispheres were dissected and collected individually. The left hemispheres of healthy zebrafish telencephalons were used as control samples. After dissection, all brain samples were transferred into an RNAprotect (Qiagen, 76104, Germany) tissue reagent immediately to prevent degradation of RNA.

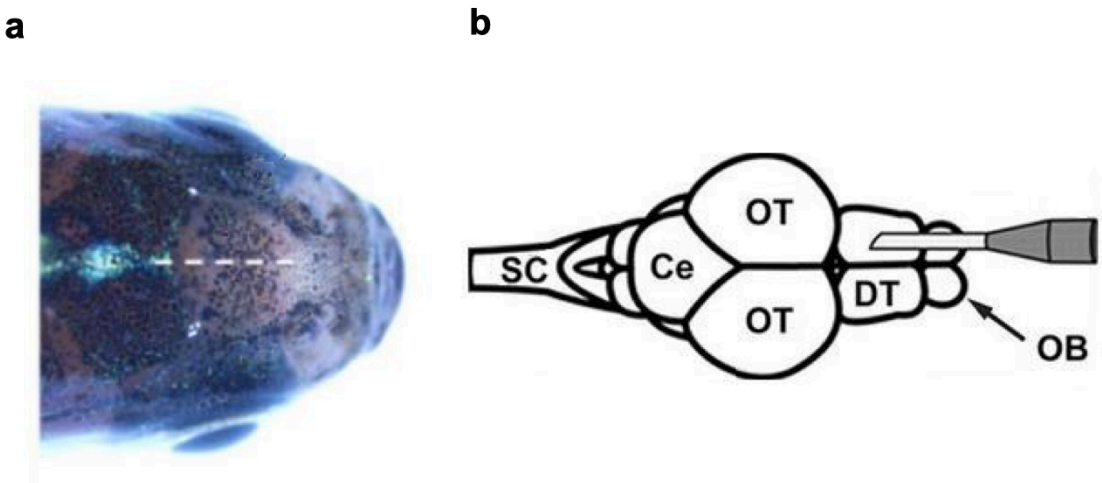

Figure 6. Schematic representation of adult zebrafish telencephalic stab injury. (a) Dorsal view of adult zebrafish *head*. The border between the two telencephalic hemispheres *is* shown by the dashed line. Note: Adapted from "Stab Wound Injury of the Zebrafish Adult Telencephalon: A Method to Investigate Vertebrate Brain Neurogenesis and Regeneration" (Schmidt et al., 2014). *J. Vis. Exp.* (90), e51753 (2014). Copyright 2014. Journal of Visualized Experiments. Published under licence to Published under licence to BioMed Central Ltd. This is an Open Access article distributed under the terms of the Creative Commons Attribution-NonCommercial-NoDerivs 3.0 Unported License (http://creativecommons.org/licenses/by-nc-nd/3.0/), which permits unrestricted use, distribution and reproduction in any medium provided that the original work is properly attributed. **(b)** A 30-G insulin syringe needle is inserted into the telencephalon of an adult zebrafish parallel*ly* to the rostro-caudal body axis along one hemisphere (dorsal view; OB*:* olfactory bulb; DT*:* dorsal telencephalon; OT*:* optic tectum*;* Ce*:* cerebellum; SC*:* spinal cord). Note: Adapted with copyright permission from John Wiley and Sons and Copyright Clearance Center from "Regeneration of the adult zebrafish brain from neurogenic radial glia-type progenitors" (Kroehne et al., 2011). Development, 2011, (138), 4831-4841. doi.org/10.1242/dev.072587. Copyright 2011. Published by The Company of Biologists.

3.3. Histological demonstration of stab lesion

3.3.1. Brain dissection and fixation

In order to show if the brain regeneration model is working properly, randomly selected fish were re-anaesthetized 1 day after lesion with 0.02% (w/v) of tricaine (Supelco, A5040, Pennsylvania, United States) solution and euthanized by putting them into ice water for 5 minutes (Schmidt et al., 2014). Fish were placed on 1x PBS-soaked tissue paper. Heads were cut and separated from the body with the help of a sharp blade behind the gills and their skulls were opened, allowing a better penetration of the solutions into the brain tissue. Then, they were kept in cold 1x PBS for 5 minutes to remove blood. Heads were transferred into cold 4% paraformaldehyde (PFA) (Merck, New Jersey, United States) in PBS and fixed overnight at 4°C. Next day, fixed heads were washed three times with cold 1x PBS for a minimum of 30 minutes each time. Next, the heads were transferred into 20% sucrose–20% EDTA (Merck, 107651, New Jersey, United States; Amresco, 0105, FPS, United States, respectively) for 2

days at 4°C and 30% sucrose–20% EDTA (Merck, 107651, New Jersey, United States; Amresco, 0105, FPS, United States, respectively) overnight at 4°C (Demirci et al., 2020).

3.3.2. Embedding of the brains for sectioning

20% sucrose-7.5% gelatine solution (Merck, 107651, New Jersey, United States; AppliChem A1693, Illinois, United States, respectively) was melted on a magnetic stirrer at 37°C and let to cool down for 3 minutes at room temperature before usage. Heads were put into this solution and waited until they sink to the bottom of the tube. A disposal embedding mould (Sigma-Aldrich, E6032, Missouri, United States) was placed into the dry ice and a 20% sucrose-7.5% gelatine solution (Merck, 107651, New Jersey, United States; AppliChem A1693, Illinois, United States, respectively) was poured at the bottom of the mould. Only one head was placed into the mould and oriented by a dissection needle rostral side down, caudal side up. The mould was filled entirely with 20% sucrose-7.5% gelatine solution (Merck, 107651, New Jersey, United States; AppliChem A1693, Illinois, United States, respectively). It was let until the solution cooled down and solidified (Demirci et al., 2020). Tissues were stored at -80°C until cryosectioning.

3.3.3. Cryosectioning

Before sectioning, the cryostat was set up at sample temperature -23°C and blade temperature -25°C. A pre-cooled sharp razor blade (Feather, C35, Japan) was used and replaced approximately after 5 brain tissues. Tissue block was removed from disposable mould carefully and trimmed. Trimmed block was stuck on tissue holder by using OCT compound (Tissue-Tek, 4583, The Netherlands). Fourteen-micrometre-thick cryosections (Grandel et al., 2006) were prepared on a Leica CM1850 (Wetzlar, Germany) cryostat and stored at -20°C until further use.

3.3.4. Hematoxylin/Eosin (HE) staining

Cryosections on slides were counterstained using Hematoxylin/Eosin (Kroehne et al., 2011). Fixation was performed by using 80% methanol (Supelco, 106009, Pennsylvania, United States) at 4°C for 20 min. After fixation, they incubated with hematoxylin (Sigma-Aldrich, MHS16, Missouri, United States) for 15 minutes. The slides were washed with dH_2O for 5 minutes. After incubation with eosin (Sigma-Aldrich, HT110116, Missouri, United States) solution for 10 minutes, dehydration was performed with 70%, 85%, 96%, 100% ethanol

solutions (Merck, 107017, New Jersey, United States) for 5 minutes each. The slides were treated with xylene for approximately 45 minutes and let until completely dry. Images were obtained using an Olympus BX5 upright microscope (Olympus, Tokyo, Japan).

3.4. RNA isolation

Before isolating RNAs, RNAprotect tissue reagent (Qiagen, 76104, Germany) was removed and 700 µl Qiazol reagent (Qiagen, 79306, Germany) was added on the brain tissues and homogenized by using a sterile disposable pestle (Fisherbrand, 12-141-364). Total RNA was isolated using the RNeasy Plus Micro Kit (Qiagen, 74034, Germany) as specified in the manufacturer's instructions. RNA samples were stored in –80 at 4°C until further experiments.

3.5. Quantitative and qualitative measurements of isolated RNA samples

NanoDrop 2000 spectrophotometer (Thermo Scientific, MA, United States) was used to quantified RNA samples. For qualitative analysis, firstly, 2100 Bioanalyzer (Agilent Technologies, CA, United States) and Agilent RNA 6000 pico kit (Agilent Genomics, 5067-1513, CA, United States) were used as indicated in the manufacturer's instructions, in order to assess the integrity of RNA samples. The samples with an RNA Integrity Number (RIN) ≥ 7 were selected for RNA sequencing and cDNA synthesis for further qPCR validations. Secondly, RT-PCR analyses were performed to show RNA integrity by using a primer pair producing an 812 bp product for zebrafish beta actin 1 (*actb1*) as a housekeeping gene (Table 1).

Table 1. Forward and reverse primers for zebrafish actb1 gene.

	Zebrafish ortholog	Forward primer sequence (5'->3')	Reverse primer sequence (5'->3')
Housekeeping gene	***actb1***	AGAGAGAAGATGACACAGATCA	TAGGCCATTTAAGGTGGCAA

3.6. Library construction and RNA-Sequencing (RNA-Seq)

According to the results of previous analyses, the selected samples were sent to the Genomics Core Facility (GeneCore, EMBL Heidelberg, Germany) for library preparation and RNA sequencing. Libraries were prepared using an Illumina TruSeq RNA Library Preparation Kit v2 (Illumina, San Diego, CA, United States) according to the manufacturer's suggestions by using 500 ng complementary DNA (cDNA) as input. Paired-end, strand-specific sequencing

platform was used on Illumina NextSeq 500 (Illumina, San Diego, CA, United States) with 75 bp read lengths.

3.7. Obtaining cancer samples from public databases

In order to compare brain regeneration and brain cancer at the gene expression level, gene expression datasets of brain cancers were obtained from public databases. RNA sequencing data of human glioblastoma (GBM) and low-grade glioma (LGG) samples were obtained from the TCGA data portal (*https://portal.gdc.cancer.gov*, 2020).

In this study, the data type for all GBM/LGG datasets downloaded from the TCGA database were gene expression quantification obtained by using HTSeq tool (Anders et al., 2015). All downstream analyses were performed by using R programming language.

The TCGA-GBM dataset (GBM=165; Normal=5) was downloaded for glioblastoma, and the TCGA-LGG dataset (LGG=529; Normal=5) was downloaded for low-grade glioma. All datasets include primary and recurrent tumour samples of both brain cancer types.

3.8. Bioinformatics analysis of zebrafish brain regeneration samples and human brain cancer samples

RNA sequencing (RNA-Seq) is a technique that allows investigation of RNA molecules in a tissue at high resolution. There are numerous commercial or non-profit software for RNA-Seq data analysis, and a typical analysis workflow includes the following steps: performing quality control of raw reads; mapping reads to the reference genome and transcriptome; quantification of gene expression levels; identification of differential gene expression and data visualization. Also, with the development of RNA-Seq technologies and their extensive data analysis methods, differential co-expression networks constructed from RNA-Seq data makes investigation of regulatory genes and functional gene annotation possible.

In this study, a customized RNA-Seq workflow was performed from start in order to identify differentially expressed genes (DEGs) and functionally enrich these DEGs for zebrafish brain regeneration data. The same analysis workflow was also applied to brain cancer data from generating a count matrix to the end (Figure 7).

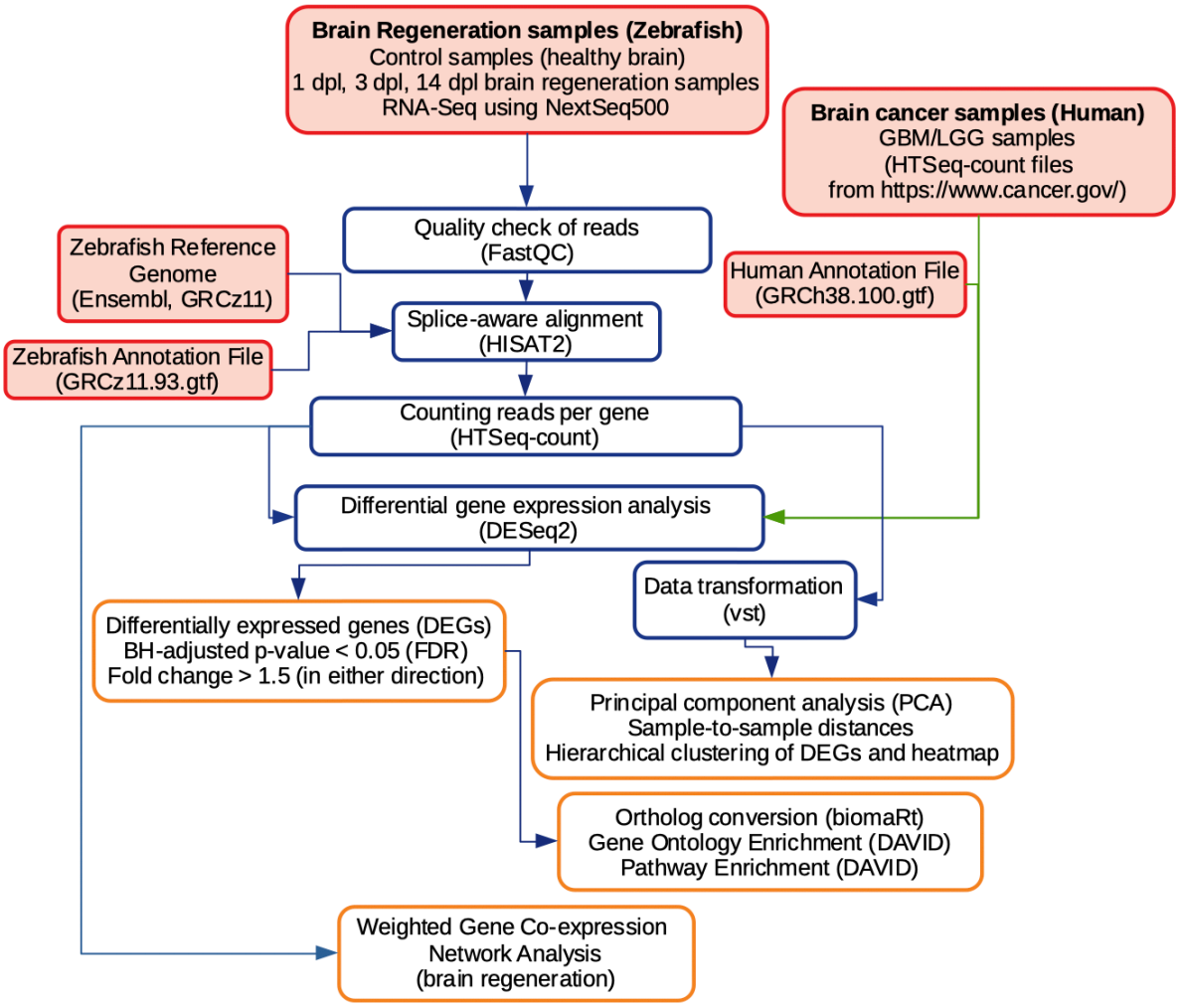

Figure 7. Bioinformatics analysis pipeline. RNA-Seq reads were generated using Illumina NextSeq 500 for zebrafish brain regeneration. The quality of reads was checked by using FastQC and MultiQC tools. Alignment and counting of reads for zebrafish brain regeneration were performed by using a zebrafish reference genome (Ensembl, GRCz11) and the annotation file (Ensembl, GRCz11.93.gtf) by HISAT2 and HTSeq-count tools, respectively. Count data were obtained from the TCGA database for human brain cancer data. For both regeneration and cancer data analysis, counts were transformed by variance-stabilizing transformation (vst) prior to calculating sample-to-sample distances, performing principal component analysis and hierarchical clustering of DEGs. In order to test differential expression for all genes, we used the DESeq2 package with the following criteria: fold change > 1.5 (in either direction) and Benjamini–Hochberg adjusted p-value (FDR) < 0.05. Gene Ontology and pathway enrichment analyses were performed by using DAVID tool (Database for Annotation, Visualization and Integrated Discovery). dpl, days post-lesion.

3.8.1. Quality check of raw RNA sequencing (RNA-Seq) data for brain regeneration

To ensure both reproducibility and reliability of the results of RNA-Seq data, quality control (QC) should be carefully applied at different steps of data analysis including raw reads and mapped reads. As an initial step, RNA-Seq data should be checked at the level of raw data before downstream analysis. To this aim, raw reads sequences generated from zebrafish brain regeneration samples were quality-controlled by using FastQC tool (Andrew, 2010). This tool includes a number of different analyses called modules such as total number of reads sequenced, the presence of adapters, GC content and the overall base quality score of samples. FASTQ-like format (text), SAM (Sequence Alignment Map), BAM (Binary Alignment Map) file formats can be used as input files. FasQC is written in the Java programming language and involves two different modes. One of them is an interactive application that displays results in a graphical user interface. The non-interactive mode can be run on command-line generating an HTML (Hypertext Markup Language) file as output. This mode is more appropriate for a large number of files. The non-interactive mode FastQC was used in this thesis to check all samples and results of all samples were consolidated with MultiQC (Ewels et al., 2016), a tool written in Python programming language to summarise and visualise the results. This tool enables the generation of a single HTML report as output from many samples.

In order to assess the quality of the raw reads, the first module of FastQC and MultiQC analyses was evaluated to show the basic statistics for the samples including the length and total number of reads sequenced for each sample. The next two important modules are “Mean Quality Scores” and “Per Sequence Quality Scores”. “Mean Quality Scores” results show the mean quality value across each base position in the read. This plot shows whether there was any problem during the sequencing. The “Per Sequence Quality Scores” plot indicates the number of reads with that average on the y-axis and the average quality score on the x-axis. Coloured horizontal lines on this plot shows the Phred quality score as red (<20), yellow (20–28), and green (>28). A Phred score >20 is acceptable for many purposes. Other quality check parameters of raw reads are “Per Base N Content” and “Adapter Content”. “Per Base N Content” analysis was performed to show the percentage of base calls at each position for which an N was called. According to this analysis, if the sequencer does not enable a base call with a sufficient confidence, it will be represented by an N rather than an ordinary base. “Adapter Content” analysis was carried out to determine the cumulative percentage of the library which has seen each of the adapter sequences at each position (Andrew, 2010; Ewels et al., 2016).

Lastly “Sequence Counts” and “Sequence Duplication levels” parameters of raw data were checked. While “Sequence Counts” analysis shows sequenced estimated unique and duplicated counts for each sample, “Sequence Duplication levels” analysis shows the relative level of duplication found for each sequence. There are generally two main sources of duplicate reads in transcriptomics data. It can be caused by PCR duplication due to biased PCR amplification of already over-represented fragments in the library. It can also be due to truly over-represented reads in an RNA-Seq library. FastQC is originally designed for quality check of whole-genome shotgun sequencing data. For whole genome shotgun data, almost 100% of the reads should be unique. As a result of this FastQC tends to raise excessive warnings for multiple sequencing data types including mRNA-Seq and small RNA-Seq in the results of the sequence duplication levels and over-represented sequences (*https://rtsf.natsci.msu.edu/genomics/tech-notes/fastqc-tutorial-and-faq/*, 2021).

3.8.2. Mapping of the brain regeneration reads to the zebrafish reference genome

After quality check of the samples, the second step of the RNA-Seq analysis is to map the reads to the reference genome. As a result of alignment, reads are aligned to loci of the genome, allowing to count reads mapped to individual genes or transcripts for identification of differentially expressed genes. For this analysis, different algorithms are used in the presence or absence of the reference genome. If the reference genome is known, there are two alternative mapping methods: (i) mapping to the reference genome or (ii) mapping to the reference transcriptome. In the absence of a reference genome, the reads are first merged as transcripts or contigs and mapped to the novel reference transcript for quantitative analysis, and then functional analyses are done (Conesa et al., 2016). If the existing genome will be used as a reference, first the reference genome must be indexed before mapping. Once the reference genome is indexed, the aligner rearranges the genome file in a format that facilitates mapping and stores it in the appropriate format. Some alignment tools provide the users with ready-to-use indexes for some of the reference organisms. After indexing, RNA-sequencing reads are mapped to the reference genome. Ailgnment tools are divided into two groups as "splice-aware" that recognize exon-exon boundaries and "splice-unaware" that do not. Several alignment tools have been developed that allow short reads to be mapped to the reference genome. These tools have different advantages in terms of performance, precision, speed and memory usage (Baruzzo et al., 2017; Pertea et al., 2016).

In this study, a "splice-aware" alignment tool, HISAT2 (2.1.0) (D. Kim et al., 2015), was used to map reads to the reference zebrafish genome. HISAT2 is a fast and sensitive alignment program for mapping next-generation sequencing reads (NGS) to the reference genome of any organism. This tool allows application programming interfaces (API) for C++, Python, and JAVA to find genomic locations from alignments for use in downstream analyses (D. Kim et al., 2015). Since pre-indexed zebrafish reference genome cannot be found online, the indexing was carried out by using the zebrafish reference genome. As a first step, the last published reference genome of the zebrafish was obtained from the Ensembl (*Danio rerio* GRCz11) database (*https://www.ensembl.org/danio_rerio/info/index*, 2019). After indexing, analyses were carried out to map the RNA-Seq reads of the samples to the reference zebrafish genome in order to determine which transcripts are expressed in the samples and at what level.

3.8.3. Quantitative analysis of mapped reads

One of the most important steps of RNA-Seq analysis is the quantification of gene expression that enables differential gene expression analysis. This allows transcripts to be counted quantitatively. Various pieces of software have been developed to quantify gene expression values such as HTSeq-count (Anders et al., 2015), Subread featureCounts (Liao et al., 2014), Cufflinks (Trapnell & Salzberg, 2009), and Ballgown (Frazee et al., 2015). The basic approach for quantitative calculation is to calculate the raw numbers of mapped reads using programs such as HTSeq and featureCounts (Anders et al., 2015; Liao et al., 2014). This gene-level quantification approach requires a gene transfer format (GTF) file containing the genomic coordinates of exons and genes (genomic features).

HTSeq, a Python package, was used in this study to calculate the numbers of mapped reads for each corresponding gene. One stand-alone script of the HTSeq package is *htseq-count* and it was used to count reads overlapping with exons of each gene. As input files, it uses a SAM/BAM file which is output of the alignment tool and a GTF/GFF file including information about gene structures (Anders et al., 2015). The latest annotation (GTF) file of zebrafish was obtained from the Ensembl database for this purpose (*https://www.ensembl.org/danio_rerio/info/index*, 2019). The outputs of *htseq-count* were then used for downstream analyses such as sample-to-sample distances, PCA, gene-level differential expression analysis and WGCNA.

3.8.4. Quality check results of brain regeneration samples after mapping to the reference genome

In addition to quality control of raw data, quality checks are performed in downstream analysis, after mapping reads to the reference genome, after quantitative analysis of transcripts, and at other steps to show variation between replicates. For this purpose, a large number of tools have been designed (García-Alcalde et al., 2012; L. Wang et al., 2012). There are also interactive tools like IGV (Integrative Genomics Viewer) to visually assist quality control (Thorvaldsdóttir et al., 2013).

Alignment results can be affected by several issues: (i) contamination with other organisms (bacteria and viruses), (ii) strandedness of the RNA-Seq process (forward-stranded, reverse-stranded or unstranded), or (iii) contamination by RNAs other than mRNA (such as ribosomal RNAs (rRNA)). MultiQC was used to show alignment rates and some statistics of quantitative analysis of the reads in this study. The module "PE Alignment Score" of MultiQC shows the number of reads aligned to the reference genome as "Number of Reads" and "Percentages". Both plots give some metrics of the alignment results: PE mapped uniquely, PE mapped discordantly uniquely, PE one mate mapped uniquely, PE multi-mapped, PE one mate multi-mapped, PE neither mate aligned. Another module, "Count Assignments", also shows the results of the quantitative analysis as "Number of Reads" and "Percentages". These plots show some statistics about counting results, such as reads assigned to a unique gene (blue), reads that are assigned to multiple overlapping genes (black), reads aligned to multiple loci (green), uniquely mapped reads that can't be assigned to a gene (orange), reads whose mapping quality is too low (purple), and reads that are not mapped to the genome (pink) (Ewels et al., 2016).

In this study, one of the tools used for quality control of the aligned reads is the Integrative Genomics Viewer (IGV) (Robinson et al., 2011; Thorvaldsdóttir et al., 2013). It is a high-performance interactive tool for the visualization of large sequencing data sets. Normally, this tool requires a BAM/SAM file with their indexes (BAI/SAI format, alignment file which is sorted by position and then indexed) as input. Since alignment results were stored in large files (BAM/SAM file format), these files were converted to bigWig (BW) format for faster visualization. BigWig files enable faster analysis than BAM files, because the alignment information is collapsed into a coverage information. In order to create bigWig files, samtools

(H. Li et al., 2009) was used to convert SAM files to sorted BAM files. The *genomecov* function of bedtools (Quinlan & Hall, 2010) was used to transform sorted BAM files to bedGraph files (textual coverage files). Finally, bigWig files (binary coverage files) were obtained using the UCSC program bedGraphToBigWig (Kent et al., 2010).

3.8.5. Batch effect correction of brain regeneration samples

Diverse technical sources of variation between libraries affect measurements in RNA sequencing and are known as batch effect. Main sources of batch effect are the difference of experimental and laboratory conditions, difference of sequencers, difference in processing times, difference of origins of samples and difference of personnel handling experiments. These differences can result in spurious results. Batch effect correction tools have been developed to remove variability from data that is not due to biological reasons.

SVA (surrogate variable analysis) package (version 3.36.0) of R was used to correct batch effect. ComBat is a function of the R package SVA, implementing an Empirical Bayes framework for batch effect correction (Leek et al., 2012). Log-transformed counts (plus a pseudo-count) were fed into ComBat for batch effect correction along with a design matrix summarizing both experimental batches (variable to integrate) and the experimental groups of interest (to be taken into account in the correction). The batch effect-corrected expression matrix was then transformed back to a "count-like" matrix using the reverse transformation (exponential minus a pseudo-count, rounded to the nearest integer). This count-like matrix was then fed into DESeq2 (Love et al., 2014) package version 1.28.1 for differential expression testing.

3.9. Sample-to-sample distances between brain regeneration samples

In order to show similarities and dissimilarities between samples, a heatmap of sample-to-sample distance matrix is generally used. Normalized count and normalized batch effect-corrected count matrices for overall gene expression were generated by *vst* (varianceStabilizingTransformation) function of DESeq2 (version 1.28.1) (Love et al., 2014). Euclidean distances were calculated for both before and after correction on the normalized, variance stabilized data by using *dist* function of the stats package of R and visualized by using *pheatmap* function of the pheatmap package (version 1.0.12) (Kolde, 2013). Both genes and

samples were hierarchically clustered using complete agglomeration method, as shown by the dendrograms of the heatmap.

3.10. Principal Component Analysis (PCA) of the brain regeneration samples

Since it is difficult to interpret large datasets such as RNA-Seq, principal component analysis (PCA) has been developed to reduce the high dimensionality of such datasets (Jolliffe & Cadima, 2016). Although there are many techniques for this aim, PCA is one of the most widely used. When it reduces the dimensionality, it minimizes loss of information and increases interpretability making possible to show the overall effect of experimental covariates and batch effects in large data. In PCA, the dimensionality of the data is reduced to a small number of dimensions called principal components (generally two for visualizing), or eigengenes in the context of RNA-Seq. A principal component (PC) is a linear combination of genes expressions where each gene is weighted according to the variance of its expression between the samples. PCs are orthogonal and independent covariates carrying most variance of the dataset in low dimensional projections. The variance of PCs decreases gradually with their rank.

In this study, normalized-count and normalized-batch-corrected count matrices for overall gene expression were generated by vst (varianceStabilizingTransformation) function of the DESeq2 package (Love et al., 2014) (version 1.28.1) of Bioconductor. Principal components (PCs) were calculated both before and after correction on the normalized, variance stabilized data by using the *prcomp* function of the stats package of R and visualized by using *ggplot2* package version 3.3.2 (Wickham, 2016).

3.11. Differential gene expression analysis

The main purpose of transcriptome studies is to investigate the alterations in gene expression occurring under various conditions by using statistical methods from raw reads. At this stage of the RNA-Seq analysis, differential gene expression analysis was performed. Differential expression analysis is to discover quantitative changes in expression levels between experimental groups from the normalized read count data with the help of statistical analysis.

To identify differentially expressed genes (DEGs), the following comparisons were performed using DESeq2: (i) 1 dpl lesioned hemisphere vs. control; (ii) 3 dpl lesioned hemisphere vs. control; (iii) 14 dpl lesioned hemisphere vs. control; (iv) LGG vs. normal tissue;

(v) GBM vs. normal tissue. The package DESeq2 of Bioconductor was used in this study to find DEGs. DESeq2 is a tool that uses a table of raw counts as input. For this purpose, the *DESeqDataSetFromHTSeqCount* function of DESeq2 was used to create a DESeqDataSet object containing raw counts and metadata of the samples (Love et al., 2014).

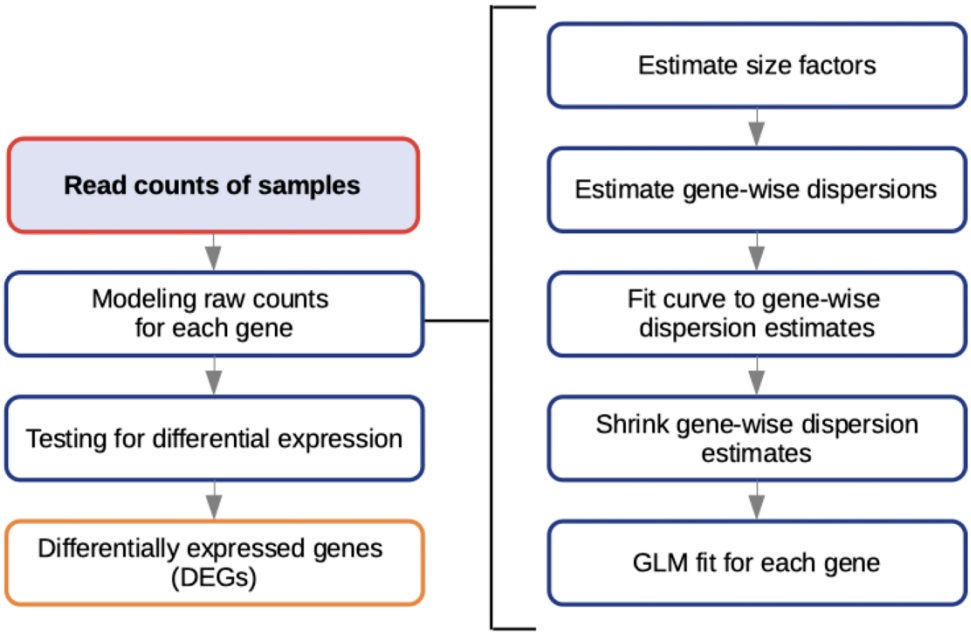

Figure 8. Statistical analysis of DESeq2. Differential expression analysis with DESeq2 includes multiple steps as shown in the figure. Note: Adapted from (https://hbctraining.github.io/DGE_workshop/lessons/04_DGE_DESeq2_analysis.html, 2021).

DESeq2 embeds a complex workflow for differential expression testing, which workflow is wrapped in a single *DESeq* function. It estimates size factors for samples to account for library size bias in the estimation of dispersion. Dispersion estimates are fitted on a curve against base mean expressions of genes. The dispersion estimates are shrunk to fit that curve closer in order to reduce the number of false positives, especially in the case of a low sample size. After that, a generalized linear model (GLM) is fitted for each gene against the design, under the assumption that gene expression counts follow a negative binomial (NB) distribution. Finally, each gene is tested for differential expression in the context of a comparison by performing a Wald test (Figure 8) (Love et al., 2014). For each comparison, each gene's differential

expression is summarised by a $\log_2$ fold change (effect size) and an (adjusted) p-value representing the significance of the expression difference between two experimental conditions.

3.12. Ortholog conversion

In order to compare events measured in zebrafish and human models, we built a table of unambiguous orthologous genes between *Homo sapiens* and *Danio rerio*. This table was made using BioMart annotations. The orthology table obtained from BioMart was first filtered to keep only pairs of genes indicated with high confidence or with similarities in genes names. In order to resolve ambiguities in this filtered table (i.e. to assign a unique human ortholog to each zebrafish gene), the table was further filtered in order to keep, for each zebrafish gene, its human ortholog with the exact same gene name when possible, or its human ortholog best ranked according to orthology metrics used sequentially, in this order: gene order conservation score, whole genome alignment coverage, percentage of identity of zebrafish gene to human gene, percentage of identity of human gene to zebrafish gene (metrics are used in this order to rank human orthologs of a given zebrafish gene, until the resulting ranking allows to choose a unique ortholog). Finally, in order to reduce the number of human genes matched to multiple zebrafish genes, only high confidence pairs were kept in that case.

3.13. Functional analysis

RNA-Seq differential gene expression analyses give a list of genes that are significant according to selected criteria including p-value and fold change. There exist downstream methods to derive biological insights from these lists of genes. Some of these methods are to determine whether these genes are enriched in any known biological functions, interactions, or pathways. Another analysis can include investigating genes by grouping them based on similar trends and to find related novel pathways or networks. These methods can be classified into three main categories: gene ontology analysis, over-representation analysis and pathway analysis. Gene ontology analyses are one of the most widely used categorization of the genes and gene ontology terms (GO terms) are grouped into three ontologies: biological processes (BP), molecular functions (MF) and cellular components (CC). For this purpose, web-based and R-based tools have been developed (Raudvere et al., 2019; Yu et al., 2012).

In this study, lists of significantly altered genes acquired from individual comparisons were used as inputs for functional analyses by using the Database for Annotation, Visualization

and Integrated Discovery (DAVID) 6.8 bioinformatics functional annotation tool (D. W. Huang et al., 2009). For functional enrichment, the EASE score, a modified one-tailed Fisher's exact test, was used to determine the GO terms and KEGG pathways by means of a user-defined gene list for each annotated DAVID GO term and KEGG pathway (Demirci et al., 2020). Significantly enriched GO terms and KEGG pathways were plotted using the ggplot2 package by using custom scripts.

3.14. Weighted gene co-expression network analysis (WGCNA)

Weighted gene co-expression network analysis (WGCNA) (Langfelder & Horvath, 2008) is a method that is used for various purposes: (i) clustering of highly co-expressed genes and delineation of gene modules, (ii) defining module eigengenes and intramodular hub genes, (iii) relating modules to each other and to phenotypic data, and (iv) finding the key drivers in modules of interest. WGCNA was used in this study to show important modules in brain regeneration.

3.14.1. Data input, cleaning and pre-processing

The first step of WGCNA is to load the expression data and pre-filter for the network analysis. According to WGCNA's manual (Langfelder & Horvath, 2008), variance-stabilized (vst) data is one of the recommended input formats for further analysis. In the tutorial of WGCNA, it is also suggested that genes whose counts are less than 10 in more than 90% of the samples should be removed, since these genes can cause noise and false correlations (Langfelder & Horvath, 2008). Genes were filtered for subsequent analysis according to these criteria in this study. As a result of this filtering, 22,853 genes were fed to WGCNA for the regeneration dataset.

3.14.2. Choosing the soft-thresholding power with scale free topology - Network construction and module detection (cluster dendrogram)

In this study, network was constructed using unsigned co-expression similarities between genes. As opposed to signed co-expression, unsigned co-expression conserves similarity between highly correlated genes, even in the case of negative correlation. Unsigned co-expression similarity between two genes *i* and *j* is defined as the absolute value of their sample correlation: $s_{i,j} = |cor(x_i, x_j)|$. For each dataset, a soft threshold (also called power) was

picked in order to construct a co-expression network. The soft threshold β expresses the way the co-expression similarity translates into an adjacency weight in the network: $a_{i,j} = s_{i,j}^{\beta}$. The higher the soft threshold, the further weak co-expressions are pushed towards 0, though without being made equal to 0 (hence the appellation of *soft* thresholding). For the data of this study (Zebrafish), a power of 9 was chosen by default, due to the small sample size (n=18) and according to the recommendation of the WGCNA manual (Langfelder & Horvath, 2008) for sample sizes less than 20. Given these parameters, a weighted co-expression network was constructed. Gene modules were then delineated from the clustering using the dynamic hybrid tree cut algorithm with a deep split parameter of 2.

3.15. Ethical committee approval

Animal experiments were approved by the Animal Experiments Local Ethics Committee of Izmir Biomedicine and Genome Center (IBG-AELEC). Ethical committee date is 29/08/2018, protocol number is 09/2018.

4. RESULTS

4.1. Histological demonstration of stab lesioned telencephalon

In order to trigger brain regeneration in adult zebrafish brain, previously described stab lesion assay that injures the central dorsal telencephalon (DT) by the insertion of a 30-gauge canula throughout left nostril along the rostro-caudal body axis was performed (Figure 6). To validate lesion method and to show lesion in the brain tissue, randomly selected fish dissected under anaesthesia. 14 um cross-sections of telencephalon were obtained by using cryostat and sections counterstained using Hematoxilin/Eosin (Kroehne et al., 2011). According to results, large lesion canal was observed in brain tissue of randomly selected zebrafish at 1 dpl. Tissue in the stab lesioned area was strongly vacuolated and blood cloth was seen in stab canal (Figure 9).

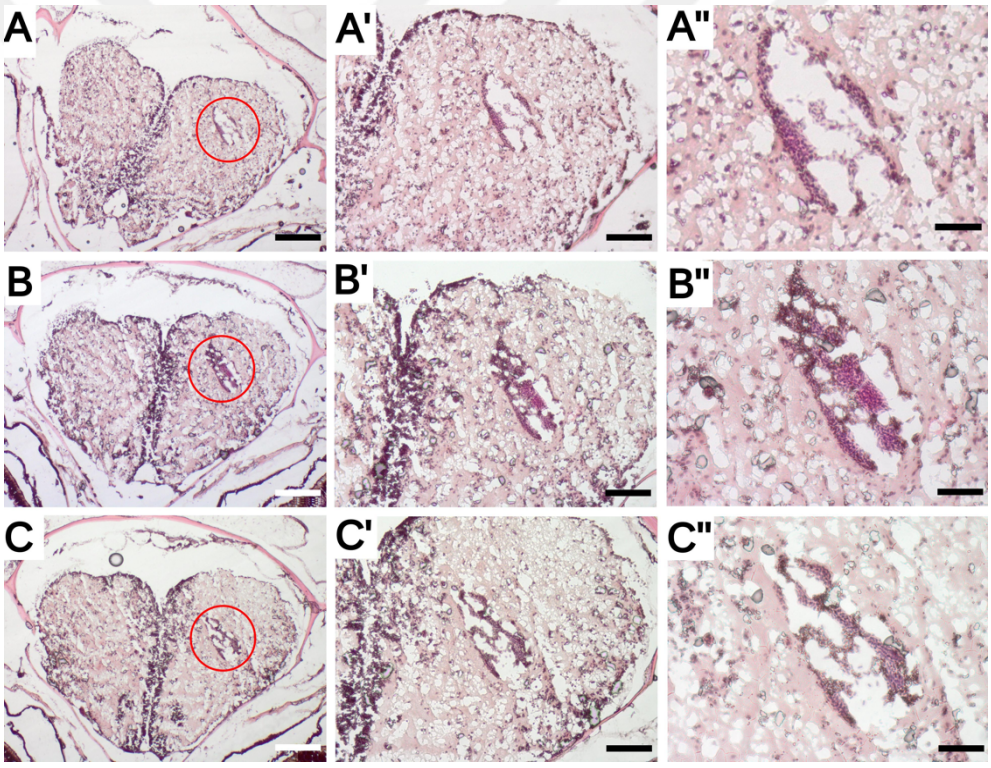

Figure 9. Histological demonstration of stab lesion assay in the adult zebrafish telencephalon. Tissue within the stab canal is strongly vacuolated and contains a blood clot as seen in Haematoxylin/Eosin (HE) stained sections of 1 day post lesion (dpl) brain samples. (A-C: 4x; A`-C`: 10x; A``-C``:40x magnification). Scale bars: 200µm in A-C; 50µm in A`-C` and 50µm in A``-C``. Red circles indicate the lesion canal.

4.2. Quantitative and qualitative measurements of isolated RNA samples

In order to perform qPCR analysis and RNA-Sequencing, total RNA isolation was performed from dissected brain samples by using RNeasy Plus Micro Kit (Qiagen, 74034, Germany). After isolation of RNA samples, several qualitative and quantitative analyses were done to check quality of samples. RNA concentration and integrity numbers of samples were measured using nanodrop and bioanalyzer, respectively.

Table 2. Qualitative and quantitative measurements of RNA samples used in this study.

No.	Sample ID	Sample name	Date	Exp. Group	ng/µl	µl	Total amount (ng)	cDNA (ng)	cDNA Dilution	RIN	Batch No.
1	Ctrl-RNA-3	Ctrl-5	16.08.18	1	67.8	12	813.6	100	1/20	10	2
2	Ctrl-RNA-5	Ctrl-1	27.08.18	1	27.5	11	302.5	100	1/20	9.7	1
3	Ctrl-RNA-6	Ctrl-2	27.08.18	1	22.7	11	249.7	100	1/20	9.7	1
4	Ctrl-RNA-7	Ctrl-3	27.08.18	1	26.5	11	291.5	100	1/20	9.9	1
5	Ctrl-RNA-8	Ctrl-4	27.08.18	1	25.5	11	280.5	100	1/20	9.8	1
6	1dpl-RNA-1	1dpl-1	30.0120	2	31.5	12	378	100	1/20	10	2
7	1dpl-RNA-2	1dpl-2	30.0120	2	33.2	12	386.4	100	1/20	10	2
8	1dpl-RNA-3	1dpl-3	30.0120	2	29.8	12	357.6	100	1/20	10	2
9	1dpl-RNA-5	1dpl-4	30.0120	2	32.5	12	390	100	1/20	10	2
10	1dpl-RNA-6	1dpl-5	30.0120	2	31.2	12	374.4	100	1/20	10	2
11	3dpl-RNA-5	3dpl-1	27.08.18	3	33.1	11	364.1	100	1/20	10	1
12	3dpl-RNA-6	3dpl-2	28.08.18	3	24.7	10	247	100	1/20	10	1
13	3dpl-RNA-7	3dpl-3	28.08.18	3	32.1	10	321	100	1/20	10	1
14	3dpl-RNA-8	3dpl-4	28.08.18	3	28.8	10	288	100	1/20	10	1
15	14dpl-RNA-2	14dpl-1	16.08.18	4	57.8	12	693.6	100	1/20	10	1
16	14dpl-RNA-3	14dpl-2	16.08.18	4	48.3	12	579.6	100	1/20	10	1
17	14dpl-RNA-4	14dpl-3	16.08.18	4	39.0	12	468	100	1/20	10	1
18	14dpl-RNA-5	14dpl-4	16.08.18	4	32.7	12	392.4	100	1/20	10	1

RNA concentrations were observed between 22.7 ng/µl – 67.8 ng/µl and their RIN values were between 9.7 and 10 (Table 2). cDNA synthesis was also performed to show RNA integrity and for further qPCR analysis. 1/20 dilution of 100 ng cDNA concentration was used as input for qPCR experiments. Zebrafish beta actin 1 (*actb1*) housekeeping gene yielding 812 bp product was chosen to check RNA integrity by RT-PCR and gel electrophoresis. Results showed that all RNA samples were intact on gel images (Figure 10).

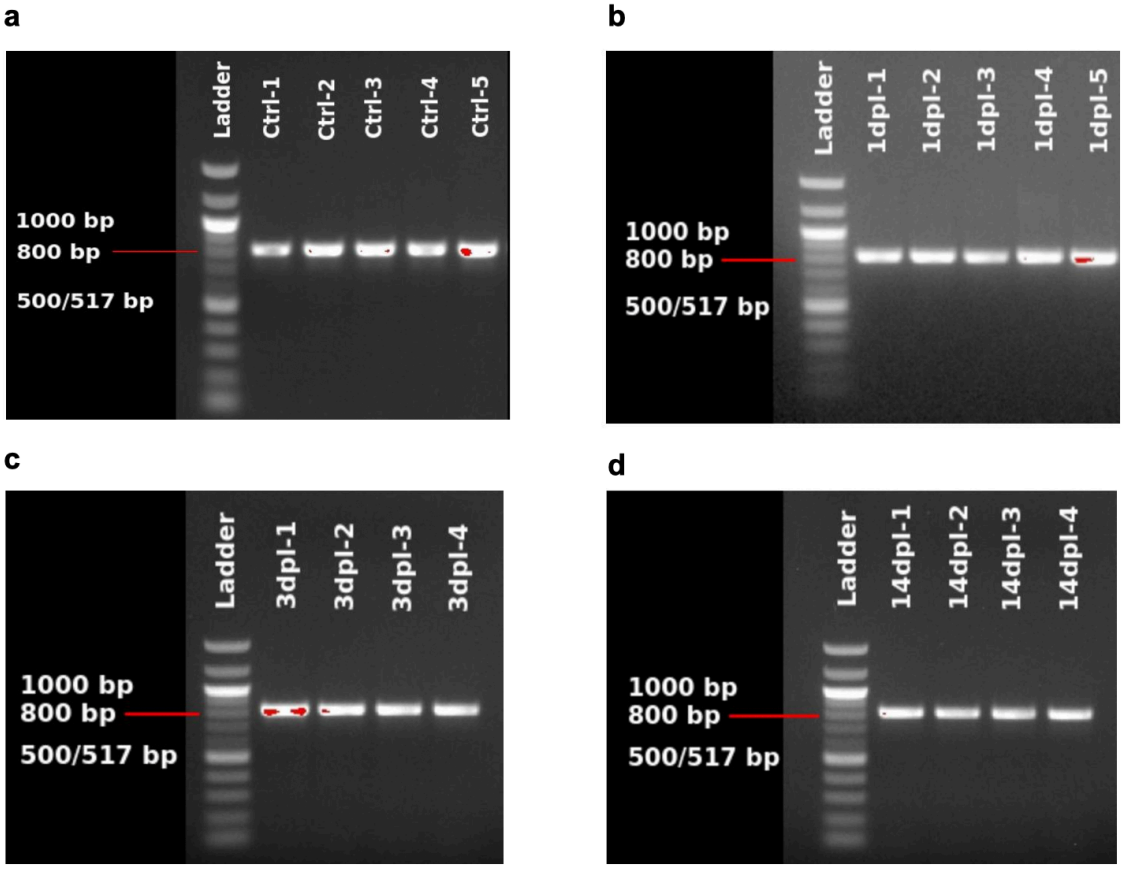

Figure 10. Integrity check of RNA samples. RT-PCR analyses were performed to show RNA integrity by using a primer pair producing an 812 bp product for zebrafish beta actin 1 (actb1) as a housekeeping gene. **(a)** Control samples (n=5); **(b)** 1 dpl samples (n=5); **(c)** 3 dpl samples (n=4); and **(d)** 14 dpl samples (n=4).

4.3. Quality check results of raw samples of brain regeneration samples

The first step in the RNA-Seq analysis workflow is to assess the quality of the sequence reads of the raw data received from the sequencing facility. The FASTQ file format contains the raw sequences of reads as well as sequence qualities and it is generated by next-generation sequencing technologies. In this study, FastQC (Andrew, 2010) and MultiQC (Ewels et al., 2016) tools were combined to do some quality checks on raw FASTQ files. These tools provide several analysing modules to give an idea to the users on whether the data has any problem for downstream analysis. For the combination of these two tools, "MultiQC" will be used hereafter.

The first module of MultiQC analysis gives the basic statistics for the samples including the length and total number of reads sequenced for each sample. According to the results, length of reads in all samples was 80 base pair (Figure 12a). Library sequencing depths were suitable for further analysis. While Ctrl-5 sample generated the lowest number of reads (48,975,486 reads), sample 14 dpl-2 generated the highest number of reads (144,965,329) (Figure 11).

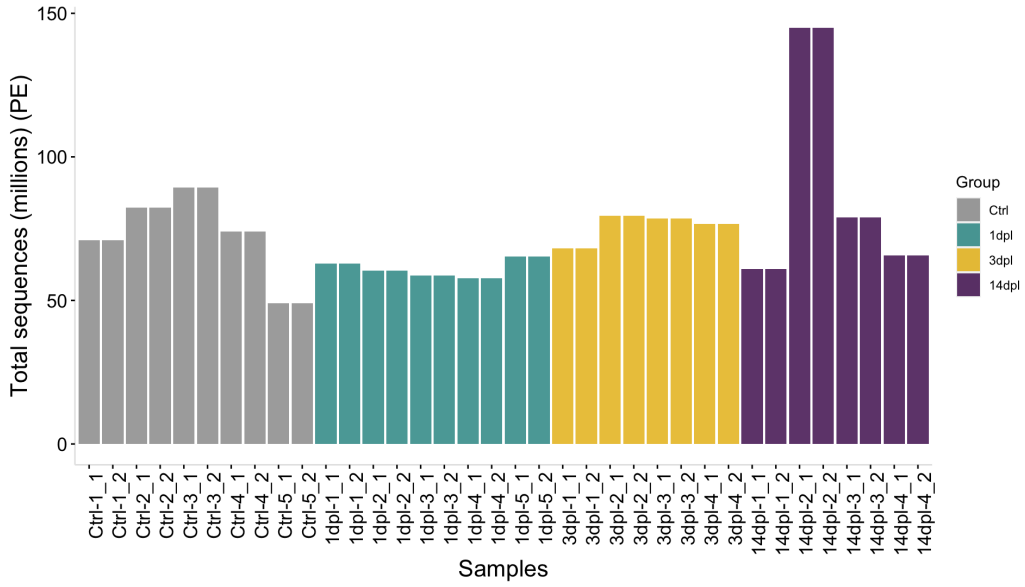

Figure 11. Total number of reads sequenced for each sample. Barplot showing total raw read numbers for each zebrafish brain sample plotted as million reads on the y-axis for the corresponding samples on the x-axis. While Ctrl-5 sample generated the lowest number of reads (48,975,486), sample 14 dpl-2 generated the highest number of reads (144,965,329). Control, grey; 1 dpl, turquoise; 3 dpl, dark yellow; 14 dpl, purple.

Next two modules of MultiQC tool are “Mean Quality Scores” and “Per Sequence Quality Scores” plots. “Mean Quality Scores” plot provides the mean quality value across each base position in the read (Figure 12a). This plot shows whether there were any problems during sequencing processes. Colour-coded lines of the plot on the y-axis represent high (green), medium (yellow) and low (red) quality scores (Phred score). The x-axis of the plot shows the position of the nucleotide on the read.

The “Per Sequence Quality Scores” plot determines the number of reads on the y-axis and average quality score on the x-axis. According to this plot, a majority of the reads should have a high average quality score. Colour-coded lines of this plot represents the Phred quality score as red (<20), yellow (20–28), and green (>28) (Figure 12b). A Phred score greater than 20 is acceptable for many purposes. According to these results, the Phred quality score for each of 18 samples (green lines) were distributed on the green area indicating sufficient quality (Figure 12a, 12b).

The other two modules of the MultiQC report are “Per Base N Content” and “Adapter Content” and can also help interpret the quality of the data. “Per Base N Content” plot shows the percentage of base calls at each position for which an N was called. If the sequencing device does not enable a base call with sufficient reliability, it will be represented by an N instead of an ordinary base. Normally, this module gives a warning message if any position shows an N content more than 5% and gives an error if any position shows an N content more than 20%. According to the results, because of the green lines showing less than 1% N content, each of the 18 samples passed this quality check (Figure 13a).

Another module showing the “Adapter Content” plot determines the cumulative percentages of libraries which has seen each of the adapter sequences at each position. This module rises a warning if any adapter sequence is present in more than 5% of all reads and gives a failure if any sequence is present in more than 10% of all reads. Results showed that all samples have less than 2% adapter sequences, which is an acceptable ratio for further analysis (Figure 13b).

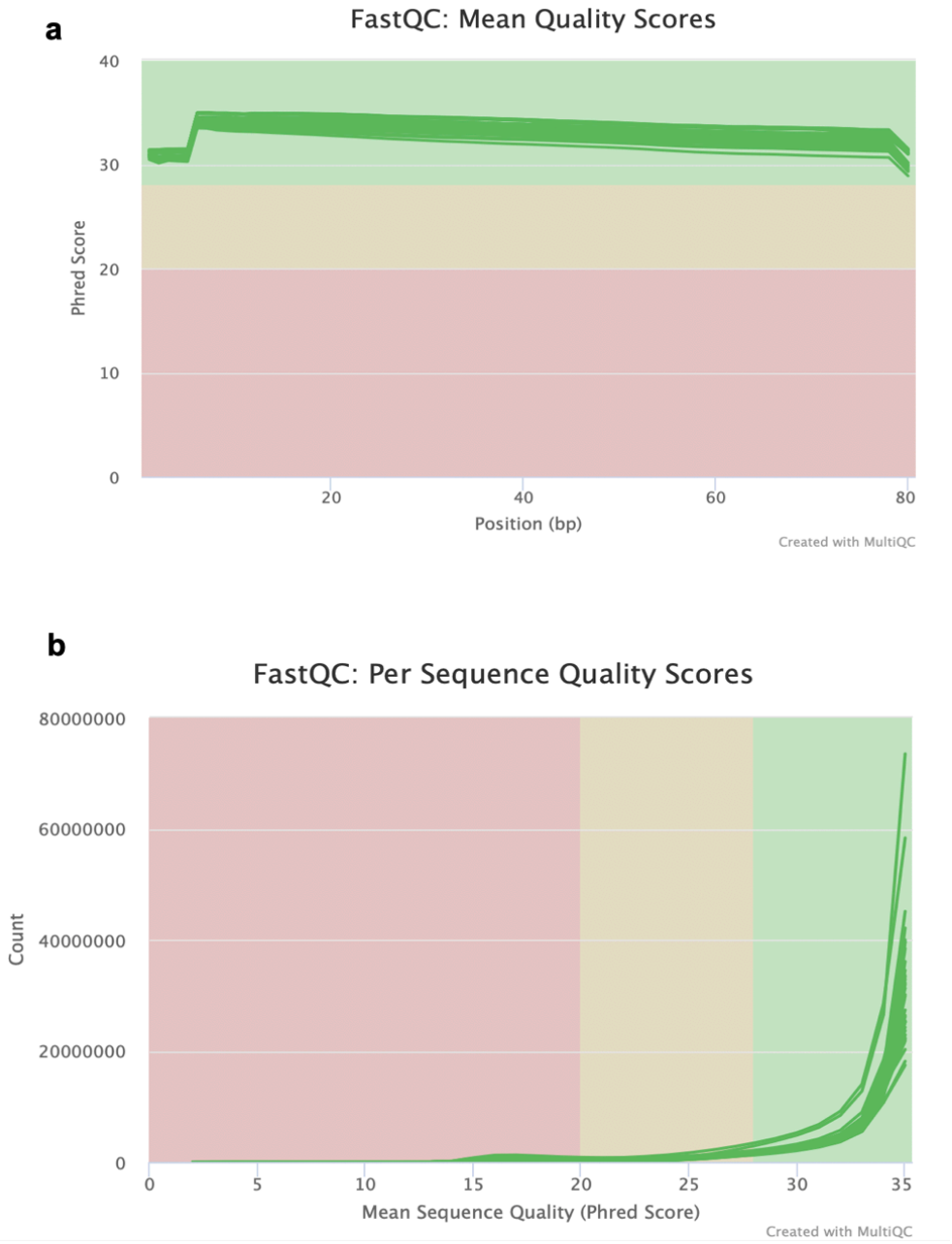

Figure 12. Results of the "Mean Quality Scores" and "Per Sequence Quality Scores" modules of MultiQC generated based on FastQC results. (a) (b) Plots show that all FASTQ sequencing files have an average per base and per sequence Phred score > 30, a threshold denoting high quality base calls. Read quality was plotted as a quality score (Phred score) on the y-axis and base position in the reads on the x-axis. Each green line represents a FASTQ file (i.e., a sample).

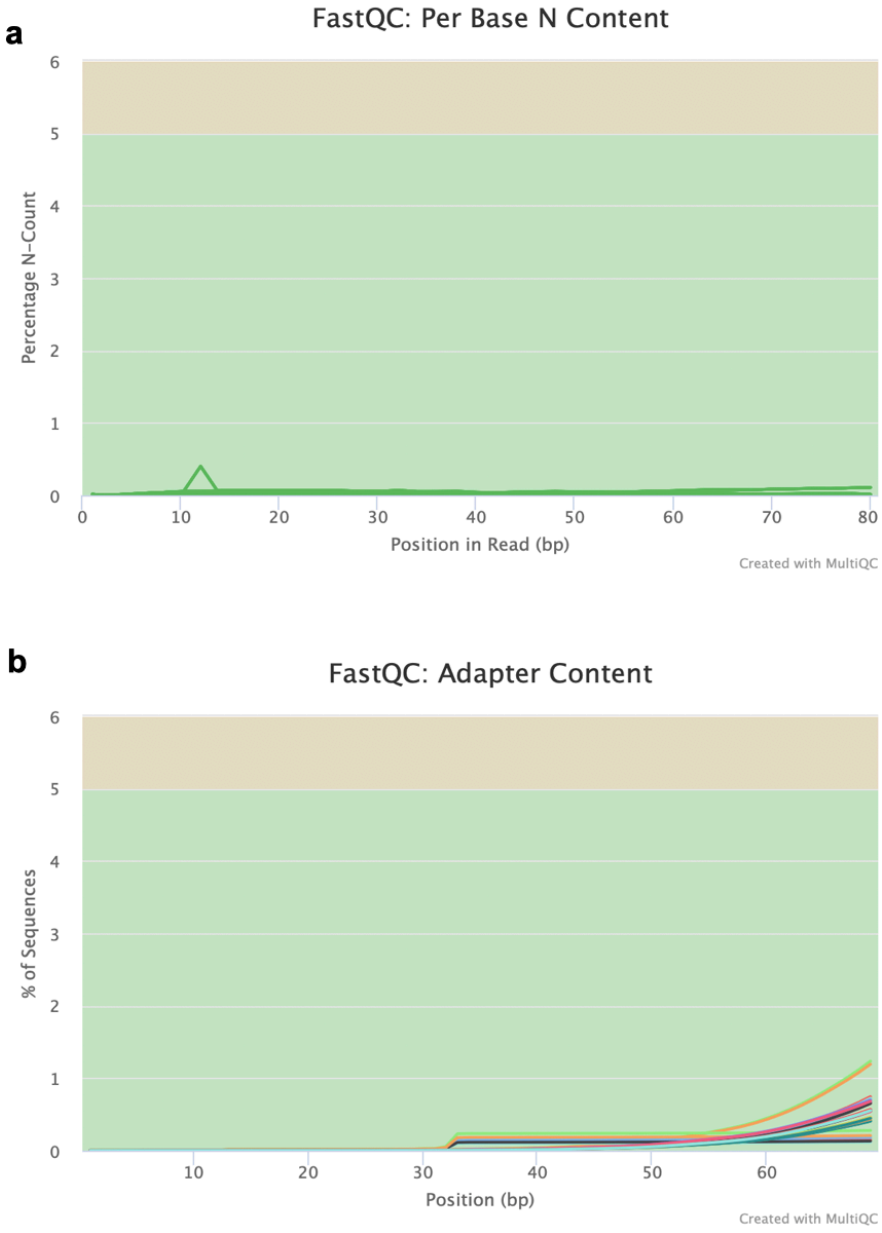

Figure 13. Results of the "Per Base N Content" and "Adapter Content" modules of MultiQC generated based on FastQC results. (a) Plot shows the percentage of counts that are not assigned to one of the conventional bases (A, T, C, G) at each position. N percentage was less than 1% across samples (in the green area). The x-axis shows position of base, the y-axis shows the percentage of N bases. **(b)** Adapter content plot determines percentage of the adapter in libraries. All samples have less than 2% adapter sequences which is an acceptable ratio for further analysis. The x-axis shows base position, the y-axis shows the percentage of adapter sequences in the sample.

Other two modules of the quality check tool were “Sequence Counts” and “Sequence Duplication Levels”. While “Sequence Counts” shows estimated duplicate read counts, “Sequence Duplication Levels” plot indicates the distribution of the duplication level across the libraries.

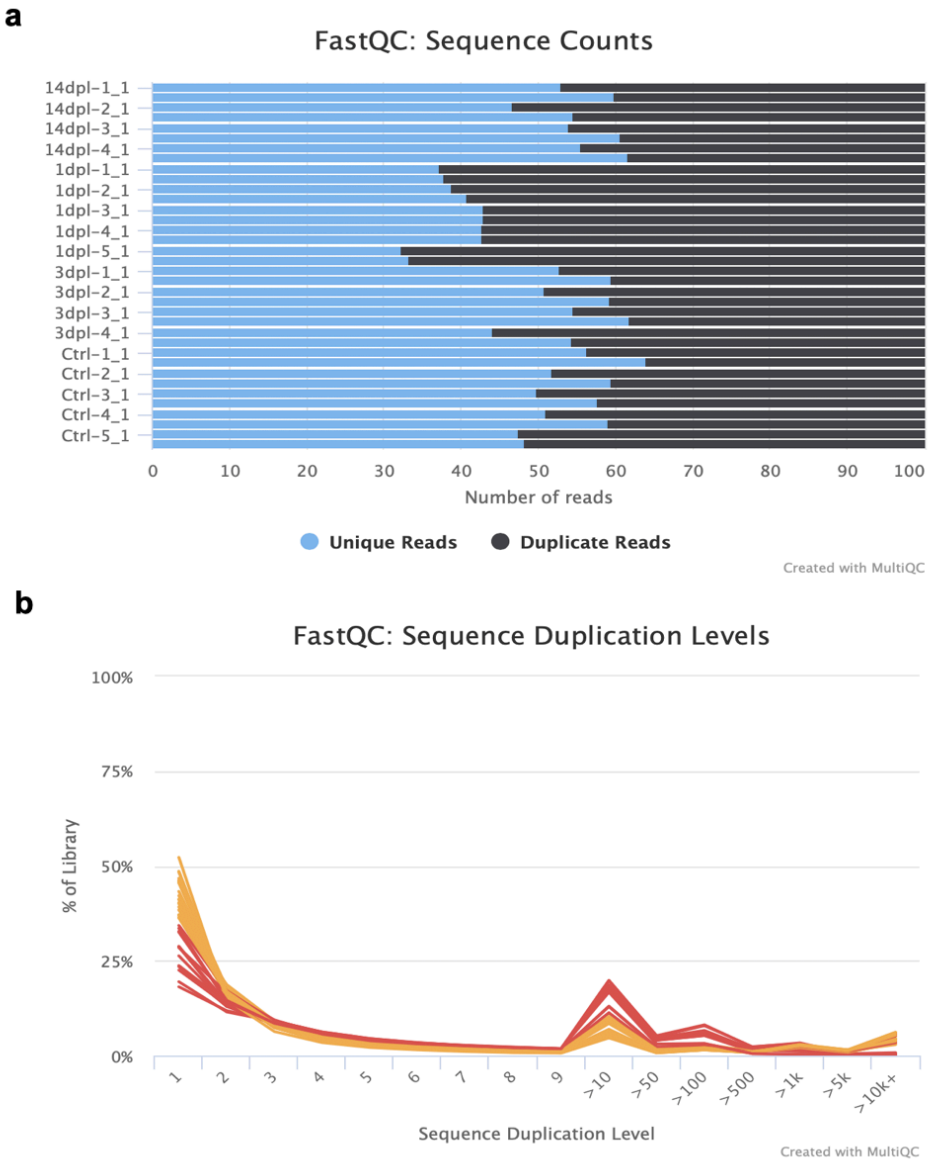

Figure 14. Results of the “Sequence Counts” and “Sequence Duplication Levels” modules of MultiQC tool generated based on the FastQC results. (a) The plot indicates the percentages of unique and duplicate reads in the libraries. The x-axis shows the number of reads as percentages, the y-axis shows the RNA-Seq libraries. **(b)** The plot determines the duplicated sequences as percentage of the library (x -axis) at different duplication levels (y-axis) across samples.

Since FastQC has been designed specifically to check quality of whole genome shotgun sequencing data, it expects that nearly 100% of the reads should be unique. For this reason, the "Sequence Counts" and "Sequence Duplication Levels" modules give a warning if the non-unique reads are more than 20% of the total sequences and give a failure if the non-unique reads are more than 50% of all sequences. In contrast to whole genome sequencing, RNA-Seq data includes, by nature, some highly and lowly abundant transcripts (*https://rtsf.natsci.msu.edu/genomics/tech-notes/fastqc-tutorial-and-faq/*, 2021; *https://www.bioinformatics.babraham.ac.uk/projects/astqc/*, 2021). This characteristic of RNA-Seq data can lead the natural duplication of highly abundant transcripts to be detected as a failure in these modules (highlighted by both FastQC and MultiQC).

According to the results of this study, percentages of duplicate reads were between 36.1% and 67.8% across the samples (Figure 14a). Sequence duplication levels plot also showed that between 18.13 and 52.27% of the duplicated sequences were at a duplication level of 1 (i.e., unique sequences), and about 4.65 – 19.84% of the total sequences were at the duplication level of 10 across samples. Some of the samples were tagged as failed (red lines) and some of the samples were tagged with warnings (orange lines) by the tool, although duplication is expected in RNA-Seq data (Figure 14b).

4.4. Quality check results of brain regeneration samples after mapping to the reference genome

One of the important steps of quality control during RNA-Seq analysis is to check the quality of the mapping process. In this study, HISAT2 aligner was used to align the reads to the reference genome and "PE alignment Scores" module of MultiQC was used to evaluate the results of the mapping in different ways across samples. One of the categories on this plot is "PE mapped uniquely" and it means that both mates are mapped to unique concordant loci. These are two loci on the same chromosome, on opposite strands, and within an expected distance from each other. According to the results, percentages of uniquely mapped reads were between 59.6% (Ctrl-1) and 78.8% (Ctrl-5). "PE mapped discordantly uniquely" shows that both mates are mapped to unique but discordant loci. These are two loci that are either on different chromosomes or on the same chromosome but on the same strand or further from each other than expected. Percentages of discordantly uniquely mapped reads were between 0.2% (1 dpl-4) and 2.8% (14 dpl-1) across the samples in this study. "PE one mate mapped uniquely"

explains that one mate is mapped to a unique locus while the other mate does not align to the genome. The percentages of reads involved in this group ranged between 6.2% (1 dpl-4) and 10.2% (Ctrl-1). “PE multi-mapped” shows that both mates are aligned to multiple concordant loci. While 1 dpl-2 was the sample having the lowest ratio with 1.8%, 3 dpl-4 was the one with the highest number of multi-mapped reads with 4.3%. If one mate is mapped to multiple loci and the other mate either is mapped to a unique discordant locus or multiple discordant loci, or does not align to the genome these reads are defined as “PE one mate multi-mapped”. Several samples including 1 dpl-1, 1 dpl-3, 1 dpl-4 and Ctrl-5 with 0.4% were in this category as lowest, 14 dpl-1, 3 dpl-4 and Ctrl-1 with 0.9% were in this category as highest. Last category of this module is “PE neither mate aligned”. In this category, neither mate is aligned to the genome. Percentages of uniquely mapped reads were between 11.9% (1 dpl-3, 1 dpl-4) and 23.9% (Ctrl-1) (Figure 15a). These statistics were also shown as number of reads for each sample (Figure 15b). Overall alignment rates of the samples were between 76.1% (1 dpl-3 and 1 dpl-4) and 88.1% (Ctrl-1), which are very satisfactory rates for downstream analysis (Figure 16).

In this study, HTSeq-count was used to determine how many reads are mapped to each gene. Another module of the MultiQC, “HTSeq: Count Assignments”, shows the quality of the quantification of the reads in different ways. Firstly, selected categories contain only the reads that are mapped to the genome and are visualized (Figure 17a), so that the proportion of assignment categories are shown as percentages of properly aligned reads only. Among these categories, “Assigned” (blue bar) shows the percentage of reads that are properly aligned to a locus with a unique gene and counted for further analyses such as differential expression. Results showed that percentages of assigned reads were between 34.6% (Ctrl-1) and 64.9% (1 dpl-1) (Figure 17a, 17b). “Ambiguous” (black bar) indicates the percentage of reads that are properly aligned to a locus where several genes overlap. While several samples such as Ctrl-1, Ctrl-2 had the lowest ambiguous reads with 0.4%, 1 dpl-2 had the highest ambiguous reads with 1.0%. Reads that are properly aligned to a locus where there is no gene annotation are categorized as “No feature” (orange bar). Percentages of these reads were between 21.1% (1 dpl-4) and 46.1% (14 dpl-3). “Too low aQual” (purple bar) indicates the reads are properly aligned to the genome but the quality of the mapping is too low. The reads having low mapping quality consisted of 13.3% (1 dpl-4) to 22.8% (Ctrl-1) of all reads that are mapped to the genome (Figure 17a). Other two categories of this module are “Alignment not unique” (green bar) and “Not aligned” (dark pink). “Alignment not unique” (green bar) determines the reads that are

mapped to several loci of the genome. The last category of this module, “Not aligned” (dark pink), represents the reads that are not aligned to the reference genome. All statistics are shown as raw numbers of reads for each sample (Figure 17b).

The mapping results were subjected to quality control to determine which region the reads correspond to on the genome, to ensure that the mapping process is done properly, and to show coverage. For this purpose, IGV tool (Thorvaldsdóttir et al., 2013) was used. Firstly, all mapped reads were visualized on the whole genome for each sample. Figure 18 shows the distribution of the reads across the entire zebrafish genome for 1 dpl, 3 dpl, 14 dpl and control samples. The tracks were shown in turquoise for 1 dpl (n=5), yellow for 3 dpl (n=4), purple for 14 dpl (n=4), and grey for normal samples (n=5). Sufficient read evidence was observed across the whole zebrafish genome. Secondly, *gfap* and *s100b* genes, two adult neurogenesis markers, were selected to show the quality of alignment at the gene level. The glial fibrillary acidic protein (*gfap*) gene is known to be expressed in brain tissue by astrocytes. Cells having astrocytic properties (GFAP-positive progenitors) can give rise to new neurons in adult neurogenesis (J. Zhang & Jiao, 2015). This gene has a length of 13,241 bp with 10 exons. It is located on the reverse strand of chromosome 3 between the coordinates 31,792,441-31,804,481 (Figure 19). The other selected gene was *s100b*, participating in cell cycle and differentiation. It is expressed by cells that are losing their neural stem cell properties and marks a mature stage (J. Zhang & Jiao, 2015). Its length is of 12,800 bp with 3 exons. It is located on the reverse strand of chromosome 22 between bases 13,846,130-13,857,729 (Figure 20).

IGV gene level results showed that, RNA-Seq read mapping to the reference genome (zebrafish, GRCz11) was performed properly for all 18 samples. It was obvious that the reads were mapped well to the 10 exons of the *gfap* gene, and 4 exons of the *s100b* gene as annotated in UCSC database (exons of genes were shown in red, bottom of the figures) (Figure 19, 20).

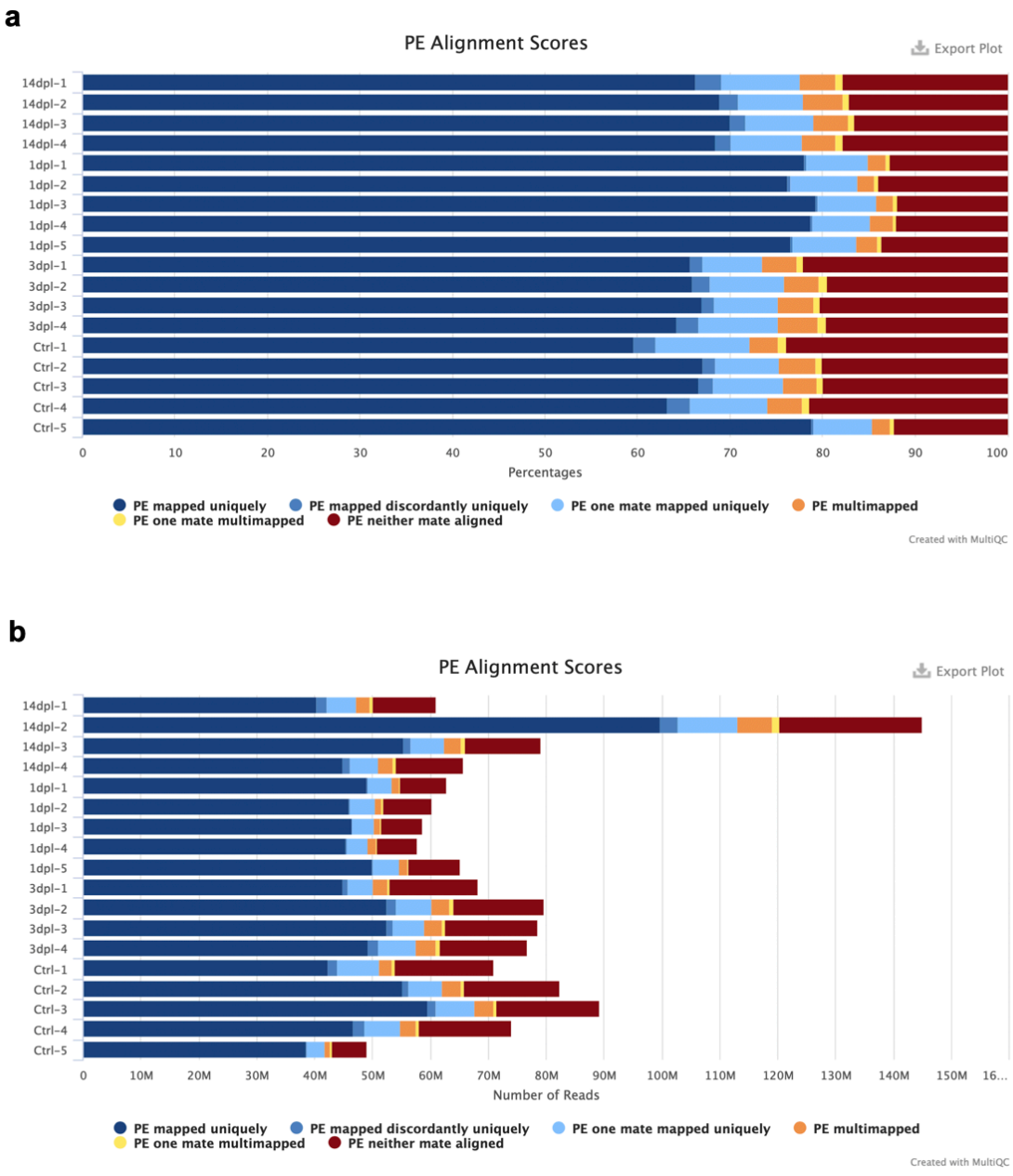

Figure 15. Results of the "PE Alignment Scores" module of MultiQC. Statistics of this module are shown as **(a)** percentages and **(b)** raw numbers of reads across the samples.

Sample Name	% Aligned
14dpl-1	82.3%
14dpl-2	83.0%
14dpl-3	83.5%
14dpl-4	82.2%
1dpl-1	87.3%
1dpl-2	86.1%
1dpl-3	88.1%
1dpl-4	88.1%
1dpl-5	86.5%
3dpl-1	77.9%
3dpl-2	80.5%
3dpl-3	79.7%
3dpl-4	80.4%
Ctrl-1	76.1%
Ctrl-2	80.0%
Ctrl-3	80.1%
Ctrl-4	78.6%
Ctrl-5	87.8%

Figure 16. Overall alignment rates of the samples to the zebrafish reference genome. Overall alignment rates of the samples were between 76.1% (Ctrl-1) and 88.1% (1 dpl-3 and 1 dpl-4) which are very satisfactory rates for downstream analysis.

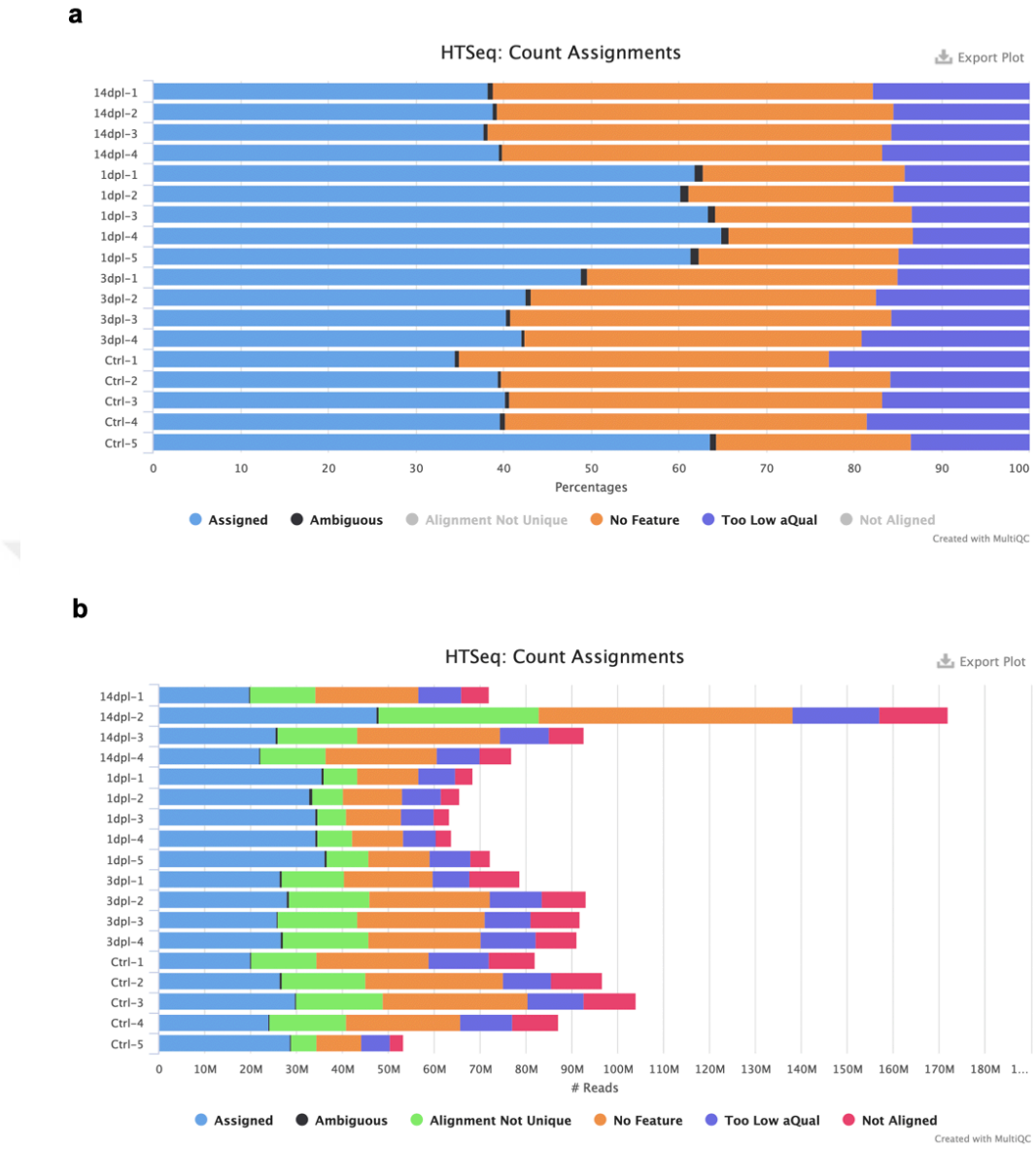

Figure 17. Results of the "HTSeq: Count Assignments" module of MultiQC. Statistics of the module were shown as **(a)** percentages and **(b)** raw numbers of reads across the samples.

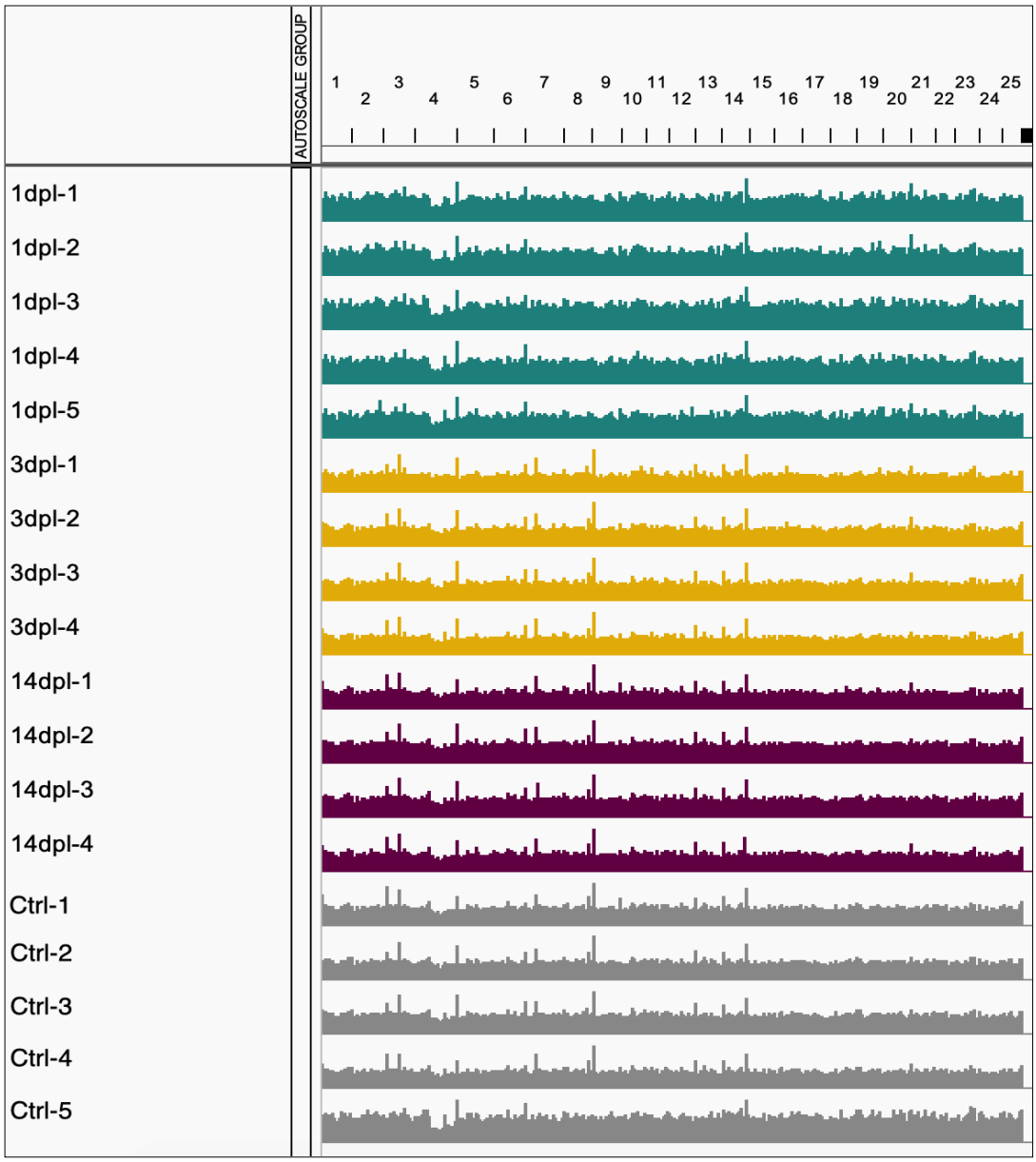

Figure 18. Visualization of alignments of RNA-Seq reads for 18 brain regeneration samples for whole genome by using Integrative Genomics Viewer (IGV). Figure shows the distribution of the reads across the entire zebrafish genome for 1 dpl, 3 dpl, 14 dpl and control samples. The tracks are shown in turquoise for 1 dpl (n=5), yellow for 3 dpl (n=4), purple for 14 dpl (n=4), and grey for control samples (n=5). The y-axis shows the number of reads overlapping each location of the genome.

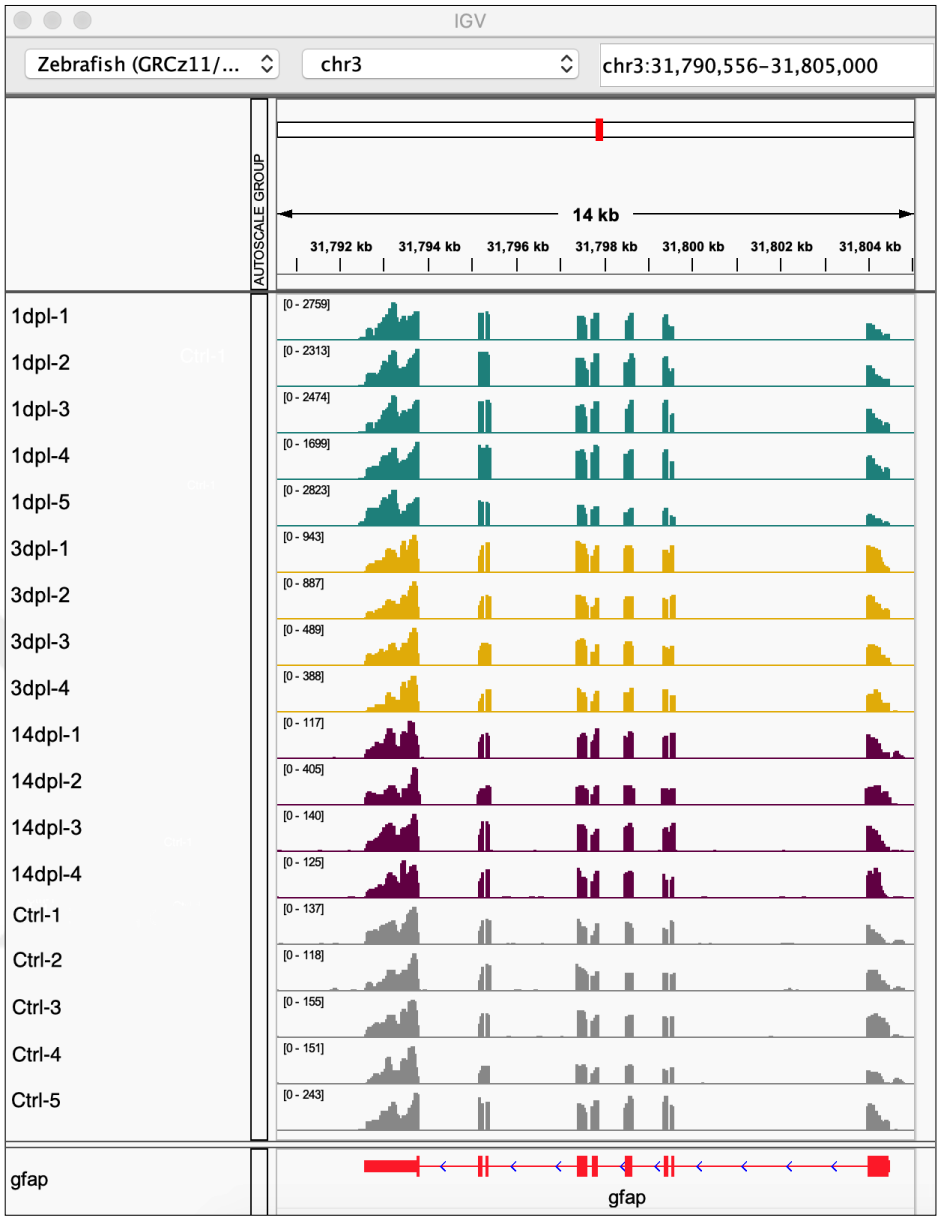

Figure 19. Visualization of alignment and coverage of RNA-Seq reads for 18 brain regeneration samples for *gfap* gene by using Integrative Genomics Viewer (IGV). Figure shows the distribution of reads for the gene *gfap* in 1 dpl, 3 dpl, 14 dpl and control samples. The tracks are shown in turquoise for 1 dpl (n=5), yellow for 3 dpl (n=4), purple for 14 dpl (n=4), and grey for control samples (n=5). The y-axis shows the number of reads overlapping each location of the locus of gene *gfap*.

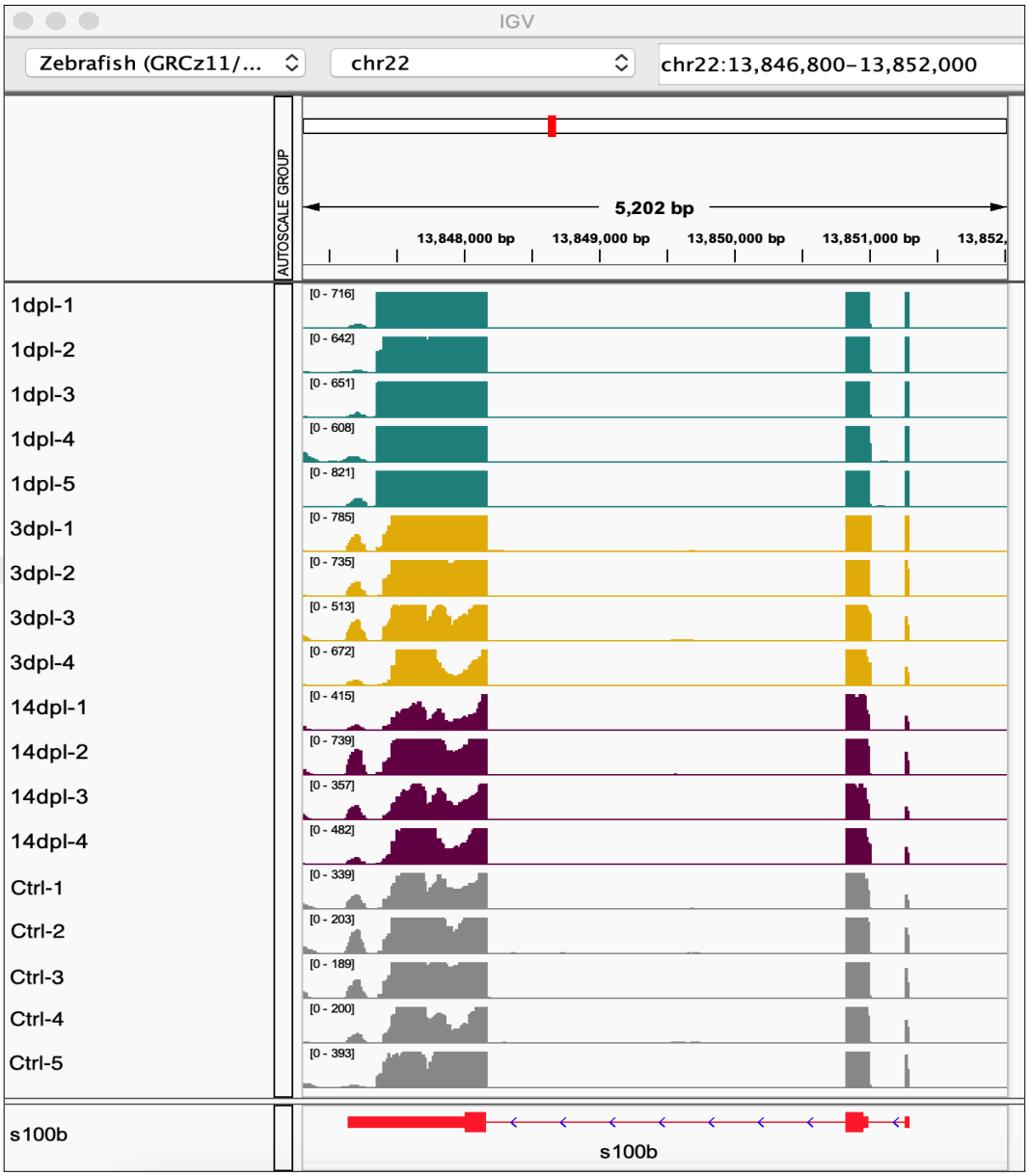

Figure 20. Visualization of alignments and coverage of RNA-Seq reads for 18 brain regeneration samples for *s100b* gene by using Integrative Genomics Viewer (IGV). Figure shows the distribution of the reads for gene *s100b* in 1 dpl, 3 dpl, 14 dpl and control samples. The tracks were shown in turquoise for 1 dpl (n=5), yellow for 3 dpl (n=4), purple for 14 dpl (n=4), and grey for control samples (n=5). The y-axis shows the number of reads overlapping each location of the locus of gene *s100b*.

4.5. Batch effect correction of brain regeneration samples

Sample-to-sample distance analysis and PCA are used to show similarities and dissimilarities between samples and groups. These analyses also show if there is any batch effect. In this study, since samples were prepared and sent for sequencing two different times, we checked if there is any variance among samples caused by this potential source of batch effect. Both genes and samples were hierarchically clustered before and after batch effect correction as shown by the dendrograms of the heatmap for sample-to-sample distance analyses (Figure 21a, 21b). According to the results, uncorrected data showed a clear difference between the batches of the control samples leading to misclustering (Figure 21a). Then, correction was done based on the control group involving in both batches. After batch correction, samples were clustered well by replicates and time points as 1 dpl, 3 dpl, 14 dpl, and Control (Figure 21b).

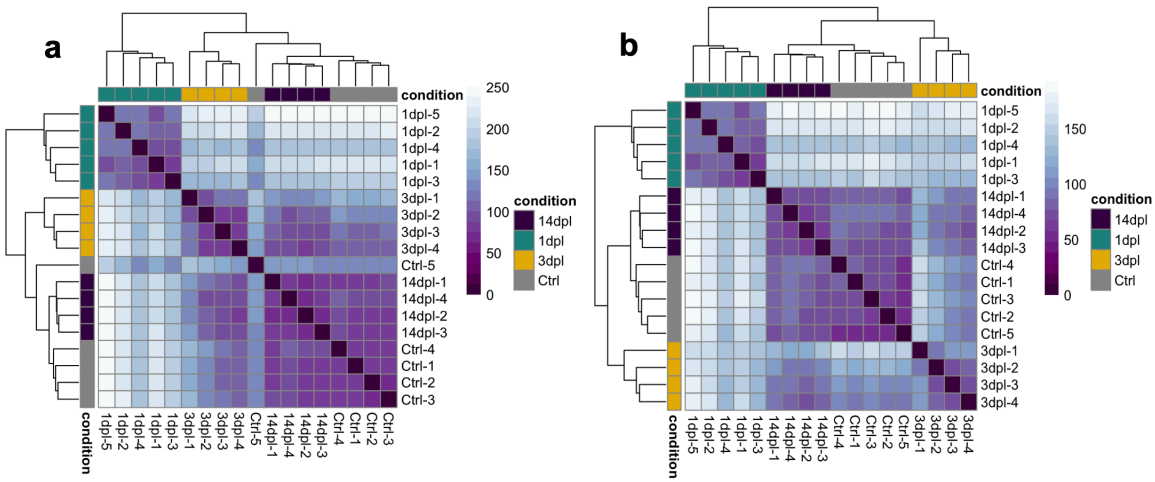

Figure 21. Heatmap of sample-to-sample distances between expression patterns of three stages of zebrafish brain regeneration and control brain samples. Heatmaps generated by using normalized count and normalized batch effect-corrected count matrices for overall gene expression generated by the DESeq2 package. **(a)** Showing uncorrected data, there was a clear difference between the batches of the control samples leading tomisclustering. **(b)** After batch effect correction, samples were clustered accordingly with time points as 1 dpl, 3 dpl, 14 dpl, and Control.

Another way to show variance between samples is to perform Principal Component Analysis (PCA). Principal components (PCs) were calculated for both uncorrected and

corrected normalized, variance-stabilized data and visualized by using *ggplot2*. PCA plots of RNA-Seq data indicated the characteristics of samples according to gene expression. According to the PCA plot of the uncorrected data, since one of the control samples (red dashed circle, Ctrl-5) was sent for sequencing in a second batch, two different batches can easily be recognized. While other four control samples (from batch 1, in blue dashed circle) clustered together, one of the control samples (from batch 2) clustered far from others. The total variance between samples was 73% [PC1 (x-axis) 60%, PC2 (y-axis) 13%] before correction (Figure 22a). Then, correction was done based on the samples of the control group, the only group having samples in both batches, and results visualized on a PCA plot. After correction, samples of the control group clustered together (green dashed circle) (Figure 22b). Principal Component 1 (PC1, x-axis) represents 53% and PC2 (y-axis) represents 17% of the total variance in the data. According to both PCA plots, samples clustered primarily based on their stages and 14 dpl samples were close to control samples than samples of the 1 dpl and 3 dpl. There was a clear separation of four groups of samples according to PC1 and PC2 for both uncorrected and corrected data (Figure 22a, 22b).

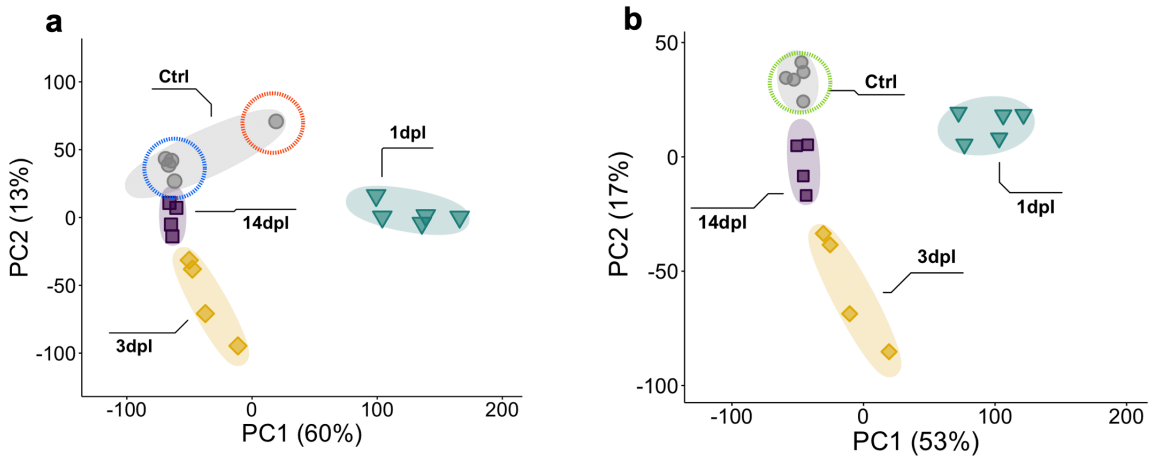

Figure 22. Principal component analysis (PCA) of expression patterns for three stages of zebrafish brain regeneration and control brain samples. Plots generated by using normalized count and normalized batch effect-corrected count matrices for overall gene expression generated by the DESeq2 package. **(a)** Showing uncorrected data, there was a clear difference between the batches of the control samples. **(b)** After batch correction, four sample groups separated well according to replicates and time points as 1 dpl, 3 dpl, 14 dpl, and Control. Different colours of dots represent the four groups of samples.

4.6. Transcriptome profiling of adult zebrafish brain regeneration

4.6.1. Differential gene expression and functional gene annotation analyses of early wound healing stage (1 dpl) of brain regeneration

In order to determine the changes in gene expression controlling early wound healing stage of brain regeneration, lesioned hemispheres at 1 dpl were compared with the equivalent hemispheres of the unlesioned brains. It was found that 6123 genes [3330 upregulated (Up) and 2793 downregulated (Down)] were significantly differentially expressed in response to injury (Figure 23a). While 5917 of those genes were protein coding, 105 of those were long intergenic non-coding RNA (lincRNAs) genes (Figure 23b). 3983 (1642 Up and 2341 Down) of DEGs were unique to this stage (Figure 32). Among these unique genes, there were several neurogenesis and neuron differentiation related genes such as *neurod2, olig1, notch3, amigo1*. Twelve semaphorin genes, a family of secreted membrane proteins involved in axonal growth and neurogenesis, were also significantly downregulated. 9 of those, playing role in neurogenesis, were unique to 1 dpl (*sema5a, sema6e, sema3h, sema5ba, sema4gb, sema4ba, sema5bb, sema6ba, sema4ga*). Several adult neurogenesis genes were also tested as differentially expressed. While *pcna, mcm2, gfap, nes, and s100b* were upregulated, *ncam3, neurod2* and *foxo3a* were downregulated.

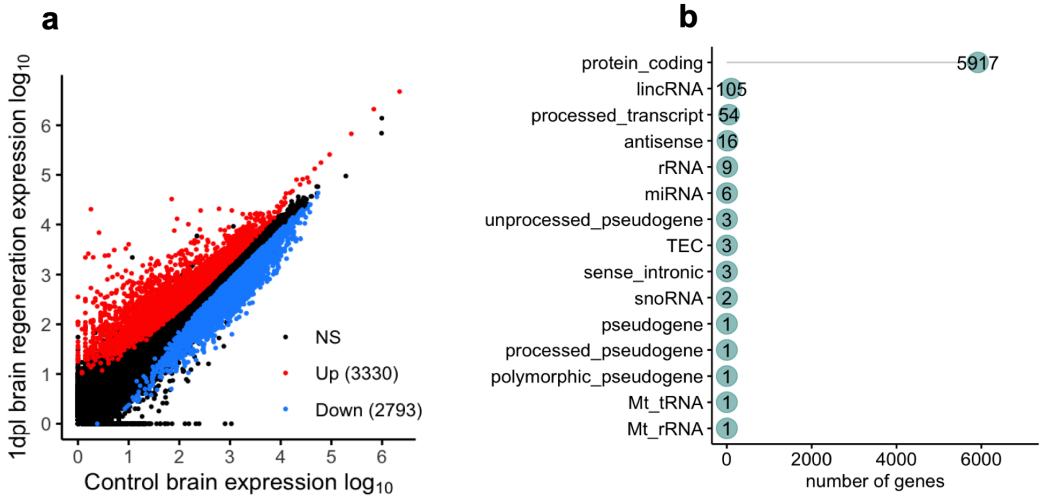

Figure 23. Transcriptome profiling of early wound healing stage (1 dpl) of zebrafish brain regeneration. (a) Scatterplot showing the number of activated (red) and reduced (blue) genes in 1 dpl brain regeneration (n=5) compared to unlesioned brain (n=5). **(b)** Dotplot shows subsets of gene biotypes and the number of the DEGs in each subset. NS, not significant.

GO term enrichment was performed based on Up and Down genes separately. Upregulated DEGs were enriched mainly in translation, ribosome-related GO terms, RNA processing, hemopoiesis, immune system development and DNA replication terms in group BP (Figure 24a). Downregulated genes were enriched in signal transduction-related terms, regulation of GTPase activity, neuron development and differentiation, neurogenesis, synaptic signaling, cell morphogenesis, axon development and axon guidance terms in BP category (Figure 24b). The top 50 GO-BP terms of up- and downregulated genes showed no overlap. The 5 most significantly enriched CC and MF categories were also shown (Figure 24a, 24b). Top 50 significantly enriched GO-BP terms and KEGG pathways in 1 dpl were also shown using all DEGs (Figure 29, Figure 30).

4.6.2. Differential gene expression and functional gene annotation analyses of early proliferative stage (3 dpl) of brain regeneration

In order to show the alterations in gene expression controlling early proliferative stage of brain regeneration, lesioned hemispheres at 3 dpl were compared with the equivalent hemispheres of the unlesioned brains. It was found that 4662 genes [3678 upregulated (Up) and 984 downregulated (Down)] were tested as differentially expressed (Figure 25a). While 4408 of those genes were protein coding, 117 of those were lincRNAs (Figure 25b). 1796 (1398 Up and 398 Down) of DEGs were unique to early proliferative stage (Figure 32). The genes involved in regulation of apoptosis, such as *bsl2a, nradd, tgfb2, cd40 casp8I2, traf2b, traf6, and bmp10*, were upregulated at this stage uniquely. Immune response, immune system process and chemotaxis-related genes, including *cxcl20, cxcl11.5, cxcl11.6, cxcl11.1, cxcl32b.1, cxcr3.1, ccl39.2, ccl19a.2, ccl39.1, ccl35.2, ccl19a.1, ccl36.1, ccl44, ccl38.1, stat1a, il6, tnfsf13, tnfsf10l4, tnfsf10,* and *cd27*, are one of the prominent gene groups significantly upregulated at this stage only. Several adult neurogenesis genes, such as *pcna, mki67, mcm2, gfap, fabp7a, neurod4, nes, rest, vim, s100b, olig4, gli2a, gli2b*, were also positively regulated genes.

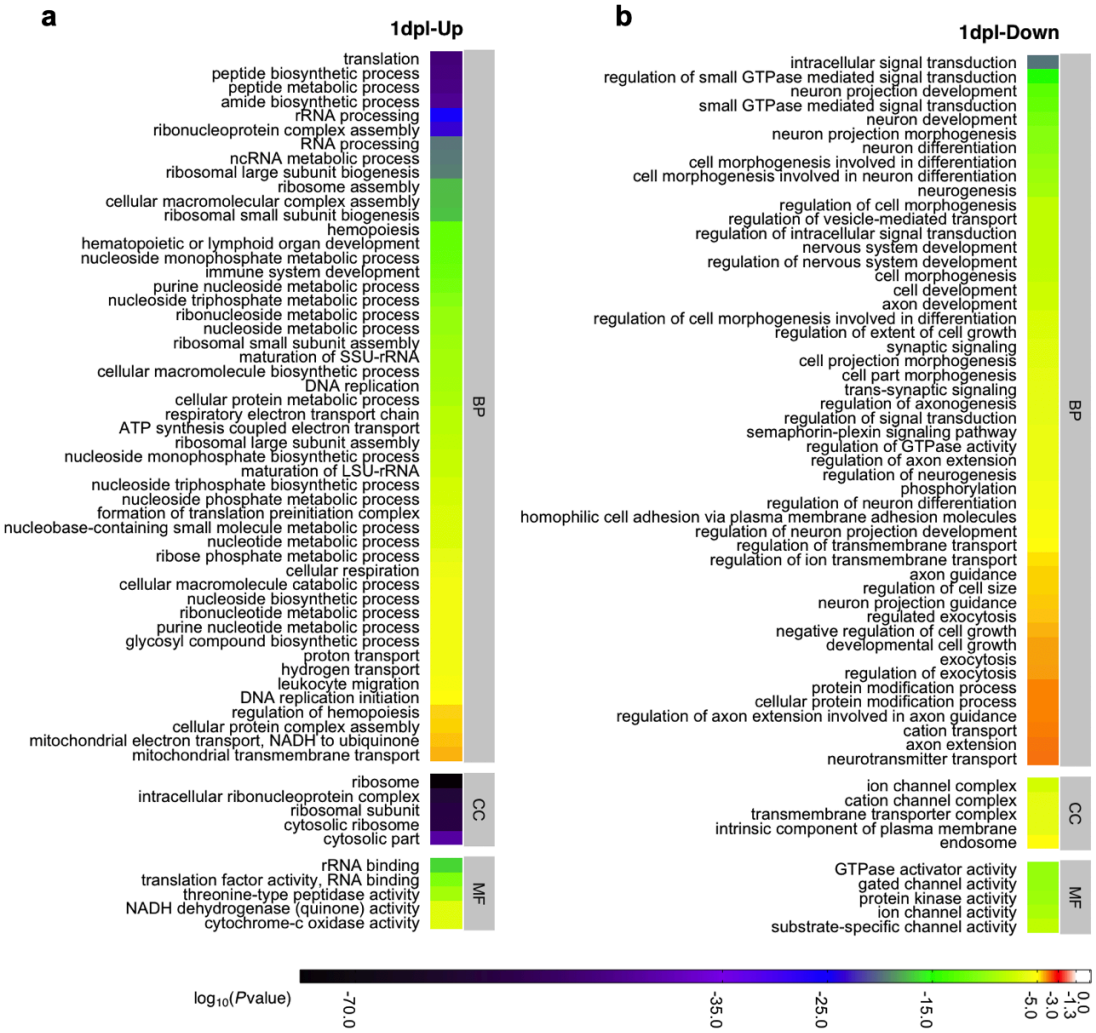

Figure 24. GO terms enriched at early wound healing stage (1 dpl) of brain regeneration by using up- and downregulated genes separately. DAVID bioinformatics tool was used to show the most significantly enriched GO terms based on the transcriptional changes at 1 dpl of brain regeneration. GO terms related with **(a)** Up (n=3330) and **(b)** Down (n=2793) regulated genes. The heatmap scale shows $\log_{10}$ of the EASE p-value for the most significantly enriched GO terms. DAVID: Database for Annotation, Visualization and Integrated Discovery, GO: Gene Ontology, BP: Biological Process, CC: Cellular Component, MF: Molecular Function.

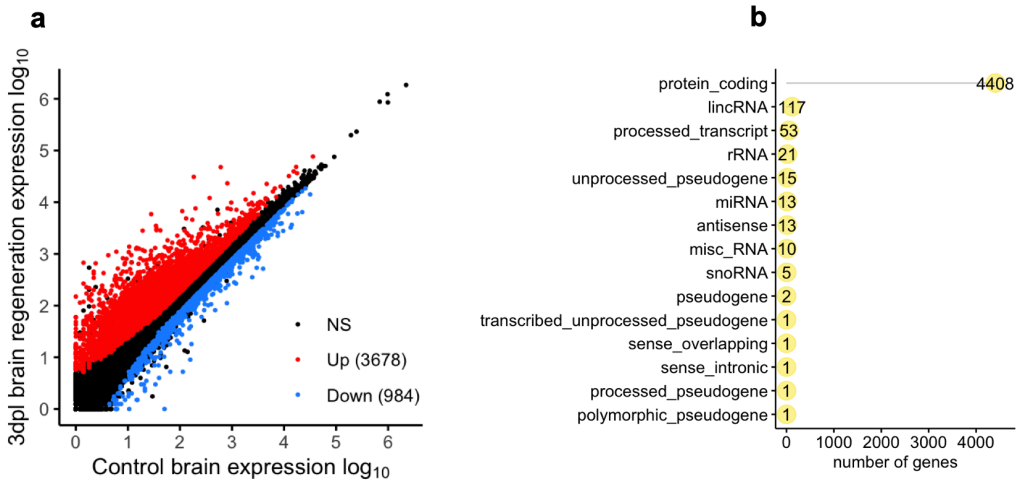

Figure 25. Transcriptome profiling of early proliferative stage (3 dpl) of zebrafish brain regeneration. (a) Scatterplot showing the number of activated (red) and reduced (blue) genes in 3 dpl brain regeneration (n=4) compared to unlesioned brain (n=5). **(b)** Dotplot shows subsets of gene biotypes and the number of the DEGs in each subset. NS, not significant.

GO term enrichment was done using Up and Down genes separately for early proliferative stage of brain regeneration. Upregulated DEGs were enriched mainly in DNA replication and cell cycle, hemopoiesis, immune system development, cell migration, leukocyte migration, chemotaxis-associated terms, leukocyte differentiation, apoptotic signaling pathway, tissue regeneration, cell death, integrin-mediated signaling pathway, and vasculature development in group BP (Figure 26a). Downregulated genes were enriched in synaptic signaling, transport, signal transduction, cellular homeostasis, neuron projection development, and negative regulation of STAT cascade terms in BP category (Figure 26b). The top 50 GO-BP terms of up- and downregulated genes showed no overlap. The 5 most significantly enriched CC and MF categories were also displayed (Figure 26a, 26b). Top 50 significantly enriched GO-BP terms and KEGG pathways were also shown using all DEGs in this stage (Figure 29, Figure 30).

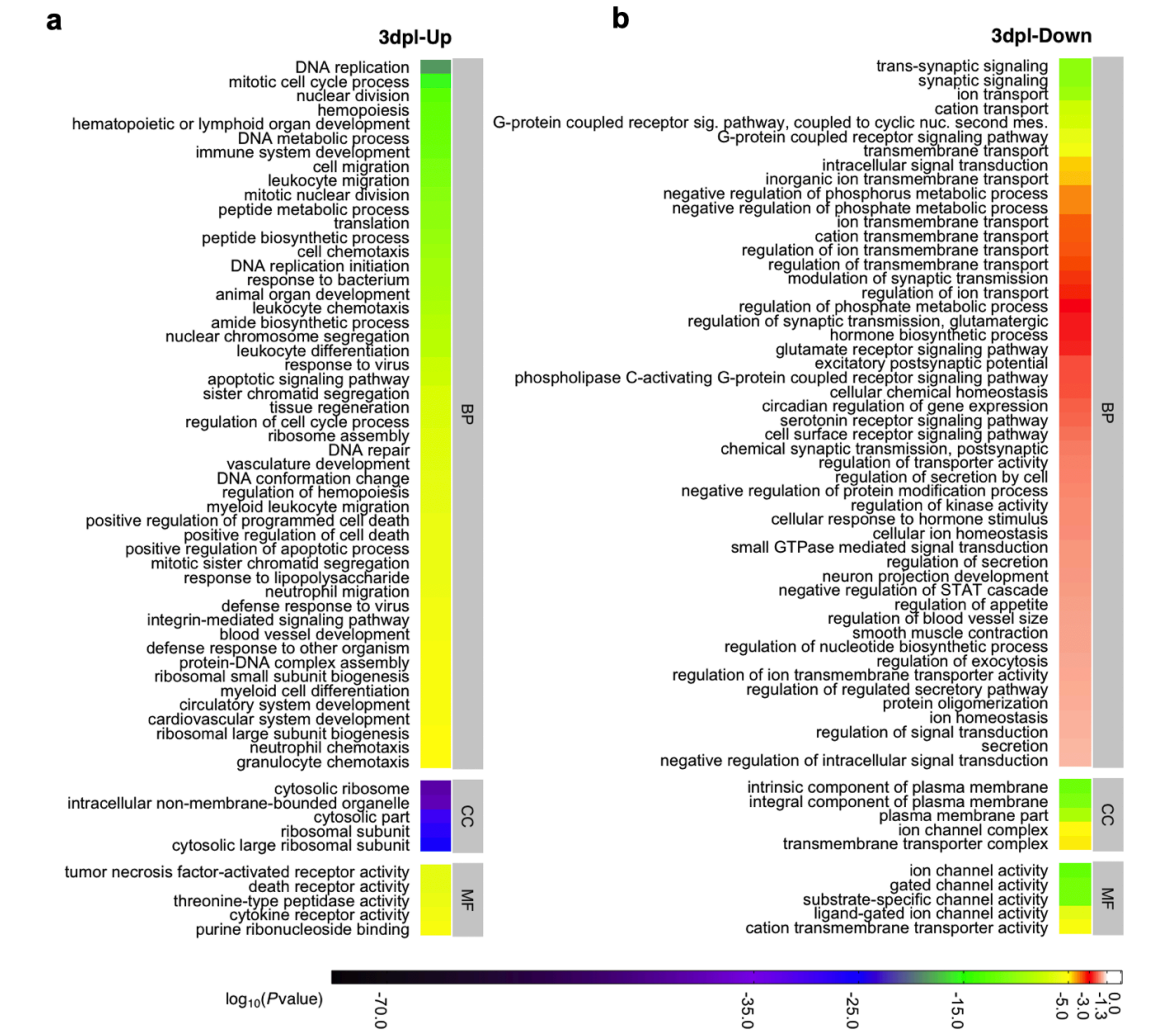

Figure 26. GO terms enriched at early proliferative stage (3 dpl) of brain regeneration by using up- and downregulated genes separately. DAVID bioinformatics tool was used to show the most significantly enriched GO terms based on the transcriptional changes in 3 dpl of brain regeneration. GO terms related with **(a)** Up (n=3678) and **(b)** Down (n=984) regulated genes. The heatmap scale shows $\log_{10}$ of the EASE p-value for the most significantly enriched GO terms. DAVID: Database for Annotation, Visualization and Integrated Discovery, GO: Gene Ontology, BP: Biological Process, CC: Cellular Component, MF: Molecular Function.

4.6.3. Differential gene expression and functional gene annotation analyses of differentiation stage (14 dpl) of brain regeneration

Lesioned hemispheres at 14 dpl were compared with the equivalent hemispheres of the unlesioned brains to determine the changes in gene expression controlling differentiation stage of the brain regeneration. The expression of 1954 genes [1330 upregulated (Up) and 624 downregulated (Down)] significantly changed at this stage (Figure 27a). Whereas 1848 of those genes were protein coding, 39 of those were lincRNAs (Figure 27b). 373 DEGs (208 Up and 165 Down) were unique to differentiation stage (Figure 32). There were several neuron differentiation genes, such as *gli1, sox11b, otpb, fzd1, fzd4*, among these uniquely altered genes. Expression of the *foxd3* gene, a cell differentiation and neural crest marker, also significantly increased. Another gene showing uniquely increased expression pattern was *her4.2* gene, having a role in neurogenesis and peripheral nervous system neuron axonogenesis. Several angiogenesis-related genes were also detected not uniquely but significantly in 14 dpl, such as *angpt1, angpt4, phkg1a, pdgfrb, fli1b, dab2, pappa2, kif11* and *ism1.* Another group of DEGs in this stage was the Notch signaling related genes. Notch signaling is involved in central nervous system development, regulation of NSC proliferation, survival and differentiation (Lathia et al., 2008). Some of these genes were *notch1a, notch1b, notch2, notchl, her15.1, dla, dlb, dlc, dld, jag1a,* and *jag1b.*

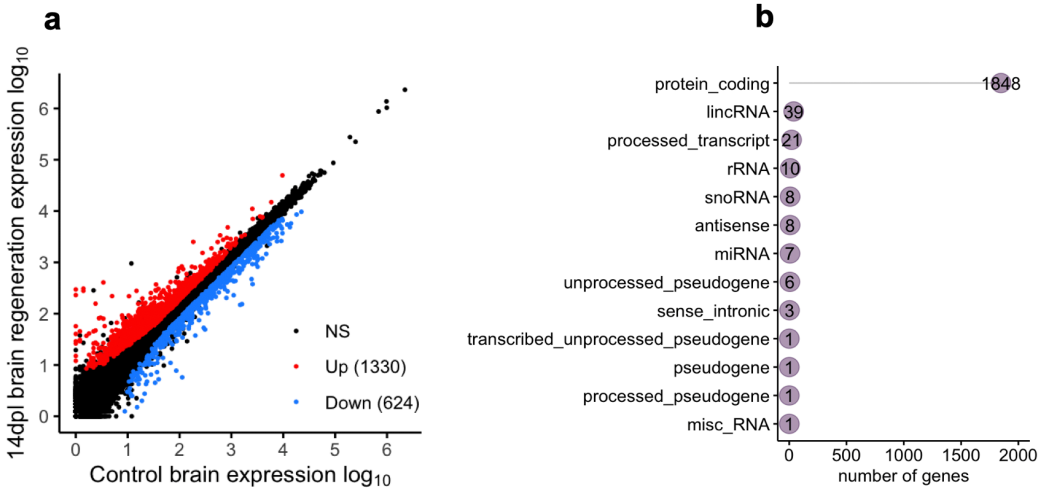

Figure 27. Transcriptome profiling of differentiation stage (14 dpl) of zebrafish brain regeneration. (a) Scatterplot showing the number of activated (red) and reduced (blue) genes in 14 dpl brain regeneration (n=4) compared to unlesioned brain (n=5). **(b)** Dotplot shows subsets of gene biotypes and the number of the DEGs in each subset. NS, not significant.

GO term enrichment was performed using Up and Down genes separately for differentiation stage of brain regeneration. Upregulated DEGs were enriched mainly in animal organ development, organ morphogenesis, cell migration, neurogenesis, tissue regeneration, nervous system development, Notch signaling pathway, immune system development, cell morphogenesis, hemopoiesis, circulatory system, vasculature development, and fin regeneration in group BP (Figure 28a). Downregulated genes were enriched in steroid biosynthetic process-related terms, circadian regulation of gene expression, signal transduction, regulation of MAPK cascade, and synaptic signaling terms in BP category (Figure 28b). The 5 most significantly enriched CC and MF categories were also shown for this stage (Figure 28a, 28b). Top 50 significantly enriched GO-BP terms and KEGG pathways were also shown using all DEGs (Figure 29, Figure 30).

4.7. Functional gene annotation analyses of zebrafish brain regeneration at all stages by using all DEGs

GO term analyses were also carried out based on all DEGs of the three stages and visualised selecting 50 most significant GO-BP terms. According to the results, translation, hemopoiesis related terms, DNA replication, hematopoietic or lymphoid organ development, and immune system development GO-BP terms were shared in both early wound healing and early proliferative stages (Figure 29a, 29b). However, cell cycle and division, leukocyte migration, cell migration, cell chemotaxis, leukocyte differentiation, apoptotic signaling pathway-related terms, MAPK cascade, cell death-associated terms, and integrin-mediated signaling pathway terms were prominently and uniquely observed at early proliferative stage (Figure 29b). Although, tissue regeneration, ameboidal-type cell migration, animal organ development, and vasculature development terms were some of the common terms in both early proliferative and differentiation stages (Figure 29b, 29c). Several organ development-related terms, organ morphogenesis, regulation of gene expression, regionalization, neurogenesis, Wnt signaling pathway, Notch signaling pathway, and glial cell development terms enriched among the 50 most significant GO-BP terms at differentiation stage of the adult zebrafish brain regeneration (Figure 29c).

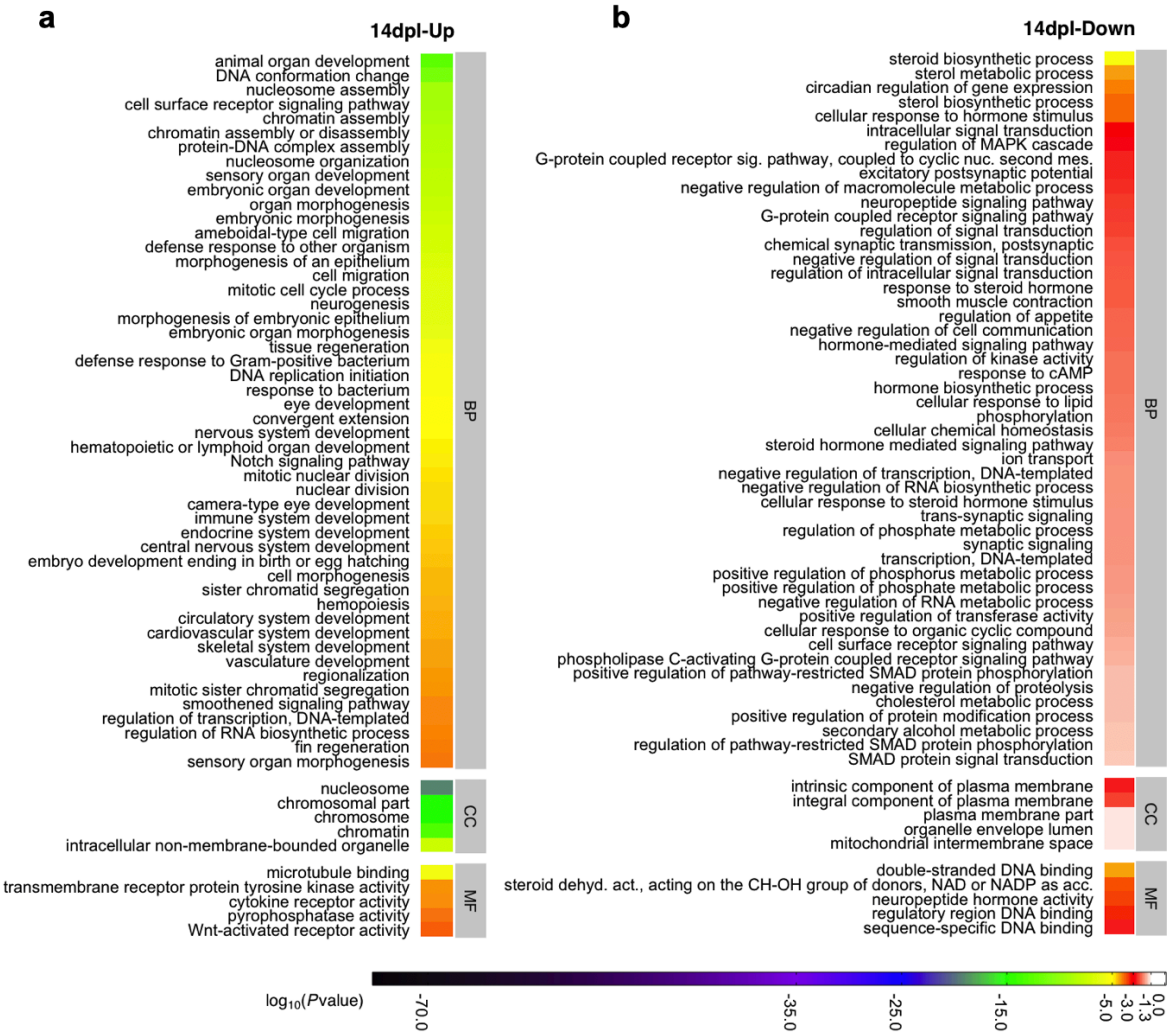

Figure 28. GO terms enriched at differentiation stage (14 dpl) of brain regeneration by using up- and downregulated genes separately. DAVID bioinformatics tool was used to show the most significantly enriched GO terms based on the transcriptional changes in 14 dpl of brain regeneration. GO terms related with **(a)** Up (n=1330) and **(b)** Down (n=624) regulated genes. The heatmap scale shows $\log_{10}$ of the EASE p-value for the most significantly enriched GO terms. DAVID: Database for Annotation, Visualization and Integrated Discovery, GO: Gene Ontology, BP: Biological Process, CC: Cellular Component, MF: Molecular Function.

KEGG pathway analyses were done and visualised based on all DEGs of the three stages. According to the results, ribosome, DNA replication, proteosome, apoptosis-related pathways enriched in both early stages. Some of the pathways shared between early proliferative and differentiation were Notch signaling pathway, ECM-receptor interaction, cell cycle, cytokine-

cytokine receptor interaction, toll-like receptor signaling pathway, herpes simplex infection, and focal adhesion. No common pathway between early wound healing and differentiation stage was detected. While MTOR signaling pathway and MAPK signaling pathway were observed only in early wound healing stage of brain regeneration, Wnt signaling pathway was detected only in differentiation stage. Jak-STAT signaling and phagosome-related pathways were some of the unique pathways for early proliferative stage. Salmonella infection and p53 signaling pathway were enriched at all stages (Figure 30).

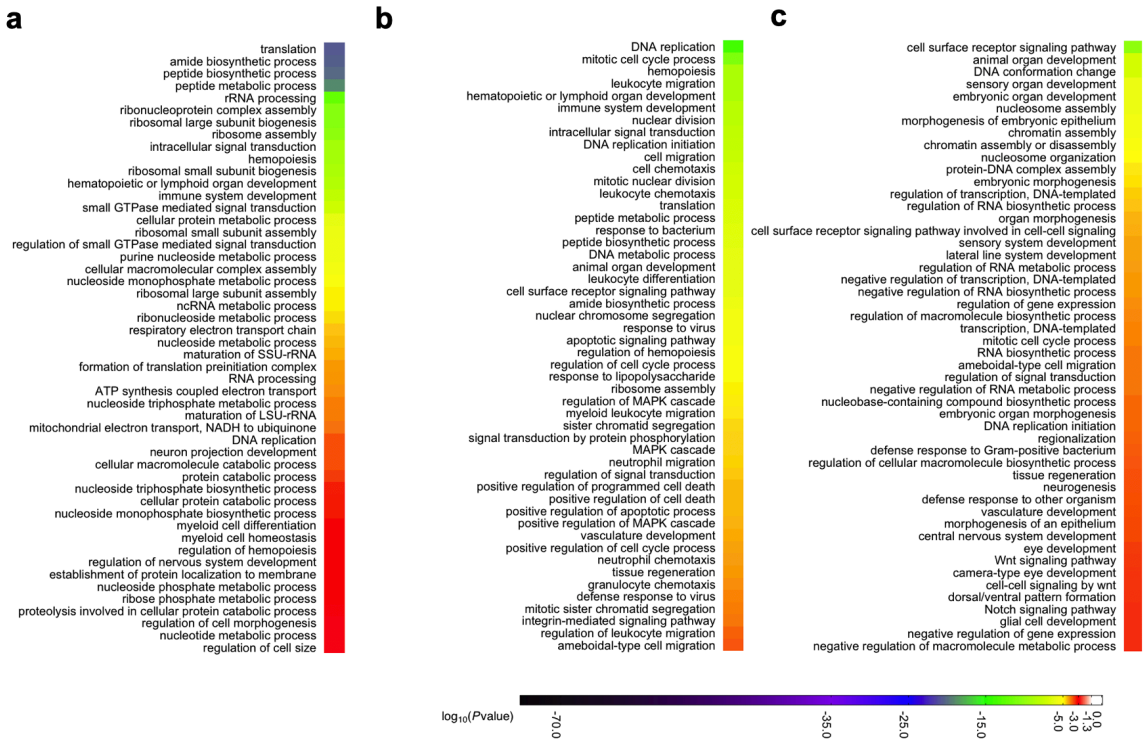

Figure 29. GO-BP terms enriched at three different stages of zebrafish brain regeneration by using all DEGs. DAVID bioinformatics tool was used to show the most significantly enriched GO-BP terms based on the transcriptional changes at **(a)** 1 dpl, **(b)** 3 dpl and **(c)** 14 dpl. All DEGs (1 dpl: 6123, 3 dpl: 4662, 14 dpl: 1954) were used for the analysis. The heatmap scale shows $\log_{10}$ of the EASE p-value for the most significantly enriched GO terms. DAVID: Database for Annotation, Visualization and Integrated Discovery, GO: Gene Ontology, BP: Biological Process.

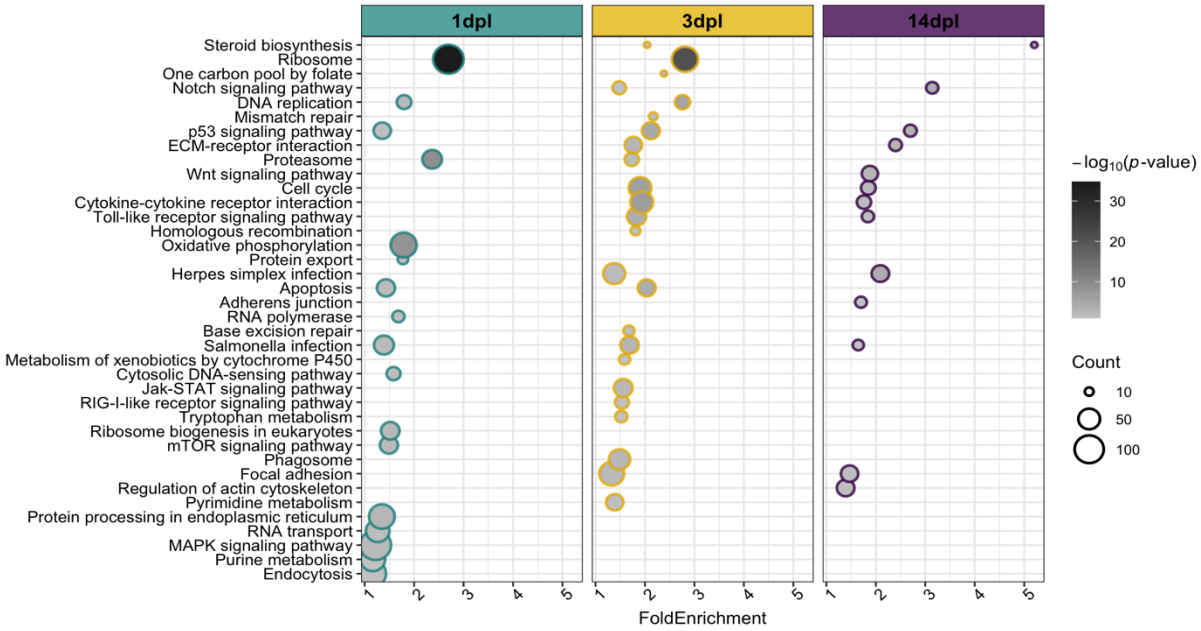

Figure 30. KEGG pathways enriched at three different stages of zebrafish brain regeneration by using all DEGs. DAVID bioinformatics tool was used to show the most significantly enriched KEGG pathways based on the transcriptional changes at **(a)** 1 dpl, **(b)** 3 dpl and **(c)** 14 dpl. All DEGs (1 dpl: 6123, 3 dpl: 4662, 14 dpl: 1954) were used for the analysis. The heatmap scale shows $\log_{10}$ of the EASE p-value for all significantly enriched GO terms.

4.8. Comparison of DEG sets between regeneration stages

In order to show global changes in gene expression, heatmap plots were drawn by using all DEGs (9136 genes) for three stages (Figure 31a, 31b). While Figure 31a shows all genes by using z-score of variance-stabilized (vst) counts for all samples, Figure 31b indicates $\log_2$ fold changes of these genes. Interestingly, although there was less variation between samples of control and 14 dpl, samples of 1 dpl and 3 dpl showed more variation between them. This may be due to the activation of intense regeneration events such as reactive proliferation and the fact that the regeneration response against the injury differs between individuals at these stages. However, since the neuronal processes are partially re-established (Kroehne et al., 2011), samples of 14 dpl showed the least variation and expression patterns of genes at that stage were similar to those the control group, explaining the least number of DEGs at this stage (Figure 31a). Curiously, most DEGs, except a small number of genes, showed a similar expression pattern across different stages. If a gene is upregulated at a stage, it is generally upregulated at all stages, and similarly for downregulated genes (Figure 31b).

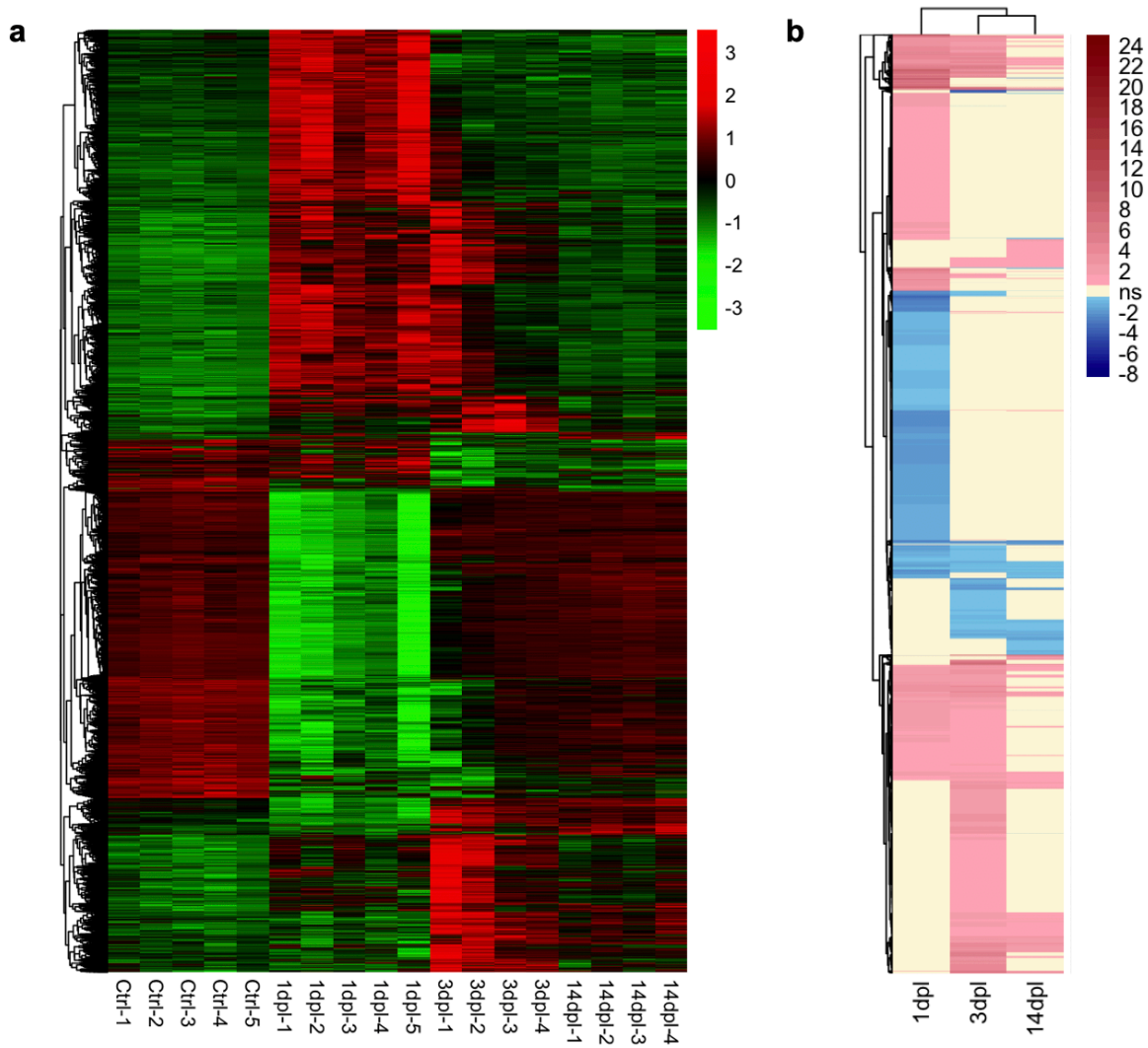

Figure 31. Heatmaps of all DEGs (9136 genes) across three stages of adult zebrafish brain regeneration. (a) The heatmap shows the z-score of variance-stabilized counts of all DEGs across stages. Each column represents samples of a time point and each row shows a single gene. Red and green shades show expressions that are respectively higher or lower than average for each particular gene. **(b)** Heatmap shows the $\log_2$ fold changes of all DEGs (9136 genes) across stages of adult zebrafish brain regeneration. Each column represents a time point, and each row shows a single gene. The scale bar shows red: upregulation; blue: downregulation; yellow: the fold change is either weak (FC < 1.5 in either direction) or not statistically significant (Benjamini–Hochberg adjusted *p*-value (FDR) > 0.1).

UpSet are alternative to Venn diagrams that can be used for visualizing intersections of multiple sets. It was used here to compare DEG sets at different regeneration stages separated by direction of change (up or down regulation). Whereas the total size of each set is shown on Figure 32a, different intersections are shown in Figure 32b. Differential expression at all stages was found asymmetrical in favour of upregulated genes. Overall, the early wound healing stage was the one with the higher number of DEGs, although there are more upregulated genes in early proliferative stage (Figure 32a). Differential expression of brain regeneration showed an important stage-specific component.

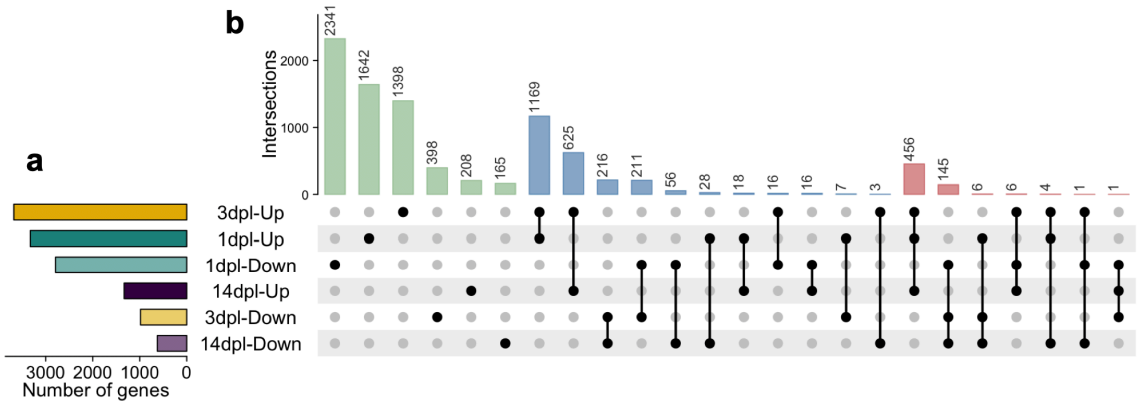

Figure 32. UpSet plot showing the comparison of DEG sets between regeneration stages. **(a)** Total number of differentially expressed genes on x-axis and at each time point, on y-axis (Up- or Down-regulated). **(b)** Intersection of sets of genes at multiple time points. Each bar represents: the genes unique to a time point (green bars), intersection of genes between two different time points (blue bars) or intersection of genes between three different time points (red bars). Black dots connected by lines correspond to time point and Up- or Down-regulation. Numbers of overlapping genes are shown above each bar.

Heatmaps of selected genes undertaking specific roles during regeneration were shown on Figure 33 indicating their $\log_2$ fold changes across stages. Several platelet-derived growth factors (PDGFs) and their receptors (PDGFRs) carrying out various functions such as animal development, blood vessel formation, regulation of cell population proliferation (Andrae et al., 2008) were mainly upregulated at early proliferative stage (Figure 33a).

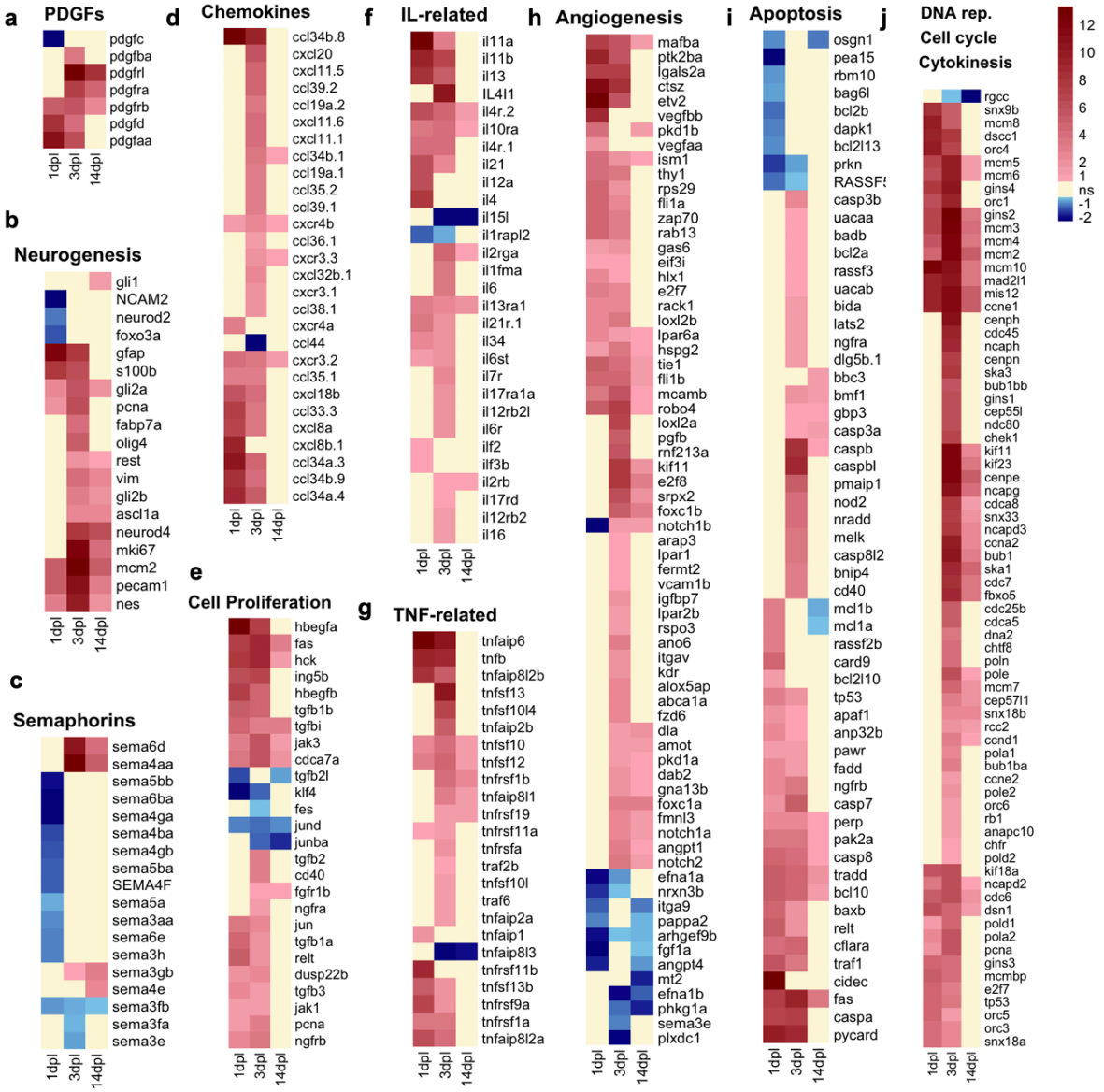

Figure 33. Heatmaps of $\log_2$ fold changes of selected genes across stages of adult zebrafish brain regeneration. **(a)** Platelet-derived growth factors and their receptors; **(b)** adult neurogenesis markers and neurogenesis-related genes; **(c)** semaphorins; **(d)** chemokines and related genes; **(e)** cell proliferation genes; **(f)** interleukines and their related genes; **(g)** tumour necrosis factor (TNF) superfamily genes and their related genes; **(h)** angiogenesis genes; **(i)** apoptosis genes; **(j)** DNA replication, cell cycle and cytokinesis genes. Each column represents a time point and each row shows a single gene. The scale bar shows red: upregulation: blue: downregulation; yellow: the fold change is either weak (FC < 1.5 in either direction) or not statistically significant (Benjamini–Hochberg adjusted *p*-value (FDR) > 0.1).

Adult neurogenesis markers have some capabilities such as, proliferation, neurogenesis, and gliogenesis. In order to determine the prominent neurogenesis events across stages, expression of selected neurogenesis markers was shown on the heatmap. *pcna* (proliferating cell nuclear antigen), *mki67* (a nuclear protein), *mcm2* (minichromosome maintenance protein 2) are used as markers for dividing cells (J. Zhang & Jiao, 2015). All these proliferation markers were upregulated at early proliferative stage. While *pcna* was upregulated at early wound healing stage, *mik67* was upregulated at differentiation stage. Increased expression of *neurod4* (neurogenic differentiation) gene, serving as a differentiation marker during adult neurogenesis, was observed at early proliferative and differentiation stages (Figure 33b). Various semaphorin genes, having important roles in neuron-axonal guidance and angiogenesis (Hu & Zhu, 2018), including *sema3aa, sema3h, sema4ba, sema5a, sema5a*, and *sema5bb*, were downregulated at early wound healing stage. s*ema4aa, sema4e, sema3gb*, and *sema6d* were upregulated at differentiation stage (Figure 33c). Cytokines and chemokines are the proteins that regulate immune response. Interleukins and tumour necrosis factor superfamily (TNF) genes, serving as cytokines, play also important role in immune system's function. Results showed prominent upregulation of several interleukin and TNF genes at early wound healing and early proliferative stages, as a consequence of immune response at these stages (Figure 33f, Figure 33g). Chemokines, a specific type of cytokines, are chemoattractant molecules that regulate immune and progenitor cell homeostasis by preventing or promoting the infiltration of cells into the injury site in CNS (Jaerve & Müller, 2012). Results showed that 26 genes [25 Up, 1 Down] at early proliferative stage, 12 genes (Up) at early wound healing stage, and only 4 genes (Up) at differentiation stage, were associated with chemokine signaling (Figure 33d).

According to the results, numerous cell proliferation-related genes and the genes having important roles in DNA replication, cell cycle and cytokinesis were upregulated at early proliferative stage. However, this number decreased at differentiation stage (Figure 33e, Figure 33j). Angiogenesis is another significant event taking place during regeneration. 55, 25, and 24 angiogenesis related genes were upregulated at early proliferative, early wound healing, and differentiation stages, respectively (Figure 33h). Apoptosis has been considered as a critical component converting the immune response into a wound healing response during the early stages of the regeneration process (Brown et al., 1997). Data showed that 43 genes [41 Up, 2 Down] at early proliferative stage, 34 genes [25 Up, 9 Down] at early wound healing stage, and 14 genes [11 Up, 3 Down] at differentiation stage were associated with apoptosis. Overall

results showed that, although it has less DEGs in total compared to early wound healing stage, the DEGs detected in pre-defined genes at early proliferative stage were more than those at early wound healing stage (Figure 33i).

Clustering of selected regeneration-related GO-BP terms enriched at each stage showed that biological events occurring during adult zebrafish brain regeneration display stage-specific patterns (Figure 34).

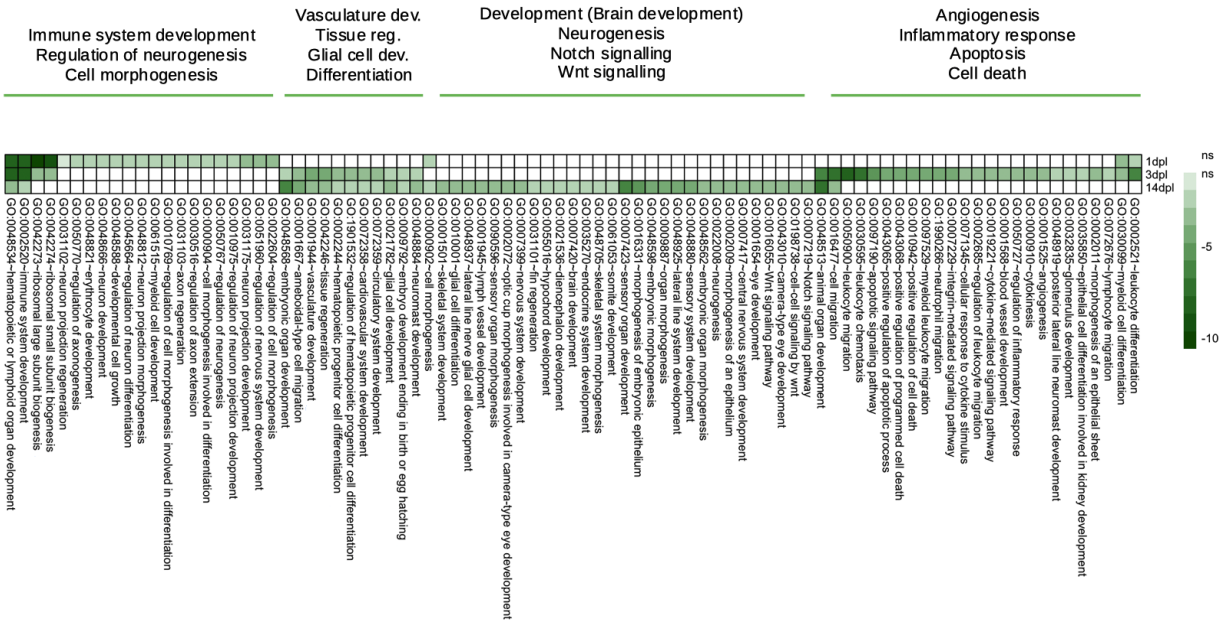

Figure 34. Heatmap representing clustering of the regeneration-related selected GO-BP terms enriched at each stage.

4.9. Weighted gene co-expression network analysis of adult zebrafish brain regeneration

In order to understand the co-expression relationships between genes, weighted gene co-expression network analysis (WGCNA) was performed. 12 distinct co-expression modules were identified, corresponding to clusters of correlated transcripts (Figure 35a, Figure 35b). The expression of the genes which are clustered in the modules showed a stage-specific component (Figure 36a). Notably, results of the GO-BP term enrichment analyses performed by using the genes clustered in the stage-specific modules of zebrafish brain regeneration showed a similar pattern with the results of the GO-BP analyses performed by using the DEGs tested for each stage (Figure 36b).

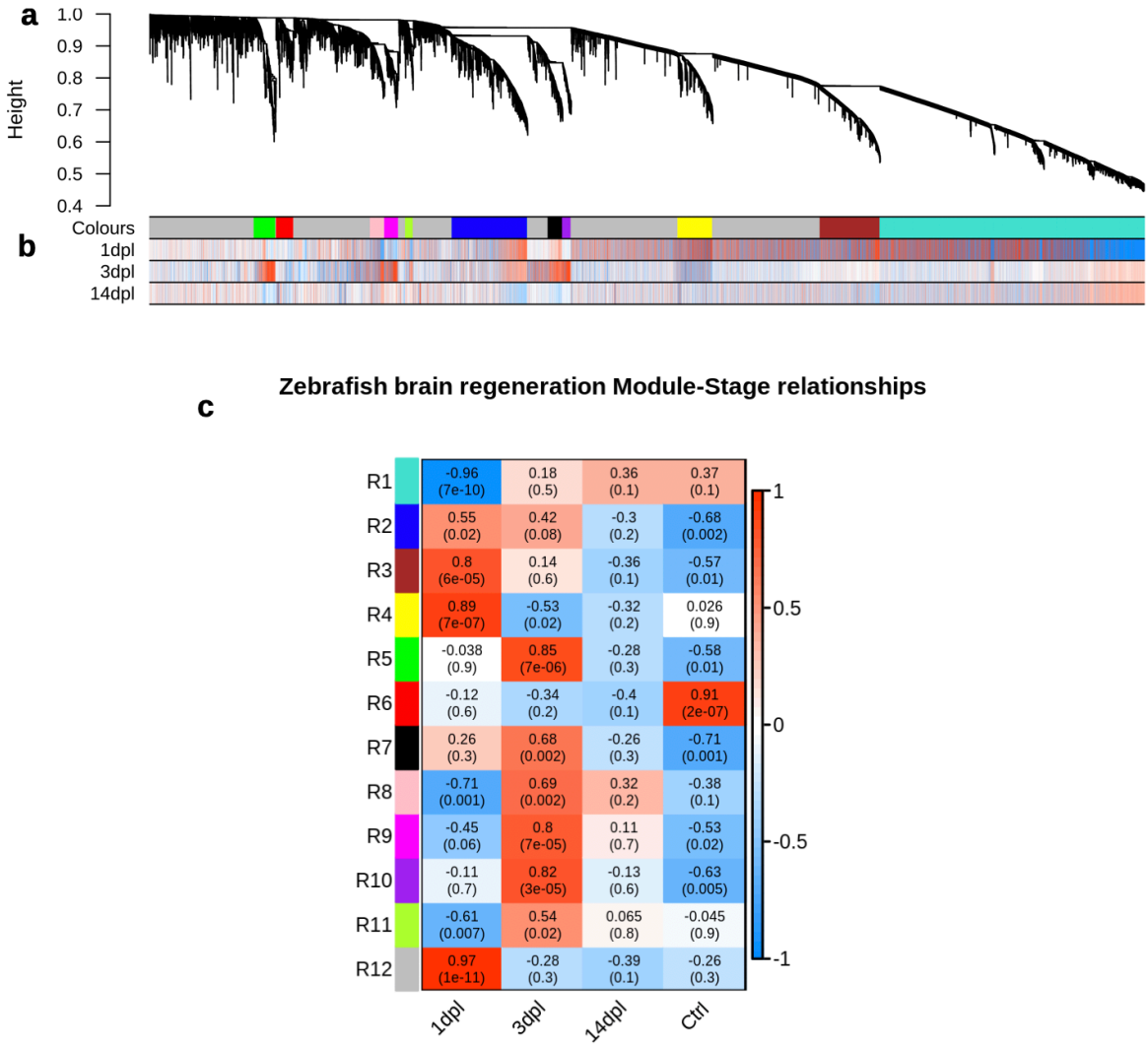

Figure 35. Network analysis of zebrafish brain regeneration. (a) Hierarchical cluster dendrogram derived from zebrafish gene expression data shows co-expression modules identified by WGCNA. **(b)** The first colour band under the dendrogram represents the modules. Colour bands underneath show highly correlated genes that are enriched in each module for each stage. **(c)** Heatmap showing correlations (and corresponding p-values) between modules and stages.

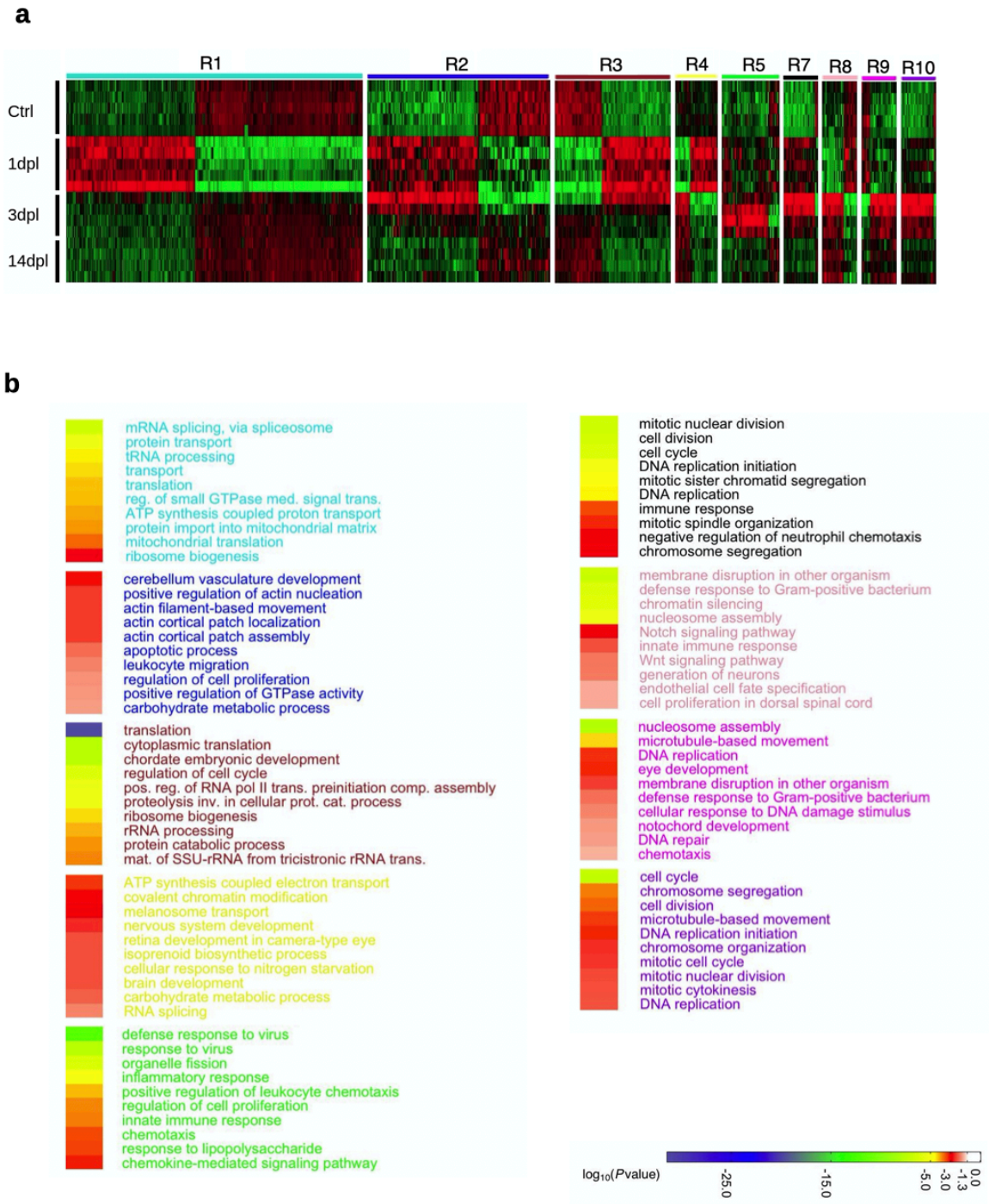

Figure 36. Heatmap and functional annotations of the genes clustered in each module. (a) Heatmap represents relative expression of genes that are enriched in each module for the three stages of the adult zebrafish brain regeneration. **(b)** Top 10 gene ontology biological process (GO-BP) terms of each significant module and their associated enrichment p-values are shown.

4.10. Transcriptome profiling of brain cancer datasets

4.10.1. Differential gene expression analysis of low-grade glioma

In order to identify differentially expressed genes in low-grade glioma, LGG (TCGA) samples were compared with normal tissue. The expression of 7992 genes [4036 upregulated (Up) and 3956 downregulated (Down)] significantly changed in low-grade glioma (Figure 37a). While 5472 of those were protein coding genes, 1680 of those were long non-coding RNA (lncRNA) genes (Figure 37b). Several cancer-related genes, proto-oncogenes, tumour suppressors, such as *ARAF, ABL1, CBLC, RELA, RAF1, TP53*, were upregulated. *POLA1, POLD1, POLD2, POLE2, POLG2, CDC25A, CDC25C, CDC45, CHECK1, MCM3, MCM5, MCM7, MCM8, MCM10, PCNA,* and *MKI67*, which are genes related with cell division and cell proliferation, were also upregulated.

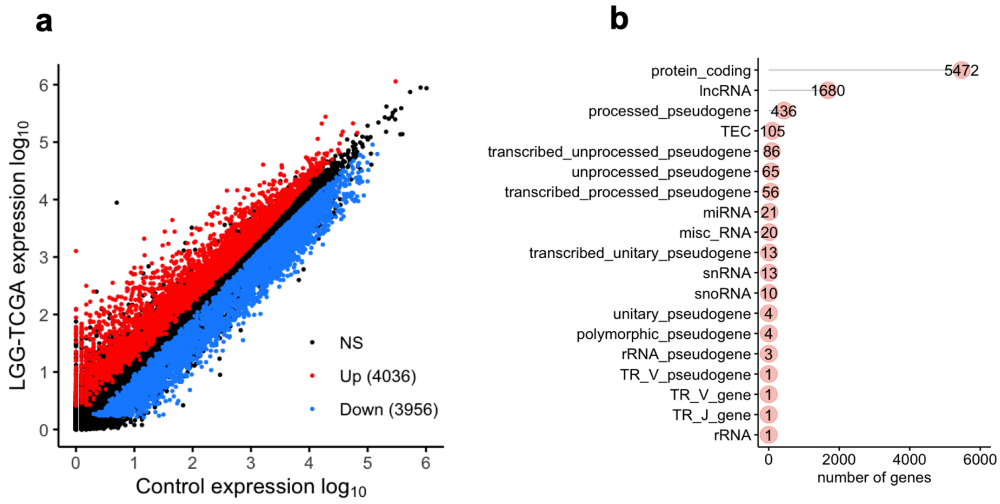

Figure 37 . Transcriptome profiling of LGG-TCGA. (a) Scatterplot showing the number of activated (red) and reduced (blue) genes in LGG-TCGA (LGG=533, Normal=4). **(b)** Dotplot shows subsets of gene biotypes and the number of DEGs in each subset. NS: not significant; Up: upregulated; Down: downregulated; lncRNA: long non-coding RNA; TEC: To be Experimentally Confirmed; miRNA: micro RNA; miscRNA: Miscellaneous RNA; snRNA: small nuclear RNA; snoRNA: small nucleolar RNA; rRNA: ribosomal RNA; TR_J: joining chain T cell receptor; TR_V: variable chain T cell receptor.

4.10.2. Differential gene expression analysis of glioblastoma

In order to identify differentially expressed genes in glioblastoma, samples of the GBM-TCGA project were compared with normal tissue samples found in the same project. The

expression of 15469 genes [8451 upregulated (Up) and 7018 downregulated (Down)] was significantly altered in glioblastoma (Figure 38a). Numbers of up and downregulated genes were very close to each other. While 8701 DEGs were protein coding genes, 2920 of those were lncRNA genes and 2833 were processed pseudogenes (Figure 38b). Studies showed that numerous lncRNAs are differentially expressed in glioblastoma (Yadav et al., 2021). Numerous oncogenes and proto-oncogenes, such as *FGR, SPI1, ARAF, CBLB, MYB, MAS1, KRAS, ETS1, ETS2, MDM2, FLI1, BRAF, RELA, YES1, FES*, MYC, and *EGFR*, were differentially expressed in glioblastoma. Similarly to the early wound healing stage of zebrafish brain regeneration, several semaphorin genes, playing roles in axonal guidance, including *SEMA3G, SEMA4A, SEMA4D, SEMA4G, SEMA5A, SEMA6B*, and *SEMA7A*, were tested as DEGs. *ANG, ANGPT1, ANGPT2, KDR, VEGFA* and *VEGFD* were some of the angiogenesis-related genes.

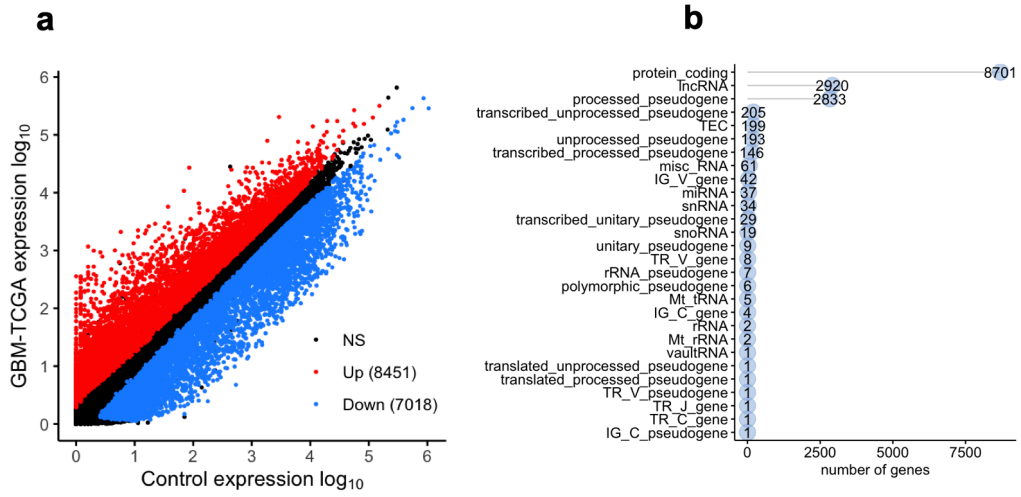

Figure 38. Transcriptome profiling of GBM-TCGA. (a) Scatterplot showing the number of activated (red) and reduced (blue) genes in GBM-TCGA (GBM=165, Normal=5). **(b)** Dotplot shows subsets of gene biotypes and the number of DEGs in each subset. NS: not significant; Up: upregulated; Down: downregulated; lncRNA: long non-coding RNA; TEC: To be Experimentally Confirmed; miscRNA: Miscellaneous RNA; IG_V: variable chain immunoglobulin; IG_C: Constant chain immunoglobulin; Mt_rRNA: mitochondrial ribosomal RNA; miRNA: micro RNA; snRNA: small nuclear RNA; snoRNA: small nucleolar RNA; rRNA: ribosomal RNA; TR_J: joining chain T cell receptor; TR_V: variable chain T cell repector; TR_C: Constant chain T cell receptor.

4.11. Comparison of early wound healing, early proliferative, and differentiation stages of adult zebrafish brain regeneration with low-grade glioma and glioblastoma

To investigate the shared genes between stages of adult zebrafish brain regeneration and low-grade glioma and glioblastoma, unique human orthologs of all DEGs across stages were defined by using biomaRT package of Bioconductor. In total, 9136 DEGs were tested in three stages of brain regeneration. After ortholog conversion, 5591 of those genes had a human ortholog to be used for downstream analysis.

4.11.1. Comparison of early wound healing stage of brain regeneration with low-grade glioma and glioblastoma

To investigate the shared genes between early wound healing stage of adult zebrafish brain regeneration and low-grade glioma and glioblastoma, unique human orthologs of DEGs at early wound healing stage were intersected with the DEGs in low-grade glioma and glioblastoma, respectively. According to the results, 1610 genes were shared between early wound healing stage and low-grade glioma. While 1246 of those show the same expression pattern, 364 of those showed opposite directions of change. 4513 zebrafish genes [2609 Up, 1904 Down] were unique to early wound healing stage (Figure 39a). Among shared genes, *TP53*, *GFAP*, and *PCNA* were upregulated genes. *NEUROD2, BRAF, KRAS, PTEN*, and *AKT3* genes were downregulated in both conditions. *CDK6, HIF1A, TET2, ITGB8, EGFL7*, and *SOX7* were oppositely regulated genes (Figure 39c).

According to results of the comparison of early wound healing stage of brain regeneration and glioblastoma, 2380 genes were shared between these two conditions. While 2056 of those show the same expression pattern, 324 of those showed opposite directions of change. In this comparison, 3743 zebrafish genes [2211 Up, 1532 Down] were unique to early wound healing stage (Figure 39b). Consistently with the DEG numbers in both cancer types, it was observed that there were more common genes intersection of glioma and early wound healing stage. Among shared DEGs, *TP53*, *PCNA, MCM2, VEGFA, VEGFB,* and *NRAS* were upregulated genes. Also, several minichromosome maintenance complex (MCM) genes, such as *MCM2, MCM3, MCM4, MCM5, MCM6, MCM8,* and *MCM10*, were also upregulated. Similarly to the low-grade glioma results, *NEUROD2, BRAF, KRAS, PTEN*, and *AKT3* genes were downregulated in both conditions. In addition to these genes, *JUND, NF1, APC, KLF4,*

ELAVL3, SHC3, PLCB1, NYAP2, and *CALN1* were also downregulated. *CDK6, HIF1A, NOTCH3, ITGB8, GPC1*, *SOX7,* and *APAF1* were oppositely regulated genes (Figure 39d).

While functional gene annotations of shared genes were done by using human gene identifiers, zebrafish gene identifiers were used for genes unique to early wound healing stage (Figures 40a, 40b, 41a, 41b). When enriching DEGs of early wound healing stage shared with low-grade glioma on one side and shared with glioblastoma on the other side, 39 terms were common to both top 50 GO-BP terms, despite the lower numbers of shared genes when comparing early wound healing stage and low-grade glioma. Neuron and neuron projection development, neuron differentiation, neurogenesis, neuron projection morphogenesis, synaptic signaling, translation, cell development, regulation of synaptic plasticity, regulation of neurogenesis, regulation of neuron differentiation and regulation of nervous system development were among these GO-BP terms (Figures 40a, 41a). The five most significantly enriched CC and MF categories were also shown (Figures 40a, 41a). Furthermore, KEGG pathway enrichment of shared DEGs showed that ribosome, mTOR signaling, GABAergic synapse, glutamatergic synapse, cholinergic synapse, ErbB signaling, oxytocin signaling, axon guidance, and pancreatic cancer were some of the shared pathways within the top 30 KEGG pathways. Interestingly, glioma was enriched by shared DEGs of early wound healing stage with both low-grade glioma and glioblastoma (Figure 42).

When enriching DEGs specific to early wound healing stage as opposed to low-grade glioma on one side and as opposed to glioblastoma on the other side, 41 terms were common to both top 50 GO-BP terms. Hemopoiesis, immune system development, hematopoietic or lymphoid organ development, leukocyte differentiation, translation, rRNA and RNA processing were among these GO-BP terms (Figures 40b, 41b). The five most significantly enriched CC and MF categories were also shown (Figures 40b, 41b). Also, KEGG pathway enrichment of the same DEG sets showed that proteasome, oxidative phosphorylation, apoptosis, RNA polymerase, herpes simplex and salmonella infection, ribosome, Jak-STAT signaling pathway, ribosome biogenesis in eukaryotes, protein processing in endoplasmic reticulum were the shared pathways within the top 30 KEGG pathways (Figure 43).

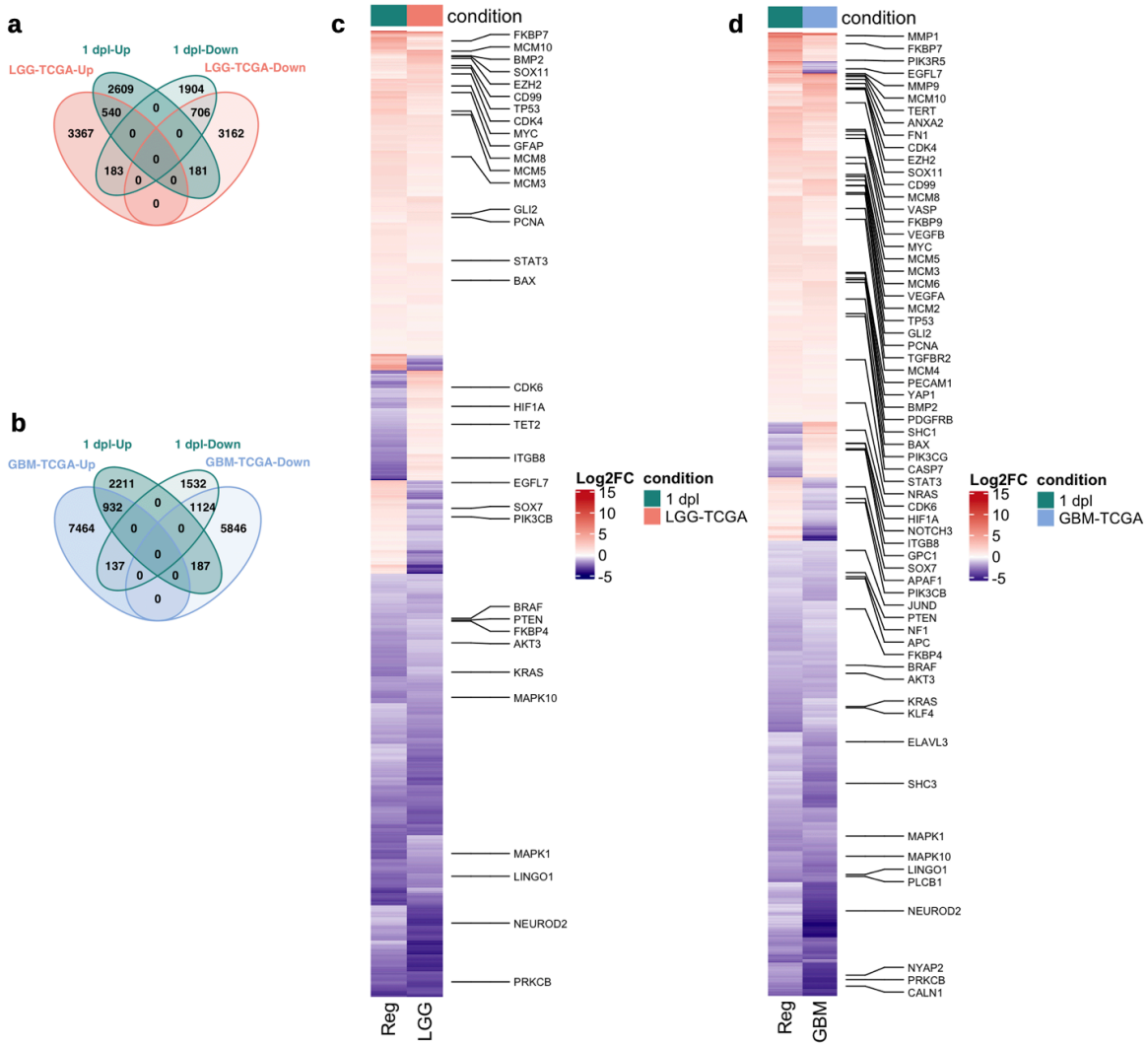

Figure 39. Comparison of early wound healing stage of brain regeneration with low-grade glioma and glioblastoma. Venn diagrams show the number of upregulated (Up) or downregulated (Down) differentially expressed genes (DEGs) and the overlap between 1 dpl (turquoise), **(a)** low-grade glioma (LGG) (pink), and **(b)** glioblastoma (GBM) (blue). Heatmaps show the expression of genes shared between 1 dpl (turquoise), and **(c)** low-grade glioma (pink), and **(d)** glioblastoma (blue). Each column represents a condition (1 dpl, LGG, GBM) and each row shows a single gene. The scale bar shows their $\log_2$ fold changes from high to low expression, represented by a colour gradient from red to purple, respectively.

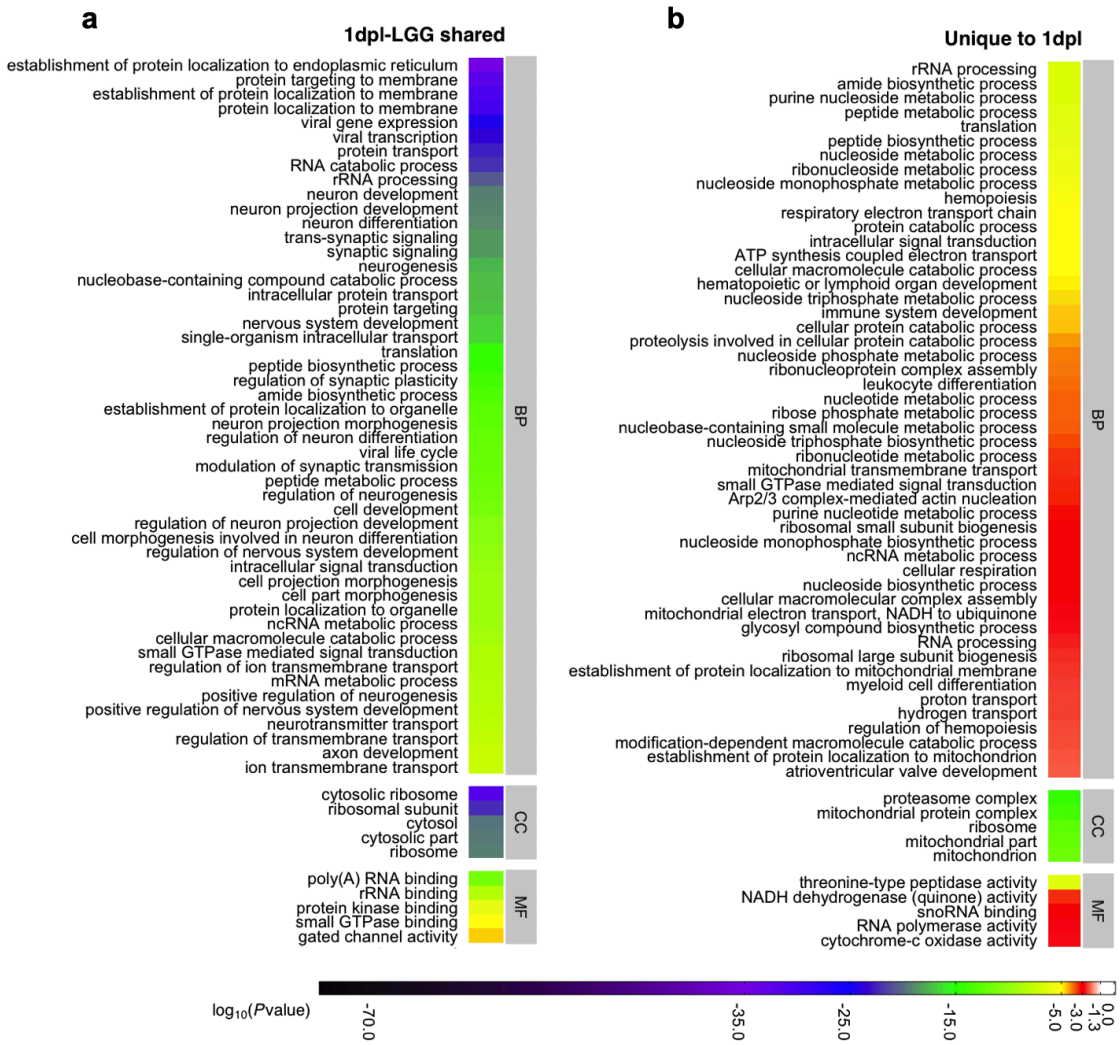

Figure 40. GO terms enriched in comparison of early wound healing stage of brain regeneration with low-grade glioma. DAVID bioinformatics tool was used to show the most significantly enriched GO-BP (top 50), CC (top 5), and MF (top 5) terms based on transcriptional changes in comparison of early wound healing stage of brain regeneration with low-grade glioma. GO terms enriched by using **(a)** human identifiers of shared DEGs between 1 dpl and low-grade glioma (1610 DEGs), **(b)** zebrafish identifiers of the DEGs unique to 1 dpl (4513 DEGs) in this comparison. The heatmap scale shows $\log_{10}$ of the EASE p-value for the most significantly enriched GO terms. DAVID: Database for Annotation, Visualization and Integrated Discovery, GO: Gene Ontology, BP: Biological Process, CC: Cellular Component, MF: Molecular Function.

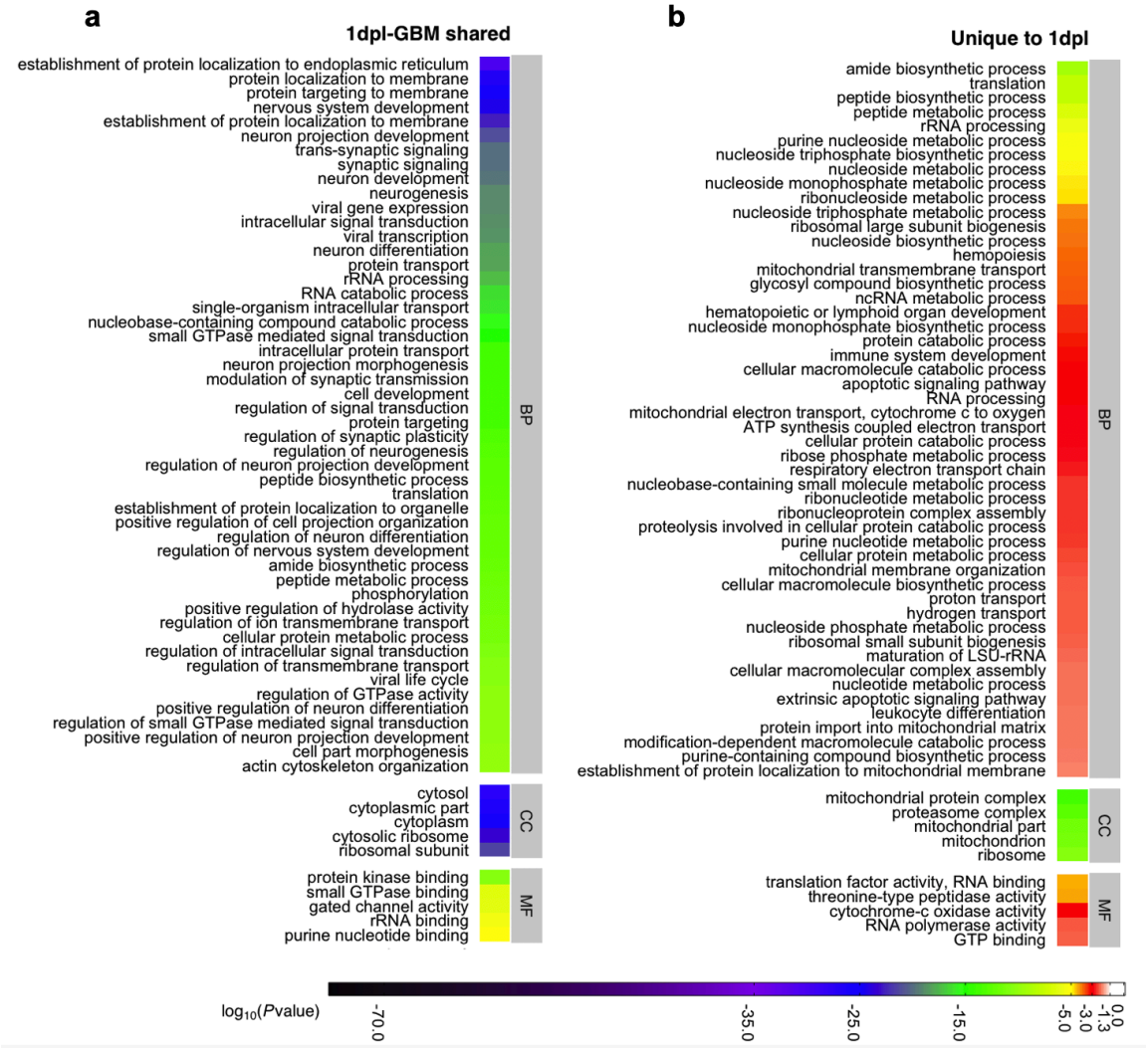

Figure 41. GO terms enriched in comparison of early wound healing stage of brain regeneration with glioblastoma. DAVID bioinformatics tool was used to show the most significantly enriched GO-BP (top 50), CC (top 5), and MF (top 5) terms based on transcriptional changes in comparison of early wound healing stage of brain regeneration with glioblastoma. GO terms enriched by using **(a)** human identifiers of shared DEGs between 1 dpl and glioblastoma (2380 DEGs), **(b)** zebrafish identifiers of the DEGs unique to 1 dpl (3743 DEGs) in this comparison. The heatmap scale shows $\log_{10}$ of the EASE p-value for the most significantly enriched GO terms. DAVID: Database for Annotation, Visualization and Integrated Discovery, GO: Gene Ontology, BP: Biological Process, CC: Cellular Component, MF: Molecular Function.

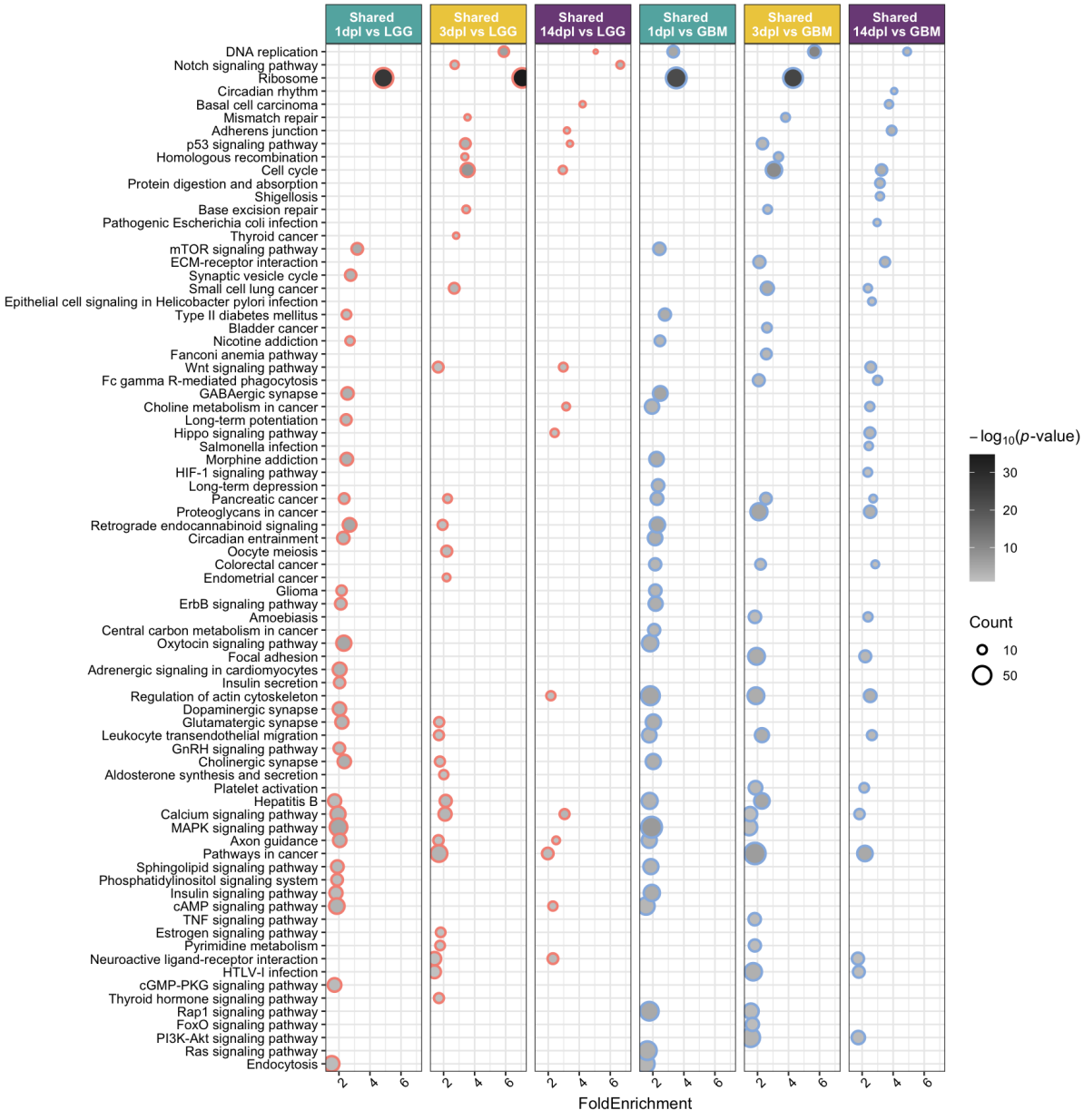

Figure 42. KEGG pathways performed by using DEGs shared between zebrafish brain regeneration and human brain cancers. DAVID bioinformatics tool was used to show the 30 most significantly enriched KEGG pathways based on the shared DEGs between zebrafish brain regeneration (1 dpl, 3 dpl and 14 dpl) and human brain cancers (LGG and GBM). The heatmap scale shows $\log_{10}$ of the EASE p-value for the most significantly enriched GO terms.

Figure 43. KEGG pathways performed by using the DEGs unique to zebrafish brain regeneration. DAVID bioinformatics tool was used to show all significantly enriched KEGG pathways based on the genes which are tested as DEG in zebrafish brain regeneration but not in the human brain cancer. The heatmap scale shows $\log_{10}$ of the EASE p-value for all significantly enriched GO terms.

4.11.2. Comparison of early proliferative stage of brain regeneration with low-grade glioma and glioblastoma

To investigate the shared genes between early proliferative stage of adult zebrafish brain regeneration and low-grade glioma and glioblastoma, unique human orthologs of DEGs at early proliferative stage were intersected with the DEGs in low-grade glioma and glioblastoma, respectively. According to the results, 952 genes were shared between early proliferative stage and low-grade glioma. While 796 of those show the same expression pattern, 156 of those showed opposite directions of change. 3710 zebrafish genes [2939 Up, 771 Down] were unique to early proliferative stage (Figure 44a). Among shared genes, *MKI67, GFAP*, and *PCNA* were upregulated genes (Figure 44c).

According to results of the comparison of early proliferative stage of brain regeneration and glioblastoma, 1513 genes were shared between these two conditions. While 1288 of those show the same expression pattern, 225 of those showed opposite directions of change. In this comparison, 3149 zebrafish genes [2484 Up, 665 Down] were unique to early wound healing stage (Figure 44c). Among shared DEGs, *ANGPT1, VIM, BRCA2*, *PCNA, MCM2,* and *MKI67* were upregulated genes. *JUND* and *KLF4* genes were downregulated. *APAF1, HIF1A, PIK3CB, KIT,* and *FKBP5* were oppositely regulated genes (Figure 44d). While functional gene annotations for shared genes were done by using human gene identifiers, zebrafish gene identifiers were used for genes unique to early proliferative stage (Figures 45a, 45b, 46a, 46b).

When enriching DEGs of early proliferative stage shared with low-grade glioma on one side and shared with glioblastoma on the other side, 31 terms were common to both top 50 GO-BP terms. Several proliferation related GO-BP terms, such as mitotic cell cycle process, G1/S transition of mitotic cell cycle, cell cycle phase transition, nuclear division, sister chromatid segregation, DNA replication, nuclear chromosome segregation, DNA replication initiation, and regulation of mitotic cell cycle, were among these GO-BP terms (Figures 45a, 46a). The five most significantly enriched CC and MF categories were also shown (Figures 45a, 46a). Furthermore, KEGG pathway enrichment of shared DEGs showed that several proliferation-related pathways, such as DNA replication and cell cycle; several signaling pathways, such as p53 signaling pathway, MAPK signaling pathway and calcium signaling; DNA repair pathways, such as mismatch repair and base excision repair; several immune response-related pathways, such as leukocyte transendothelial migration, hepatitis B and HTLV-I infection were

some of the shared pathways within the top 30 KEGG pathways. Interestingly, several cancer-related pathways, such as small cell lung cancer, pancreatic cancer and pathways in cancer were enriched by shared DEGs of early proliferative stage with both low-grade glioma and glioblastoma (Figure 42).

When enriching DEGs specific to early wound healing stage as opposed to low-grade glioma on one side and as opposed to glioblastoma on the other side, 38 terms were common to both top 50 GO-BP terms. Several immune response-related terms, such as response to virus, bacterium and lipopolysaccharide, defence response to virus, defence response to other organism, leukocyte chemotaxis, lymphocyte migration, leukocyte migration, neutrophil chemotaxis, cell chemotaxis, granulocyte chemotaxis, leukocyte differentiation, cytokine-mediated signaling pathway, cellular response to cytokine stimulus, response to interferon-gamma, neutrophil migration, myeloid leukocyte migration and regulation of inflammatory response; several apoptosis and cell death associated terms, such as apoptotic signaling pathway, positive regulation of apoptotic process, positive regulation of programmed cell death and positive regulation of cell death; several terms related with MAPK signaling, such as MAPK cascade, positive regulation of MAPK cascade and regulation of MAPK cascade, were among these GO-BP terms (Figures 45b, 46b). The five most significantly enriched CC and MF categories were also shown (Figures 45b, 46b). Also, KEGG pathway enrichment of the same DEG sets showed that p53 signaling pathway, Toll-like receptor signaling pathway, cytokine-cytokine receptor interaction, apoptosis, herpes simplex infection, salmonella infection, phagosome, Jak-STAT signaling pathway were the shared pathways within the top 30 KEGG pathways (Figure 43).

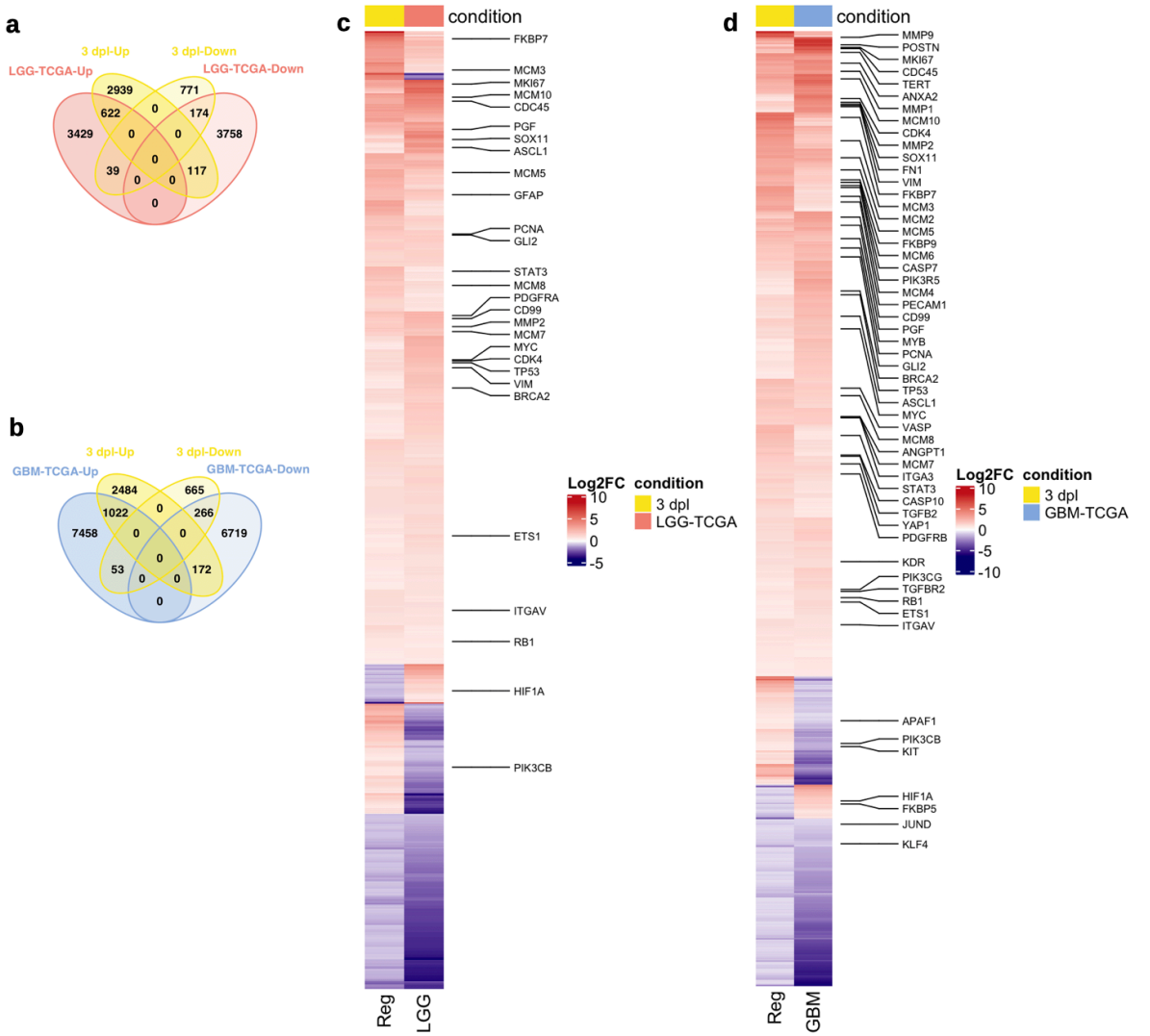

Figure 44. Comparison of early proliferative stage of brain regeneration with low-grade glioma and glioblastoma. Venn diagrams show the numbers of upregulated (Up) or downregulated (Down) differentially expressed genes (DEGs) and the overlap between 3 dpl (yellow), **(a)** low-grade glioma (LGG) (pink), and **(b)** glioblastoma (GBM) (blue). Heatmaps show the expression of genes shared between 3 dpl (yellow), and **(c)** low-grade glioma (pink), and **(d)** glioblastoma (blue). Each column represents a condition (3 dpl, LGG, GBM) and each row shows a single gene. The scale bar shows their $\log_2$ fold changes from high to low expression, represented by a colour gradient from red to purple, respectively.

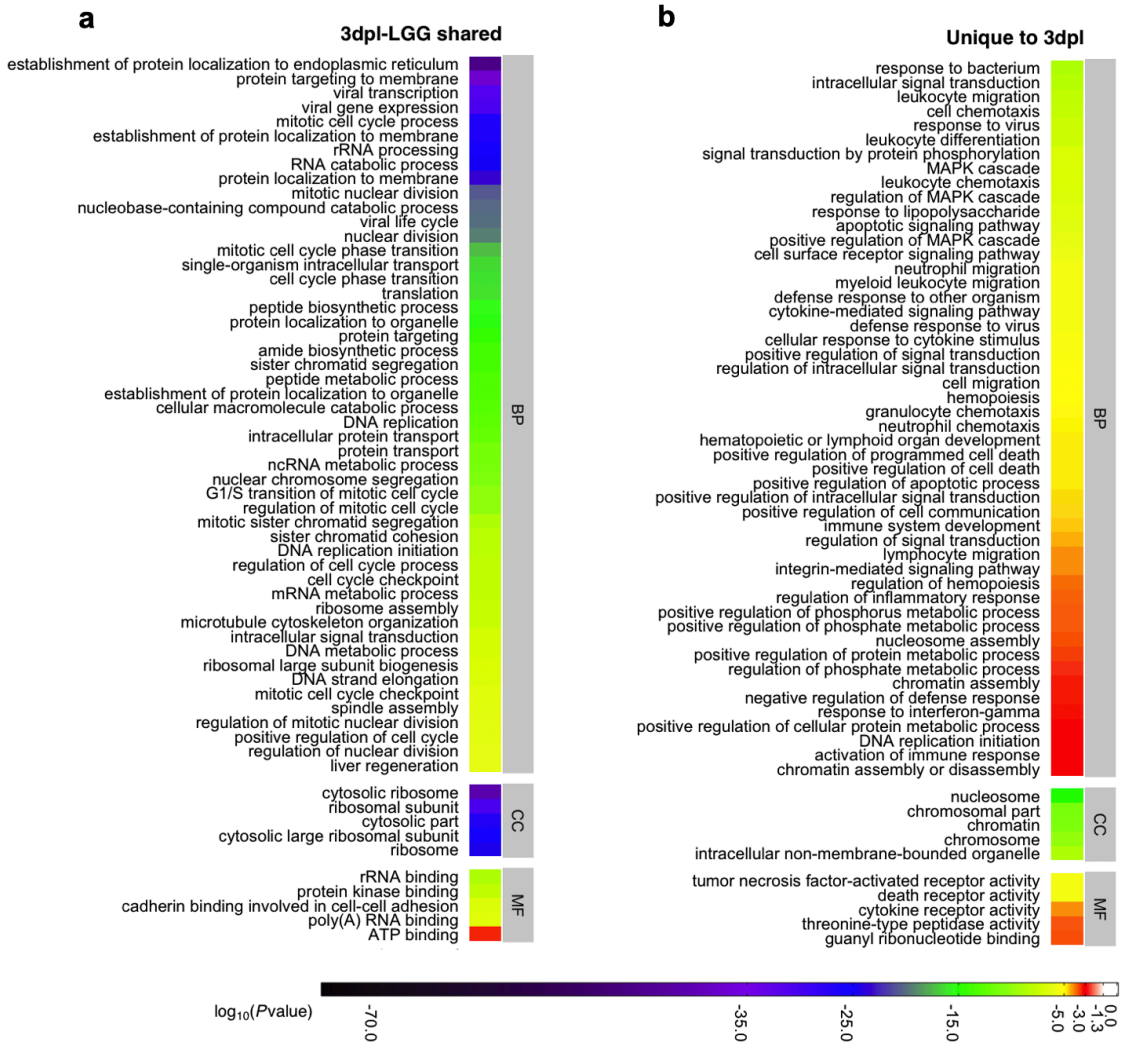

Figure 45. GO terms enriched in comparison of early proliferative stage of brain regeneration with low-grade glioma. DAVID bioinformatics tool was used to show the most significantly enriched GO-BP (top 50), CC (top 5), and MF (top 5) terms based on transcriptional changes in comparison of early proliferative stage of brain regeneration with low-grade glioma. GO terms enriched by using **(a)** human identifiers of shared DEGs between 3 dpl and low-grade glioma (952 DEGs), **(b)** zebrafish identifiers of the DEGs unique to 3 dpl (3710 DEGs) in this comparison. The heatmap scale shows log10 of the EASE p-value for the most significantly enriched GO terms. DAVID: Database for Annotation, Visualization and Integrated Discovery, GO: Gene Ontology, BP: Biological Process, CC: Cellular Component, MF: Molecular Function.

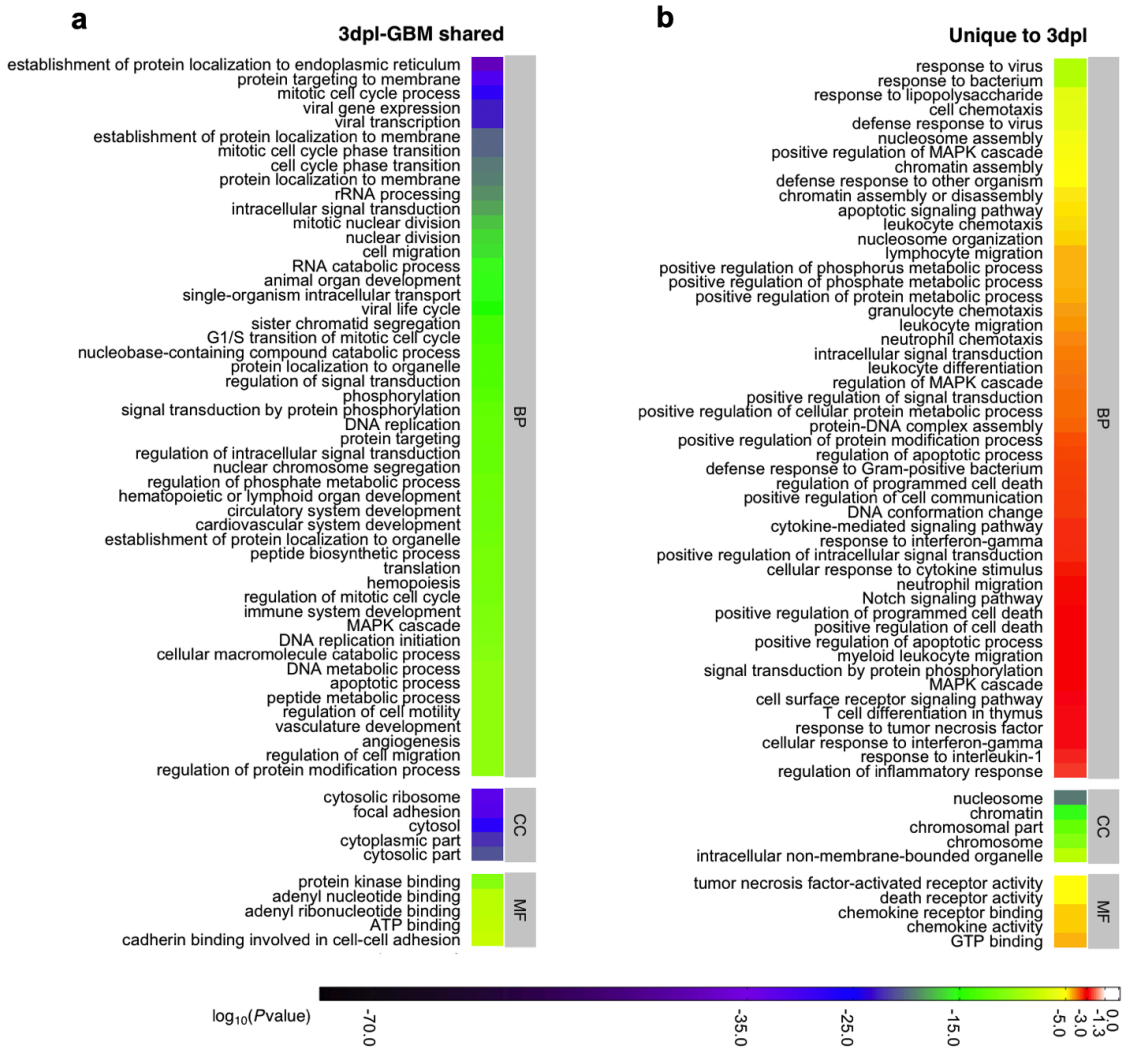

Figure 46. GO terms enriched in comparison of early proliferative stage of brain regeneration with glioblastoma. DAVID bioinformatics tool was used to show the most significantly enriched GO-BP (top 50), CC (top 5), and MF (top 5) terms based on transcriptional changes in comparison of early proliferative stage of brain regeneration with glioblastoma. GO terms enriched by using **(a)** human identifiers of shared DEGs between 3 dpl and glioblastoma (1513 DEGs), **(b)** zebrafish identifiers of the DEGs unique to 3 dpl (3149 DEGs) in this comparison. The heatmap scale shows log10 of the EASE p-value for the most significantly enriched GO terms. DAVID: Database for Annotation, Visualization and Integrated Discovery, GO: Gene Ontology, BP: Biological Process, CC: Cellular Component, MF: Molecular Function.

4.11.3. Comparison of differentiation stage of brain regeneration with low-grade glioma and glioblastoma

To investigate the shared genes between differentiation stage of adult zebrafish brain regeneration and low-grade glioma and glioblastoma, unique human orthologs of DEGs at differentiation stage were intersected with the DEGs in low-grade glioma and glioblastoma, respectively. According to the results, 380 genes were shared between differentiation stage and low-grade glioma. While 319 of those show the same expression pattern, 61 showed opposite directions of change. 1574 zebrafish genes [1073 Up, 501 Down] were unique to differentiation stage (Figure 47a). Among shared genes, *ASCL1*, *MKI67, MCM3, MCM5, MCM7* and *MCM10* were upregulated genes (Figure 47c). According to results of the comparison of differentiation stage of brain regeneration and glioblastoma, 629 genes were shared between these two conditions. While 504 of those show the same expression pattern, 125 showed opposite directions of changes. In this comparison, 1325 zebrafish genes [901 Up, 424 Down] were unique to differentiation stage (Figure 47b). Among shared DEGs, *TERT, MMP2, ANXA2, FN1*, *CASP3* and *PECAM1* were upregulated genes. *JUND* and *NRSN1* genes were downregulated. *HIF1A* and *NYAP2*, were oppositely regulated genes (Figure 47d).

While functional gene annotations for shared genes were done by using human gene identifiers, zebrafish gene identifiers were used for genes unique to differentiation stage (Figures 48a, 48b, 49a, 49b). When enriching DEGs of differentiation stage shared with low-grade glioma on one side and shared with glioblastoma on the other side, 31 terms were common to both top 50 GO-BP terms. Several development and morphogenesis related GO-BP terms, such as cell development, animal organ development, nervous system development, regulation of nervous system development, sensory organ development, organ morphogenesis and embryonic morphogenesis; several neurogenesis-related terms, such as neurogenesis, regulation of neurogenesis, neuron differentiation; several angiogenesis-related terms, such as angiogenesis, vasculature and blood vessel development, cardiovascular system development, circulatory system development, were among these GO-BP terms (Figures 48a, 49a). The five most significantly enriched CC and MF categories were also shown (Figures 48a, 49a). Furthermore, KEGG pathway enrichment of shared DEGs showed that DNA replication, cell cycle, adherens junction, Wnt signaling pathway, Hippo signaling pathway, regulation of actin cytoskeleton, calcium signaling pathway and neuroactive ligand-receptor interaction were some of the shared pathways within the top 30 KEGG pathways. Interestingly, several cancer-related

pathways, such as basal cell carcinoma, choline metabolism in cancer and pathways in cancer were enriched by shared DEGs of differentiation stage with both low-grade glioma and glioblastoma (Figure 42).

When enriching DEGs specific to differentiation stage as opposed to low-grade glioma on one side and as opposed to glioblastoma on the other side, 38 terms were common to both top 50 GO-BP terms. Similarly to results of the early proliferative stage, several immune response-related terms were also significantly enriched in BP category, such as defence response to other organism, defence response to Gram-positive bacterium, response to virus, response to bacterium, defence response to virus. In addition to these pathways, circadian regulation of gene expression, negative regulation of gene expression, regulation of gene expression, lateral line system development, sensory system development, neuromast development and embryonic organ development were also among the top 50 GO-BP terms (Figures 48b, 49b). The five most significantly enriched CC and MF categories were also shown (Figures 48b, 49b). Also, KEGG pathway enrichment of the same DEG sets showed that steroid biosynthesis, p53 signaling pathway, Toll-like receptor signaling pathway, cytokine-cytokine receptor interaction, herpes simplex infection and Wnt signaling pathway were the shared pathways within the top 30 KEGG pathways (Figure 43).

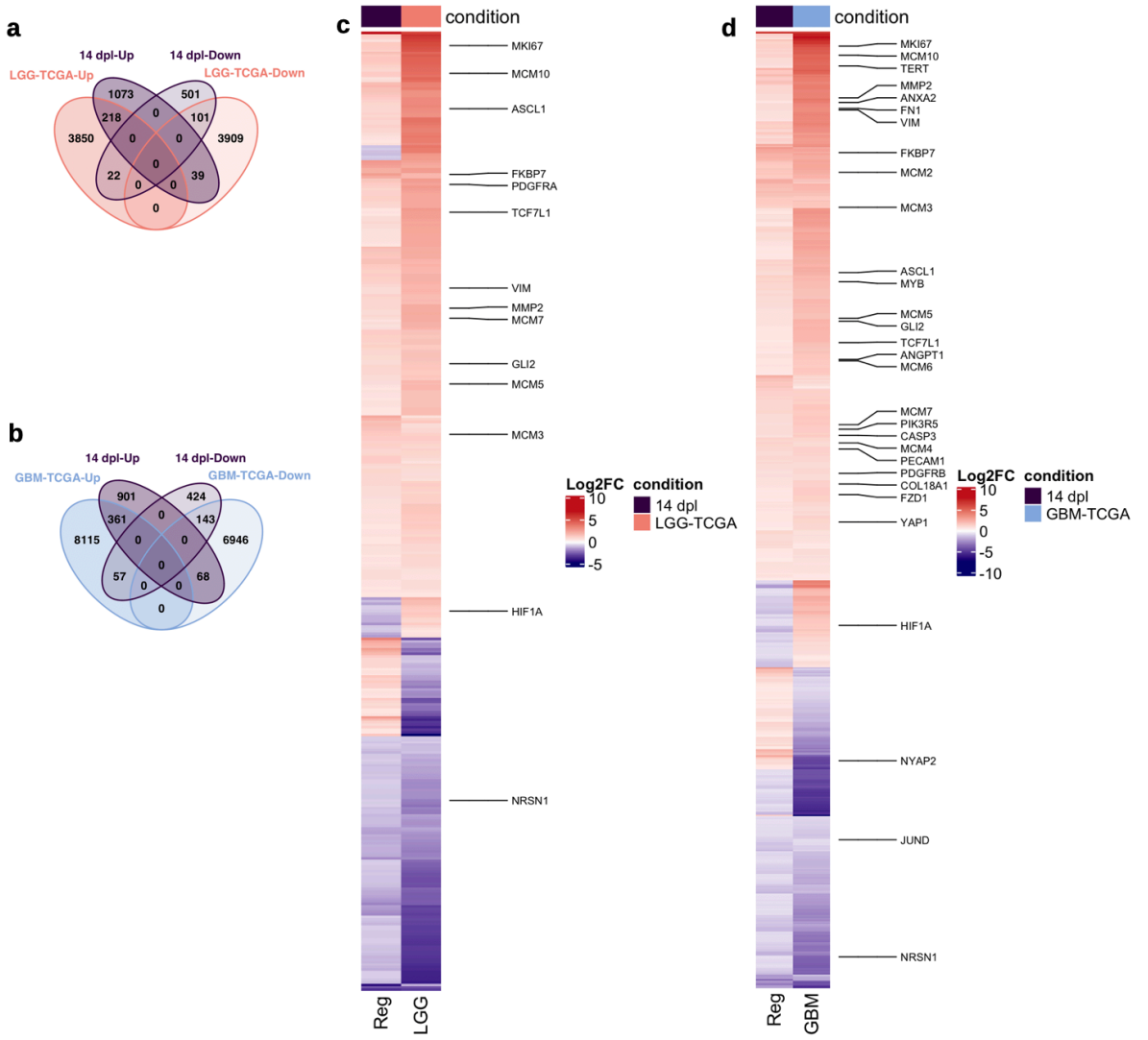

Figure 47. Comparison of differentiation stage of brain regeneration with low-grade glioma and glioblastoma. Venn diagrams show the numbers of upregulated (Up) or downregulated (Down) differentially expressed genes (DEGs) and the overlap between 14 dpl (purple), **(a)** low-grade glioma (LGG) (pink), and **(b)** glioblastoma (GBM) (blue). Heatmaps show the expression of genes shared between 14 dpl (purple), and **(c)** low-grade glioma (pink), and **(d)** glioblastoma (blue). Each column represents a condition (14 dpl, LGG, GBM) and each row shows a single gene. The scale bar shows their $\log_2$ fold changes from high to low expression, represented by a colour gradient from red to purple, respectively.

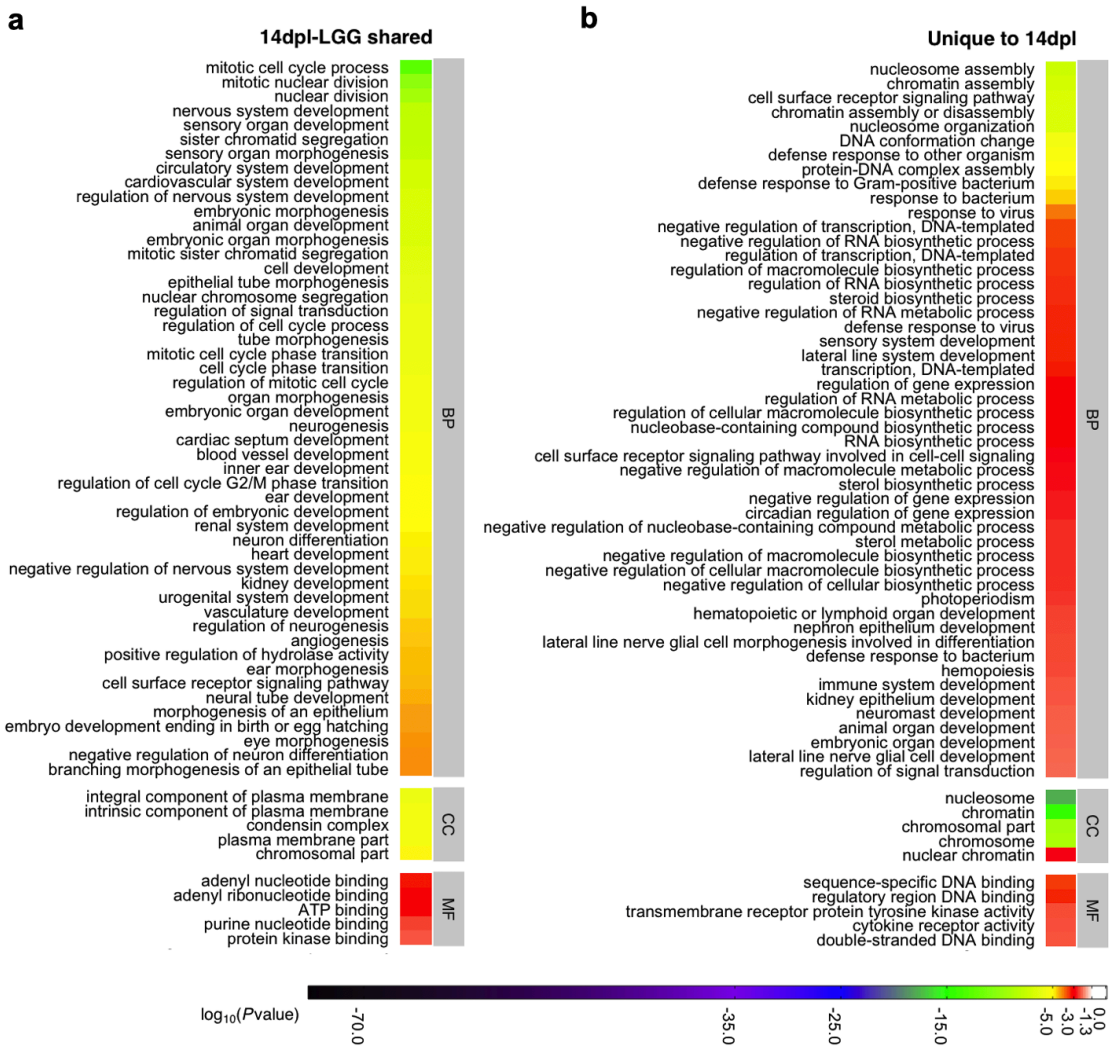

Figure 48. GO terms enriched in comparison of differentiation stage of brain regeneration with low-grade glioma. DAVID bioinformatics tool was used to show the most significantly enriched GO-BP (top 50), CC (top 5), and MF (top 5) terms based on transcriptional changes in comparison of differentiation stage of brain regeneration with low-grade glioma. GO terms enriched by using **(a)** human identifiers of shared DEGs between 14 dpl and low-grade glioma (380 DEGs), **(b)** zebrafish identifiers of the DEGs unique to 14 dpl (1574 DEGs) in this comparison. The heatmap scale shows log10 of the EASE p-value for the most significantly enriched GO terms. DAVID: Database for Annotation, Visualization and Integrated Discovery, GO: Gene Ontology, BP: Biological Process, CC: Cellular Component, MF: Molecular Function.

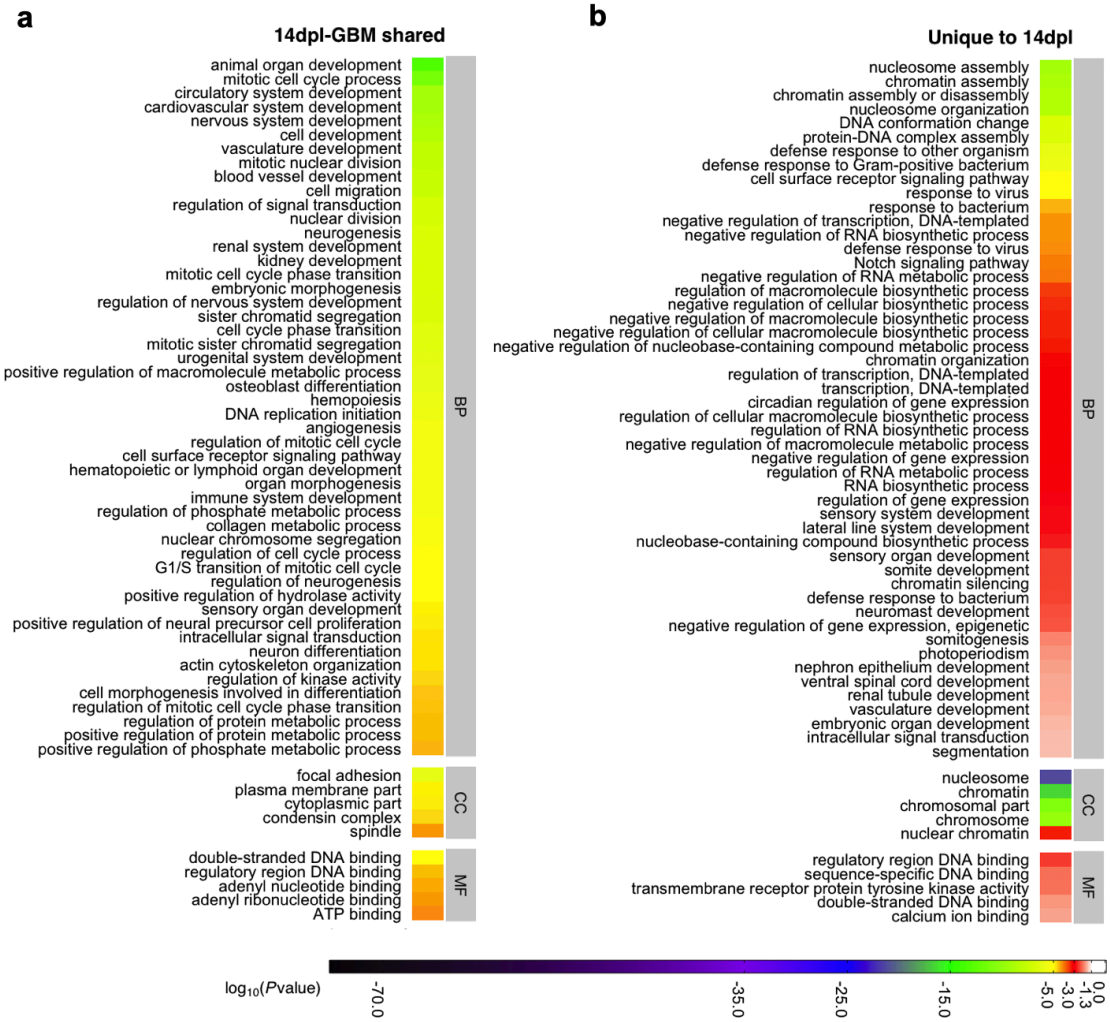

Figure 49. GO terms enriched in comparison of differentiation stage of brain regeneration with glioblastoma. DAVID bioinformatics tool was used to show the most significantly enriched GO-BP (top 50), CC (top 5), and MF (top 5) terms based on transcriptional changes in comparison of differentiation stage of brain regeneration with glioblastoma. GO terms enriched by using **(a)** human identifiers of shared DEGs between 14 dpl and glioblastoma (629 DEGs), **(b)** zebrafish identifiers of the DEGs unique to 14 dpl (1325 DEGs) in this comparison. The heatmap scale shows the log10 of the EASE p-value for the most significantly enriched GO terms. DAVID: Database for Annotation, Visualization and Integrated Discovery, GO: Gene Ontology, BP: Biological Process, CC: Cellular Component, MF: Molecular Function.

4.12. Comparison of the DEG sets of three different stages of zebrafish brain regeneration and two different human brain cancers

In order to show global changes in gene expression between three stages of the brain regeneration and two types of brain cancers, heatmaps were drawn by using $\log_2$ fold changes of the genes (3615 genes) differentially expressed in at least one stage of adult zebrafish brain regeneration and shared with at least one type of brain cancer (Figure 50).

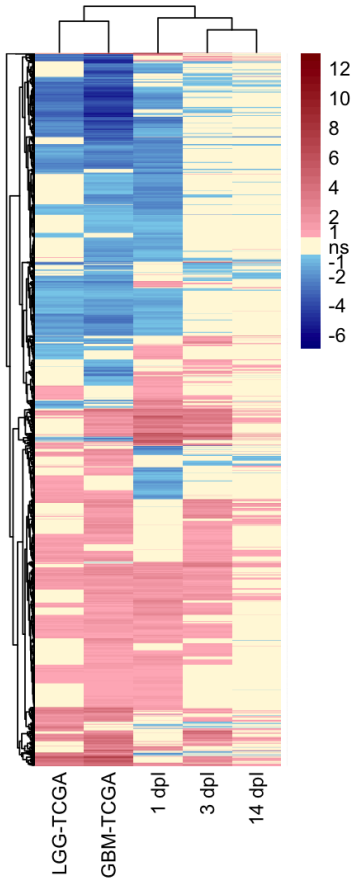

Figure 50. Heatmaps of the DEGs (3615 genes) across three stages of adult zebrafish brain regeneration and two brain cancers. Heatmap shows the $\log_2$ fold changes of genes (3615 genes) differentially expressed in at least one stage of adult zebrafish brain regeneration and shared with at least one type of brain cancer. Each column represents a time point of adult zebrafish brain regeneration or a cancer type and each row shows a single gene. The scale bar shows red: upregulation; blue: downregulation; yellow: the fold change is either weak (FC < 1.5 in either direction) or not statistically significant (Benjamini–Hochberg adjusted p-value (FDR) > 0.1).

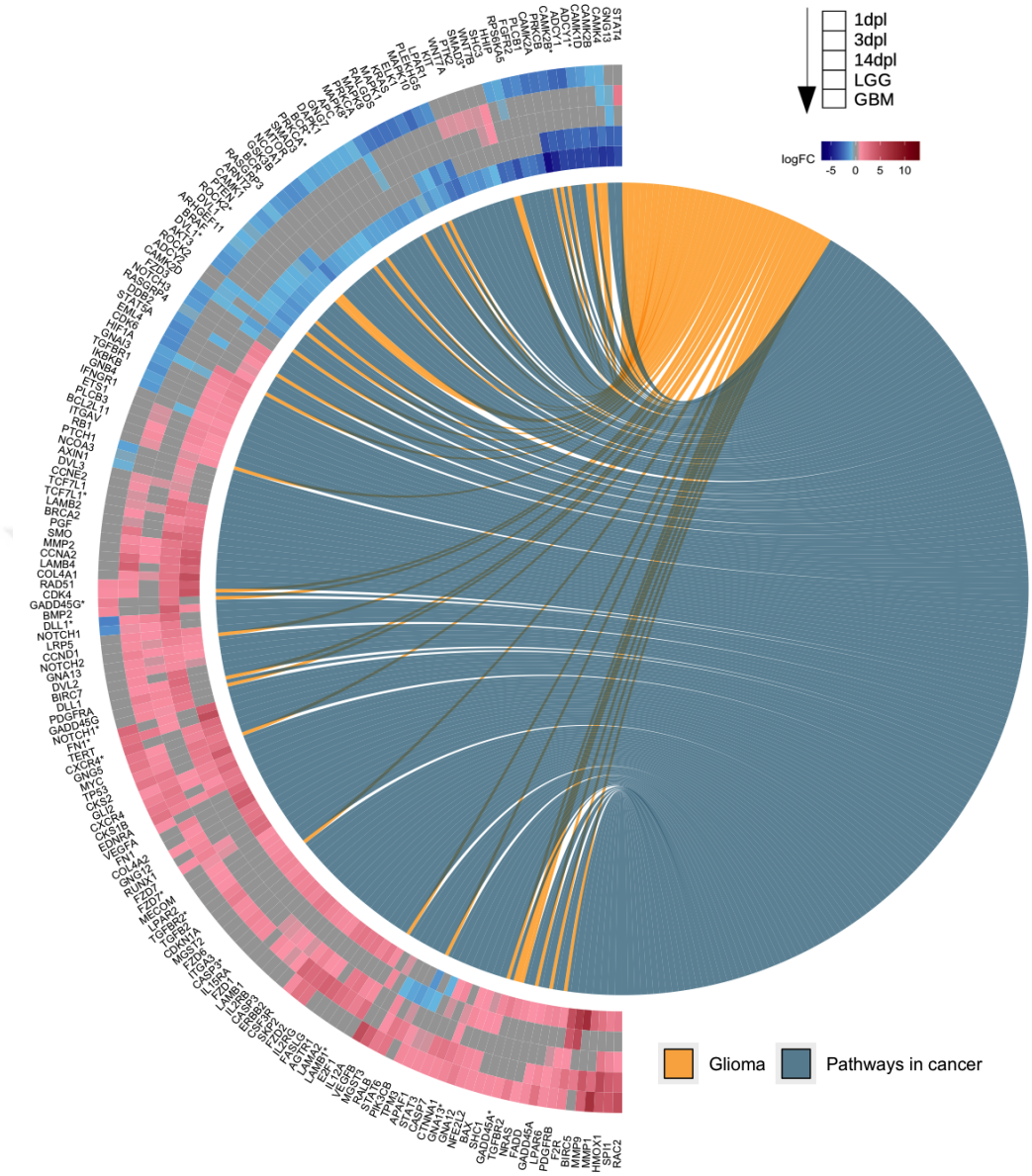

Figure 51. Chord plot shows log_2 fold changes of the genes annotated in selected KEGG pathways (Glioma and Pathways in cancer) for three stages of the zebrafish brain regeneration and two different types of human brain cancers. The genes are linked to their assigned pathways by ribbons and ordered according to their log_2 fold change from high to low fold change, represented by a colour gradient from blue to red, respectively. log2 fold changes are shown for different conditions in this order from the outer annulus to the inner annulus: 1 dpl, 3 dpl, 14 dpl, LGG and GBM. For human genes associated as orthologs to several zebrafish genes in the list, an asterisk (*) was appended to human gene name.

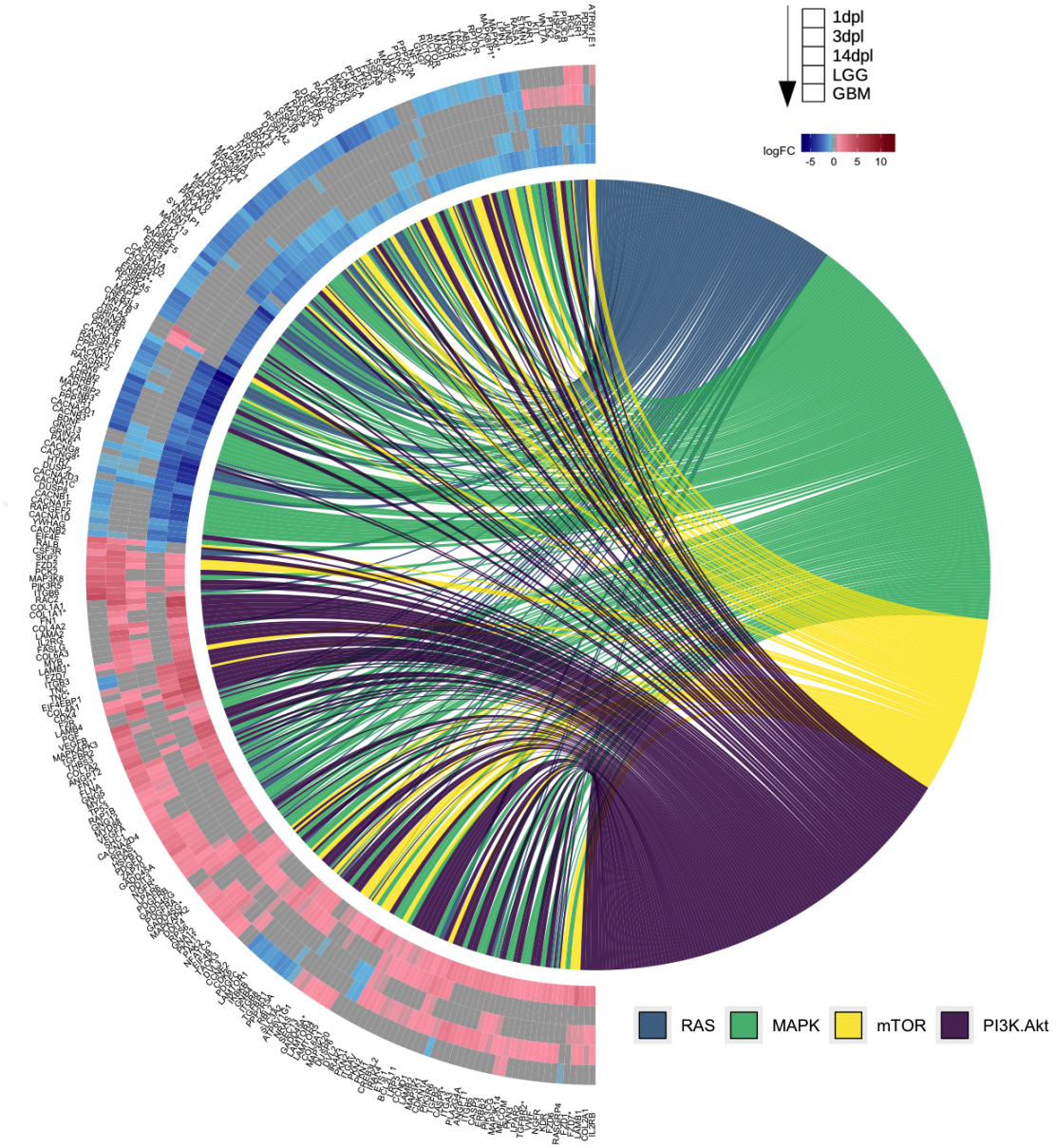

Figure 52. Chord plot shows log_2 fold changes of the genes annotated in selected KEGG pathways (RAS, MAPK, mTOR and PI3K-Akt pathways) for three stages of the zebrafish brain regeneration and two different types of human brain cancers. The genes are linked to their assigned pathways by ribbons and ordered according to their log_2 fold change from high to low fold change, represented by a colour gradient from blue to red, respectively. log_2 fold changes are shown for different conditions in this order from the outer annulus to the inner annulus: 1 dpl, 3 dpl, 14 dpl, LGG and GBM. For human genes associated as orthologs to several zebrafish genes in the list, an asterisk (*) was appended to human gene name.

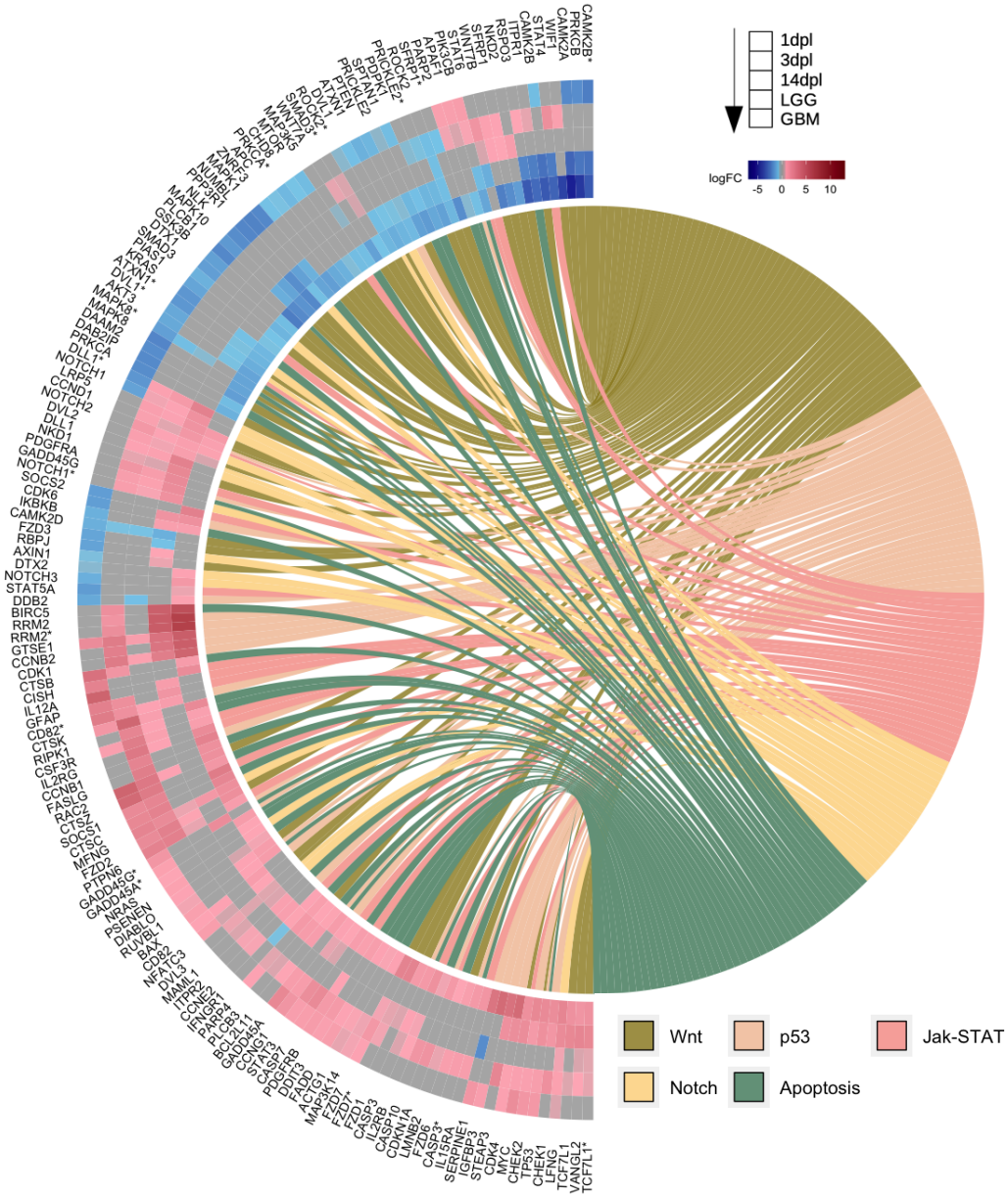

Figure 53. Chord plot shows log_2 fold changes of the genes annotated in selected KEGG pathways (Wnt signaling, p53 signaling, Jak-STAT signaling, Apoptosis and Notch signaling pathways) for three stages of the zebrafish brain regeneration and two different types of human brain cancers. The genes are linked to their assigned pathways by ribbons and ordered according to their log_2 fold change from high to low fold change, represented by a colour gradient from blue to red, respectively. log_2 fold changes are shown for different conditions in this order from the outer annulus to the inner annulus: 1 dpl, 3 dpl, 14 dpl, LGG and GBM. For human genes associated as orthologs to several zebrafish genes in the list, an asterisk (*) was appended to human gene name.

Interestingly, most DEGs of the early wound healing stage of the zebrafish brain regeneration, except a small number of genes, showed the similar expression pattern with two types of human brain cancers, but mostly with GBM. In general, if a gene is upregulated in early wound healing stage, it is generally upregulated in brain cancers, and similarly for downregulated genes (Figure 50).

The genes obtained from the KEGG database included substantial numbers of genes involved in Glioma, Pathways in cancer, RAS, MAPK, mTOR, PI3K-Akt, Wnt, p53, Jak-STAT, apoptosis and Notch signaling pathways (Figures 51 - 53). In order to compare the changes in gene expression associated with these selected pathways during three regenerative stages and two human brain cancers, the genes annotated in these pathways were intersected with DEG sets. The number of significantly altered genes in early wound healing stage were decreased at early proliferative and differentiation stage for all pathways. Interestingly, the DEGs tested in early wound healing stage showed similar expression pattern with LGG but mostly GBM (Figures 51-53). While most Wnt signaling pathway-related genes were downregulated or absent across DEG sets, p53 signaling pathway-related genes were mainly upregulated or absent across DEG sets (Figure 53). Expression of some of the Pathways in cancer genes, such as *PTK2, KIT, LPAR1, NOTCH1, NOTCH3, RASGRP4, IFNGR1, PTCH1, NCOA3, PIK3CB, TPM3, APAF1* and *DLL1*, and Wnt pathway-related genes, such as *WIF1, RSPO3, NKD2, SFRP1, SMAD3, WNT7A, WNT7B*, and *AXIN1*, showed opposite expression pattern between brain regeneration and brain cancers (Figures 51, 53).

5. DISCUSSION

Although there are several studies searching the common and distinct molecular mechanisms underlying brain regeneration and brain cancers, the way how both processes are elaborately controlled at the level of gene expression has been overlooked. This is the first study that unravels gene expression patterns of the regenerating adult zebrafish telencephalon at two early stages and one relatively late stage: 1 dpl, which corresponds to the early wound healing stage; 3 dpl, which is the early proliferative stage; and 14 dpl, which is the differentiation stage. Also, this is the first study that compares gene expression profiles of the three different stages of regenerating adult zebrafish telencephalon with two different brain cancers: low-grade glioma (LGG) and glioblastoma (GBM).

Quality of the novel adult brain regeneration data was inspected throughout several steps of the RNA-Seq analysis pipeline. Overall, the data had an appropriate quality to carry on downstream analyses, such as differential expression analysis. Overall, results showed that the total number of DEGs at early wound healing stage is far higher than at early proliferative and differentiation stages. The number of DEGs gradually decreased as a result of tissue healing. Finally, the stage at which the least genes were differentially expressed was 14 dpl.

Tissue regeneration follows a route starting with injury-induced initiation of regeneration events. Tissue loss including blood vessels, wound closure and immune response are involved in the early phases of the regeneration process (Marques et al., 2019). Furthermore, as a consequence of inflammation and bleeding, the lesion site is infiltrated by platelets and immune cells (Krafts, 2010; Kroehne et al., 2011; Marques et al., 2019). Platelet-derived growth factors (PDGFs) are potential inducers for mesenchymal-based cells. It has been shown that crucial cell types that are required for tissue regeneration, such as fibroblasts, macrophages and monocytes are induced by PDGFs for proliferation, chemotaxis and gene expression (Andrae et al., 2008; Krafts, 2010; Pierce et al., 1991). Research indicated that PDGFs are important for myelin regeneration in CNS by stimulating the proliferation, differentiation and survival of cells in the oligodendroglial lineage (Webster, 1997). The results of this study confirmed that a significant upregulation of platelet-derived growth factor genes, such as *pdgfaa, pdgfd, pdgfrb*, at both early stages and platelet/endothelial cell adhesion molecule *pecam1* at all stages.

Besides growth factors, cytokines secreted by cells of the immune system, also include essential signals during tissue regeneration. They act as immunomodulators to regulate the

acute inflammatory response that is necessary for functional regeneration of the zebrafish CNS after injury (Elsaeidi et al., 2014; Fuller-Carter et al., 2015; Krafts, 2010; Kyritsis et al., 2012; Tsarouchas et al., 2018). Results showed that several anti-inflammatory cytokines, *il6st, il11a, il11b, il13* and *il21* (at both early stages)*, il4* (at early wound healing stage)*, il6* (at early proliferative stage), were significantly upregulated during early brain regeneration. Tumour necrosis factor superfamily (TNFSF) genes acting as cytokines, and its receptor superfamily (TNFSRF) genes are expressed mainly by immune cells and regulates several functions in the CNS, such as neuroinflammation and autoimmunity (Sonar & Lal, 2015). Several TNFSF and TNFRSF genes, such as *tnfb, tnfsf10, tnfsf12, tnfrsf11a, tnfsf13b*, *tnfrsf9a* and *tnfrsf1a*, were significantly upregulated at both early stages, whereas *tnfsf13* and *tnfrsfa* were upregulated at early proliferative stage only. Although several TNFSF and TNFRSF genes had their expression significantly altered during the differentiation stage, their numbers were far less than in the early stages. Chemokines and their receptors, play key roles in activation and infiltration of the cells to the wound site and regulate regeneration of several tissues in zebrafish (Bussmann & Raz, 2015; Kizil, Dudczig, et al., 2012; Xu et al., 2014). Remarkably, a significant upregulation of chemokines and related genes, including *cxcl20, cxcl11.5, ccl39.2, cxcl11.6, ccl19a.1, ccl36.1*, was observed at early proliferative stage of brain regeneration. Overall, the results suggest that this early response of cytokines and chemokines is essential to the regulation of the innate immune response (Kizil, Dudczig, et al., 2012; Opal & DePalo, 2000; Placke et al., 2010).

Apoptosis is also one of the most prominent events that are activated in the early phases of brain regeneration for effective wound healing (Wilson et al., 2007). Results showed significant upregulation of the apoptosis-related genes *tp53, apaf1, caspa, casp7, baxa,* and *baxb* at both early stages. Whereas the expression of *asp3b, casp8l2, nradd, bcl2a, bcl2l11, cd40, tgfb2, traf2b, traf6,* and *bmp10* increased uniquely at early proliferative stage, the expression of genes such as *sgk1, bcl2l10,* and *bmp2b*, increased only at early wound healing stage of brain regeneration. Apoptosis is considered to have a critical role in solving inflammation by converting the immune response in early stages of tissue repair into a wound healing response (Brown et al., 1997; Wu & Chen, 2014). The capability of zebrafish telencephalon to convert an early inflammatory reaction into a healing capacity could be underpinned by parallel increasing in gene expression levels associated with cytokine signaling and apoptosis at early wound healing stage, corroborating the early wound healing stage as an

important stage of telencephalon regeneration (Demirci et al., 2020). Angiogenic sprouting into the wound site has been shown as another essential event of the regeneration process, which occurs 15 hours after injury during heart regeneration in zebrafish (Marín-Juez et al., 2016). It has been shown that vascular endothelial growth factor a-a (*vegfaa*) gene, an important regulator of angiogenesis, is upregulated during heart regeneration of zebrafish (Marín-Juez et al., 2016). According to results, *vegfaa* was upregulated specifically at early wound healing stage, showing that injury triggers a rapid angiogenic sprouting at early brain regeneration. Angiopoietin-1 (*angpt1*) has been shown essential to mouse vasculature during response to injury (Jeansson et al., 2011). Upregulated *angpt1* gene was observed at early proliferative and differentiation stages of the zebrafish brain regeneration.

In brain regeneration, injury-induced proliferation is one of the main molecular events and it is regulated by radial glial cells (RGCs) (Ghosh & Hui, 2016). Glial fibrillary acidic protein (*gfap*), a neuroregeneration marker, is expressed by radial astrocytes (Jurisch-Yaksi et al., 2020) giving rise to new neurons during adult neurogenesis (Ghosh & Hui, 2016). Results showed that the expression of *gfap* increased during both early stages. As a proliferation marker, *pcna* (proliferating cell nuclear antigen) is released by actively dividing cells as an indicator of neural stem cells (NSCs) (Zacchetti et al., 2003), and is remarkably upregulated at both early stages. Also, *mki6* and *mcm2* (J. Zhang & Jiao, 2015), two cell cycle-related genes used as markers of dividing cells, were upregulated significantly during the regeneration process at both early and late stages. It was also shown that while some quiescent RGC genes such as *s100b* (Kaslin et al., 2017; Lange et al., 2020) were upregulated at both early stages, *fabp7a* (Lange et al., 2020) was upregulated only at early proliferative stage. Also, several adult neurogenesis markers were identified as upregulated at different stages. A neuron differentiation marker, *neurod2* (J. Zhang & Jiao, 2015), was expressed at later stages of neurogenesis, and upregulated significantly at early proliferative stage and differentiation stage.

Comparison of two different cancer types with the three stages of brain regeneration showed that the numbers of shared and unshared DEGs detected in each comparison were determined the highest between early wound healing stage of regeneration and GBM, perhaps as a consequence of the total DEG numbers being highest at this stage of regeneration and in GBM. Interestingly, shared genes between early wound healing stage and both LGG and GBM were enriched in glioma KEGG pathway showing its similarity with LGG and GBM.

Expression of several glioma/glioblastoma-related genes has also been altered in adult zebrafish brain regeneration. Since the minichromosome maintenance (MCMs) family genes are involved in initiation of the DNA replication, they are considered as potential markers for proliferating cells (Schrader et al., 2005). High expression of MCM genes (MCM2-7 and MCM10) has been previously shown in precancerous cells, cancer cells, and also recurrent tumours (Alison et al., 2002; Freeman et al., 1999; Going, 2002; Hunt et al., 2002; Ishimi et al., 2003; H. Mao et al., 2012; Meng et al., 2001; Ramnath et al., 2001; Rodins et al., 2002). Furthermore, since their high expression has been also associated with glioma tumour grade, they might be used as potential prognostic markers for glioma. Among these genes, overexpression of MCM2, MCM3 and MCM7 is correlated with weak prognosis and glioma tumour progression (Erkan et al., 2014; Hua et al., 2014). Expression of several MCMs (*MCM2-MCM8*, and *MCM10*) was significantly increased in both brain cancers and brain regeneration. A recent study showed that overexpression of Annexin A2 (ANXA2) raised the expression of Glypican 1 (GPC1) gene through MYC, creating a positive feedback loop, which increases the proliferation of glioma cells (Xin Li et al., 2021). *ANXA2*, and *MYC* expression increased at two early regeneration stages and GBM. Interestingly, *GPC1* expression decreased at early wound healing stage but it did not test positive for differential expression at early proliferative stage.

Stem-like cells, (GSCs), a highly tumorigenic cell group in GBMs (Hemmati et al., 2003; Singh et al., 2004) are in charge of progression, resistance to traditional treatment, and recurrence of glioma (Bao et al., 2006; Chen et al., 2012; Gilbert & Ross, 2009; Zhou et al., 2009). The sustainability of GSCs and progression of glioma rely on the EZH2 (Enhancer of Zeste 2 Polycomb Repressive Complex 2 Subunit) gene. Research suggests that STAT3 (signal transducer and activator of transcription 3) is also a key player for propagation and sustainability of multipotency in glioblastoma stem cells (GBM-SCs) (Rahaman et al., 2002; Sherry et al., 2009). EZH2-STAT3 interaction has been shown in GSCs by knock down of EZH2 using shRNA causing reduced expression of STAT3 via decreasing H3K27 trimethylation (E. Kim et al., 2013). It has also been shown that expression of *EZH2* gene was crucial for proliferation of progenitor cells in hippocampal and cortical neurogenesis in mice (Pereira et al., 2010; J. Zhang et al., 2014). According to the results, expression of *EZH2* and *STAT3* genes have been found remarkably increased, not only in both LGG and GBM, but also at early wound healing stage.

Expression of several genes related with apoptosis, proliferation, angiogenesis and invasion showed opposite directions of change between stages of the zebrafish brain regeneration and human brain cancers. These genes can serve as potential targets. Suppression of SOX7 (SRY-related HMG-box 7), a transcription factor which also acts as a tumour suppressor gene (Liu et al., 2014; T. Zhao et al., 2016), has been demonstrated in several cancers (Chan et al., 2012; Guo et al., 2008; Hayano et al., 2013; Katoh, 2002; Stovall et al., 2013; Y. Zhang et al., 2009; Zhong et al., 2012) and its downregulation has been associated with poor prognosis (Oh et al., 2017; Stovall et al., 2013). Results showed that *SOX7* expression was decreased in LGG and GBM cancers, confirming previous studies, but interestingly it was only increased at early wound healing stage, but not at other stages of brain regeneration. Similarly, APAF1 (Apoptosis protease-activating factor-1), as a marker of tumour progression, has been found downregulated in many cancer types (Soengas et al., 2006; Tanase et al., 2014). Results showed that, whereas expression of the *APAF1* gene was decreased in GBM, its expression increased at both early stages of brain regeneration. Hypoxia and its main regulator HIF-1 (hypoxia inducible factor 1) are important elements in the invasion of glioma. HIF-1 can also induce angiogenesis by regulating the expression of VEGF, PDGFβ, and PGF (Méndez et al., 2010). According to the results, while expression of *HIF-1* gene was increased in both LGG and GBM as a result of hypoxia, its expression was decreased in all three stages of brain regeneration. CDK6 gene, a cyclin-dependent kinase, having essential roles in regulation of cell-cycle progression, has been shown upregulated in glioma cells, and the upregulation of CDK6 has been linked with the malignancy of the glioma (Lu, 2012). Similarly to HIF-1 gene, *CDK6* expression has been detected as upregulated in both LGG and GBM. Curiously, its expression level is decreased at the early wound healing stage of zebrafish brain regeneration.

6. CONCLUSIONS AND FUTURE DIRECTIONS

In conclusion, this comparative transcriptome analysis of the three stages of the adult zebrafish brain regeneration and two different types of the human brain cancers uncovers the shared significantly altered genes and pathways regulating zebrafish brain regeneration and human brain cancers. Treatments and outcomes of the brain cancers have remained stable for over four decades, resulting in a growing burden for humanity, and the development of new approaches and therapies is required. The results of this study will be able to contribute to the literature as a resource comparing regeneration and cancer at the whole transcriptome level for the first time and it can also contribute to the development of new approaches for treatment of brain cancers.

As for future aspects, a comprehensive transcriptome analysis of zebrafish glioma/glioblastoma, along with zebrafish brain regeneration and human glioma/glioblastoma could help unravelling similarities and differences between these two phenomena at a more detailed resolution. Targeting of selected candidate genes or pathways by genetic manipulation techniques or by using potential drug candidates in cell cultures or in animal models could redirect the glioma/glioblastoma to a regeneration-like state, making possible the discovery of new treatments for glioma/glioblastoma.

7. REFERENCES

Agata, K., & Watanabe, K. (1999). Molecular and cellular aspects of planarian regeneration. *Seminars in Cell & Developmental Biology*, *10*(4), 377–383. https://doi.org/10.1006/scdb.1999.0324

Agnihotri, S., Burrell, K. E., Wolf, A., Jalali, S., Hawkins, C., Rutka, J. T., & Zadeh, G. (2013). Glioblastoma, a brief review of history, molecular genetics, animal models and novel therapeutic strategies. *Archivum Immunologiae et Therapiae Experimentalis*, *61*(1), 25–41. https://doi.org/10.1007/s00005-012-0203-0

Alison, M. R., Hunt, T., & Forbes, S. J. (2002). Minichromosome maintenance (MCM) proteins may be pre-cancer markers. *Gut*, *50*(3), 290–291. https://doi.org/10.1136/gut.50.3.290

Alvarado, A. S., & Tsonis, P. A. (2006). Bridging the regeneration gap: genetic insights from diverse animal models. *Nature Reviews Genetics*, *7*(11), 873–884. https://doi.org/10.1038/nrg1923

Alvarez-Buylla, A., García-Verdugo, J. M., & Tramontin, A. D. (2001). A unified hypothesis on the lineage of neural stem cells. *Nature Reviews Neuroscience*, *2*(4), 287–293. https://doi.org/10.1038/35067582

Anders, S., Pyl, P. T., & Huber, W. (2015). HTSeq--a Python framework to work with high-throughput sequencing data. *Bioinformatics (Oxford, England)*, *31*(2), 166–169. https://doi.org/10.1093/bioinformatics/btu638

Anderson, M. A., Burda, J. E., Ren, Y., Ao, Y., O'Shea, T. M., Kawaguchi, R., Coppola, G., Khakh, B. S., Deming, T. J., & Sofroniew, M. V. (2016). Astrocyte scar formation aids central nervous system axon regeneration. *Nature*, *532*(7598), 195–200. https://doi.org/10.1038/nature17623

Andrae, J., Gallini, R., & Betsholtz, C. (2008). Role of platelet-derived growth factors in physiology and medicine. *Genes & Development*, *22*(10), 1276–1312. https://doi.org/10.1101/gad.1653708

Andrew, S. (2010). *A quality control tool for high throughput sequence data* (p. 391).

Ansari, M., Nasrolahi, H., Kani, A.-A., Mohammadianpanah, M., Ahmadloo, N., Omidvari, S., & Mosalaei, A. (2012). Pediatric glioblastoma multiforme: A single-institution experience. *Indian Journal of Medical and Paediatric Oncology: Official Journal of Indian Society of Medical & Paediatric Oncology*, *33*(3), 155–160. https://doi.org/10.4103/0971-5851.103142

Antos, C. L., & Tanaka, E. M. (2010). *Vertebrates that regenerate as models for guiding stem cells* (pp. 184–214). https://doi.org/10.1007/978-1-4419-7037-4_13

Bao, S., Wu, Q., McLendon, R. E., Hao, Y., Shi, Q., Hjelmeland, A. B., Dewhirst, M. W., Bigner, D. D., & Rich, J. N. (2006). Glioma stem cells promote radioresistance by preferential activation of the DNA damage response. *Nature*, *444*(7120), 756–760. https://doi.org/10.1038/nature05236

Barnett, S. C., Robertson, L., Graham, D., Allan, D., & Rampling, R. (1998). Oligodendrocyte-type-2 astrocyte (O-2A) progenitor cells transformed with c-myc and H-ras form high-grade glioma after stereotactic injection into the rat brain. *Carcinogenesis*, *19*(9), 1529–1537. https://doi.org/10.1093/carcin/19.9.1529

Baruzzo, G., Hayer, K. E., Kim, E. J., Di Camillo, B., FitzGerald, G. A., & Grant, G. R. (2017). Simulation-based comprehensive benchmarking of RNA-seq aligners. *Nature Methods*, *14*(2), 135–139. https://doi.org/10.1038/nmeth.4106

Baumgart, E. V., Barbosa, J. S., Bally-cuif, L., Götz, M., & Ninkovic, J. (2012). Stab wound injury of the zebrafish telencephalon: A model for comparative analysis of reactive gliosis. *Glia*, *60*(3), 343–357. https://doi.org/10.1002/glia.22269

Beachy, P. A., Karhadkar, S. S., & Berman, D. M. (2004). Tissue repair and stem cell renewal in carcinogenesis. *Nature*, *432*(7015), 324–331. https://doi.org/10.1038/nature03100

Becker, C. G., & Becker, T. (2002). Repellent guidance of regenerating optic axons by chondroitin sulfate glycosaminoglycans in zebrafish. *The Journal of Neuroscience*, *22*(3), 842–853. https://doi.org/10.1523/JNEUROSCI.22-03-00842.2002

Bernardos, R. L., Barthel, L. K., Meyers, J. R., & Raymond, P. A. (2007). Late-stage neuronal progenitors in the retina are radial muller glia that function as retinal stem cells. *Journal of Neuroscience*, *27*(26), 7028–7040. https://doi.org/10.1523/JNEUROSCI.1624-07.2007

Best, J. B., & Morita, M. (1982). Planarians as a model system for in vitro teratogenesis studies. *Teratogenesis, Carcinogenesis, and Mutagenesis*, *2*(3–4), 277–291. https://doi.org/10.1002/1520-6866(1990)2:3/4<277::aid-tcm1770020309>3.0.co;2-8

Boffetta, P., Boccia, S., & La Vecchia, C. (2014). *A quick guide to cancer epidemiology*. Springer International Publishing. https://doi.org/10.1007/978-3-319-05068-3

Bond, A. M., Ming, G.-L., & Song, H. (2015). Adult mammalian neural stem cells and neurogenesis: five decades later. *Cell Stem Cell*, *17*(4), 385–395. https://doi.org/10.1016/j.stem.2015.09.003

Bondy, M. L., Scheurer, M. E., Malmer, B., Barnholtz-Sloan, J. S., Davis, F. G., Il'yasova, D., Kruchko, C., McCarthy, B. J., Rajaraman, P., Schwartzbaum, J. A., Sadetzki, S., Schlehofer, B., Tihan, T., Wiemels, J. L., Wrensch, M., Buffler, P. A., & Brain Tumor Epidemiology Consortium. (2008). Brain tumor epidemiology: consensus from the Brain Tumor Epidemiology Consortium. *Cancer*, *113*(7 Suppl), 1953–1968. https://doi.org/10.1002/cncr.23741

Bonfanti, L., & Peretto, P. (2011). Adult neurogenesis in mammals - a theme with many variations. *European Journal of Neuroscience*, *34*(6), 930–950. https://doi.org/10.1111/j.1460-9568.2011.07832.x

Bonnans, C., Chou, J., & Werb, Z. (2014). Remodelling the extracellular matrix in development and disease. *Nature Reviews. Molecular Cell Biology*, *15*(12), 786–801. https://doi.org/10.1038/nrm3904

Brennan, C., Momota, H., Hambardzumyan, D., Ozawa, T., Tandon, A., Pedraza, A., & Holland, E. (2009). Glioblastoma subclasses can be defined by activity among signal transduction pathways and associated genomic alterations. *PLoS ONE*, *4*(11), e7752. https://doi.org/10.1371/journal.pone.0007752

Brockes, J. (1998). Regeneration and cancer. *Biochimica et Biophysica Acta (BBA) - Reviews on Cancer*, *1377*(1), M1–M11. https://doi.org/10.1016/S0304-419X(97)00029-2

Brockes, J. P. (2005). Appendage regeneration in adult vertebrates and implications for regenerative medicine. *Science*, *310*(5756), 1919–1923. https://doi.org/10.1126/science.1115200

Brockes, Jeremy P. (1997). Amphibian limb regeneration: rebuilding a complex structure. *Science*, *276*(5309), 81–87. https://doi.org/10.1126/science.276.5309.81

Brockes, Jeremy P., & Kumar, A. (2008). Comparative aspects of animal regeneration. *Annual Review of Cell and Developmental Biology*, *24*(1), 525–549. https://doi.org/10.1146/annurev.cellbio.24.110707.175336

Brosius Lutz, A., & Barres, B. A. (2014). Contrasting the glial response to axon injury in the central and peripheral nervous systems. *Developmental Cell*, *28*(1), 7–17. https://doi.org/10.1016/j.devcel.2013.12.002

Brown, D. L., Kao, W. W.-Y., & Greenhalgh, D. G. (1997). Apoptosis down-regulates inflammation under the advancing epithelial wound edge: Delayed patterns in diabetes and improvement with topical growth factors. *Surgery*, *121*(4), 372–380. https://doi.org/10.1016/S0039-6060(97)90306-8

Bussmann, J., & Raz, E. (2015). Chemokine-guided cell migration and motility in zebrafish development. *The EMBO Journal*, *34*(10), 1309–1318. https://doi.org/10.15252/embj.201490105

Cajal, S. R. y. (1928). *Degeneration and regeneration in the nervous system*. Oxford University Press.

Chan, D. W., Mak, C. S. L., Leung, T. H. Y., Chan, K. K. L., & Ngan, H. Y. S. (2012). Down-regulation of Sox7 is associated with aberrant activation of Wnt/b-catenin signaling in endometrial cancer. *Oncotarget*, *3*(12), 1546–1556. https://doi.org/10.18632/oncotarget.667

Chang, H. Y., Sneddon, J. B., Alizadeh, A. A., Sood, R., West, R. B., Montgomery, K., Chi, J.-T., Rijn, M. van de, Botstein, D., & Brown, P. O. (2004). Gene expression signature of fibroblast serum response predicts human cancer progression: similarities between tumors and wounds. *PLoS Biology*, *2*(2), e7. https://doi.org/10.1371/journal.pbio.0020007

Chapouton, P., Jagasia, R., & Bally-Cuif, L. (2007). Adult neurogenesis in non-mammalian vertebrates. *BioEssays*, *29*(8), 745–757. https://doi.org/10.1002/bies.20615

Chapouton, P., Skupien, P., Hesl, B., Coolen, M., Moore, J. C., Madelaine, R., Kremmer, E., Faus-Kessler, T., Blader, P., Lawson, N. D., & Bally-Cuif, L. (2010). Notch activity levels control the balance between quiescence and recruitment of adult neural stem cells. *The Journal of Neuroscience: The Official Journal of the Society for Neuroscience*, *30*(23), 7961–7974. https://doi.org/10.1523/JNEUROSCI.6170-09.2010

Chen, J., Li, Y., Yu, T.-S., McKay, R. M., Burns, D. K., Kernie, S. G., & Parada, L. F. (2012). A restricted cell population propagates glioblastoma growth after chemotherapy. *Nature*, *488*(7412), 522–526. https://doi.org/10.1038/nature11287

Choi, T., Ninov, N., Stainier, D. Y. R., & Shin, D. (2014). Extensive conversion of hepatic biliary epithelial cells to hepatocytes after near total loss of hepatocytes in zebrafish. *Gastroenterology*, *146*(3), 776–788. https://doi.org/10.1053/j.gastro.2013.10.019

Claus, E. B., Bondy, M. L., Schildkraut, J. M., Wiemels, J. L., Wrensch, M., & Black, P. M. (2005). Epidemiology of intracranial meningioma. *Neurosurgery*, *57*(6), 1088–1095; discussion 1088-95. https://doi.org/10.1227/01.neu.0000188281.91351.b9

Conesa, A., Madrigal, P., Tarazona, S., Gomez-Cabrero, D., Cervera, A., McPherson, A., Szcześniak, M. W., Gaffney, D. J., Elo, L. L., Zhang, X., & Mortazavi, A. (2016). A survey of best practices for RNA-seq data analysis. *Genome Biology*, *17*(1), 13. https://doi.org/10.1186/s13059-016-0881-8

Coussens, L. M., & Werb, Z. (2002). Inflammation and cancer. *Nature*, *420*(6917), 860–867. https://doi.org/10.1038/nature01322

Crusz, S. M., & Balkwill, F. R. (2015). Inflammation and cancer: advances and new agents. *Nature Reviews Clinical Oncology*, *12*(10), 584–596. https://doi.org/10.1038/nrclinonc.2015.105

Curado, S., Anderson, R. M., Jungblut, B., Mumm, J., Schroeter, E., & Stainier, D. Y. R. (2007). Conditional targeted cell ablation in zebrafish: A new tool for regeneration studies. *Developmental Dynamics*, *236*(4), 1025–1035. https://doi.org/10.1002/dvdy.21100

Curado, S., Stainier, D. Y. R., & Anderson, R. M. (2008). Nitroreductase-mediated cell/tissue ablation in zebrafish: a spatially and temporally controlled ablation method with applications in developmental and regeneration studies. *Nature Protocols*, *3*(6), 948–954. https://doi.org/10.1038/nprot.2008.58

Dahlstrand, J., Collins, V. P., & Lendahl, U. (1992). Expression of the class VI intermediate filament nestin in human central nervous system tumors. *Cancer Research*, *52*(19), 5334–5341. http://www.ncbi.nlm.nih.gov/pubmed/1382841

Dahm, R., & Geisler, R. (2006). Learning from small fry: the zebrafish as a genetic model organism for aquaculture fish species. *Marine Biotechnology*, *8*(4), 329–345. https://doi.org/10.1007/s10126-006-5139-0

Dai, Y.-J., Jia, Y.-F., Chen, N., Bian, W.-P., Li, Q.-K., Ma, Y.-B., Chen, Y.-L., & Pei, D.-S. (2014). Zebrafish as a model system to study toxicology. *Environmental Toxicology and Chemistry*, *33*(1), 11–17. https://doi.org/10.1002/etc.2406

de Almeida Sassi, F., Lunardi Brunetto, A., Schwartsmann, G., Roesler, R., & Abujamra, A. L. (2012). Glioma revisited: from neurogenesis and cancer stem cells to the epigenetic regulation of the niche. *Journal of Oncology*, *2012*, 1–20. https://doi.org/10.1155/2012/537861

de Visser, K. E., Eichten, A., & Coussens, L. M. (2006). Paradoxical roles of the immune system during cancer development. *Nature Reviews Cancer*, *6*(1), 24–37. https://doi.org/10.1038/nrc1782

Demirci, Y., Cucun, G., Poyraz, Y. K., Mohammed, S., Heger, G., Papatheodorou, I., & Ozhan, G. (2020). Comparative transcriptome analysis of the regenerating zebrafish telencephalon unravels a resource with key pathways during two early stages and activation of Wnt/β-catenin signaling at the early wound healing stage. *Frontiers in Cell and Developmental Biology*, *8*, 584604. https://doi.org/10.3389/fcell.2020.584604

Dhaliwal, J., & Lagace, D. C. (2011). Visualization and genetic manipulation of adult neurogenesis using transgenic mice. *European Journal of Neuroscience*, *33*(6), 1025–1036. https://doi.org/10.1111/j.1460-9568.2011.07600.x

DiPietro, L. A. (2013). Angiogenesis and scar formation in healing wounds. *Current Opinion in Rheumatology*, *25*(1), 87–91. https://doi.org/10.1097/BOR.0b013e32835b13b6

DiPietro, L. A. (2016). Angiogenesis and wound repair: when enough is enough. *Journal of Leukocyte Biology*, *100*(5), 979–984. https://doi.org/10.1189/jlb.4MR0316-102R

Doetsch, F., Caillé, I., Lim, D. A., García-Verdugo, J. M., & Alvarez-Buylla, A. (1999). Subventricular zone astrocytes are neural stem cells in the adult mammalian brain. *Cell*, *97*(6), 703–716. https://doi.org/10.1016/s0092-8674(00)80783-7

Doetsch, F., & Scharff, C. (2001). Challenges for brain repair: insights from adult neurogenesis in birds and mammals. *Brain, Behavior and Evolution*, *58*(5), 306–322. https://doi.org/10.1159/000057572

Dvorak, H. F. (1986). Tumors: wounds that do not heal. Similarities between tumor stroma generation and wound healing. *The New England Journal of Medicine*, *315*(26), 1650–1659. https://doi.org/10.1056/NEJM198612253152606

Ekdahl, C. T., Claasen, J.-H., Bonde, S., Kokaia, Z., & Lindvall, O. (2003). Inflammation is detrimental for neurogenesis in adult brain. *Proceedings of the National Academy of Sciences*, *100*(23), 13632–13637. https://doi.org/10.1073/pnas.2234031100

Elsaeidi, F., Bemben, M. A., Zhao, X.-F., & Goldman, D. (2014). Jak/Stat signaling stimulates zebrafish optic nerve regeneration and overcomes the inhibitory actions of Socs3 and Sfpq. *Journal of Neuroscience*, *34*(7), 2632–2644. https://doi.org/10.1523/JNEUROSCI.3898-13.2014

Erkan, E. P., Ströbel, T., Lewandrowski, G., Tannous, B., Madlener, S., Czech, T., Saydam, N., & Saydam, O. (2014). Depletion of minichromosome maintenance protein 7 inhibits glioblastoma multiforme tumor growth in vivo. *Oncogene*, *33*(39), 4778–4785. https://doi.org/10.1038/onc.2013.423

Ewels, P., Magnusson, M., Lundin, S., & Käller, M. (2016). MultiQC: summarize analysis results for multiple tools and samples in a single report. *Bioinformatics*, *32*(19), 3047–3048. https://doi.org/10.1093/bioinformatics/btw354

Faijerson, J., Tinsley, R. B., Apricó, K., Thorsell, A., Nodin, C., Nilsson, M., Blomstrand, F., & Eriksson, P. S. (2006). Reactive astrogliosis induces astrocytic differentiation of adult neural stem/progenitor cells in vitro. *Journal of Neuroscience Research*, *84*(7), 1415–1424. https://doi.org/10.1002/jnr.21044

Fernandes, C., Costa, A., Osório, L., Lago, R. C., Linhares, P., Carvalho, B., & Caeiro, C. (2017). Current standards of care in glioblastoma therapy. In *Glioblastoma*. http://www.ncbi.nlm.nih.gov/pubmed/29251860

Fitch, M. T., & Silver, J. (2008). CNS injury, glial scars, and inflammation: Inhibitory extracellular matrices and regeneration failure. *Experimental Neurology*, *209*(2), 294–301. https://doi.org/10.1016/j.expneurol.2007.05.014

Fleisch, V. C., Fraser, B., & Allison, W. T. (2011). Investigating regeneration and functional integration of CNS neurons: Lessons from zebrafish genetics and other fish species. *Biochimica et Biophysica Acta (BBA) - Molecular Basis of Disease*, *1812*(3), 364–380. https://doi.org/10.1016/j.bbadis.2010.10.012

Foster, J. A. (1963). Induction of neoplasms in planarians with carcinogens. *Cancer Research*, *23*, 300–303. http://www.ncbi.nlm.nih.gov/pubmed/13958897

Foster, J. A. (1969). Malformations and lethal growths in planaria treated with carcinogens. *National Cancer Institute Monograph*, *31*, 683–691. http://www.ncbi.nlm.nih.gov/pubmed/5374700

Franceschi, E., Minichillo, S., & Brandes, A. A. (2017). Pharmacotherapy of glioblastoma: established treatments and emerging concepts. *CNS Drugs*, *31*(8), 675–684. https://doi.org/10.1007/s40263-017-0454-8

Frazee, A. C., Pertea, G., Jaffe, A. E., Langmead, B., Salzberg, S. L., & Leek, J. T. (2015). Ballgown bridges the gap between transcriptome assembly and expression analysis. *Nature Biotechnology*, *33*(3), 243–246. https://doi.org/10.1038/nbt.3172

Freeman, A., Morris, L. S., Mills, A. D., Stoeber, K., Laskey, R. A., Williams, G. H., & Coleman, N. (1999). Minichromosome maintenance proteins as biological markers of dysplasia and malignancy. *Clinical Cancer Research: An Official Journal of the American Association for Cancer Research*, *5*(8), 2121–2132. http://www.ncbi.nlm.nih.gov/pubmed/10473096

Fukunaga-Kalabis, M., Martinez, G., Nguyen, T. K., Kim, D., Santiago-Walker, A., Roesch, A., & Herlyn, M. (2010). Tenascin-C promotes melanoma progression by maintaining the ABCB5-positive side population. *Oncogene*, *29*(46), 6115–6124. https://doi.org/10.1038/onc.2010.350

Fuller-Carter, P. I., Carter, K. W., Anderson, D., Harvey, A. R., Giles, K. M., & Rodger, J. (2015). Integrated analyses of zebrafish miRNA and mRNA expression profiles identify miR-29b and miR-223 as potential regulators of optic nerve regeneration. *BMC Genomics*, *16*(1), 591. https://doi.org/10.1186/s12864-015-1772-1

Gage, F. H. (2000). Mammalian Neural Stem Cells. *Science*, *287*(5457), 1433–1438. https://doi.org/10.1126/science.287.5457.1433

Ganz, J., Kaslin, J., Hochmann, S., Freudenreich, D., & Brand, M. (2010). Heterogeneity and Fgf dependence of adult neural progenitors in the zebrafish telencephalon. *Glia*, *58*(11), 1345–1363. https://doi.org/10.1002/glia.21012

García-Alcalde, F., Okonechnikov, K., Carbonell, J., Cruz, L. M., Götz, S., Tarazona, S., Dopazo, J., Meyer, T. F., & Conesa, A. (2012). Qualimap: evaluating next-generation sequencing alignment data. *Bioinformatics (Oxford, England)*, *28*(20), 2678–2679. https://doi.org/10.1093/bioinformatics/bts503

Gemberling, M., Bailey, T. J., Hyde, D. R., & Poss, K. D. (2013). The zebrafish as a model for complex tissue regeneration. *Trends in Genetics*, *29*(11), 611–620. https://doi.org/10.1016/j.tig.2013.07.003

Geurtzen, K., Knopf, F., Wehner, D., Huitema, L. F. A., Schulte-Merker, S., & Weidinger, G. (2014). Mature osteoblasts dedifferentiate in response to traumatic bone injury in the zebrafish fin and skull. *Development*, *141*(11), 2225–2234. https://doi.org/10.1242/dev.105817

Ghosh, S., & Hui, S. P. (2016). Regeneration of zebrafish CNS: adult neurogenesis. *Neural Plasticity*, *2016*, 1–21. https://doi.org/10.1155/2016/5815439

Gilbert, C. A., & Ross, A. H. (2009). Cancer stem cells: cell culture, markers, and targets for new therapies. *Journal of Cellular Biochemistry*, *108*(5), 1031–1038. https://doi.org/10.1002/jcb.22350

Going, J. J. (2002). Aberrant expression of minichromosome maintenance proteins 2 and 5, and Ki-67 in dysplastic squamous oesophageal epithelium and Barrett's mucosa. *Gut*, *50*(3), 373–377. https://doi.org/10.1136/gut.50.3.373

González-Granero, S., Lezameta, M., & García-Verdugo, J. (2011). *Neurogenesis in the adult brain I* (T. Seki, K. Sawamoto, J. M. Parent, & A. Alvarez-Buylla (Eds.)). Springer Japan. https://doi.org/10.1007/978-4-431-53933-9

González-Rosa, J. M., Peralta, M., & Mercader, N. (2012). Pan-epicardial lineage tracing reveals that epicardium derived cells give rise to myofibroblasts and perivascular cells during zebrafish heart regeneration. *Developmental Biology*, *370*(2), 173–186. https://doi.org/10.1016/j.ydbio.2012.07.007

Grandel, H., & Brand, M. (2013). Comparative aspects of adult neural stem cell activity in vertebrates. *Development Genes and Evolution*, *223*(1–2), 131–147. https://doi.org/10.1007/s00427-012-0425-5

Grandel, H., Kaslin, J., Ganz, J., Wenzel, I., & Brand, M. (2006). Neural stem cells and neurogenesis in the adult zebrafish brain: Origin, proliferation dynamics, migration and cell fate. *Developmental Biology*, *295*(1), 263–277. https://doi.org/10.1016/j.ydbio.2006.03.040

Guo, L., Zhong, D., Lau, S., Liu, X., Dong, X.-Y., Sun, X., Yang, V. W., Vertino, P. M., Moreno, C. S., Varma, V., Dong, J.-T., & Zhou, W. (2008). Sox7 Is an independent checkpoint for beta-catenin function in prostate and colon epithelial cells. *Molecular Cancer Research: MCR*, *6*(9), 1421–1430. https://doi.org/10.1158/1541-7786.MCR-07-2175

Gurtner, G. C., Werner, S., Barrandon, Y., & Longaker, M. T. (2008). Wound repair and regeneration. *Nature*, *453*(7193), 314–321. https://doi.org/10.1038/nature07039

Haddow, A. (1972). Molecular repair, wound healing, and carcinogenesis: tumor production a possible overhealing? *Advances in Cancer Research*, *16*, 181–234. https://doi.org/10.1016/s0065-230x(08)60341-3

Hagedorn, M., Siegfried, G., Hooks, K. B., & Khatib, A.-M. (2016). Integration of zebrafish fin regeneration genes with expression data of human tumors in silico uncovers potential novel melanoma markers. *Oncotarget*, *7*(44), 71567–71579. https://doi.org/10.18632/oncotarget.12257

Hall, F., Morita, M., & Best, J. B. (1986). Neoplastic transformation in the planarian: II. Ultrastructure of malignant reticuloma. *Journal of Experimental Zoology*, *240*(2), 229–244. https://doi.org/10.1002/jez.1402400210

Hanif, F., Muzaffar, K., Perveen, K., Malhi, S. M., & Simjee, S. U. (2017). Glioblastoma multiforme: A review of its epidemiology and pathogenesis through clinical presentation and treatment. *Asian Pacific Journal of Cancer Prevention: APJCP*, *18*(1), 3–9. https://doi.org/10.22034/APJCP.2017.18.1.3

Hata, S., Namae, M., & Nishina, H. (2007). Liver development and regeneration: From laboratory study to clinical therapy. *Development, Growth & Differentiation*, *49*(2), 163–170. https://doi.org/10.1111/j.1440-169X.2007.00910.x

Hayano, T., Garg, M., Yin, D., Sudo, M., Kawamata, N., Shi, S., Chien, W., Ding, L.-W., Leong, G., Mori, S., Xie, D., Tan, P., & Koeffler, H. P. (2013). SOX7 is downregulated in lung cancer. *Journal of Experimental & Clinical Cancer Research: CR*, *32*, 17. https://doi.org/10.1186/1756-9966-32-17

He, J., Lu, H., Zou, Q., & Luo, L. (2014). Regeneration of liver after extreme hepatocyte loss occurs mainly via biliary transdifferentiation in zebrafish. *Gastroenterology*, *146*(3), 789-800.e8. https://doi.org/10.1053/j.gastro.2013.11.045

Hemmati, H. D., Nakano, I., Lazareff, J. A., Masterman-Smith, M., Geschwind, D. H., Bronner-Fraser, M., & Kornblum, H. I. (2003). Cancerous stem cells can arise from pediatric brain tumors. *Proceedings of the National Academy of Sciences of the United States of America*, *100*(25), 15178–15183. https://doi.org/10.1073/pnas.2036535100

Hill, D. A., Inskip, P. D., Shapiro, W. R., Selker, R. G., Fine, H. A., Black, P. M., & Linet, M. S. (2003). Cancer in first-degree relatives and risk of glioma in adults. *Cancer Epidemiology, Biomarkers & Prevention: A Publication of the American Association for Cancer Research, Cosponsored by the American Society of Preventive Oncology*, *12*(12), 1443–1448. http://www.ncbi.nlm.nih.gov/pubmed/14693735

Holland, E. C., Celestino, J., Dai, C., Schaefer, L., Sawaya, R. E., & Fuller, G. N. (2000). Combined activation of Ras and Akt in neural progenitors induces glioblastoma formation in mice. *Nature Genetics*, *25*(1), 55–57. https://doi.org/10.1038/75596

Howe, K., Clark, M. D., Torroja, C. F., Torrance, J., Berthelot, C., Muffato, M., Collins, J. E., Humphray, S., McLaren, K., Matthews, L., McLaren, S., Sealy, I., Caccamo, M., Churcher, C., Scott, C., Barrett, J. C., Koch, R., Rauch, G.-J., White, S., … Stemple, D. L. (2013). The zebrafish reference genome sequence and its relationship to the human genome. *Nature*, *496*(7446), 498–503. https://doi.org/10.1038/nature12111

https://hbctraining.github.io/DGE_workshop/lessons/04_DGE_DESeq2_analysis.html. (2021).

https://portal.gdc.cancer.gov. (2020).

https://rtsf.natsci.msu.edu/genomics/tech-notes/fastqc-tutorial-and-faq/. (2021).

https://www.bioinformatics.babraham.ac.uk/projects/fastqc/. (2021).

https://www.ensembl.org/Danio_rerio/Info/Index. (2019).

Hu, S., & Zhu, L. (2018). Semaphorins and their receptors: from axonal guidance to atherosclerosis. *Frontiers in Physiology*, *9*. https://doi.org/10.3389/fphys.2018.01236

Hua, C., Zhao, G., Li, Y., & Bie, L. (2014). Minichromosome Maintenance (MCM) Family as potential diagnostic and prognostic tumor markers for human gliomas. *BMC Cancer*, *14*, 526. https://doi.org/10.1186/1471-2407-14-526

Huang, D. W., Sherman, B. T., & Lempicki, R. A. (2009). Systematic and integrative analysis of large gene lists using DAVID bioinformatics resources. *Nature Protocols*, *4*(1), 44–57. https://doi.org/10.1038/nprot.2008.211

Huang, H.-T., & Zon, L. I. (2008). Regulation of stem cells in the zebrafish hematopoietic system. *Cold Spring Harbor Symposia on Quantitative Biology*, *73*, 111–118. https://doi.org/10.1101/sqb.2008.73.029

Hunt, D. P. J., Freeman, A., Morris, L. S., Burnet, N. G., Bird, K., Davies, T. W., Laskey, R. A., & Coleman, N. (2002). Early recurrence of benign meningioma correlates with expression of mini-chromosome maintenance-2 protein. *British Journal of Neurosurgery*, *16*(1), 10–15. https://doi.org/10.1080/02688690120114174

Iacob, G., & Dinca, E. B. (2009). Current data and strategy in glioblastoma multiforme. *Journal of Medicine and Life*, *2*(4), 386–393. http://www.ncbi.nlm.nih.gov/pubmed/20108752

Idilli, A. I., Precazzini, F., Mione, M. C., & Anelli, V. (2017). Zebrafish in translational cancer research: insight into leukemia, melanoma, glioma and endocrine tumor biology. *Genes*, *8*(9). https://doi.org/10.3390/genes8090236

Ignatova, T. N., Kukekov, V. G., Laywell, E. D., Suslov, O. N., Vrionis, F. D., & Steindler, D. A. (2002). Human cortical glial tumors contain neural stem-like cells expressing astroglial and neuronal markers in vitro. *Glia*, *39*(3), 193–206. https://doi.org/10.1002/glia.10094

Ishimi, Y., Okayasu, I., Kato, C., Kwon, H.-J., Kimura, H., Yamada, K., & Song, S.-Y. (2003). Enhanced expression of Mcm proteins in cancer cells derived from uterine cervix. *European Journal of Biochemistry*, *270*(6), 1089–1101. https://doi.org/10.1046/j.1432-1033.2003.03440.x

Jaerve, A., & Müller, H. W. (2012). Chemokines in CNS injury and repair. *Cell and Tissue Research*, *349*(1), 229–248. https://doi.org/10.1007/s00441-012-1427-3

Jeansson, M., Gawlik, A., Anderson, G., Li, C., Kerjaschki, D., Henkelman, M., & Quaggin, S. E. (2011). Angiopoietin-1 is essential in mouse vasculature during development and in response to injury. *Journal of Clinical Investigation*, *121*(6), 2278–2289. https://doi.org/10.1172/JCI46322

Jolliffe, I. T., & Cadima, J. (2016). Principal component analysis: a review and recent developments. *Philosophical Transactions. Series A, Mathematical, Physical, and Engineering Sciences*, *374*(2065), 20150202. https://doi.org/10.1098/rsta.2015.0202

Jopling, C., Sleep, E., Raya, M., Martí, M., Raya, A., & Belmonte, J. C. I. (2010). Zebrafish heart regeneration occurs by cardiomyocyte dedifferentiation and proliferation. *Nature*, *464*(7288), 606–609. https://doi.org/10.1038/nature08899

Joven, A., Elewa, A., & Simon, A. (2019). Model systems for regeneration: salamanders. *Development*, *146*(14). https://doi.org/10.1242/dev.167700

Ju, B., Chen, W., Orr, B. A., Spitsbergen, J. M., Jia, S., Eden, C. J., Henson, H. E., & Taylor, M. R. (2015). Oncogenic KRAS promotes malignant brain tumors in zebrafish. *Molecular Cancer*, *14*(1), 18. https://doi.org/10.1186/s12943-015-0288-2

Jurisch-Yaksi, N., Yaksi, E., & Kizil, C. (2020). Radial glia in the zebrafish brain: Functional, structural, and physiological comparison with the mammalian glia. *Glia*, *68*(12), 2451–2470. https://doi.org/10.1002/glia.23849

Kääriäinen, E., Nummela, P., Soikkeli, J., Yin, M., Lukk, M., Jahkola, T., Virolainen, S., Ora, A., Ukkonen, E., Saksela, O., & Hölttä, E. (2006). Switch to an invasive growth phase in melanoma is associated with tenascin-C, fibronectin, and procollagen-I forming specific channel structures for invasion. *The Journal of Pathology*, *210*(2), 181–191. https://doi.org/10.1002/path.2045

Kanti Das, K., & Kumar, R. (2017). Pediatric Glioblastoma. In *Glioblastoma* (pp. 297–312). Codon Publications. https://doi.org/10.15586/codon.glioblastoma.2017.ch15

Karin, M., & Clevers, H. (2016). Reparative inflammation takes charge of tissue regeneration. *Nature*, *529*(7586), 307–315. https://doi.org/10.1038/nature17039

Kaslin, J., Ganz, J., & Brand, M. (2008). Proliferation, neurogenesis and regeneration in the non-mammalian vertebrate brain. *Philosophical Transactions of the Royal Society B: Biological Sciences*, *363*(1489), 101–122. https://doi.org/10.1098/rstb.2006.2015

Kaslin, J., Kroehne, V., Ganz, J., Hans, S., & Brand, M. (2017). Distinct roles of neuroepithelial-like and radial glia-like progenitor cells in cerebellar regeneration. *Development*. https://doi.org/10.1242/dev.144907

Katoh, M. (2002). Expression of human SOX7 in normal tissues and tumors. *International Journal of Molecular Medicine*, *9*(4), 363–368. http://www.ncbi.nlm.nih.gov/pubmed/11891528

Keating, M. T. (2004). Genetic approaches to disease and regeneration. *Philosophical Transactions of the Royal Society of London. Series B: Biological Sciences*, *359*(1445), 795–798. https://doi.org/10.1098/rstb.2004.1469

Kent, W. J., Zweig, A. S., Barber, G., Hinrichs, A. S., & Karolchik, D. (2010). BigWig and BigBed: enabling browsing of large, distributed datasets. *Bioinformatics (Oxford, England)*, *26*(17), 2204–2207. https://doi.org/10.1093/bioinformatics/btq351

Kettleborough, R. N. W., Busch-Nentwich, E. M., Harvey, S. A., Dooley, C. M., de Bruijn, E., van Eeden, F., Sealy, I., White, R. J., Herd, C., Nijman, I. J., Fényes, F., Mehroke, S., Scahill, C., Gibbons, R., Wali, N., Carruthers, S., Hall, A., Yen, J., Cuppen, E., & Stemple, D. L. (2013). A systematic genome-wide analysis of zebrafish protein-coding gene function. *Nature*, *496*(7446), 494–497. https://doi.org/10.1038/nature11992

Kikuchi, K., Holdway, J. E., Werdich, A. A., Anderson, R. M., Fang, Y., Egnaczyk, G. F., Evans, T., MacRae, C. A., Stainier, D. Y. R., & Poss, K. D. (2010). Primary contribution to zebrafish heart regeneration by gata4+ cardiomyocytes. *Nature*, *464*(7288), 601–605. https://doi.org/10.1038/nature08804

Killela, P. J., Pirozzi, C. J., Healy, P., Reitman, Z. J., Lipp, E., Rasheed, B. A., Yang, R., Diplas, B. H., Wang, Z., Greer, P. K., Zhu, H., Wang, C. Y., Carpenter, A. B., Friedman, H., Friedman, A. H., Keir, S. T., He, J., He, Y., McLendon, R. E., … Bigner, D. D. (2014). Mutations in IDH1, IDH2, and in the TERT promoter define clinically distinct subgroups of adult malignant gliomas. *Oncotarget*, *5*(6), 1515–1525. https://doi.org/10.18632/oncotarget.1765

Kim, D., Langmead, B., & Salzberg, S. L. (2015). HISAT: a fast spliced aligner with low memory requirements. *Nature Methods*, *12*(4), 357–360. https://doi.org/10.1038/nmeth.3317

Kim, E., Kim, M., Woo, D.-H., Shin, Y., Shin, J., Chang, N., Oh, Y. T., Kim, H., Rheey, J., Nakano, I., Lee, C., Joo, K. M., Rich, J. N., Nam, D.-H., & Lee, J. (2013). Phosphorylation of EZH2 activates STAT3 signaling via STAT3 methylation and promotes tumorigenicity of glioblastoma stem-like cells. *Cancer Cell*, *23*(6), 839–852. https://doi.org/10.1016/j.ccr.2013.04.008

Kim, I. S., Heilmann, S., Kansler, E. R., Zhang, Y., Zimmer, M., Ratnakumar, K., Bowman, R. L., Simon-Vermot, T., Fennell, M., Garippa, R., Lu, L., Lee, W., Hollmann, T., Xavier, J. B., & White, R. M. (2017). Microenvironment-derived factors driving metastatic plasticity in melanoma. *Nature Communications*, *8*(1), 14343. https://doi.org/10.1038/ncomms14343

Kizil, C., Dudczig, S., Kyritsis, N., Machate, A., Blaesche, J., Kroehne, V., & Brand, M. (2012). The chemokine receptor cxcr5 regulates the regenerative neurogenesis response in the adult zebrafish brain. *Neural Development*, *7*, 27. https://doi.org/10.1186/1749-8104-7-27

Kizil, C., Kaslin, J., Kroehne, V., & Brand, M. (2012). Adult neurogenesis and brain regeneration in zebrafish. *Developmental Neurobiology*, *72*(3), 429–461. https://doi.org/10.1002/dneu.20918

Knopf, F., Hammond, C., Chekuru, A., Kurth, T., Hans, S., Weber, C. W., Mahatma, G., Fisher, S., Brand, M., Schulte-Merker, S., & Weidinger, G. (2011). Bone regenerates via dedifferentiation of osteoblasts in the zebrafish fin. *Developmental Cell*, *20*(5), 713–724. https://doi.org/10.1016/j.devcel.2011.04.014

Kolde, R. (2013). *pheatmap: Pretty heatmaps. R package version 0.7.7. http://CRAN.R-project.org/package=pheatmap.*

Krafts, K. P. (2010). Tissue repair: The hidden drama. *Organogenesis*, *6*(4), 225–233. https://doi.org/10.4161/org.6.4.12555

Kriegstein, A., & Alvarez-Buylla, A. (2009). The Glial nature of embryonic and adult neural stem cells. *Annual Review of Neuroscience*, *32*(1), 149–184. https://doi.org/10.1146/annurev.neuro.051508.135600

Kroehne, V., Freudenreich, D., Hans, S., Kaslin, J., & Brand, M. (2011). Regeneration of the adult zebrafish brain from neurogenic radial glia-type progenitors. *Development*, *138*(22), 4831–4841. https://doi.org/10.1242/dev.072587

Kyritsis, N., Kizil, C., Zocher, S., Kroehne, V., Kaslin, J., Freudenreich, D., Iltzsche, A., & Brand, M. (2012). Acute inflammation initiates the regenerative response in the adult zebrafish brain. *Science*, *338*(6112), 1353–1356. https://doi.org/10.1126/science.1228773

Ladomersky, E., Scholtens, D. M., Kocherginsky, M., Hibler, E. A., Bartom, E. T., Otto-Meyer, S., Zhai, L., Lauing, K. L., Choi, J., Sosman, J. A., Wu, J. D., Zhang, B., Lukas, R. V., & Wainwright, D. A. (2019). The Coincidence between increasing age, immunosuppression, and the incidence of patients with glioblastoma. *Frontiers in Pharmacology*, *10*. https://doi.org/10.3389/fphar.2019.00200

Lange, C., Rost, F., Machate, A., Reinhardt, S., Lesche, M., Weber, A., Kuscha, V., Dahl, A., Rulands, S., & Brand, M. (2020). Single cell sequencing of radial glia progeny reveals diversity of newborn neurons in the adult zebrafish brain. *Development*, 1855951. https://doi.org/10.1242/dev.185595

Langfelder, P., & Horvath, S. (2008). WGCNA: an R package for weighted correlation network analysis. *BMC Bioinformatics*, *9*(1), 559. https://doi.org/10.1186/1471-2105-9-559

LaPelusa, A., & Dave, H. D. (2021). Physiology, hemostasis. In *StatPearls*. http://www.ncbi.nlm.nih.gov/pubmed/31424847

Lathia, J. D., Mattson, M. P., & Cheng, A. (2008). Notch: from neural development to neurological disorders. *Journal of Neurochemistry*, *107*(6), 1471–1481. https://doi.org/10.1111/j.1471-4159.2008.05715.x

Leek, J. T., Johnson, W. E., Parker, H. S., Jaffe, A. E., & Storey, J. D. (2012). The sva package for removing batch effects and other unwanted variation in high-throughput experiments. *Bioinformatics (Oxford, England)*, *28*(6), 882–883. https://doi.org/10.1093/bioinformatics/bts034

Lessman, C. A. (2011). The developing zebrafish (Danio rerio): A vertebrate model for high-throughput screening of chemical libraries. *Birth Defects Research Part C: Embryo Today: Reviews*, *93*(3), 268–280. https://doi.org/10.1002/bdrc.20212

Li, H., Handsaker, B., Wysoker, A., Fennell, T., Ruan, J., Homer, N., Marth, G., Abecasis, G., & Durbin, R. (2009). The Sequence alignment/map format and SAMtools. *Bioinformatics*, *25*(16), 2078–2079. https://doi.org/10.1093/bioinformatics/btp352

Li, Xiaoman, Wu, C., Chen, N., Gu, H., Yen, A., Cao, L., Wang, E., & Wang, L. (2016). PI3K/Akt/mTOR signaling pathway and targeted therapy for glioblastoma. *Oncotarget*, *7*(22), 33440–33450. https://doi.org/10.18632/oncotarget.7961

Li, Xin, Nie, S., Lv, Z., Ma, L., Song, Y., Hu, Z., Hu, X., Liu, Z., Zhou, G., Dai, Z., Song, T., Liu, J., & Wang, S. (2021). Overexpression of Annexin A2 promotes proliferation by forming a Glypican 1/c-Myc positive feedback loop: prognostic significance in human glioma. *Cell Death & Disease*, *12*(3), 261. https://doi.org/10.1038/s41419-021-03547-5

Liao, Y., Smyth, G. K., & Shi, W. (2014). featureCounts: an efficient general purpose program for assigning sequence reads to genomic features. *Bioinformatics (Oxford, England)*, *30*(7), 923–930. https://doi.org/10.1093/bioinformatics/btt656

Lim, D. A., Cha, S., Mayo, M. C., Chen, M.-H., Keles, E., VandenBerg, S., & Berger, M. S. (2007). Relationship of glioblastoma multiforme to neural stem cell regions predicts invasive and multifocal tumor phenotype. *Neuro-Oncology*, *9*(4), 424–429. https://doi.org/10.1215/15228517-2007-023

Lindsey, B. W., Darabie, A., & Tropepe, V. (2012). The cellular composition of neurogenic periventricular zones in the adult zebrafish forebrain. *The Journal of Comparative Neurology*, *520*(10), 2275–2316. https://doi.org/10.1002/cne.23065

Lindsey, B. W., & Tropepe, V. (2006). A comparative framework for understanding the biological principles of adult neurogenesis. *Progress in Neurobiology*, *80*(6), 281–307. https://doi.org/10.1016/j.pneurobio.2006.11.007

Liu, H., Yan, Z.-Q., Li, B., Yin, S.-Y., Sun, Q., Kou, J.-J., Ye, D., Ferns, K., Liu, H.-Y., & Liu, S.-L. (2014). Reduced expression of SOX7 in ovarian cancer: a novel tumor suppressor through the Wnt/β-catenin signaling pathway. *Journal of Ovarian Research*, *7*, 87. https://doi.org/10.1186/s13048-014-0087-1

Louis, D. N., Ohgaki, H., Wiestler, O. D., Cavenee, W. K., Burger, P. C., Jouvet, A., Scheithauer, B. W., & Kleihues, P. (2007). The 2007 WHO classification of tumours of

the central nervous system. *Acta Neuropathologica*, *114*(2), 97–109. https://doi.org/10.1007/s00401-007-0243-4

Louis, D. N., Perry, A., Reifenberger, G., von Deimling, A., Figarella-Branger, D., Cavenee, W. K., Ohgaki, H., Wiestler, O. D., Kleihues, P., & Ellison, D. W. (2016). The 2016 World Health Organization classification of tumors of the central nervous system: a summary. *Acta Neuropathologica*, *131*(6), 803–820. https://doi.org/10.1007/s00401-016-1545-1

Love, M. I., Huber, W., & Anders, S. (2014). Moderated estimation of fold change and dispersion for RNA-seq data with DESeq2. *Genome Biology*, *15*(12), 550. https://doi.org/10.1186/s13059-014-0550-8

Lu, Y.-C. (2012). Knockdown of CDK6 enhances glioma sensitivity to chemotherapy. *Oncology Reports*. https://doi.org/10.3892/or.2012.1884

Ma, S. K. Y., Chan, A. S. F., Rubab, A., Chan, W. C. W., & Chan, D. (2020). Extracellular matrix and cellular plasticity in musculoskeletal development. *Frontiers in Cell and Developmental Biology*, *8*, 781. https://doi.org/10.3389/fcell.2020.00781

Mao, A. S., & Mooney, D. J. (2015). Regenerative medicine: Current therapies and future directions. *Proceedings of the National Academy of Sciences of the United States of America*, *112*(47), 14452–14459. https://doi.org/10.1073/pnas.1508520112

Mao, H., LeBrun, D. G., Yang, J., Zhu, V. F., & Li, M. (2012). Deregulated signaling pathways in glioblastoma multiforme: molecular mechanisms and therapeutic targets. *Cancer Investigation*, *30*(1), 48–56. https://doi.org/10.3109/07357907.2011.630050

Marín-Juez, R., Marass, M., Gauvrit, S., Rossi, A., Lai, S.-L., Materna, S. C., Black, B. L., & Stainier, D. Y. R. (2016). Fast revascularization of the injured area is essential to support zebrafish heart regeneration. *Proceedings of the National Academy of Sciences of the United States of America*, *113*(40), 11237–11242. https://doi.org/10.1073/pnas.1605431113

Marques, I. J., Lupi, E., & Mercader, N. (2019). Model systems for regeneration: zebrafish. *Development*, *146*(18). https://doi.org/10.1242/dev.167692

Martin, P., & Leibovich, S. J. (2005). Inflammatory cells during wound repair: the good, the bad and the ugly. *Trends in Cell Biology*, *15*(11), 599–607. https://doi.org/10.1016/j.tcb.2005.09.002

Méndez, O., Zavadil, J., Esencay, M., Lukyanov, Y., Santovasi, D., Wang, S.-C., Newcomb, E. W., & Zagzag, D. (2010). Knock down of HIF-1α in glioma cells reduces migration in vitro and invasion in vivo and impairs their ability to form tumor spheres. *Molecular Cancer*, *9*(1), 133. https://doi.org/10.1186/1476-4598-9-133

Meng, M. V, Grossfeld, G. D., Williams, G. H., Dilworth, S., Stoeber, K., Mulley, T. W., Weinberg, V., Carroll, P. R., & Tlsty, T. D. (2001). Minichromosome maintenance protein

2 expression in prostate: characterization and association with outcome after therapy for cancer. *Clinical Cancer Research: An Official Journal of the American Association for Cancer Research*, *7*(9), 2712–2718. http://www.ncbi.nlm.nih.gov/pubmed/11555583

Merchant, T. E., Pollack, I. F., & Loeffler, J. S. (2010). Brain tumors across the age spectrum: biology, therapy, and late effects. *Seminars in Radiation Oncology*, *20*(1), 58–66. https://doi.org/10.1016/j.semradonc.2009.09.005

Messali, A., Villacorta, R., & Hay, J. W. (2014). A review of the economic burden of glioblastoma and the cost effectiveness of pharmacologic treatments. *PharmacoEconomics*, *32*(12), 1201–1212. https://doi.org/10.1007/s40273-014-0198-y

Ming, G., & Song, H. (2011). Adult neurogenesis in the mammalian brain: significant answers and significant questions. *Neuron*, *70*(4), 687–702. https://doi.org/10.1016/j.neuron.2011.05.001

Modrek, A. S. (2014). Brain stem cells as the cell of origin in glioma. *World Journal of Stem Cells*, *6*(1), 43. https://doi.org/10.4252/wjsc.v6.i1.43

Moss, J. B., Koustubhan, P., Greenman, M., Parsons, M. J., Walter, I., & Moss, L. G. (2009). Regeneration of the pancreas in adult zebrafish. *Diabetes*, *58*(8), 1844–1851. https://doi.org/10.2337/db08-0628

Nakano, A., Kanemura, Y., Mori, K., Kodama, E., Yamamoto, A., Sakamoto, H., Nakamura, Y., Okano, H., Yamasaki, M., & Arita, N. (2007). Expression of the neural RNA-binding protein Musashi1 in pediatric brain tumors. *Pediatric Neurosurgery*, *43*(4), 279–284. https://doi.org/10.1159/000103307

Nasser, M. M., & Mehdipour, P. (2018). Exploration of involved key genes and signaling diversity in brain tumors. *Cellular and Molecular Neurobiology*, *38*(2), 393–419. https://doi.org/10.1007/s10571-017-0498-9

Noble, M., & Mayer-Pröschel, M. (1997). Growth factors, glia and gliomas. *Journal of Neuro-Oncology*, *35*(3), 193–209. https://doi.org/10.1023/a:1005898228116

Noctor, S. C., Flint, A. C., Weissman, T. A., Dammerman, R. S., & Kriegstein, A. R. (2001). Neurons derived from radial glial cells establish radial units in neocortex. *Nature*, *409*(6821), 714–720. https://doi.org/10.1038/35055553

Odelberg, S. J. (2002). Inducing cellular dedifferentiation: a potential method for enhancing endogenous regeneration in mammals. *Seminars in Cell & Developmental Biology*, *13*(5), 335–343. https://doi.org/10.1016/s1084952102000897

Oh, K.-Y., Hong, K.-O., Huh, Y.-S., Lee, J.-I., & Hong, S.-D. (2017). Decreased expression of SOX7 induces cell proliferation and invasion and correlates with poor prognosis in oral squamous cell carcinoma. *Journal of Oral Pathology & Medicine*, *46*(9), 752–758. https://doi.org/10.1111/jop.12566

Ohgaki, H., & Kleihues, P. (2005). Epidemiology and etiology of gliomas. *Acta Neuropathologica*, *109*(1), 93–108. https://doi.org/10.1007/s00401-005-0991-y

Ohgaki, H., & Kleihues, P. (2007). Genetic pathways to primary and secondary glioblastoma. *The American Journal of Pathology*, *170*(5), 1445–1453. https://doi.org/10.2353/ajpath.2007.070011

Ohka, F., Natsume, A., & Wakabayashi, T. (2012). Current trends in targeted therapies for glioblastoma multiforme. *Neurology Research International*, *2012*, 878425. https://doi.org/10.1155/2012/878425

Opal, S. M., & DePalo, V. A. (2000). Anti-Inflammatory cytokines. *Chest*, *117*(4), 1162–1172. https://doi.org/10.1378/chest.117.4.1162

Ostrom, Q. T., Bauchet, L., Davis, F. G., Deltour, I., Fisher, J. L., Langer, C. E., Pekmezci, M., Schwartzbaum, J. A., Turner, M. C., Walsh, K. M., Wrensch, M. R., & Barnholtz-Sloan, J. S. (2014). The epidemiology of glioma in adults: a "state of the science" review. *Neuro-Oncology*, *16*(7), 896–913. https://doi.org/10.1093/neuonc/nou087

Ostrom, Q. T., Gittleman, H., Farah, P., Ondracek, A., Chen, Y., Wolinsky, Y., Stroup, N. E., Kruchko, C., & Barnholtz-Sloan, J. S. (2013). CBTRUS statistical report: Primary brain and central nervous system tumors diagnosed in the United States in 2006-2010. *Neuro-Oncology*, *15 Suppl 2*, ii1-56. https://doi.org/10.1093/neuonc/not151

Oviedo, N. J., & Beane, W. S. (2009). Regeneration: The origin of cancer or a possible cure? *Seminars in Cell & Developmental Biology*, *20*(5), 557–564. https://doi.org/10.1016/j.semcdb.2009.04.005

Oyarce, K., Bongarzone, E. R., & Nualart, F. (2014). Unconventional neurogenic niches and neurogenesis modulation by vitamins. *Journal of Stem Cell Research & Therapy*, *4*(3), 184. https://doi.org/10.4172/2157-7633.1000184

Parsons, D. W., Jones, S., Zhang, X., Lin, J. C.-H., Leary, R. J., Angenendt, P., Mankoo, P., Carter, H., Siu, I.-M., Gallia, G. L., Olivi, A., McLendon, R., Rasheed, B. A., Keir, S., Nikolskaya, T., Nikolsky, Y., Busam, D. A., Tekleab, H., Diaz, L. A., … Kinzler, K. W. (2008). An integrated genomic analysis of human glioblastoma multiforme. *Science*, *321*(5897), 1807–1812. https://doi.org/10.1126/science.1164382

Pearson, B. J., & Alvarado, A. S. (2008). Regeneration, stem cells, and the evolution of tumor suppression. *Cold Spring Harbor Symposia on Quantitative Biology*, *73*, 565–572. https://doi.org/10.1101/sqb.2008.73.045

Pedersen, T. X., Leethanakul, C., Patel, V., Mitola, D., Lund, L. R., Danø, K., Johnsen, M., Gutkind, J. S., & Bugge, T. H. (2003). Laser capture microdissection-based in vivo genomic profiling of wound keratinocytes identifies similarities and differences to

squamous cell carcinoma. *Oncogene*, *22*(25), 3964–3976. https://doi.org/10.1038/sj.onc.1206614

Peng, W. M., Yu, L. L., Bao, C. Y., Liao, F., Li, X. S., & Zuo, M. X. (2002). Transplanted neuronal precursors migrate and differentiate in the developing mouse brain. *Cell Research*, *12*(3–4), 223–228. https://doi.org/10.1038/sj.cr.7290128

Pereira, J. D., Sansom, S. N., Smith, J., Dobenecker, M.-W., Tarakhovsky, A., & Livesey, F. J. (2010). Ezh2, the histone methyltransferase of PRC2, regulates the balance between self-renewal and differentiation in the cerebral cortex. *Proceedings of the National Academy of Sciences of the United States of America*, *107*(36), 15957–15962. https://doi.org/10.1073/pnas.1002530107

Pertea, M., Kim, D., Pertea, G. M., Leek, J. T., & Salzberg, S. L. (2016). Transcript-level expression analysis of RNA-seq experiments with HISAT, StringTie and Ballgown. *Nature Protocols*, *11*(9), 1650–1667. https://doi.org/10.1038/nprot.2016.095

Pierce, G. F., Mustoe, T. A., Altrock, B. W., Deuel, T. F., & Thomason, A. (1991). Role of platelet-derived growth factor in wound healing. *Journal of Cellular Biochemistry*, *45*(4), 319–326. https://doi.org/10.1002/jcb.240450403

Placke, T., Kopp, H.-G., & Salih, H. R. (2010). Glucocorticoid-Induced TNFR-Related (GITR) Protein and Its Ligand in Antitumor Immunity: Functional Role and Therapeutic Modulation. *Clinical and Developmental Immunology*, *2010*, 1–10. https://doi.org/10.1155/2010/239083

Poss, K. D., Keating, M. T., & Nechiporuk, A. (2003). Tales of regeneration in zebrafish. *Developmental Dynamics*, *226*(2), 202–210. https://doi.org/10.1002/dvdy.10220

Prasad, G., & Haas-Kogan, D. A. (2009). Radiation-induced gliomas. *Expert Review of Neurotherapeutics*, *9*(10), 1511–1517. https://doi.org/10.1002/pmic.200800802

Quinlan, A. R., & Hall, I. M. (2010). BEDTools: a flexible suite of utilities for comparing genomic features. *Bioinformatics*, *26*(6), 841–842. https://doi.org/10.1093/bioinformatics/btq033

Rahaman, S. O., Harbor, P. C., Chernova, O., Barnett, G. H., Vogelbaum, M. A., & Haque, S. J. (2002). Inhibition of constitutively active Stat3 suppresses proliferation and induces apoptosis in glioblastoma multiforme cells. *Oncogene*, *21*(55), 8404–8413. https://doi.org/10.1038/sj.onc.1206047

Rakic, P. (2002). Neurogenesis in adult primate neocortex: an evaluation of the evidence. *Nature Reviews Neuroscience*, *3*(1), 65–71. https://doi.org/10.1038/nrn700

Ramnath, N., Hernandez, F. J., Tan, D. F., Huberman, J. A., Natarajan, N., Beck, A. F., Hyland, A., Todorov, I. T., Brooks, J. S., & Bepler, G. (2001). MCM2 is an independent predictor of survival in patients with non-small-cell lung cancer. *Journal of Clinical Oncology:*

Official Journal of the American Society of Clinical Oncology, *19*(22), 4259–4266. https://doi.org/10.1200/JCO.2001.19.22.4259

Raudvere, U., Kolberg, L., Kuzmin, I., Arak, T., Adler, P., Peterson, H., & Vilo, J. (2019). g:Profiler: a web server for functional enrichment analysis and conversions of gene lists (2019 update). *Nucleic Acids Research*, *47*(W1), W191–W198. https://doi.org/10.1093/nar/gkz369

Reddien, P. W., & Alvarado, A. S. (2004). Fundamentals of planarian regeneration. *Annual Review of Cell and Developmental Biology*, *20*(1), 725–757. https://doi.org/10.1146/annurev.cellbio.20.010403.095114

Reilly, K. M. (2009). Brain tumor susceptibility: the role of genetic factors and uses of mouse models to unravel risk. *Brain Pathology (Zurich, Switzerland)*, *19*(1), 121–131. https://doi.org/10.1111/j.1750-3639.2008.00236.x

Riss, J., Khanna, C., Koo, S., Chandramouli, G. V. R., Yang, H. H., Hu, Y., Kleiner, D. E., Rosenwald, A., Schaefer, C. F., Ben-Sasson, S. A., Yang, L., Powell, J., Kane, D. W., Star, R. A., Aprelikova, O., Bauer, K., Vasselli, J. R., Maranchie, J. K., Kohn, K. W., … Barrett, J. C. (2006). Cancers as wounds that do not heal: differences and similarities between renal regeneration/repair and renal cell carcinoma. *Cancer Research*, *66*(14), 7216–7224. https://doi.org/10.1158/0008-5472.CAN-06-0040

Robinson, J. T., Thorvaldsdóttir, H., Winckler, W., Guttman, M., Lander, E. S., Getz, G., & Mesirov, J. P. (2011). Integrative genomics viewer. *Nature Biotechnology*, *29*(1), 24–26. https://doi.org/10.1038/nbt.1754

Rodins, K., Cheale, M., Coleman, N., & Fox, S. B. (2002). Minichromosome maintenance protein 2 expression in normal kidney and renal cell carcinomas: relationship to tumor dormancy and potential clinical utility. *Clinical Cancer Research: An Official Journal of the American Association for Cancer Research*, *8*(4), 1075–1081. http://www.ncbi.nlm.nih.gov/pubmed/11948116

Rolls, A., Shechter, R., & Schwartz, M. (2009). The bright side of the glial scar in CNS repair. *Nature Reviews Neuroscience*, *10*(3), 235–241. https://doi.org/10.1038/nrn2591

Ron, E. (2003). Cancer risks from medical radiation. *Health Physics*, *85*(1), 47–59. https://doi.org/10.1097/00004032-200307000-00011

Rose, S. M., & Rose, F. C. (1952). Tumor agent transformations in Amphibia. *Cancer Research*, *12*(1), 1–12. http://www.ncbi.nlm.nih.gov/pubmed/14886955

Rose, S. M., & Wallingford, H. M. (1948). Transformation of renal tumors of frogs to normal tissues in regenerating limbs of salamanders. *Science (New York, N.Y.)*, *107*(2784), 457. http://www.ncbi.nlm.nih.gov/pubmed/18938459

Rothenaigner, I., Krecsmarik, M., Hayes, J. A., Bahn, B., Lepier, A., Fortin, G., Götz, M., Jagasia, R., & Bally-Cuif, L. (2011). Clonal analysis by distinct viral vectors identifies bona fide neural stem cells in the adult zebrafish telencephalon and characterizes their division properties and fate. *Development (Cambridge, England)*, *138*(8), 1459–1469. https://doi.org/10.1242/dev.058156

Roy, S., & Gatien, S. (2008). Regeneration in axolotls: a model to aim for! *Experimental Gerontology*, *43*(11), 968–973. https://doi.org/10.1016/j.exger.2008.09.003

Saló, E. (2006). The power of regeneration and the stem-cell kingdom: freshwater planarians (Platyhelminthes). *BioEssays*, *28*(5), 546–559. https://doi.org/10.1002/bies.20416

Sanai, N., Alvarez-Buylla, A., & Berger, M. S. (2005). Neural stem cells and the origin of gliomas. *New England Journal of Medicine*, *353*(8), 811–822. https://doi.org/10.1056/NEJMra043666

Sánchez Alvarado, A. (2000). Regeneration in the metazoans: why does it happen? *BioEssays : News and Reviews in Molecular, Cellular and Developmental Biology*, *22*(6), 578–590. https://doi.org/10.1002/(SICI)1521-1878(200006)22:6<578::AID-BIES11>3.0.CO;2-#

Schaeffer, D. J. (1993). Planarians as a model system for in vivo tumorigenesis studies. *Ecotoxicology and Environmental Safety*, *25*(1), 1–18. https://doi.org/10.1006/eesa.1993.1001

Schäfer, M., & Werner, S. (2008). Cancer as an overhealing wound: an old hypothesis revisited. *Nature Reviews Molecular Cell Biology*, *9*(8), 628–638. https://doi.org/10.1038/nrm2455

Schmidt, R., Beil, T., Strähle, U., & Rastegar, S. (2014). Stab wound injury of the zebrafish adult telencephalon: a method to investigate vertebrate brain neurogenesis and regeneration. *Journal of Visualized Experiments*, *90*. https://doi.org/10.3791/51753

Schmidt, R., Strähle, U., & Scholpp, S. (2013). Neurogenesis in zebrafish - from embryo to adult. *Neural Development*, *8*, 3. https://doi.org/10.1186/1749-8104-8-3

Schrader, C., Janssen, D., Klapper, W., Siebmann, J.-U., Meusers, P., Brittinger, G., Kneba, M., Tiemann, M., & Parwaresch, R. (2005). Minichromosome maintenance protein 6, a proliferation marker superior to Ki-67 and independent predictor of survival in patients with mantle cell lymphoma. *British Journal of Cancer*, *93*(8), 939–945. https://doi.org/10.1038/sj.bjc.6602795

Schwartzbaum, J. A., Fisher, J. L., Aldape, K. D., & Wrensch, M. (2006). Epidemiology and molecular pathology of glioma. *Nature Clinical Practice. Neurology*, *2*(9), 494–503; quiz 1 p following 516. https://doi.org/10.1038/ncpneuro0289

Seilern-Aspang, F., & Kratochwill, K. (1965). *Regeneration in animals and related problems* (V. Kiortsis & H. Trampusch (Eds.)). North-Holland Publishing Company.

Seri, B., García-Verdugo, J. M., McEwen, B. S., & Alvarez-Buylla, A. (2001). Astrocytes give rise to new neurons in the adult mammalian hippocampus. *The Journal of Neuroscience: The Official Journal of the Society for Neuroscience*, *21*(18), 7153–7160. http://www.ncbi.nlm.nih.gov/pubmed/11549726

Sherry, M. M., Reeves, A., Wu, J. K., & Cochran, B. H. (2009). STAT3 is required for proliferation and maintenance of multipotency in glioblastoma stem cells. *Stem Cells (Dayton, Ohio)*, *27*(10), 2383–2392. https://doi.org/10.1002/stem.185

Sherwood, L. M., Parris, E. E., & Folkman, J. (1971). Tumor angiogenesis: therapeutic implications. *New England Journal of Medicine*, *285*(21), 1182–1186. https://doi.org/10.1056/NEJM197111182852108

Shih, C.-H., Lacagnina, M., Leuer-Bisciotti, K., & Proschel, C. (2014). Astroglial-Derived Periostin Promotes Axonal Regeneration after Spinal Cord Injury. *Journal of Neuroscience*, *34*(7), 2438–2443. https://doi.org/10.1523/JNEUROSCI.2947-13.2014

Shihabuddin, L. S., Horner, P. J., Ray, J., & Gage, F. H. (2000). Adult spinal cord stem cells generate neurons after transplantation in the adult dentate gyrus. *The Journal of Neuroscience*, *20*(23), 8727–8735. https://doi.org/10.1523/JNEUROSCI.20-23-08727.2000

Silva, A. C., Pereira, C., Fonseca, A. C. R. G., Pinto-do-Ó, P., & Nascimento, D. S. (2021). Bearing my heart: the role of extracellular matrix on cardiac development, homeostasis, and injury response. *Frontiers in Cell and Developmental Biology*, *8*. https://doi.org/10.3389/fcell.2020.621644

Singh, S. K., Hawkins, C., Clarke, I. D., Squire, J. A., Bayani, J., Hide, T., Henkelman, R. M., Cusimano, M. D., & Dirks, P. B. (2004). Identification of human brain tumour initiating cells. *Nature*, *432*(7015), 396–401. https://doi.org/10.1038/nature03128

Soengas, M. S., Gerald, W. L., Cordon-Cardo, C., Lazebnik, Y., & Lowe, S. W. (2006). Apaf-1 expression in malignant melanoma. *Cell Death & Differentiation*, *13*(2), 352–353. https://doi.org/10.1038/sj.cdd.4401755

Sofroniew, M. V. (2009). Molecular dissection of reactive astrogliosis and glial scar formation. *Trends in Neurosciences*, *32*(12), 638–647. https://doi.org/10.1016/j.tins.2009.08.002

Sonar, S., & Lal, G. (2015). Role of tumor necrosis factor superfamily in neuroinflammation and autoimmunity. *Frontiers in Immunology*, *6*, 364. https://doi.org/10.3389/fimmu.2015.00364

Speidel, D. (2015). The role of DNA damage responses in p53 biology. *Archives of Toxicology*, *89*(4), 501–517. https://doi.org/10.1007/s00204-015-1459-z

Spemann, H., & Mangold, H. (2001). Induction of embryonic primordia by implantation of organizers from a different species.1923. *The International Journal of Developmental Biology*, *45*(1), 13–38.

Stern, C. D. (2000). Conrad H. Waddington's contributions to avian and mammalian development, 1930-1940. *The International Journal of Developmental Biology*, *44*(1), 15–22. http://www.ncbi.nlm.nih.gov/pubmed/10761841

Stoick-Cooper, C. L., Weidinger, G., Riehle, K. J., Hubbert, C., Major, M. B., Fausto, N., & Moon, R. T. (2007). Distinct Wnt signaling pathways have opposing roles in appendage regeneration. *Development*, *134*(3), 479–489. https://doi.org/10.1242/dev.001123

Stovall, D. B., Wan, M., Miller, L. D., Cao, P., Maglic, D., Zhang, Q., Stampfer, M. R., Liu, W., Xu, J., & Sui, G. (2013). The regulation of SOX7 and its tumor suppressive role in breast cancer. *The American Journal of Pathology*, *183*(5), 1645–1653. https://doi.org/10.1016/j.ajpath.2013.07.025

Tamimi, A. F., & Juweid, M. (2017). Epidemiology and Outcome of Glioblastoma. In *Glioblastoma*. https://doi.org/10.15586/codon.glioblastoma.2017.ch8

Tanaka, E. M., & Ferretti, P. (2009). Considering the evolution of regeneration in the central nervous system. *Nature Reviews Neuroscience*, *10*(10), 713–723. https://doi.org/10.1038/nrn2707

Tanase, C., Albulescu, R., Codrici, E., Calenic, B., Popescu, I. D., Mihai, S., Necula, L., Cruceru, M. L., & Hinescu, M. E. (2014). Decreased expression of APAF-1 and increased expression of cathepsin B in invasive pituitary adenoma. *OncoTargets and Therapy*, 81. https://doi.org/10.2147/OTT.S70886

Thompson, D. E., Mabuchi, K., Ron, E., Soda, M., Tokunaga, M., Ochikubo, S., Sugimoto, S., Ikeda, T., Terasaki, M., & Izumi, S. (1994). Cancer incidence in atomic bomb survivors. Part II: Solid tumors, 1958-1987. *Radiation Research*, *137*(2 Suppl), S17-67. http://www.ncbi.nlm.nih.gov/pubmed/8127952

Thorvaldsdóttir, H., Robinson, J. T., & Mesirov, J. P. (2013). Integrative Genomics Viewer (IGV): high-performance genomics data visualization and exploration. *Briefings in Bioinformatics*, *14*(2), 178–192. https://doi.org/10.1093/bib/bbs017

Thummel, R., Kassen, S. C., Enright, J. M., Nelson, C. M., Montgomery, J. E., & Hyde, D. R. (2008). Characterization of Müller glia and neuronal progenitors during adult zebrafish retinal regeneration. *Experimental Eye Research*, *87*(5), 433–444. https://doi.org/10.1016/j.exer.2008.07.009

Trapnell, C., & Salzberg, S. L. (2009). How to map billions of short reads onto genomes. *Nature Biotechnology*, *27*(5), 455–457. https://doi.org/10.1038/nbt0509-455

Tsarouchas, T. M., Wehner, D., Cavone, L., Munir, T., Keatinge, M., Lambertus, M., Underhill, A., Barrett, T., Kassapis, E., Ogryzko, N., Feng, Y., van Ham, T. J., Becker, T., & Becker, C. G. (2018). Dynamic control of proinflammatory cytokines Il-1β and Tnf-α by macrophages in zebrafish spinal cord regeneration. *Nature Communications*, *9*(1), 4670. https://doi.org/10.1038/s41467-018-07036-w

Tsonis, P. A. (1983). Effects of carcinogens on regenerating and non-regenerating limbs in amphibia (review). *Anticancer Research*, *3*(3), 195–202. http://www.ncbi.nlm.nih.gov/pubmed/6347032

Venkatesan, S., Lamfers, M. L. M., Dirven, C. M. F., & Leenstra, S. (2016). Genetic biomarkers of drug response for small-molecule therapeutics targeting the RTK/Ras/PI3K, p53 or Rb pathway in glioblastoma. *CNS Oncology*, *5*(2), 77–90. https://doi.org/10.2217/cns-2015-0005

Verhaak, R. G. W., Hoadley, K. A., Purdom, E., Wang, V., Qi, Y., Wilkerson, M. D., Miller, C. R., Ding, L., Golub, T., Mesirov, J. P., Alexe, G., Lawrence, M., O'Kelly, M., Tamayo, P., Weir, B. A., Gabriel, S., Winckler, W., Gupta, S., Jakkula, L., … Hayes, D. N. (2010). Integrated genomic analysis identifies clinically relevant subtypes of glioblastoma characterized by abnormalities in PDGFRA, IDH1, EGFR, and NF1. *Cancer Cell*, *17*(1), 98–110. https://doi.org/10.1016/j.ccr.2009.12.020

Verkhratsky, A., & Butt, A. (2013). *Glial physiology and pathophysiology*. John Wiley & Sons, Ltd. https://doi.org/10.1002/9781118402061

Viotti, J., Duplan, E., Caillava, C., Condat, J., Goiran, T., Giordano, C., Marie, Y., Idbaih, A., Delattre, J.-Y., Honnorat, J., Checler, F., & Alves da Costa, C. (2014). Glioma tumor grade correlates with parkin depletion in mutant p53-linked tumors and results from loss of function of p53 transcriptional activity. *Oncogene*, *33*(14), 1764–1775. https://doi.org/10.1038/onc.2013.124

Waddington, C. H. (1935). Cancer and the Theory of Organisers. *Nature*, *135*(3416), 606–608. https://doi.org/10.1038/135606a0

Wang, L., Wang, S., & Li, W. (2012). RSeQC: quality control of RNA-seq experiments. *Bioinformatics (Oxford, England)*, *28*(16), 2184–2185. https://doi.org/10.1093/bioinformatics/bts356

Wang, X., Pei, Z., Hossain, A., Bai, Y., & Chen, G. (2021). Transcription factor-based gene therapy to treat glioblastoma through direct neuronal conversion. *Cancer Biology and Medicine*, *18*, 0–0. https://doi.org/10.20892/j.issn.2095-3941.2020.0499

Wanner, I. B., Anderson, M. A., Song, B., Levine, J., Fernandez, A., Gray-Thompson, Z., Ao, Y., & Sofroniew, M. V. (2013). Glial scar borders are formed by newly proliferated, elongated astrocytes that interact to corral inflammatory and fibrotic cells via STAT3-

dependent mechanisms after spinal cord injury. *Journal of Neuroscience*, *33*(31), 12870–12886. https://doi.org/10.1523/JNEUROSCI.2121-13.2013

Webster, H. de F. (1997). Growth factors and myelin regeneration in multiple sclerosis. *Multiple Sclerosis Journal*, *3*(2), 113–120. https://doi.org/10.1177/135245859700300210

Wee, B., Charles, N., & Holland, E. C. (2011). Animal models to study cancer-initiating cells from glioblastoma. *Frontiers in Bioscience (Landmark Edition)*, *16*, 2243–2258. https://doi.org/10.2741/3851

White, R. M., & Zon, L. I. (2008). Melanocytes in development, regeneration, and cancer. *Cell Stem Cell*, *3*(3), 242–252. https://doi.org/10.1016/j.stem.2008.08.005

Wickham, H. (2016). ggplot2: Elegant graphics for data analysis. In *Springer-Verlag New York*.

Wilson, S. E., Chaurasia, S. S., & Medeiros, F. W. (2007). Apoptosis in the initiation, modulation and termination of the corneal wound healing response. *Experimental Eye Research*, *85*(3), 305–311. https://doi.org/10.1016/j.exer.2007.06.009

Wu, Y.-S., & Chen, S.-N. (2014). Apoptotic cell: linkage of inflammation and wound healing. *Frontiers in Pharmacology*, *5*. https://doi.org/10.3389/fphar.2014.00001

Xu, C., Hasan, S. S., Schmidt, I., Rocha, S. F., Pitulescu, M. E., Bussmann, J., Meyen, D., Raz, E., Adams, R. H., & Siekmann, A. F. (2014). Arteries are formed by vein-derived endothelial tip cells. *Nature Communications*, *5*, 5758. https://doi.org/10.1038/ncomms6758

Yadav, B., Pal, S., Rubstov, Y., Goel, A., Garg, M., Pavlyukov, M., & Pandey, A. K. (2021). LncRNAs associated with glioblastoma: From transcriptional noise to novel regulators with a promising role in therapeutics. *Molecular Therapy - Nucleic Acids*, *24*, 728–742. https://doi.org/10.1016/j.omtn.2021.03.018

Yu, G., Wang, L.-G., Han, Y., & He, Q.-Y. (2012). clusterProfiler: an R package for comparing biological themes among gene clusters. *Omics: A Journal of Integrative Biology*, *16*(5), 284–287. https://doi.org/10.1089/omi.2011.0118

Zacchetti, A., Van Garderen, E., Teske, E., Nederbragt, H., Dierendonck, J. H., & Rutteman, G. R. (2003). Validation of the use of proliferation markers in canine neoplastic and non-neoplastic tissues: comparison of KI-67 and proliferating cell nuclear antigen (PCNA) expression versus in vivo bromodeoxyuridine labelling by immunohistochemistry. *Apmis*, *111*(3), 430–438. https://doi.org/10.1034/j.1600-0463.2003.t01-1-1110208.x

Zhang, J., Ji, F., Liu, Y., Lei, X., Li, H., Ji, G., Yuan, Z., & Jiao, J. (2014). Ezh2 regulates adult hippocampal neurogenesis and memory. *The Journal of Neuroscience: The Official Journal of the Society for Neuroscience*, *34*(15), 5184–5199. https://doi.org/10.1523/JNEUROSCI.4129-13.2014

Zhang, J., & Jiao, J. (2015). Molecular biomarkers for embryonic and adult neural stem cell and neurogenesis. *BioMed Research International*, *2015*, 727542. https://doi.org/10.1155/2015/727542

Zhang, Y., Huang, S., Dong, W., Li, L., Feng, Y., Pan, L., Han, Z., Wang, X., Ren, G., Su, D., Huang, B., & Lu, J. (2009). SOX7, downregulated in colorectal cancer, induces apoptosis and inhibits proliferation of colorectal cancer cells. *Cancer Letters*, *277*(1), 29–37. https://doi.org/10.1016/j.canlet.2008.11.014

Zhao, S., Huang, J., & Ye, J. (2015). A fresh look at zebrafish from the perspective of cancer research. *Journal of Experimental & Clinical Cancer Research*, *34*(1), 80. https://doi.org/10.1186/s13046-015-0196-8

Zhao, T., Yang, H., Tian, Y., Xie, Q., Lu, Y., Wang, Y., Su, N., Dong, B., Liu, X., Wang, C., Jiang, C., & Liu, X. (2016). SOX7 is associated with the suppression of human glioma by HMG-box dependent regulation of Wnt/β-catenin signaling. *Cancer Letters*, *375*(1), 100–107. https://doi.org/10.1016/j.canlet.2016.02.044

Zhong, W., Qin, G., Dai, Q., Han, Z., Chen, S., Ling, X., Fu, X., Cai, C., Chen, J., Chen, X., Lin, Z., Deng, Y., Wu, S., He, H., & Wu, C. (2012). SOXs in human prostate cancer: implication as progression and prognosis factors. *BMC Cancer*, *12*, 248. https://doi.org/10.1186/1471-2407-12-248

Zhou, B.-B. S., Zhang, H., Damelin, M., Geles, K. G., Grindley, J. C., & Dirks, P. B. (2009). Tumour-initiating cells: challenges and opportunities for anticancer drug discovery. *Nature Reviews. Drug Discovery*, *8*(10), 806–823. https://doi.org/10.1038/nrd2137

Zoncu, R., Efeyan, A., & Sabatini, D. M. (2011). mTOR: from growth signal integration to cancer, diabetes and ageing. *Nature Reviews. Molecular Cell Biology*, *12*(1), 21–35. https://doi.org/10.1038/nrm3025

Zullo, L., Bozzo, M., Daya, A., Di Clemente, A., Mancini, F. P., Megighian, A., Nesher, N., Röttinger, E., Shomrat, T., Tiozzo, S., Zullo, A., & Candiani, S. (2020). The diversity of muscles and their regenerative potential across animals. *Cells*, *9*(9), 1925. https://doi.org/10.3390/cells9091925

8. APPENDICES

Appendix-1

Ethical committee approval

İZMİR BİYOTIP VE GENOM MERKEZİ
HAYVAN DENEYLERİ YEREL ETİK KURULU
(İBG-HADYEK)
KARARI

TOPLANTI TARİHİ	29/08/2018	TOPLANTI GÜNÜ	Çarşamba
TOPLANTI SAYISI	08	TOPLANTI SAATİ	15.00

Sayın Doç. Dr. Güneş Özhan Baykan,

09/2018 Protokol No'lu; yürütücüsü olduğunuz "Comparative Analysis of the Molecular Mechanisms of Brain Regeneration and Glioma Using Zebrafish Model to Develop Therapeutic Approaches for Gliomas" başlıklı projenin uygulanmasında etik açıdan sakınca olmadığına oy birliği ile karar verilmiştir.

Bilgilerinizi ve gereğini rica ederiz.

(Proje Yürütücüsü) Doç. Dr. H. Güneş ÖZHAN Başkan	Vet. Hek. Kerem ESMEN Başkan Yardımcısı
Prof.Dr. H. Alper BAĞRIYANIK Üye	(Proje Ekibi Üyesi) Dr. Gülçin Çakan Akdoğan Üye
(Katılmamıştır) Yrd. Doç. Dr. Ayşe Banu DEMİR Üye	Prof.Dr. Eusari GÜNELİ Üye
Doç. Dr. Kasım Diril Üye	Vet. Hek. Umur KELEŞ Üye
H. Muammer KARAGÖZ Üye	

Appendix-2

Curriculum vitae

YELİZ DEMİRCİ (CV)

==========

Education
PhD in Molecular Biology and Genetics, 2021
Dokuz Eylül University, İzmir Biomedicine and Genome Institute,
Genome Sciences and Molecular Biotechnology Department,
Molecular Biology and Genetics Doctorate Programme – İzmir, Turkey

MSc in Biotechnology, 2015
Ankara University, Institute of Biotechnology, Ankara, Turkey

Bsc in Biology, 2009
İstanbul University, Faculty of Sciences, İstanbul, Turkey

Research Experience
EMBL-EBI, Functional Genomics Group
Advisor: Dr. Alvis Brazma, Feb. 2020 - Jul. 2021

EMBL-EBI, Gene expression Team
Advisor: Dr. Irene Papatheodorou, Apr. 01 - Aug. 02, 2019

EMBL-EBI, **Gene expression Team**
Advisor: Dr. Irene Papatheodorou, Sep. 03 - Dec. 07, 2018

Awards & Grants
Federation of European Biochemical Society - Short Term Fellowship

European Molecular Biology Organization - Short Term Fellowship

The Scientific and Technological Research Council of Turkey-2214/A
2214-International Research Fellowship Programme (for PhD Students)

The Scientific and Technological Research Council of Turkey-2211/C
Domestic Priority Areas Doctoral Scholarship Program

The Council of Higher Education (CoHE) of Turkey-100/2000, PhD Scholarship Program

Publications
Demirci Y, Cucun G, Poyraz YK, Mohammed S, Heger G, Papatheodorou I, Ozhan G (2020). Comparative Transcriptome Analysis of the Regenerating Zebrafish Telencephalon Unravels a Resource with Key Pathways During Two Early Stages and Activation of Wnt/β-Catenin Signaling at the Early Wound Healing Stage. Front Cell Dev Biol Volume 8 (2020) p.584604.

Demirci Y, Zhang B & Unver T (2018). CRISPR/Cas9: an RNA-guided highly precise synthetic tool for plant genome editing. J Cell Physiol 233, 1844-1859.

Duman M, Polat E, Ozer M, **Demirci Y**, Yasar NF, Akyuz C, Uzun O, Peker KD, Genc E & Yol S (2013). The Effect of Rabeprazole on Lower Esophageal Sphincter Tone in Experimental Rat Model. J Invest Surg 26(4), 186-190.

Ozer M, **Demirci Y,** Hizel C, Sarikaya S, Karalti I, Kaspar C, Alpan S & Genc E (2012). Impact of Genetic Factors (CYP2C9, VKORC1 and CYP4F2) on Warfarin Dose Requirement in the Turkish Population. Basic Clin Pharmacol Toxicol 112(3), 209-214.

Reyhan E, Duman M, **Demirci Y,** Atici AE, Ozer M, Cevreli B, Ekiz F, Dalgic T, Akoglu M & Genc E (2012). Superiority of Ceftriaxon to Cefazolin in a Rat Model of Obstructive Jaundice: An Experimental Study. J Invest Surg 26(1), 11-15.

Ozer M, Duman M, Tas S, **Demirci Y,** Aydın MF, Reyhan E, Atici AE, Bostanci EB, Akoglu M & Genc E (2012). In vitro effects of famotidine and ranitidine on lower esophageal sphincter tone in rats. Turk J Gastroenterol 23(5), 438-443.

Duman M, Ozer M, Reyhan E, **Demirci Y**, Atici AE, Dalgic T, Bostanci EB & Genc E (2011). In vitro effect of pantoprazole on lower esophageal sphincter tone in rats. World J Gastroenterol 17(46), 5105-5109.

Ozer M, **Demirci Y,** Sarikaya S, Karalti I, Kaspar C, Hizel C, Alpan RS & Genc E (2011). The effect of polymorphisms in CYP2C9, CYP4F2, EPHX1 and VKORC1 on warfarin dose in Turkish patients. Curr Opin in Biotechnol 22, S125-S125.

Work Experiences
Teaching and Research Assistant; Feb. - Oct. 2015
İzmir University of Economics (İzmir, Turkey)

Lab Manager; 2004-2012
Yeditepe University (İstanbul, Turkey), Faculty of Medicine,
Department of Basic Medical Sciences, Education and Research Laboratories

Appendix-3

Article

frontiers in Cell and Developmental Biology

ORIGINAL RESEARCH
published: 09 October 2020
doi: 10.3389/fcell.2020.584604

Comparative Transcriptome Analysis of the Regenerating Zebrafish Telencephalon Unravels a Resource With Key Pathways During Two Early Stages and Activation of Wnt/β-Catenin Signaling at the Early Wound Healing Stage

Yeliz Demirci[1,2,3†], Gokhan Cucun[1,2†], Yusuf Kaan Poyraz[1,2], Suhaib Mohammed[3], Guillaume Heger[4], Irene Papatheodorou[3] and Gunes Ozhan[1,2]*

[1] İzmir Biomedicine and Genome Center (IBG), Dokuz Eylül University Health Campus, İzmir, Turkey, [2] İzmir International Biomedicine and Genome Institute (IBG-İzmir), Dokuz Eylül University, İzmir, Turkey, [3] European Molecular Biology Laboratory – European Bioinformatics Institute (EMBL-EBI), Cambridge, United Kingdom, [4] École Centrale de Nantes, Nantes, France

OPEN ACCESS

Edited by:
Alicia Guemez-Gamboa,
Northwestern University,
United States

Reviewed by:
Sepand Rastegar,
Karlsruhe Institute of Technology (KIT), Germany
Jan Kaslin,
Australian Regenerative Medicine Institute (ARMI), Australia
Shawn M. Burgess,
National Human Genome Research Institute (NHGRI), United States

***Correspondence:**
Gunes Ozhan
gunes.ozhan@ibg.edu.tr

[†]These authors have contributed equally to this work

Specialty section:
This article was submitted to Molecular Medicine, a section of the journal Frontiers in Cell and Developmental Biology

Received: 17 July 2020
Accepted: 11 September 2020
Published: 09 October 2020

Citation:
Demirci Y, Cucun G, Poyraz YK, Mohammed S, Heger G, Papatheodorou I and Ozhan G (2020) Comparative Transcriptome Analysis of the Regenerating Zebrafish Telencephalon Unravels a Resource With Key Pathways During Two Early Stages and Activation of Wnt/β-Catenin Signaling at the Early Wound Healing Stage. Front. Cell Dev. Biol. 8:584604. doi: 10.3389/fcell.2020.584604

Owing to its pronounced regenerative capacity in many tissues and organs, the zebrafish brain represents an ideal platform to understand the endogenous regeneration mechanisms that restore tissue integrity and function upon injury or disease. Although radial glial and neuronal cell populations have been characterized with respect to specific marker genes, comprehensive transcriptomic profiling of the regenerating telencephalon has not been conducted so far. Here, by processing the lesioned and unlesioned hemispheres of the telencephalon separately, we reveal the differentially expressed genes (DEGs) at the early wound healing and early proliferative stages of regeneration, i.e., 20 h post-lesion (hpl) and 3 days post-lesion (dpl), respectively. At 20 hpl, we detect a far higher number of DEGs in the lesioned hemisphere than in the unlesioned half and only 7% of all DEGs in both halves. However, this difference disappears at 3 dpl, where the lesioned and unlesioned hemispheres share 40% of all DEGs. By performing an extensive comparison of the gene expression profiles in these stages, we unravel that the lesioned hemispheres at 20 hpl and 3 dpl exhibit distinct transcriptional profiles. We further unveil a prominent activation of Wnt/β-catenin signaling at 20 hpl, returning to control level in the lesioned site at 3 dpl. Wnt/β-catenin signaling indeed appears to control a large number of genes associated primarily with the p53, apoptosis, forkhead box O (FoxO), mitogen-activated protein kinase (MAPK), and mammalian target of rapamycin (mTOR) signaling pathways specifically at 20 hpl. Based on these results, we propose that the lesioned and unlesioned hemispheres react to injury dynamically during telencephalon regeneration and that the activation of Wnt/β-catenin signaling at the early wound healing stage plays a key role in the regulation of cellular and molecular events.

Keywords: brain regeneration, telencephalon, comparative transcriptome analysis, zebrafish, Wnt/β-catenin pathway, wound healing

INTRODUCTION

All vertebrate brains studied so far undergo adult neurogenesis, where they generate functional new neurons and integrate them into the existing brain circuitry after fetal and early postnatal development. Adult neurogenesis is achieved *via* stem or progenitor cells, in particular zones that exhibit varying degrees of abundance and neurogenic capacity among vertebrate species, and correlates with the capacity to regenerate upon damage to neuronal networks caused by injury (Doetsch and Scharff, 2001; Chapouton et al., 2007; Kaslin et al., 2008; Bonfanti and Peretto, 2011; Alunni and Bally-Cuif, 2016). Radial glia or glia-like cells (RGCs) have the characteristics of astrocytes, the star-shaped glial cells of the central nervous system (CNS), and act as primary neural stem cells (NSCs) that generate new neurons in the adult brain (Doetsch et al., 1999; Noctor et al., 2001; Seri et al., 2001; Dhaliwal and Lagace, 2011; Ming and Song, 2011).

Mammalian adult neurogenesis takes place predominantly *via* the NSCs confined to two distinct parts of the forebrain, i.e., the subventricular zone (SVZ) of the lateral ventricles in the telencephalon and the subgranular zone (SGZ) of the dentate gyrus in the hippocampus (Alvarez-Buylla et al., 2001; Kriegstein and Alvarez-Buylla, 2009; Bonfanti and Peretto, 2011). The restricted capacity of the neurogenic niches is explained partially by the reduction of constitutively active adult proliferation zones in mammalian brain during evolution (Rakic, 2002; Lindsey and Tropepe, 2006; Tanaka and Ferretti, 2009), a specific or general resistance against cell proliferation due to the evolution of tight control mechanisms against tumorigenesis (Pearson and Sanchez Alvarado, 2008), resistance to integrate new cells into a mature neural network (Kempermann et al., 2004; Kaslin et al., 2008), an altered cellular plasticity that affects stem or progenitor cell characteristics (Shihabuddin et al., 2000; Peng et al., 2002; Kizil et al., 2012b), or a non-permissive environment related to scar formation at the wound site after injury (Ekdahl et al., 2003; Fitch and Silver, 2008; Rolls et al., 2009). Low neurogenecity is paralleled by a limited potential in the integration of the newborn neurons in most regions of the mammalian brain, necessitating the use of another platform free of these constraints for the development of new therapeutic approaches (Bhardwaj et al., 2006; Ernst and Frisen, 2015; Alunni and Bally-Cuif, 2016).

In contrast to mammals, adult neurogenesis in zebrafish is robust and widespread, with 16 distinct constitutively proliferative zones that are mostly located along the ventricular surface but also deeper in the brain parenchyma (Kaslin et al., 2008). These zones are detected along the entire rostro-caudal axis of the zebrafish brain and contain ventricularly positioned self-renewing neural progenitors (Grandel et al., 2006; Kaslin et al., 2008; Kizil et al., 2012b; Grandel and Brand, 2013). Zebrafish CNS regenerates *via* the proliferation and differentiation of the radial glial cells (RGCs), also referred to as ependymoglia due to their functional orthology to the mammalian ependymal cells, and the neuroepithelial-like progenitor cells (Grandel et al., 2006; Ganz et al., 2010; Fleisch et al., 2011; Kizil et al., 2012b; Kaslin et al., 2017; Lindsey et al., 2017; Zambusi and Ninkovic, 2020). The permissive environment, which is necessary for these progenitors—upon injury—to become activated and differentiate into functional neurons, results most likely from the fact that zebrafish does not form any obvious scar tissue after injury in the CNS, thus granting zebrafish a regeneration potential higher than that of mammals (Becker and Becker, 2002; Kroehne et al., 2011).

Being one of the best-characterized regions of the adult zebrafish brain, the telencephalon harbors at least two distinct neurogenic zones, the dorsal and the medio-ventral neurogenic niches, with ependymoglial cells that differ in their proliferation and progeny characteristics (Marz et al., 2010; Zambusi and Ninkovic, 2020). Accordingly, these cells express different markers including glial fibrillary acidic protein (Gfap), S100β, nestin, brain lipid-binding protein (Blbp), aromatase, and SRY-box 2 (Sox2), confirming their radial glia-like nature (Adolf et al., 2006; Pellegrini et al., 2007; Lam et al., 2009; Ganz et al., 2010; Marz et al., 2010; Kroehne et al., 2011). A recent study on transcriptome analysis has identified novel markers for radial glia, newborn neurons, and mature neurons (Lange et al., 2020). Several inflammation-related programs including the chemokine receptor Cxcr5, the zinc finger transcription factor Gata3, and cysteinyl leukotriene signaling have been shown to promote the proliferation and generation of newborn neurons, thus enhancing neuronal regeneration in response to injury (Kizil et al., 2012a,b; Kyritsis et al., 2012). Fibroblast growth factor (Fgf) signaling and aryl hydrocarbon receptor (AhR) signaling have also been reported to directly regulate ependymoglial cell proliferation in the adult zebrafish telencephalon (Ganz et al., 2010; Di Giaimo et al., 2018). Yet, little is known about the neural signaling pathways and the molecular interaction networks that are involved in zebrafish brain regeneration. This is particularly in question for the early stages of brain regeneration, where a deeper knowledge of the contributory pathways with a special focus on their crosstalk is necessary to understand the underlying mechanisms.

To address these questions, we have set out to identify the genes that are differentially expressed in the zebrafish telencephalon during early regeneration in response to stab wound injury and focused on two early stages: (1) the early wound healing stage at 20 h post-lesion (hpl) and (2) the early proliferative stage at 3 days post-lesion (dpl). To this end, we have performed whole transcriptome analyses of the telencephalon by comparing (a) the lesioned and unlesioned hemispheres at two regenerative stages separately and (b) the lesioned hemispheres of the two stages to each other. Upon comparing the injury responses of the hemispheres at the early wound healing stage, we have found that the number of differentially expressed genes (DEGs) in the lesioned hemisphere is by far higher than that of the unlesioned hemisphere. In the early proliferative stage, however, the difference between the responses of the hemispheres declined noticeably and more than 40% of all DEGs are shared. Our comparative transcriptome analyses of the lesioned hemispheres at the wound healing and proliferative stages have revealed a considerably large pool of DEGs that are not shared, reflecting a discrepancy in the transcriptional profiles of these stages. Using Gene Ontology (GO) term and Kyoto Encyclopedia of Genes and Genomes (KEGG) pathway analysis,

we have deciphered an enrichment of the gene sets related to the Wnt/β-catenin signaling pathway predominantly at 20 hpl and confirmed this experimentally at the messenger RNA (mRNA) and protein levels. To further investigate how Wnt/β-catenin signaling regulates regeneration at the molecular level, we have unveiled the Wnt targetome by analyzing the transcriptomes of the lesioned hemispheres where Wnt signaling is suppressed from the time of injury to 20 hpl or 3 dpl. Our data have demonstrated that the Wnt targetome at 20 hpl is considerably larger than that at 3 dpl and that Wnt/β-catenin signaling controls a variety of key signaling pathways including p53, apoptosis, forkhead box O (FoxO), mitogen-activated protein kinase (MAPK), and mammalian target of rapamycin (mTOR) at the early wound healing stage of brain regeneration. Overall, by using a prominent combination of bioinformatics and experimental validation of the bioinformatics data, we unravel the whole transcriptomes of the lesioned and unlesioned hemispheres at the early wound healing and proliferative stages of brain regeneration and highlight the significance of Wnt/β-catenin signaling in the regulation of cellular and molecular events taking place during early regeneration.

MATERIALS AND METHODS

Stab Wound Assay

A transgenic reporter of Tcf/Lef-mediated transcription 6xTCF/Lef-miniP:2dGFP [Tg(6XTCF:dGFP)] (Shimizu et al., 2012) was used for RNA isolation and transcriptome analysis. Wild-type (wt) AB zebrafish were used for immunofluorescence staining. Before surgery, fish were anesthetized with 0.02% of Tricaine (MS-222, Sigma-Aldrich). Stab injury was performed in 6–9-months-old male fish as previously described (Kroehne et al., 2011; Baumgart et al., 2012). A 30-gauge needle was inserted through the left nostril until the end of the telencephalon. Afterward, the fish were transferred into a tank with freshwater. Animal experiments were approved by the Animal Experiments Local Ethics Committee of İzmir Biomedicine and Genome Center (IBG-AELEC).

Drug Treatment

To inhibit Wnt/β-catenin signaling during regeneration, zebrafish that are exposed to stab wound injury of the brain were immersed in fish water containing 20 μM IWR-1 (Sigma-Aldrich, MO, United States) dissolved in dimethyl sulfoxide (DMSO). Inhibitor of Wnt response (IWR) treatment was initiated directly after stab injury and terminated at either 20 hpl or 3 dpl. IWR-1 containing fish water was refreshed daily.

Tissue Preparation

After performing stab wound injury in the telencephalon, the fish were euthanized and severed heads were fixed in 4% paraformaldehyde (PFA) overnight at 4°C. Next, the heads were transferred into 20% sucrose–20% EDTA for 2 days at 4°C and 30% sucrose–20% EDTA overnight at 4°C. The heads were embedded in 20% sucrose–7.5% gelatin solution kept in a box filled with dry ice. Brain sections of 14 μm were cut at −20°C using a cryostat (CM1850, Leica, Wetzlar, Germany) and stored at -20°C until further use.

Immunohistochemistry and Imaging

The brain sections on slides were dried at room temperature (RT) for 20 min. The slides were washed twice with PBSTX (1× PBS/0.3% Triton X-100) for 10 min. After incubation with 10 mM sodium citrate for 15 min at 85°C, they were washed with 1 × PBS twice for 5 min and incubated with diluted primary antibody in PBSTX at 4°C overnight. The next day, the slides were washed three times with PBSTX for 10 min at RT, incubated with secondary antibody, and washed three times with 1× PBS for 5 min at RT. Images were obtained using an LSM 880 laser scanning confocal microscope (Carl Zeiss AG, Oberkochen, Germany). The primary antibodies are as follows: mouse anti-GFAP (1:500, ab154474, Abcam, Cambridge, United Kingdom), mouse anti-PCNA (1:500, M0879, Dako, Agilent, CA, United States), rabbit anti-S100β (1:500, Z0311, Dako, Agilent), mouse anti-acetylated tubulin (1:250, T6793, Sigma-Aldrich, MO, United States), and rabbit anti-phospho-β-catenin (1:100, D2F1, Cell Signaling Technology, MA, United States). The secondary antibodies are as follows: rhodamine (TRITC) AffiniPure donkey anti-rabbit IgG (1:200, 711-025-152, Jackson Immunoresearch Laboratories, PA, United States) and Cy5 AffiniPure donkey anti-rat IgG (H+L) (1:400, 712-175-150, Jackson Immunoresearch Laboratories). Nuclear staining was performed with 4′,6-diamidino-2-phenylindole (DAPI; 4083S, Cell Signaling Technology).

RNA Isolation and cDNA Preparation

After stab wound injury was performed, zebrafish were anesthetized using 0.02% Tricaine-S solution and sacrificed at either 20 h post-lesion (hpl) or 3 days post-lesion (dpl). Firstly, the heads were separated from the fish and then the lesioned (left) and unlesioned (right) hemispheres were dissected individually to examine the influence of the injury between them (**Figures 1A,B**). The left and right hemispheres of healthy zebrafish telencephalon were used as control samples. The experiments were carried out in triplicate for each group. All brain samples were transferred into an RNAprotect tissue reagent (Qiagen, Hilden, Germany) immediately to prevent RNA degradation. Total RNA was extracted using the RNeasy Plus Micro Kit (Qiagen) according to the manufacturer's instructions. RNA samples were quantified by using a NanoDrop 2000 spectrophotometer (Thermo Scientific, MA, United States). RNA integrity was assessed using an Agilent RNA 6000 Pico with the Agilent 2100 Bioanalyzer (Agilent Technologies, CA, United States). The samples were sent to the Genomics Core Facility (GeneCore, EMBL Heidelberg, Germany) for library preparation and RNA sequencing.

Library Preparation and RNA Sequencing

Libraries were prepared using an Illumina TruSeq RNA Library Preparation Kit v2 (Illumina, San Diego, CA, United States) according to the manufacturer's recommendations by using 500 ng complementary DNA (cDNA) as input. For size selection, 300

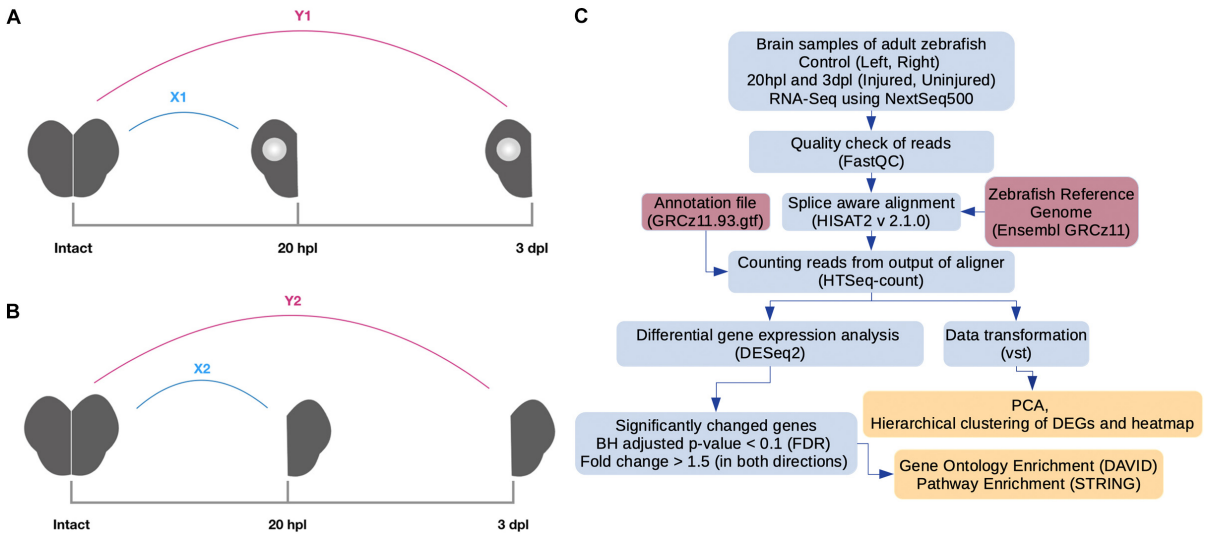

FIGURE 1 | Pipeline for RNA preparation and analysis of RNA sequencing (RNA-seq) data. **(A)** Preparation of RNA samples from the lesioned hemispheres at 20 hpl or 3 dpl. *X1*: comparison of the lesioned hemisphere at 20 hpl with the intact brain; *Y1*: comparison of the lesioned hemisphere at 3 dpl with the intact brain. **(B)** Preparation of RNA samples from the unlesioned hemispheres at 20 hpl or 3 dpl. *X2*: comparison of the unlesioned hemisphere at 20 hpl with the intact brain; *Y2*: comparison of the unlesioned hemisphere at 3 dpl with the intact brain. **(C)** RNA-seq reads were generated using Illumina NextSeq 500. The quality of reads was checked by the FastQC tool. Next, alignment and counting of reads were performed by using a zebrafish reference genome (Ensembl, GRCz11) and the annotation file (Ensembl, GRCz11.93) by HISAT2 and HTSeq-count tools, respectively. Counts were transformed with variance stabilizing transformation (vst) to perform principal component analysis and hierarchical clustering. To select genes as differentially expressed, we used the DESeq2 package with the following criteria: fold change > 1.5 (in both directions) and Benjamini–Hochberg adjusted *p*-value (FDR) < 0.1. Gene Ontology and pathway enrichment analyses were performed by using DAVID and the STRING tool of Cytoscape, respectively. *hpl*, hours post-lesion; *dpl*, days post-lesion.

bp cDNAs were selected. Paired-end, strand-specific sequencing for total RNA was performed on Illumina NextSeq 500 with 75 bp read lengths.

Bioinformatics Analysis

For each sample, quality control of the reads was inspected by using the FastQC tool; low-quality reads and adapter sequences were removed by using Trimmomatic (Bolger et al., 2014). RNA sequencing (RNA-seq) reads were aligned to the zebrafish reference genome (Ensembl, GRCz11) using HISAT2 (2.1.0) (Kim et al., 2015). After alignment, the transcripts were assembled and counted by HTSeq (Anders et al., 2015) by using the annotation file from the Ensembl website (Danio_rerio.GRCz11.93.gtf) (**Figure 1C**). The DESeq2 package (Love et al., 2014) of Bioconductor (Gentleman et al., 2004) was used to carry out normalization of read counts, their transformation (vst), and differential expression analysis. Principal component analysis (PCA) was performed to check the vst-transformed read counts and visualized with ggplot2 (Wickham, 2016; **Supplementary Figure S1**). To find DEGs, we performed Wald tests for the following comparisons using DESeq2: 20 hpl lesioned hemisphere vs. control (X1); 20 hpl unlesioned hemisphere vs. control (X2); 20 hpl lesioned hemisphere after IWR treatment vs. 20 hpl lesioned hemisphere (X3); 20 hpl lesioned hemisphere after IWR treatment vs. control (X4); 3 dpl lesioned hemisphere vs. control (Y1); 3 dpl unlesioned hemisphere vs. control (Y2); 3 dpl lesioned hemisphere after IWR treatment vs. 3-dpl lesioned hemisphere (Y3); and 3 dpl lesioned hemisphere after IWR treatment vs. control (Y4) (**Figures 1A,B**, **6B**). For all eight groups, we selected a gene as upregulated if the fold change > 1.5 and downregulated if the fold change < 0.67 (= 1/1.5), which we will simply refer to as "FC > 1.5 in both directions" hereafter (**Supplementary Table S1**). The lists of the significantly downregulated and upregulated genes obtained from individual comparisons were used as inputs for statistical enrichment analyses with regard to GO terms by using the Database for Annotation, Visualization and Integrated Discovery (DAVID) 6.8 bioinformatics functional annotation tool (Huang da et al., 2009). Functional enrichment was performed in three categories of GO terms: biological process (BP), molecular function (MF), and cellular component (CC). The EASE score, a modified one-tailed Fisher's exact test, was used to identify the GO terms by means of a user-defined gene list for each defined DAVID GO term. KEGG pathway (Kanehisa and Goto, 2000) and Reactome pathway (Fabregat et al., 2018) analyses were performed using all significantly changed genes with the StringApp tool of Cytoscape 3.7.2 (Shannon et al., 2003; Doncheva et al., 2019). Gene lists related to the selected GO terms and KEGG pathways were obtained from the KEGG and AmiGO databases and plotted using the GOplot package (Walter et al., 2015).

qPCR and Statistical Analysis

All samples with RIN ≥ 7.0 (our samples ranged from 8.1 to 10) were converted to cDNA using ProtoScript II First Strand cDNA Synthesis Kit (New England BioLabs, MA, United States)

according to the manufacturer's instructions. Zebrafish *rpl13a* (*ribosomal protein L13a*) was used as the reference gene for normalization to determine the relative gene expression levels. Quantitative PCR (qPCR) was performed in triplicate using GoTaq qPCR Master Mix (Promega, Madison, WI, United States) at an Applied Biosystems 7500 Fast Real Time PCR machine (Foster City, CA, United States). The data were analyzed using the GraphPad Prism 8 software (Graphpad Software Inc., CA, United States). The values are the mean ± SEM (standard error of mean) of three samples. Primer sequences for the following zebrafish genes are listed in **Supplementary Table S2**: *adam8a*, *c1qc*, *capgb*, *cd74b*, *cdk2*, *csf1ra*, *ctgfa*, *egfp*, *epha2a*, *foxo1a*, *fsta*, *gadd45ga*, *gfap*, *grem1b*, *il6st*, *inhbab*, *isl1*, *klf11b*, *lef1*, *mCherry*, *mpeg1.1*, *pappaa*, *pcna*, *prg4b*, *rpl13a*, *sgk2b*, *tbx2a*, and *tfa*.

RESULTS

Transcriptome Profiling of the Telencephalon During the Early Wound Healing Stage of Regeneration

While the later stages of brain regeneration have been relatively better understood, little is known about the early stages especially at the level of differential gene expression. To determine the changes in gene expression that control the molecular mechanisms underlying early brain regeneration, we aimed to identify and compare the entire transcriptomes of the zebrafish telencephalon at two early regenerative stages, i.e., 20 hpl and 3 dpl. Several telencephalon genes have been found to be significantly upregulated in the lesioned and unlesioned hemispheres (Kroehne et al., 2011; Kizil et al., 2012b). However, their injury responses have not been compared at the transcriptome level before. Thus, to distinguish between the responses of the lesioned and unlesioned hemispheres and avoid the dilution of genes that are differentially expressed mainly in the lesioned hemisphere, we decided to dissect the telencephalic hemispheres and have their transcriptome sequenced separately (**Figure 1**). Before sequencing, we validated the injury response by measuring the expression levels of *gfap* and *gata3* that are known to be strongly upregulated in the lesioned hemisphere upon injury (**Supplementary Figure S1**) (Kroehne et al., 2011). We found that 1,472 genes [829 upregulated (Up) and 643 downregulated (Down)] were significantly differentially expressed in the lesioned hemisphere at 20 hpl (X1) as compared to the equivalent hemisphere of the unlesioned brain, and 1,356 (785 Up and 571 Down) of them were unique to X1 (**Figure 2A** and **Supplementary Table S3**). *en1a*, *abhd2b*, and *lyrm5b* were in the top 10 Down genes while *mthfd1l*, *tbx2a*, and *entpd2b* were in the top 10 Up genes in X1 (**Figure 2B**). In the unlesioned hemisphere at 20 hpl (X2), we detected 211 DEGs (76 Up and 135 Down) with lower fold changes in both the Up and Down genes as compared to X1, and 95 genes (32 Up and 63 Down) were unique to X2 (**Figure 2A** and **Supplementary Table S3**). *igfbp1a*, *cd74a*, and *nt5c2l1* were the top three Down genes while *stat3*, *anxa2a*, and *mid1ip1b* were the top three Up genes in X2 (**Figure 2C**). Only 7% of all DEGs, i.e., 116 genes (44 Up and 72 Down), including those encoding for several heat shock proteins, leucine-rich repeat-containing proteins, and phosphatases were shared between X1 and X2 (**Figure 2A** and **Supplementary Table S3**). The top GO terms in X1 and X2 showed no overlap, parallel to the low number of genes shared between them (**Figures 2D,E**). We also determined altered GO terms and Reactome pathways by comparing the X1 and X2 groups (**Supplementary Figures S2, S3** and **Supplementary Tables S4, S5**). While there were 20 KEGG pathways significantly enriched in X1, only four pathways were enriched in X2 (**Figure 2F** and **Supplementary Table S5**). To confirm the results of the bioinformatics analyses, we quantified the expressions of several genes related to tissue regeneration (Kroehne et al., 2011; Tsujioka et al., 2017; Galvao et al., 2018; Yu et al., 2019). *prg4a* and *klf11* were indeed upregulated only in the lesioned hemisphere (**Figure 2G**), while *gfap* and *il6st* were so in both hemispheres (**Figure 2H**). Several tubulin genes (*tubb6*, *tuba1b*, *tuba8l*, *tub*, and *tubb4b*) were upregulated not only in X1 but also in X2 (*tuba8l4*) (**Supplementary Table S1**). We confirmed this by immunofluorescence staining for acetylated tubulin, a neuronal microtubule marker that mainly labeled the parenchyma cells in the control and became strongly upregulated in the cells lining the ventricle after injury (**Figures 2I,J**). These data collectively indicate that, at the early wound healing stage, remarkably, i.e., seven times, higher numbers of genes are differentially expressed in the lesioned hemisphere as compared to the unlesioned hemisphere.

Transcriptome Profiling of the Telencephalon During the Early Proliferative Stage of Regeneration

The telencephalon is known to react to injury by a strong induction of proliferation that peaks at 3 dpl mainly in the ventricular zone of the lesioned hemisphere (Kroehne et al., 2011; Marz et al., 2011; Lindsey et al., 2017). By analyzing the transcriptomics data at 3 dpl, we identified 1,707 genes (924 Up and 783 Down) to be significantly differentially expressed in the lesioned hemisphere at 3 dpl (Y1) as compared to the corresponding hemisphere of the unlesioned brain, and 861 (589 Up and 272 Down) of them were unique to Y1 (**Figure 3A** and **Supplementary Tables S1, S3**). In contrast to 20 hpl, most DEGs were shared between Y1 and Y2 (unlesioned hemisphere at 3 dpl), where we identified a total of 1,215 DEGs (530 Up and 685 Down), only 369 (195 Up and 174 Down) of which were unique to Y2 (**Figure 3A** and **Supplementary Tables S1, S3**). *en1a*, *mhc1uba*, and *mhc2dab* were in the top 10 Down genes in both Y1 and Y2, while *capgb*, *c1qb*, and *entpd2b* were in the top 10 Up genes in Y1 (**Figure 3B**) and *isl1*, *msh4*, and *tfa* were in the top 11 Up genes in Y2 (**Figure 3C**). Eight hundred forty-six genes (335 Up and 511 Down) were shared between Y1 and Y2 and harbored many members of gene families encoding for solute carriers, calcium channels, ring finger proteins, and protocadherins (**Figure 3A** and **Supplementary Table S3**). The top 40 GO terms in Y1 and Y2 overlapped by 25% (**Figures 3D,E**). We also defined altered GO terms and Reactome pathways by comparing the Y1 and Y2 groups (**Supplementary Figures S4, S5** and

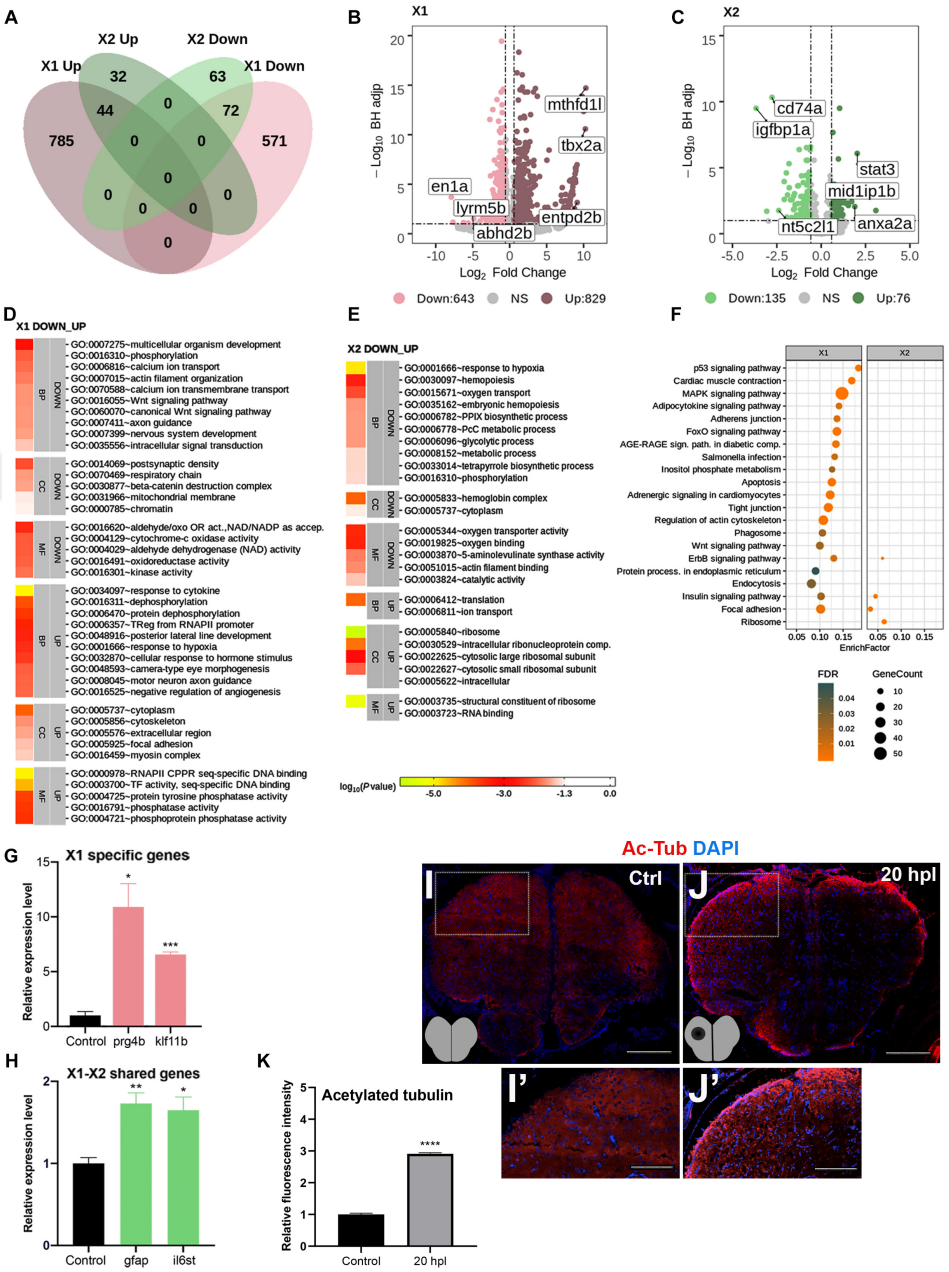

FIGURE 2 | Transcriptome profiling of the telencephalon during the early wound healing stage of regeneration. **(A)** The Venn diagram shows the number of upregulated (*Up*) or downregulated (*Down*) differentially expressed genes (DEGs) in the lesioned (*X1*, *pink*) and unlesioned (*X2*, *green*) hemispheres and the overlap between each set of DEGs at 20 hpl. A total of 1,472 and 211 genes were significantly changed in X1 and X2, respectively. There were 116 genes shared between X1 and X2. **(B,C)** Volcano plots representing changes in the gene expression levels in X1 and X2. *Each point* represents a gene. The *X*-axis shows $\log_2$ of fold change in the condition compared to control and the *vertical dashed lines* indicate the fold change cutoffs. The *Y*-axis represents -$\log_{10}$ of the Benjamini–Hochberg adjusted *p*-value, where the significance threshold is indicated by the *dashed horizontal line*. Number of upregulated genes in X1 and X2: 829 and 76, respectively, and downregulated genes in X1 and X2: 643 and 135, respectively. *Darker* and *lighter shades* in **(A–C)** indicate upregulation and downregulation, respectively. **(D,E)** DAVID bioinformatics tool was used to show the most significantly enriched GO terms based on the transcriptional changes in X1 and X2 comparisons. The heatmap scale shows $\log_{10}$ of the EASE *p*-value for the most significantly enriched GO terms. **(F)** STRING bioinformatics tool was used to show the most significantly enriched KEGG pathways based on the transcriptional changes in X1 and X2. The *dot plot* represents KEGG pathways enriched in X1 and X2 by using all significantly changed genes in these comparisons based on FDR and EnrichFactor. **(G,H)** Relative expression levels of X1-specific genes (*prg4b* and *klf11b*) and the genes shared between X1 and X2 (*gfap* and *il6st*). Statistical significance was evaluated using unpaired *t*-test. $^*p < 0.05$, $^{**}p < 0.01$, and $^{***}p < 0.001$. *Error bars* represent ± standard error of the mean (SEM, $n = 3$). **(I–I',J–J')** Anti-acetylated tubulin staining of the control and 20 hpl brain sections with *boxed* areas magnified. Sections are counterstained for DAPI. *Scale bars*, 200 μm in **(I,J)**; 100 μm in **(I')** and **(J')**. **(K)** Relative fluorescence intensity in brain sections stained for anti-acetylated tubulin. *DAVID*, Database for Annotation, Visualization and Integrated Discovery; *GO*, Gene Ontology; *BP*, biological process; *CC*, cellular component; *MF*, molecular function; *STRING*, Search Tool for the Retrieval of Interacting Genes/Proteins; *KEGG*, Kyoto Encyclopedia of Genes and Genomes; *FDR*, false discovery rate; *hpl*, hours post-lesion. See section "Materials and Methods" for the definition of DEGs covered in X and Y comparisons. $^*p < 0.05$, $^{**}p < 0.01$, $^{***}p < 0.001$, and $^{****}p < 0.0001$.

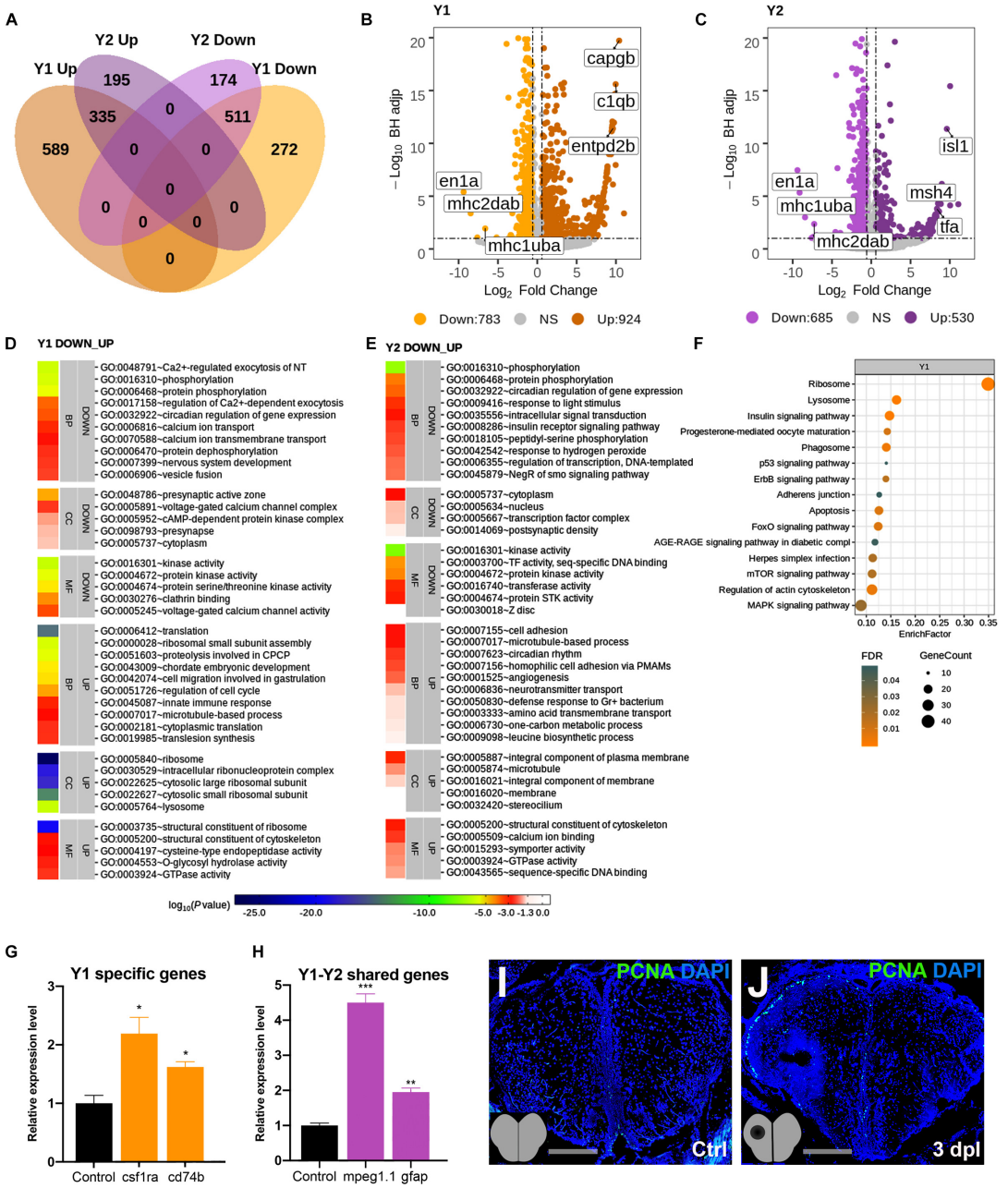

FIGURE 3 | Transcriptome profiling of the telencephalon during the early proliferative stage of regeneration. **(A)** The Venn diagram shows the number of upregulated (*Up*) or downregulated (*Down*) differentially expressed genes (DEGs) in the lesioned (*Y1*, *orange*) and unlesioned (*Y2*, *purple*) hemispheres and the overlap between each set of DEGs at 3 dpl. A total of 1,707 and 1,215 genes were significantly changed in Y1 and Y2, respectively. There were 846 genes shared between Y1 and Y2. **(B,C)** Volcano plots representing changes in the gene expression levels in Y1 and Y2. *Each point* represents a gene. The *X*-axis shows $\log_2$ of fold change in the condition compared to the control and *dashed vertical lines* indicate the fold change cutoff. The *Y*-axis represents $-\log_{10}$ of the Benjamini–Hochberg adjusted *p*-value, where the significance threshold is indicated by the *dashed horizontal line*. Number of upregulated genes in Y1 and Y2: 924 and 530, respectively, and downregulated genes in Y1 and Y2: 783 and 685, respectively. *Darker* and *lighter shades* in **(A–C)** indicate upregulation and downregulation, respectively. **(D,E)** DAVID bioinformatics tool was used to show the most significantly enriched GO terms based on the transcriptional changes in Y1 and Y2 comparisons. The heatmap scale shows $\log_{10}$ of the EASE *p*-value for the most significantly enriched GO terms. **(F)** STRING bioinformatics tool was used to show the most significantly enriched KEGG pathways based on the transcriptional changes in X1 and X2. The *dot plot* represents KEGG pathways enriched in X1 and X2 by using all significantly changed genes in these comparisons based on FDR and EnrichFactor. **(G,H)** Relative expression levels of Y1-specific genes (*csf1ra* and *cd74b*) and the genes shared between Y1 and Y2 (*mpeg1.1* and *gfap*). Statistical significance was evaluated using unpaired *t*-test. $^*p < 0.05$, $^{**}p < 0.01$, and $^{***}p < 0.001$. *Error bars* represent ± standard error of the mean (SEM, $n = 3$). **(I,J)** Anti-PCNA staining of the control and 3 dpl brain sections. Sections are counterstained for DAPI. *DAVID*, Database for Annotation, Visualization and Integrated Discovery; *GO*, Gene Ontology; *BP*, biological process; *CC*, cellular component; *MF*, molecular function; *STRING*, Search Tool for the Retrieval of Interacting Genes/Proteins; *KEGG*, Kyoto Encyclopedia of Genes and Genomes; *FDR*, false discovery rate; *dpl*, days post-lesion. See section "Materials and Methods" for the definition of DEGs covered in X and Y comparisons.

Supplementary Tables S4, S5). There were 15 KEGG pathways significantly enriched in Y1 (**Figure 3F** and **Supplementary Table S5**). The qPCR results confirmed that the regeneration-related DEGs *csf1ra* and *cd74b* (Chitu et al., 2016; Hwang et al., 2017) were upregulated in the lesioned hemisphere (**Figure 3G**) and *mpeg1.1* and *gfap* (Kroehne et al., 2011; Paredes et al., 2015) in both hemispheres (**Figure 3H**). Moreover, we observed a remarkable increase in the number of proliferating cells at the ventricular zone of the telencephalon in the lesioned hemisphere, detected by proliferating cell nuclear antigen (PCNA) antibody staining (**Figures 3I,J**). Thus, we conclude that the number of DEGs is higher in both hemispheres during the proliferative stage in comparison to the early wound healing stage and that 41% of all DEGs are shared between the lesioned and unlesioned hemispheres at this stage.

The Early Wound Healing and Proliferative Stages of Brain Regeneration Are More Different Than Similar

Next, to compare the molecular and cellular events that occur in the lesioned hemisphere of the telencephalon at its early wound healing and proliferative stages, we compared the transcriptome profiles of the X1 and Y1 groups in detail. There were 1,015 DEGs (566 Up and 449 Down) that were unique to X1 and 1,250 DEGs (705 Up and 545 Down) were unique to Y1 (**Figure 4A** and **Supplementary Table S6**). We found that 457 genes (27% of X1 DEGs and 31% of Y1 DEGs) were shared between X1 and Y1 (**Figure 4A** and **Supplementary Table S6**). Among them, 395 genes were regulated in the same way, i.e., Up in both or Down in both, while 62 were regulated inversely. We next intersected the DEGs in X1 and Y1 to reveal genes differentially expressed at both time points. The heatmap displayed four groups of shared genes: group 1 with nine genes (e.g., *caspb* and *notch3*) Down in X1 and Up in Y1; group 2 with 185 genes (e.g., *hif1an*) Down in both X1 and Y1; group 3 with 53 genes (e.g., *mapk6*) Up in X1 and Down in Y1; and group 4 with 210 genes (e.g., *stat3*, *il6st*, *slc7a11*, and *s100b*) Up in both X1 and Y1 (**Figures 4B,C** and **Supplementary Table S6**). To compare the molecular data obtained from 20 hpl and 3 dpl using GO term enrichment, we used three groups of DEGs: (1) DEGs unique to X1; (2) DEGs unique to Y1; and (3) DEGs shared between X1 and Y1. GO term and KEGG pathway analyses showed enrichment of the Wnt signaling pathway exclusively in X1, whereas several other signaling pathways including p53, ErbB, FoxO, apoptosis, insulin, and MAPK were shared between X1 and Y1; mTOR signaling was uniquely enriched in Y1 (**Figure 4D**, **Supplementary Figure S6**, and **Supplementary Table S5**). To validate differential gene expression, we selected DEGs that are unique to X1 (*tbx2a* and *grem1b*), unique to Y1 (*cdk2* and *c1qc*), or shared between X1 and Y1 (*adam8a* and *capgb*), which are all known to be involved in tissue regeneration (Schlomann et al., 2000; Garnier et al., 2009; Satoh and Makanae, 2014; Peterson et al., 2015; Wang et al., 2015; Tang et al., 2017). All selected DEGs became upregulated after injury in the corresponding hemisphere, as detected by qPCR (**Figures 4E–H**). Furthermore, immunofluorescence staining for the glial cell markers S100β and glial fibrillary acidic protein (GFAP) confirmed upregulation at both 20 hpl and 3 dpl (**Figures 4I–N**). Overall, the early wound healing and proliferative stages of brain regeneration share less than a third of their individual pools of DEGs, strongly suggesting that the molecular and cellular mechanisms of regeneration substantially differ at these stages.

Wnt/β-Catenin Signaling Is Activated During the Early Wound Healing Stage in the Regenerating Brain

Comparative analyses of the GO terms and KEGG pathways for the genes that are differentially expressed at 20 hpl and 3 dpl have disclosed a strong and specific enrichment of gene sets related to Wnt signaling at 20 hpl: "Wnt signaling pathway," "canonical Wnt signaling pathway," "β-catenin destruction complex," and "negative regulation of canonical Wnt signaling pathway" (**Figure 4D**, **Supplementary Figure S6**, and **Supplementary Tables S4, S5**). Thus, we next aimed to address the role and molecular targets of Wnt/β-catenin signaling, the so-called canonical Wnt pathway, during the early wound healing stage of brain regeneration. Wnt/β-catenin signaling is one of the most common intracellular signal transduction pathways activated in response to injury of virtually all tissues/organs (Ozhan and Weidinger, 2014). While Wnt signaling has been revealed to promote regeneration of the optic tectum, the spinal cord, and the tectum of the midbrain in zebrafish (Shimizu et al., 2012, 2018; Strand et al., 2016; Wehner et al., 2017; Lindsey et al., 2019), it has not yet been associated with the regeneration of the telencephalon. We have used the Tg(6XTCF:dGFP) transgenic zebrafish reporter of Tcf/Lef-mediated transcription, which has been shown to sensitively detect Wnt/β-catenin pathway activity in several cellular contexts (Shimizu et al., 2012). GFP expression in the reporter line is difficult to detect because of the unstable nature of GFP, leading to a low level of fluorescence in the adult zebrafish. We have performed immunofluorescence staining for anti-GFP at 20 hpl and detected Wnt activity in the lesioned area, most likely in the brain endothelial and blood cells (**Supplementary Figure S7**). Quantification of pathway activity by qPCR in the reporter line indeed showed an upregulation of Wnt signaling in both the lesioned and unlesioned hemispheres at 20 hpl (**Figure 5A**). Interestingly, signaling became downregulated in the lesioned hemisphere at 3 dpl while staying elevated in the unlesioned hemisphere, suggesting that it is specifically suppressed in the lesioned hemisphere after the wound healing stage. We also verified the significant activation of Wnt/β-catenin signaling at 20 hpl in the lesioned telencephalic hemispheres of the samples that were sent for RNA sequencing (**Figure 5B**). The Wnt/β-catenin target genes *lef1* and *egr2a* were likewise upregulated at 20 hpl in the lesioned hemispheres (**Figure 5C**). Immunofluorescence staining of brain sections showed an elevation of phospho-β-catenin (Ser675) levels in the lesioned hemisphere, especially in the vicinity of the lesion, indicating an increased transcriptional activity of β-catenin (**Figures 5D–I**). Considering the high levels of Wnt/β-catenin activity in the

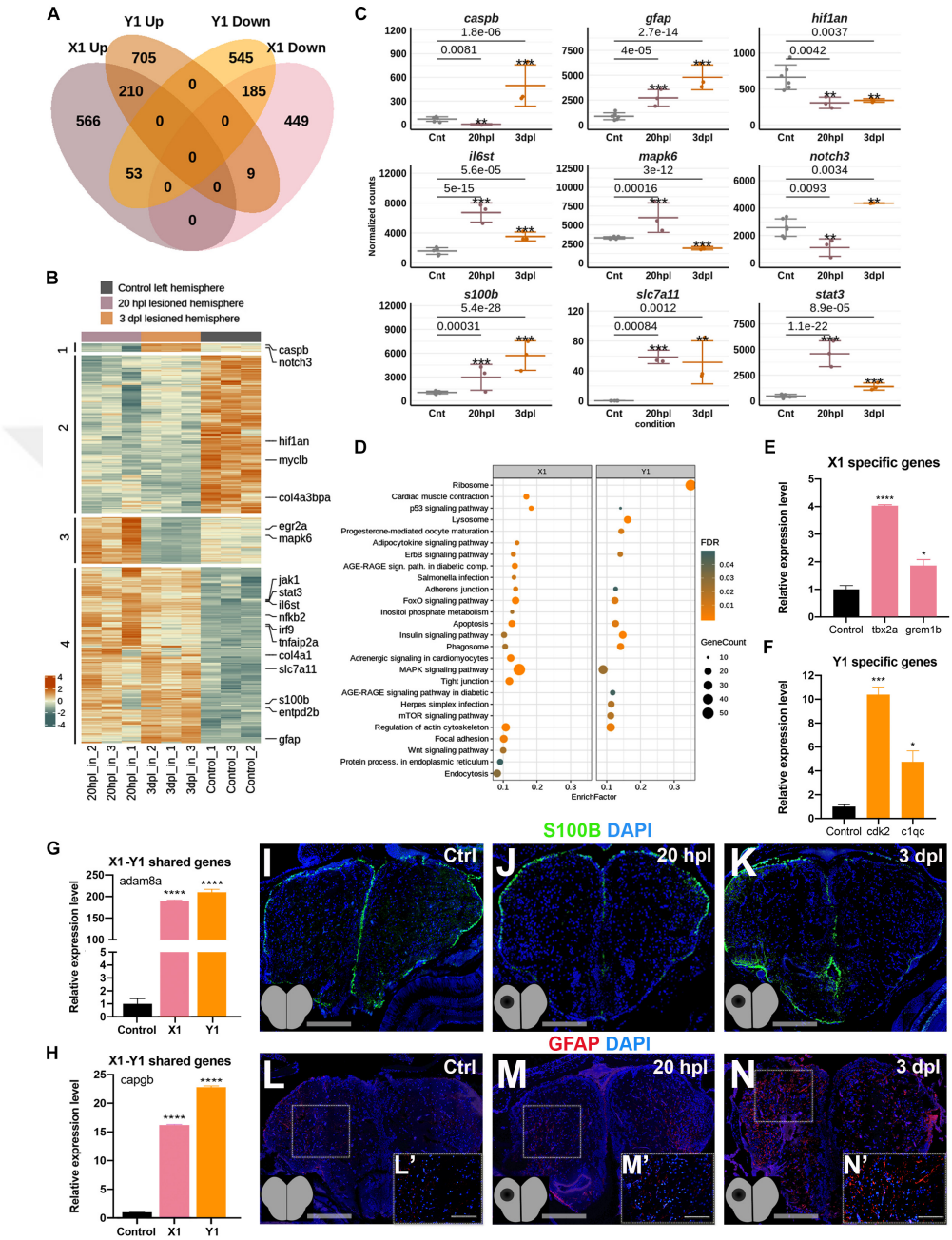

FIGURE 4 | Early wound healing and proliferative stages of brain regeneration are more different than similar. **(A)** The Venn diagram shows the number of upregulated (*Up*) or downregulated (*Down*) differentially expressed genes (DEGs) in the lesioned 20-hpl (*X1*, *pink*) and lesioned 3-dpl (*Y1*, *orange*) hemispheres and the overlap between each set of DEGs. Out of 1,472 genes, 1,015 were significantly changed only in X1, while 1,250 out of 1,707 genes were so in Y1. There were 457 genes shared between X1 and Y1. *Darker* and *lighter shades* indicate upregulation and downregulation, respectively. **(B)** The heatmap shows the expressions of genes shared between X1 and Y1. Each *column* represents a single hemisphere from a single telencephalon and each *row* shows a single gene. The *scale bar* shows counts *Z*-scores from high to low expression, represented by a color gradient from *orange* to *green*, respectively. **(C)** Dot plot representation of normalized transformed read counts of a representative set of genes shared between X1 and Y1 (*gray*: control samples; *pink*: 20-hpl lesioned hemisphere; *orange*: 3 dpl lesioned hemisphere). The mean ± standard deviations (SD) of three independent experiments are plotted. **(D)** STRING bioinformatics tool was used to show the most significantly enriched KEGG pathways based on the transcriptional changes in X1 and X2. The *dot plot* represents KEGG pathways enriched in X1 and Y1 by using all significantly changed genes in these comparisons based on FDR and EnrichFactor. **(E,F)** Relative expression levels of DEGs that are unique to X1 (*tbx2a* and *grem1b*) or unique to Y1 (*cdk2* and *c1qc*). **(G,H)** Relative expression levels of DEGs shared between X1 and Y1 (*adam8a* and *capgb*). Statistical significance was evaluated using unpaired *t*-test. ****$p < 0.0001$. *Error bars* represent ± standard error of the mean (SEM, $n = 3$). **(I–K)** Anti-S100β staining of the control, 20 hpl, and 3 dpl brain sections. **(L–N,L′–N′)** Anti-GFAP staining of the control, 20 hpl, and 3 dpl brain sections with *boxed* areas magnified. Sections are counterstained for DAPI. *Scale bars*, 200 μm in **(L–N)**; 100 μm in **(L′–N′)**. *STRING*, Search Tool for the Retrieval of Interacting Genes/Proteins; *KEGG*, Kyoto Encyclopedia of Genes and Genomes; *FDR*, false discovery rate; *hpl*, hours post-lesion; *dpl*, days post-lesion. See section "Materials and Methods" for the definition of DEGs covered in X and Y comparisons. *$p < 0.05$, **$p < 0.01$, ***$p < 0.001$, and ****$p < 0.0001$.

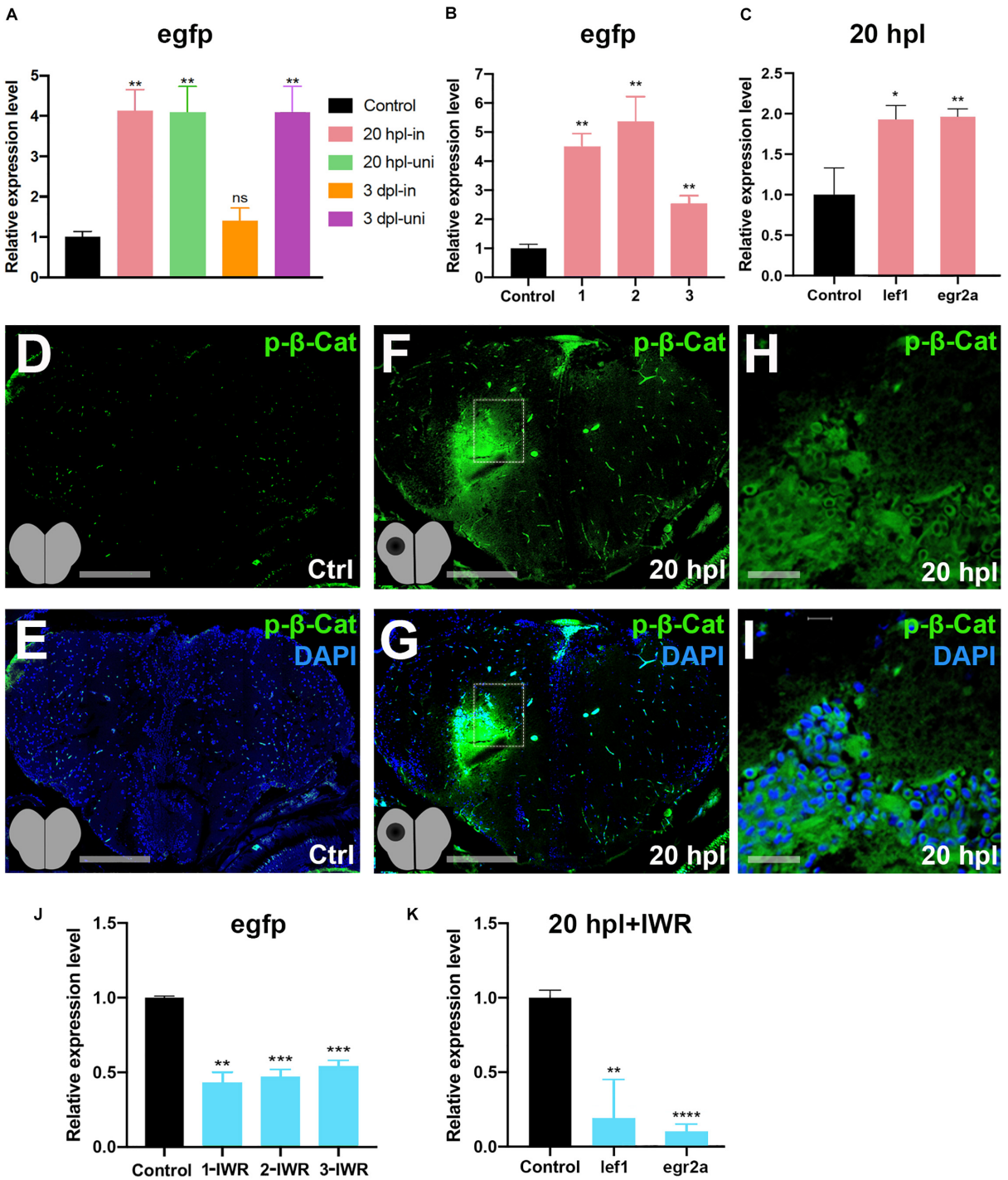

FIGURE 5 | Wnt/β-catenin signaling is activated during the early wound healing stage in the regenerating brain. **(A)** Relative expression levels of *egfp* as a reporter of Wnt/β-catenin signaling activity in the lesioned and unlesioned hemispheres of the telencephalon during the early wound healing and proliferative stages of regeneration. Three hemispheres were pooled for each sample. **(B)** Relative expression levels of *EGFP* as a reporter of Wnt/β-catenin signaling activity in the lesioned hemispheres of three independent telencephalon samples used for RNA sequencing during the early wound healing stage. **(C)** Relative expression levels of the known Wnt target genes *lef1* and *egr2a* in the lesioned hemisphere of the telencephalon during the early wound healing stage. **(D,E)** Anti-phospho-β-catenin staining of control brain sections. **(F,G)** Anti-phospho-β-catenin staining of 20-hpl brain sections. The lesioned area is *boxed* and shown in **(H,I)**. Sections are counterstained for DAPI. *Scale bars*, 200 μm in **(D–G)**; 25 μm in **(H,I)**. **(J)** Relative expression levels of *egfp* as a reporter of Wnt/β-catenin signaling activity in lesioned + IWR-1-treated hemispheres of three independent telencephalon samples collected at 20 hpl. **(K)** Relative expression levels of the Wnt target genes *lef-1* and *egr2a* in the pooled three lesioned + IWR-1-treated hemispheres at 20 hpl. Statistical significance was evaluated using unpaired *t*-test. $^{**}p < 0.01$ and $^{***}p < 0.001$. *Error bars* represent ± standard error of the mean (SEM, $n = 3$). *hpl*, hours post-lesion. $^{*}p < 0.05$, $^{**}p < 0.01$, $^{***}p < 0.001$, and $^{****}p < 0.0001$.

endothelial compartment of the zebrafish and mouse brains (Moro et al., 2012; Martowicz et al., 2019), it is likely that these Wnt-positive cells are non-CNS cells. To unravel how Wnt/β-catenin signaling regulates brain regeneration at the molecular level, we set out to identify its target genes in the early stage where signaling was significantly enhanced. To this purpose, we initially confirmed that Wnt/β-catenin signaling could be efficiently inhibited by the Wnt antagonist IWR-1, as evidenced by the significant reduction in the expressions of *egfp* in the Tg(6XTCF:dGFP) Wnt reporter and the canonical Wnt target genes *lef1* and *egr2a* in the lesioned hemisphere at 20 hpl (**Figures 5J,K**). Thus, we conclude that Wnt/β-catenin signaling is activated in the early wound healing stage of brain regeneration and returns to control level in the lesioned site at the early proliferative phase.

Inhibition of Wnt/β-Catenin Signaling During the Early Wound Healing Stage Identifies 119 Target Genes That Are Positively Regulated by the Pathway

Next, to identify the Wnt targetome at the early wound healing and proliferative stages of brain regeneration, we suppressed Wnt/β-catenin signaling starting from the time of injury to 20 hpl or to 3 dpl by treating the zebrafish with the Wnt antagonist IWR-1 and had the transcriptome of the lesioned hemispheres sequenced at 20 hpl or 3 dpl. There were 293 genes (64 Up and 229 Down) in X3 and 103 genes (70 Up and 33 Down) in Y3 comparisons (**Figure 6A** and **Supplementary Table S1**). We termed DEGs that are Up in X1 and Down in X3 as the positively regulated Wnt targetome at 20 hpl and the genes that are Up in Y1 and Down in Y3 as the positively regulated Wnt targetome at 3 dpl (**Figures 1A**, **6B**). The Wnt targetome that was composed of 119 genes at 20 hpl (**Figures 6C,D** and **Supplementary Table S7**) sharply narrowed down to nine genes at 3 dpl (**Supplementary Figure S9** and **Supplementary Table S7**). Next, to validate the Wnt targetome at 20 hpl, we measured the expression levels of some genes selected from the targetome by qPCR. All selected genes were significantly upregulated in the lesioned hemisphere following injury and became downregulated when Wnt signaling was inhibited by IWR-1 from the time of injury until 20 hpl (**Figures 6E,F**). These results strongly suggest a key role for Wnt/β-catenin signaling in the early wound healing stage of regeneration.

Inhibition of Wnt/β-Catenin Signaling During the Early Wound Stage Results in a Marked Alteration of the Gene Expression Profiles Represented in KEGG Pathway Enrichment

Among the KEGG pathways that were significantly enriched in the lesioned hemisphere at 20 hpl (X1) or 3 dpl (Y1), several of them, including the p53 signaling pathway, apoptosis, MAPK signaling pathway, and FoxO signaling pathway, were shared between X1 and Y1, whereas the Wnt and mTOR signaling pathways were unique to X1 and Y1, respectively (**Figures 2F**, **3F**, **4D**). Thus, we set out to compare how these KEGG pathways are altered in the lesioned hemisphere at 20 hpl and 3 dpl in response to inhibition of Wnt/β-catenin signaling. We termed the comparison of the 20 hpl lesioned hemisphere + IWR treatment to control as X4 and the comparison of the 3 dpl lesioned hemisphere + IWR treatment to control as Y4 (**Figure 6B**). There were 868 genes (387 Up and 481 Down) differentially expressed in X4 and 1,977 (1,179 Up and 798 Down) were so in Y4 (**Supplementary Table S1**). The genes we obtained from the KEGG and AmiGO databases included substantial numbers of genes involved in the Wnt, MAPK, apoptosis, mTOR, p53, and FoxO signaling pathways (**Supplementary Table S8**). To compare the alterations in the gene expression profiles related with these pathways during two regenerative stages, we intersected these genes with DEGs in X1, X4, Y1, and Y4. Strikingly, the number of significantly altered genes in X1 decreased dramatically after IWR treatment in X4 for all pathways (**Figures 7A–D** and **Supplementary Figure S10** compare the total number of brown and blue shaded boxes in X1 and X4; **Supplementary Table S8**). Among the Wnt signaling pathway genes that were detected in the two KEGG pathways, "WNT signaling pathway" (**Figure 7A**) and "WNT_GO signaling pathway" (**Supplementary Figure S10A**), 12 of the 14 genes that were Up in X1 (*csnk2a4*, *wnt5b*, *fosl1a*, *jun*, *mycb*, *dkk1a*, *gskip*, *ppm1ab*, *tnksa*, *fermt2*, *tmem198b*, and *tle3b*) did not significantly change any more after IWR treatment in X4, indicating that these 12 genes are positively regulated Wnt targets (**Figure 7A** and **Supplementary Figure S10A** compare the number of brown shaded boxes in X1 and X4). 18 of the 24 genes that were Down in X1 (*lrp6*, *ctbp1*, *fzd3b*, *apc*, *ctnnd2b*, *fzd3a*, *camk2d2*, *daam1b*, *ppp3r1a*, *fzd9b*, *tcf7l2*, *ccnd2a*, *rac3b*, *ndrg2*, *fto*, *reck*, *ankrd6b*, and *ccdc136b*) did not change any more in X4, suggesting that these 18 genes are negatively regulated Wnt targets (**Figure 7A** and **Supplementary Figure S10A** compare the number of blue shaded boxes in X1 and X4). On the contrary, the number of altered genes in Y1 did not change much either in Y4 (**Figure 7A** and **Supplementary Figure S10** compare the total number of brown and blue shaded boxes in Y1 and Y4; **Supplementary Table S8**). Accordingly, 20 out of 30 DEGs determined in the Wnt pathway-related genes that were differentially regulated in Y1 were likewise regulated after IWR treatment in Y4 (**Figure 7A** and **Supplementary Figure S10A**). Finally, we were able to validate some selected genes, i.e., *epha2a* as a MAPK pathway-related gene, *sgk2b* and *foxo1a* as FoxO signaling-related genes, and *gadd45ga* as a p53 pathway-related gene at 20 hpl (**Figure 7B**). Taken together, these data indicate that Wnt/β-catenin signaling controls the expression of a wide range of genes related to various signaling pathways, including p53, apoptosis, FoxO, MAPK, and mTOR, at the early wound healing stage of brain regeneration.

DISCUSSION

Although the zebrafish telencephalon has been carefully explored for its neurogenic niches that harbor stem or progenitor cells

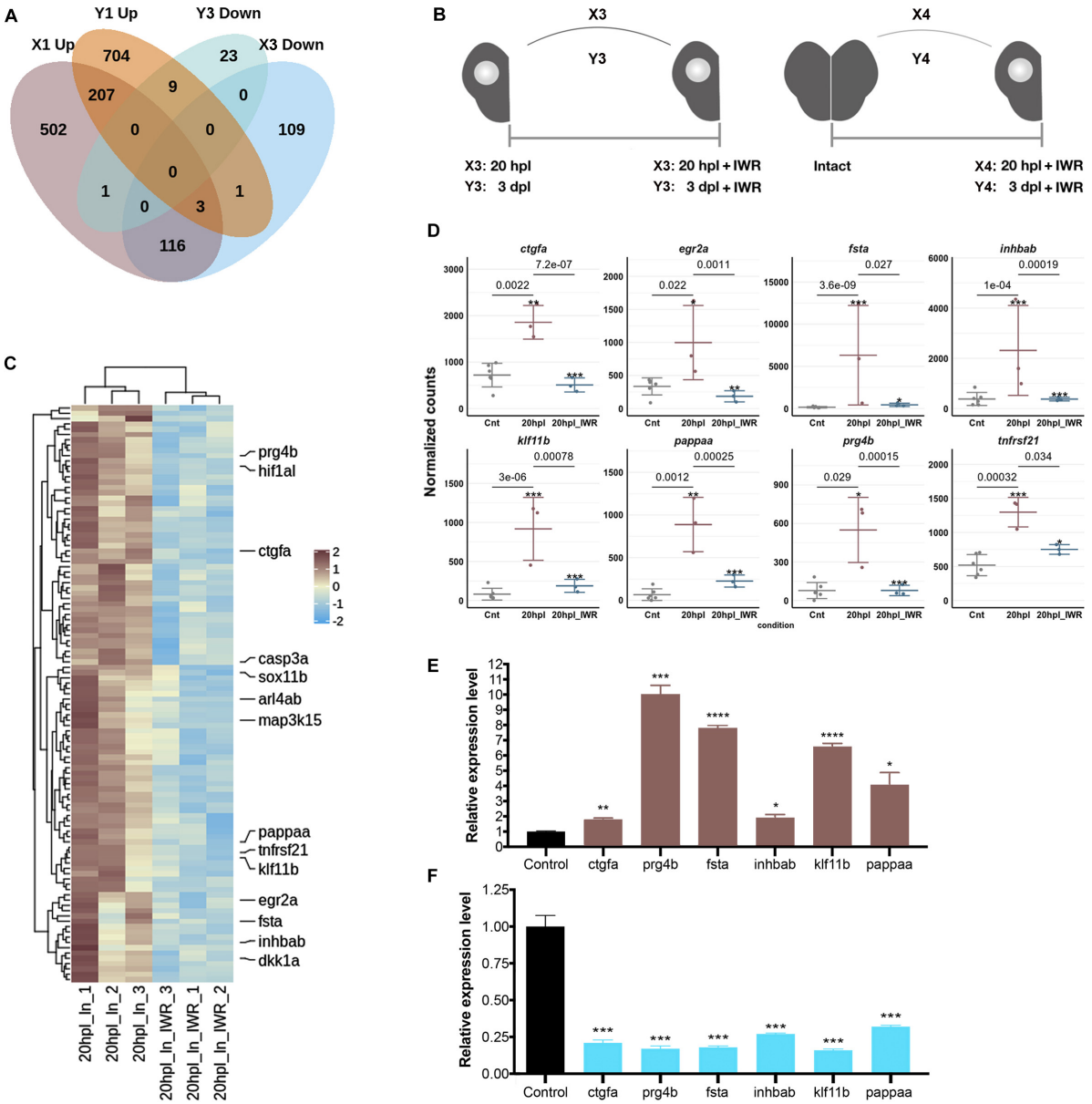

FIGURE 6 | Inhibition of Wnt/β-catenin signaling during the early wound healing stage identifies 119 target genes that are positively regulated by the pathway. **(A)** The Venn diagram shows the number of differentially expressed genes (DEGs) that are upregulated (*Up*) in the lesioned 20-hpl (*X1*, *dark pink*), downregulated (*Down*) in the lesioned + IWR-1-treated 20-hpl (*X3*, *light blue*), Up in the lesioned 3-dpl (*Y1*, *dark orange*), or Down in the lesioned + IWR-1-treated 3-dpl (*Y3*, *turquoise*) hemispheres and the overlap between each set of DEGs. There were 119 genes Up in X1 and Down in X3, while only nine genes were Up in Y1 and Down in Y3. **(B)** Preparation of RNA samples from the lesioned hemisphere at 20 hpl or 3 dpl. *X3*: 20-hpl lesioned hemisphere after IWR treatment vs. 20-hpl lesioned hemisphere; *Y3*: 3-dpl lesioned hemisphere after IWR treatment vs. 3-dpl lesioned hemisphere; *X4*: 20-hpl lesioned hemisphere after IWR treatment vs. control; *Y4*: 3-dpl lesioned hemisphere after IWR treatment vs. control. **(C)** The heatmap shows the Wnt target genes that are Up in X1 and Down in X3. Each *column* represents a single hemisphere from a single telencephalon and each *row* shows a single gene. The *scale bar* shows counts *Z*-scores from high to low expression, represented by a color gradient from *orange* to *green*, respectively. **(D)** Dot plot representation of normalized transformed read counts of a representative set of Wnt target genes that are Up in X1 and Down in X3 (*brown*: 20-hpl lesioned hemispheres; *blue*: 20-hpl lesioned + IWR-1-treated hemispheres). The mean ± standard deviations (SD) of three independent experiments are plotted. **(E,F)** Relative expression levels of the Wnt target genes that are Up in X1 and Down in X3 (*ctgfa*, *prg4b*, *fsta*, *inhbab*, *klf11b*, and *pappaa*). Statistical significance was evaluated using unpaired *t*-test. $^{*}p < 0.05$, $^{**}p < 0.01$, $^{***}p < 0.001$, and $^{****}p < 0.0001$. *Error bars* represent ± standard error of the mean (SEM, $n = 3$). See section "Materials and Methods" for the definition of DEGs covered in X and Y comparisons.

expressing different marker genes, comparative analysis of the transcriptome profiles at the early stages of telencephalon regeneration has not been performed yet. This is the first study that uncovers the global gene expression profiles of the regenerating zebrafish telencephalon in the lesioned and unlesioned hemispheres at two early stages of regeneration,

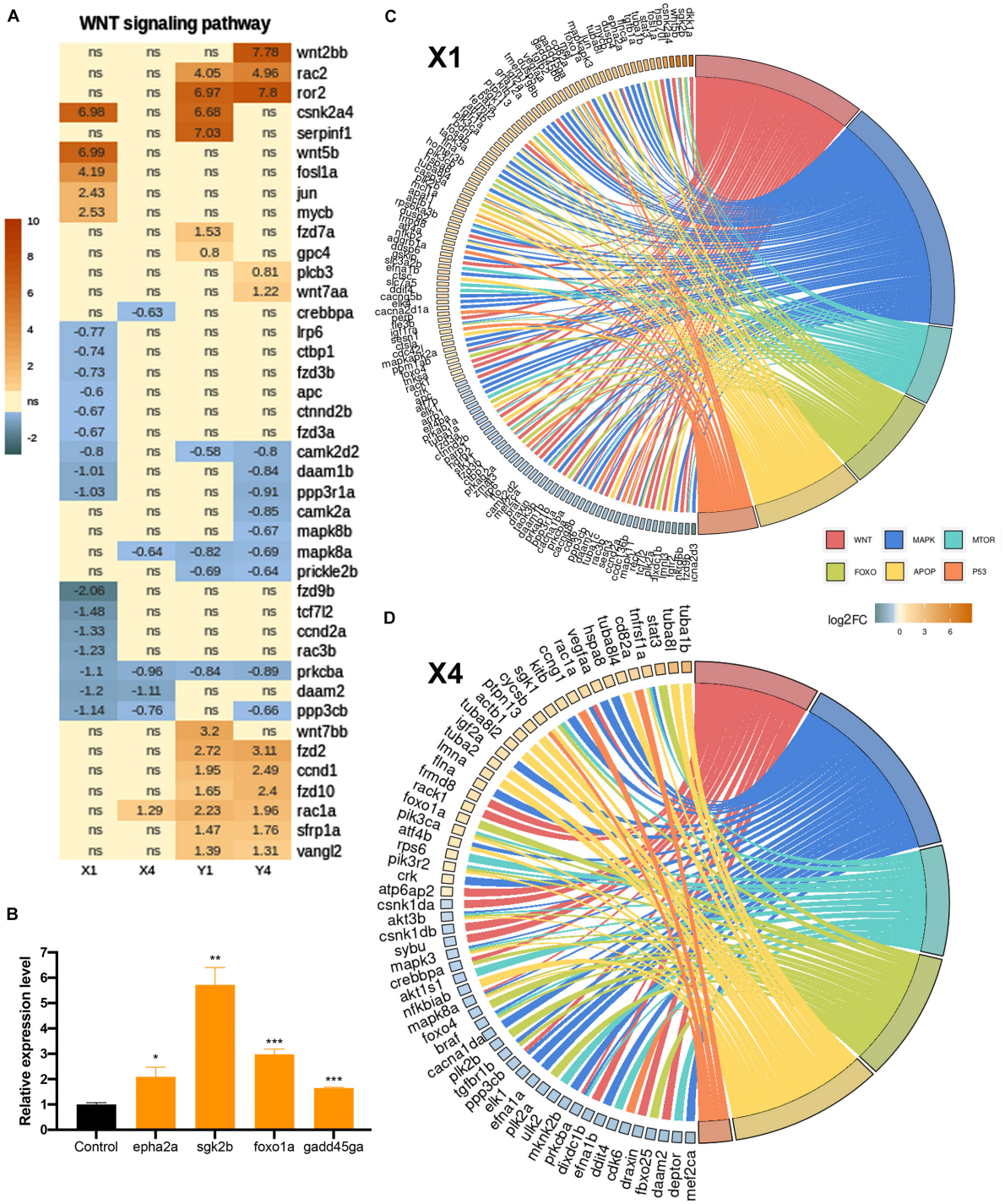

FIGURE 7 | Inhibition of Wnt/β-catenin signaling during the early wound stage results in a marked alteration of the gene expression profiles represented in Kyoto Encyclopedia of Genes and Genomes (KEGG) pathway enrichment. Heatmap representation of the uniquely changed genes in **(A)** the Wnt signaling pathway in X1, X4, Y1, and Y4 comparisons. Each *column* represents a comparison according to the DESeq2 results and each *row* shows a single gene. The *scale bar* shows $\log_2$ of the fold change values (when statistically significant) from high to low fold change, represented by a color gradient from *orange* to *blue*, respectively. Statistical significance was evaluated using Wald test. *ns*, non-significant. **(B,C)** GOChord plot of selected GO terms belonging to the biological process (BP) sub-ontology and KEGG pathways for X1 and X4 comparisons, respectively. The genes related to the Wnt-KEGG pathway and Wnt-Gene Ontology BP are intersected and represented as one group. The genes are linked to their assigned pathways by *ribbons* and ordered according to their $\log_2$ of the fold change values from high to low fold change, represented by a color gradient from *orange* to *blue*, respectively. **(D)** Relative expression levels of pathway-related genes (*epha2a*, *sgk2b*, *foxo1a*, and *gadd45ga*). Statistical significance was evaluated using unpaired *t*-test. $^{*}p < 0.05$, $^{**}p < 0.01$, and $^{***}p < 0.001$. *Error bars* represent ± standard error of the mean (SEM, $n = 3$). See section "Materials and Methods" for the definition of DEGs covered in X and Y comparisons.

which we defined as 20 hpl, corresponding to the early wound healing stage, and 3 dpl, to the early proliferative stage. Using comparative gene expression profiling, we describe for the first time that: (i) the total number of DEGs in the lesioned hemisphere is substantially higher than that in the unlesioned one at 20 hpl; (ii) the number of DEGs in 3 dpl is elevated as compared to 20 hpl and that 40% of all DEGs at 3 dpl are shared between the lesioned and unlesioned hemispheres; (iii) transcriptomes at 20 hpl and 3 dpl share less than a third of their DEGs; (iv) Wnt/β-catenin signaling is activated at 20 hpl, controlling the transcription of a large pool of target genes, 119 of which are positively regulated by the pathway; and (v) Wnt/β-catenin signaling results in a marked alteration of the gene expression profiles represented as enrichment of the KEGG pathways, including p53, apoptosis, MAPK, mTOR, and FoxO, at the early wound healing stage of brain regeneration.

Injury-induced proliferative response has been proposed to be primarily confined to the lesioned hemisphere of the telencephalon (Marz et al., 2011). Nevertheless, several genes are upregulated both in the lesioned and unlesioned hemispheres, though not to the same degree (Kroehne et al., 2011; Kizil et al., 2012b). The difference in the responses of the two hemispheres to injury could be due to differences in the methods used to induce a telencephalic injury. Nevertheless, whether the unlesioned part could be used as an effective internal control is a matter of debate. Strikingly, studies of hemispherectomy, where one cerebral hemisphere is completely removed or functionally disconnected, have demonstrated that the contralesional hemisphere is able to undertake various functions of the lesioned side, most likely due to a strong interaction between the lesioned and the intact halves in brain injuries (Sebastianelli et al., 2017). Such an interplay would be inevitably reflected as differential gene expression after injury not only in the lesioned but also in the unlesioned site of the telencephalon. Our results show that, at both 20 hpl and 3 dpl, many DEGs were shared between the lesioned (X1 or Y1) and the unlesioned (X2 or Y2) hemispheres and that the number of shared DEGs at 3 dpl was far higher than that at 20 hpl (see **Figures 2A**, **3A**). Thus, the lesioned and unlesioned hemispheres indeed appear to interact during telencephalon regeneration, and the level of this interaction increases from the early wound healing to the proliferative stage. The injury response appears to be most intense and peculiar at the wound site during the early wound healing stage and extends outside as the proliferative stage starts, leading to a considerable difference between the transcriptional programs activated at these two stages.

Cytokines released from innate immune cells play key roles in the regulation of the acute inflammatory response that is required for functional regeneration of the zebrafish CNS after injury (Kyritsis et al., 2012; Elsaeidi et al., 2014; Fuller-Carter et al., 2015; Tsarouchas et al., 2018). Our data showed prominent upregulation of the anti-inflammatory cytokine genes *il11a*, *il21*, and *il6st*, cytokine receptor encoding *il17ra1a*, the tumor necrosis factor receptor superfamily (TNFRSF) genes *tnfrsf18*, *tnfrsf21*, and the genes related to cytokine response *junba*, *jun*, *rel*, and *timp2a* at 20 hpl, suggesting that signaling through these early response cytokines is essential to orchestrate innate immune response (Opal and DePalo, 2000; Placke et al., 2010). Apoptosis is also activated in the early regenerative phase of various tissues including *Xenopus* tail, mouse liver, and cornea and is indispensable for effective wound healing (Tseng et al., 2007; Wilson et al., 2007; Li et al., 2010). Remarkably, we observed a significant upregulation of the apoptosis-related genes including *apaf1*, *baxa*, *traf4b*, *tgfb2*, *sgk1*, and *casp3a* selectively in the lesioned hemisphere at 20 hpl (Elmore, 2007; Gilbert et al., 2016; Liu et al., 2017; Kreckel et al., 2019). Strikingly, many of them were downregulated when Wnt/β-catenin signaling was suppressed, pointing out a positive regulatory role for Wnt signaling in apoptosis during early brain regeneration. Dual-specific phosphatase (DUSP) genes were also upregulated in the lesioned hemisphere. Among these, *dusp6* has been shown to promote cell death in different contexts (Domercq et al., 2011; Piya et al., 2012). Apoptosis has been proposed as a key factor to resolve inflammation by driving the conversion of immune response into a wound healing response in the early phases of tissue repair (Brown et al., 1997; Wu and Chen, 2014). Thus, parallel elevations in the expression levels of genes related to cytokine signaling and apoptosis at 20 hpl could underlie the capacity of zebrafish telencephalon to convert the early inflammatory response into a healing ability and consolidate this time point as a representative of the early wound healing stage during telencephalon regeneration.

Angiogenic sprouting into the injured area has been described as another prominent event that takes place as early as 15 h after injury during heart regeneration in zebrafish (Marin-Juez et al., 2016). Significantly upregulated *vascular endothelial growth factor a-a* (*vegfaa*), a key regulator of angiogenesis, is essential for cardiomyocyte proliferation and heart regeneration (Marin-Juez et al., 2016). Likewise, the neuropilin genes *nrp1a*, *nrp1b*, and *nrp2a*, which encode for transmembrane receptors of vascular endothelial growth factors (VEGFs), are upregulated in injured hearts at 1 dpl and the glucose transporter gene *slc2a1b* upregulated in vascular endothelial cells in response to hypoxia (Delcourt et al., 2015; Guo and Vander Kooi, 2015; Lowe et al., 2019). CNS regeneration also involves an intense crosstalk between neurons and vascular niches that mediates angiogenesis mainly through the activation of VEGF and contributes to neuroprotection (Ruiz de Almodovar et al., 2009). We noted a significant upregulation of *vegfaa*, *nrp1a*, *nrp1b*, and *slc2a1b* genes specifically in the lesioned hemisphere at 20 hpl, arguing that injury activates a fast angiogenic sprouting mechanism during telencephalon regeneration.

Optic nerve injury in adult zebrafish induces the expression of the axon growth inhibitor suppressor of cytokine signaling 3 (*socs3*) in retinal ganglion cells, ultimately attenuating regeneration (Smith et al., 2009; Elsaeidi et al., 2014). We found that while upregulated at 20 hpl, *socs3a* was strongly downregulated at 3 dpl. *socs3b*, *sox11b*, and *klf6a*, which are associated with optic nerve regeneration (Veldman et al., 2007), were likewise induced at 20 hpl, with *sox11b* becoming downregulated at 3 dpl. More axon guidance genes including *robo1*, *tnc*, and *boc* (Lee et al., 2001; Connor et al., 2005; Schweitzer et al., 2005) were downregulated primarily in the

lesioned hemisphere at 20 hpl. Such biphasic expression of axon growth inhibitors during brain regeneration suggests a stage-specific regulation of axon growth.

The proliferative response of the injured zebrafish telencephalon is driven by the RGCs and reaches a peak at the lesioned site around 3 dpl (Marz et al., 2011; Kizil et al., 2012c). At this stage, we observed that some quiescent RGC genes such as *fabp7a*, *mt-atp8*, *hipk1a*, *s100b*, and *mgll* were upregulated in both hemispheres, while *ptn*, *luzp2*, *psap*, *hepacama*, and *anxa11b* were only upregulated in the lesioned side (Kaslin et al., 2017; Lange et al., 2020). On the other hand, proliferating RGC genes including *tmsb4x*, *hmgb2a*, *hmga1a*, *rps23*, and *ran* were exclusively upregulated in the lesioned half, whereas the general proliferation marker *ccnd1* was upregulated in both halves (Lange et al., 2020). Besides, we found that many cell cycle-associated genes such as *pcna*, *mki67*, *rpl35*, *mdka*, *ccna2*, and *cdk1* were upregulated predominantly in the lesioned hemisphere (Sobecki et al., 2017). Together, these results validate 3 dpl as a highly proliferative phase dominated by RGC activities and reveal that this proliferative response is clearly more pronounced in the lesioned hemisphere.

As the resident macrophages of the CNS, microglia have been shown to engulf dead cells after brain injury in zebrafish (Herzog et al., 2019). Previous studies have identified various microglia- and/or macrophage-specific markers that are differentially regulated during regeneration of the retina and olfactory bulb (Oosterhof et al., 2017; Mitchell et al., 2019). At 3 dpl, a considerable number of microglial genes including *mhc1zba*, *marco*, *spi1b*, *csf1ra*, and *mfap4* were upregulated exclusively in the lesioned hemisphere, while a few including *mpeg1.1* and *sall3a* were upregulated in both hemispheres. This prominent emanation of microglial signature at 3 dpl correlates with the extensive proliferation of microglia induced by neuronal cell death (Oosterhof et al., 2017). Furthermore, we found 18 innate immune response genes (see **Supplementary Table S4**) to be upregulated at 3 dpl. Among them, *nfkb2* and *csf1ra* are involved in the activation of innate immune response during heart and tail fin regeneration (Petrie et al., 2014; Karra et al., 2015; Morales and Allende, 2019). Activation of the immune response thus needs to be analyzed together with the related signaling pathways to understand the mechanisms of proper tissue healing.

Wnt/β-catenin signaling appears to play a positive, regeneration-promoting role in most systems, from invertebrates that display whole-body regeneration to organs that mammals can completely or partially regenerate, such as the liver, skeletal muscle, and kidney (Whyte et al., 2012; Ozhan and Weidinger, 2014). Wnt signaling is also essential for the organs that regenerate completely only in the lower vertebrates, such as the appendages (Stoick-Cooper et al., 2007; Singh et al., 2018) and the eye (Hayashi et al., 2008; Patel et al., 2017). In the adult zebrafish, Wnt/β-catenin signaling is involved in the proliferation and differentiation of neural stem or progenitor cells in the hypothalamus, optic tectum, and spinal cord (Wang et al., 2009; Shi et al., 2015; Shitasako et al., 2017; Wehner et al., 2017). Our results further support the role of canonical Wnt signaling in regeneration by providing the first evidence of active signaling in the zebrafish telencephalon at a very early stage of regeneration, i.e., 20 hpl. Wnt/β-catenin signaling activity has been identified around the necrotic lesions in mouse liver and hair follicle regeneration models (Ito et al., 2007; Whyte et al., 2012; Zhao et al., 2019). Likewise, we have demonstrated the early activation of Wnt/β-catenin signaling near the lesioned area of the telencephalon. At 1 dpl, the telencephalic lesion is known to be filled with blood cells and is surrounded by macrophages/microglial cells, indicating an early infiltration of these cells into the site of tissue damage (Ayari et al., 2010). Therefore, identification of the types of blood and immune cells with active Wnt/β-catenin signaling at 20 hpl would unravel its role in the early wound healing process of brain regeneration. Interestingly, signaling becomes downregulated to control levels in the lesioned hemisphere at 3 dpl. Wnt/β-catenin signaling has been reported to have biphasic roles during heart, muscle, and liver development, where early and late signaling activities have diverse roles (Monga et al., 2001; Naito et al., 2006; Klaus et al., 2007; Ueno et al., 2007; Brack et al., 2008; Gessert and Kuhl, 2010). Thus, it is likely that Wnt signaling is regulated at least in a biphasic manner in the course of adult brain response to injury.

Several of the Wnt target genes we identified, including *sox11b*, *casp3a*, *klf11*, and *egr2a*, are known to be involved in the regulation of Wnt/β-catenin activity (Spittau and Krieglstein, 2012; Zaman et al., 2012; Zimmerman et al., 2013; Liu et al., 2019). Moreover, a wide range of genes related to the p53, apoptosis, MAPK, mTOR, and FoxO pathways are regulated by Wnt/β-catenin signaling during early wound healing, but become far less responsive to Wnt later at the proliferative stage. Wnt/β-catenin signaling has been implicated in the regulation of proliferation and differentiation of various progenitor cells during tissue regeneration *via* controlling the p53, mTOR, and FoxO pathways (Hirose et al., 2014; Peng et al., 2014; Maiese, 2015; Lund-Ricard et al., 2020). Besides, an intense crosstalk between the MAPK and Wnt signaling pathways has been deciphered in development, cancer, and regeneration (Caverzasio and Manen, 2007; Bikkavilli et al., 2008; Zhang et al., 2014). Our results reveal for the first time that these signaling pathways are activated in response to canonical Wnt pathway early after the telencephalon injury. Further functional studies will clarify how Wnt signaling interacts with these pathways to regulate the early regenerative response in brain regeneration.

In conclusion, our comparative transcriptome analyses of the regenerating zebrafish telencephalon at the early wound healing and proliferative stages reveal differentially expressed genes and altered biological pathways that control the cellular and molecular mechanisms of regeneration. The great burden caused by traumatic brain injuries and neurodegenerative diseases to humanity necessitates the development of therapeutic interventions, which is tightly dependent on unraveling these mechanisms that render possible effective brain regeneration.

DATA AVAILABILITY STATEMENT

All datasets have been deposited in ArrayExpress under the link: https://www.ebi.ac.uk/arrayexpress/experiments/E-MTAB-9321/ with the accession number "E-MTAB-9321".

ETHICS STATEMENT

The animal study was reviewed and approved by the Animal Experiments Local Ethics Committee of İzmir Biomedicine and Genome Center (IBG AELEC/IBG-HADYEK).

AUTHOR CONTRIBUTIONS

GO, YD, and GC designed the experiments. GC and YP performed the molecular and cell biology experiments. YD, SM, GH, and IP conducted the bioinformatics analyses. GO, YD, and GC wrote the manuscript. All authors contributed to the discussion.

FUNDING

This work was supported by the Scientific and Technological Research Council of Turkey (TUBITAK, grant number 215Z365). GO Lab is funded by EMBO Installation Grant (IG 3024). YD was supported by an EMBO Short-Term Fellowship (#7783) and a FEBS Short-Term Fellowship. GH was supported by an EMBL-EBI/Embassy of France in London Fellowship.

ACKNOWLEDGMENTS

We thank İzmir Biomedicine and Genome Center Vivarium-Zebrafish Core Facility, Optical Imaging Core Facility, and Histopathology Core Facility for providing zebrafish care, microscope facility support, and histopathology service support, respectively. We also would like to thank the Genomics Core Facility (GeneCore) of EMBL, Heidelberg.

SUPPLEMENTARY MATERIAL

The Supplementary Material for this article can be found online at: https://www.frontiersin.org/articles/10.3389/fcell.2020.584604/full#supplementary-material

REFERENCES

Adolf, B., Chapouton, P., Lam, C. S., Topp, S., Tannhauser, B., Strahle, U., et al. (2006). Conserved and acquired features of adult neurogenesis in the zebrafish telencephalon. *Dev. Biol.* 295, 278–293. doi: 10.1016/j.ydbio.2006.03.023

Alunni, A., and Bally-Cuif, L. (2016). A comparative view of regenerative neurogenesis in vertebrates. *Development* 143, 741–753. doi: 10.1242/dev.122796

Alvarez-Buylla, A., Garcia-Verdugo, J. M., and Tramontin, A. D. (2001). A unified hypothesis on the lineage of neural stem cells. *Nat. Rev. Neurosci.* 2, 287–293. doi: 10.1038/35067582

Anders, S., Pyl, P. T., and Huber, W. (2015). HTSeq–a python framework to work with high-throughput sequencing data. *Bioinformatics* 31, 166–169. doi: 10.1093/bioinformatics/btu638

Ayari, B., El Hachimi, K. H., Yanicostas, C., Landoulsi, A., and Soussi-Yanicostas, N. (2010). Prokineticin 2 expression is associated with neural repair of injured adult zebrafish telencephalon. *J. Neurotrauma* 27, 959–972. doi: 10.1089/neu.2009.0972

Baumgart, E. V., Barbosa, J. S., Bally-Cuif, L., Gotz, M., and Ninkovic, J. (2012). Stab wound injury of the zebrafish telencephalon: a model for comparative analysis of reactive gliosis. *Glia* 60, 343–357. doi: 10.1002/glia.22269

Becker, C. G., and Becker, T. (2002). Repellent guidance of regenerating optic axons by chondroitin sulfate glycosaminoglycans in zebrafish. *J. Neurosci.* 22, 842–853. doi: 10.1523/jneurosci.22-03-00842.2002

Bhardwaj, R. D., Curtis, M. A., Spalding, K. L., Buchholz, B. A., Fink, D., Bjork-Eriksson, T., et al. (2006). Neocortical neurogenesis in humans is restricted to development. *Proc. Natl. Acad. Sci. U.S.A.* 103, 12564–12568. doi: 10.1073/pnas.0605177103

Bikkavilli, R. K., Feigin, M. E., and Malbon, C. C. (2008). p38 mitogen-activated protein kinase regulates canonical Wnt-beta-catenin signaling by inactivation of GSK3beta. *J. Cell Sci.* 121(Pt 21), 3598–3607. doi: 10.1242/jcs.032854

Bolger, A. M., Lohse, M., and Usadel, B. (2014). Trimmomatic: a flexible trimmer for Illumina sequence data. *Bioinformatics* 30, 2114–2120. doi: 10.1093/bioinformatics/btu170

Bonfanti, L., and Peretto, P. (2011). Adult neurogenesis in mammals–a theme with many variations. *Eur. J. Neurosci.* 34, 930–950. doi: 10.1111/j.1460-9568.2011.07832.x

Brack, A. S., Conboy, I. M., Conboy, M. J., Shen, J., and Rando, T. A. (2008). A temporal switch from notch to Wnt signaling in muscle stem cells is necessary for normal adult myogenesis. *Cell Stem Cell* 2, 50–59. doi: 10.1016/j.stem.2007.10.006

Brown, D. L., Kao, W. W., and Greenhalgh, D. G. (1997). Apoptosis down-regulates inflammation under the advancing epithelial wound edge: delayed patterns in diabetes and improvement with topical growth factors. *Surgery* 121, 372–380. doi: 10.1016/s0039-6060(97)90306-8

Caverzasio, J., and Manen, D. (2007). Essential role of Wnt3a-mediated activation of mitogen-activated protein kinase p38 for the stimulation of alkaline phosphatase activity and matrix mineralization in C3H10T1/2 mesenchymal cells. *Endocrinology* 148, 5323–5330. doi: 10.1210/en.2007-0520

Chapouton, P., Jagasia, R., and Bally-Cuif, L. (2007). Adult neurogenesis in non-mammalian vertebrates. *Bioessays* 29, 745–757. doi: 10.1002/bies.20615

Chitu, V., Gokhan, S., Nandi, S., Mehler, M. F., and Stanley, E. R. (2016). Emerging roles for CSF-1 receptor and its ligands in the nervous system. *Trends Neurosci.* 39, 378–393. doi: 10.1016/j.tins.2016.03.005

Connor, R. M., Allen, C. L., Devine, C. A., Claxton, C., and Key, B. (2005). BOC, brother of CDO, is a dorsoventral axon-guidance molecule in the embryonic vertebrate brain. *J. Comp. Neurol.* 485, 32–42. doi: 10.1002/cne.20503

Delcourt, N., Quevedo, C., Nonne, C., Fons, P., O'Brien, D., Loyaux, D., et al. (2015). Targeted identification of sialoglycoproteins in hypoxic endothelial cells and validation in zebrafish reveal roles for proteins in angiogenesis. *J. Biol. Chem.* 290, 3405–3417. doi: 10.1074/jbc.M114.618611

Dhaliwal, J., and Lagace, D. C. (2011). Visualization and genetic manipulation of adult neurogenesis using transgenic mice. *Eur. J. Neurosci.* 33, 1025–1036. doi: 10.1111/j.1460-9568.2011.07600.x

Di Giaimo, R., Durovic, T., Barquin, P., Kociaj, A., Lepko, T., Aschenbroich, S., et al. (2018). The aryl hydrocarbon receptor pathway defines the time frame for restorative neurogenesis. *Cell Rep.* 25, 3241–3251.e5. doi: 10.1016/j.celrep.2018.11.055

Doetsch, F., Caille, I., Lim, D. A., Garcia-Verdugo, J. M., and Alvarez-Buylla, A. (1999). Subventricular zone astrocytes are neural stem cells in the adult mammalian brain. *Cell* 97, 703–716. doi: 10.1016/s0092-8674(00)80783-7

Doetsch, F., and Scharff, C. (2001). Challenges for brain repair: insights from adult neurogenesis in birds and mammals. *Brain Behav. Evol.* 58, 306–322. doi: 10.1159/000057572

Domercq, M., Alberdi, E., Sanchez-Gomez, M. V., Ariz, U., Perez-Samartin, A., and Matute, C. (2011). Dual-specific phosphatase-6 (Dusp6) and ERK mediate AMPA receptor-induced oligodendrocyte death. *J. Biol. Chem.* 286, 11825–11836. doi: 10.1074/jbc.M110.153049

Doncheva, N. T., Morris, J. H., Gorodkin, J., and Jensen, L. J. (2019). Cytoscape stringapp: network analysis and visualization of proteomics data. *J. Proteome Res.* 18, 623–632. doi: 10.1021/acs.jproteome.8b00702

Ekdahl, C. T., Claasen, J. H., Bonde, S., Kokaia, Z., and Lindvall, O. (2003). Inflammation is detrimental for neurogenesis in adult brain. *Proc. Natl. Acad. Sci. U.S.A.* 100, 13632–13637. doi: 10.1073/pnas.2234031100

Elmore, S. (2007). Apoptosis: a review of programmed cell death. *Toxicol. Pathol.* 35, 495–516. doi: 10.1080/01926230701320337

Elsaeidi, F., Bemben, M. A., Zhao, X. F., and Goldman, D. (2014). Jak/Stat signaling stimulates zebrafish optic nerve regeneration and overcomes the inhibitory actions of Socs3 and Sfpq. *J. Neurosci.* 34, 2632–2644. doi: 10.1523/JNEUROSCI.3898-13.2014

Ernst, A., and Frisen, J. (2015). Adult neurogenesis in humans- common and unique traits in mammals. *PLoS Biol.* 13:e1002045. doi: 10.1371/journal.pbio.1002045

Fabregat, A., Jupe, S., Matthews, L., Sidiropoulos, K., Gillespie, M., Garapati, P., et al. (2018). The reactome pathway knowledgebase. *Nucleic Acids Res.* 46, D649–D655. doi: 10.1093/nar/gkx1132

Fitch, M. T., and Silver, J. (2008). CNS injury, glial scars, and inflammation: inhibitory extracellular matrices and regeneration failure. *Exp. Neurol.* 209, 294–301. doi: 10.1016/j.expneurol.2007.05.014

Fleisch, V. C., Fraser, B., and Allison, W. T. (2011). Investigating regeneration and functional integration of CNS neurons: lessons from zebrafish genetics and other fish species. *Biochim. Biophys. Acta* 1812, 364–380. doi: 10.1016/j.bbadis.2010.10.012

Fuller-Carter, P. I., Carter, K. W., Anderson, D., Harvey, A. R., Giles, K. M., and Rodger, J. (2015). Integrated analyses of zebrafish miRNA and mRNA expression profiles identify miR-29b and miR-223 as potential regulators of optic nerve regeneration. *BMC Genomics* 16:591. doi: 10.1186/s12864-015-1772-1

Galvao, J., Iwao, K., Apara, A., Wang, Y., Ashouri, M., Shah, T. N., et al. (2018). The kruppel-like factor gene target dusp14 regulates axon growth and regeneration. *Invest. Ophthalmol. Vis. Sci.* 59, 2736–2747. doi: 10.1167/iovs.17-23319

Ganz, J., Kaslin, J., Hochmann, S., Freudenreich, D., and Brand, M. (2010). Heterogeneity and Fgf dependence of adult neural progenitors in the zebrafish telencephalon. *Glia* 58, 1345–1363. doi: 10.1002/glia.21012

Garnier, D., Loyer, P., Ribault, C., Guguen-Guillouzo, C., and Corlu, A. (2009). Cyclin-dependent kinase 1 plays a critical role in DNA replication control during rat liver regeneration. *Hepatology* 50, 1946–1956. doi: 10.1002/hep.23225

Gentleman, R. C., Carey, V. J., Bates, D. M., Bolstad, B., Dettling, M., Dudoit, S., et al. (2004). Bioconductor: open software development for computational biology and bioinformatics. *Genome Biol.* 5:R80. doi: 10.1186/gb-2004-5-10-r80

Gessert, S., and Kuhl, M. (2010). The multiple phases and faces of wnt signaling during cardiac differentiation and development. *Circ. Res.* 107, 186–199. doi: 10.1161/circresaha.110.221531

Gilbert, R. W. D., Vickaryous, M. K., and Viloria-Petit, A. M. (2016). Signalling by transforming growth factor beta isoforms in wound healing and tissue regeneration. *J. Dev. Biol.* 4:21. doi: 10.3390/jdb4020021

Grandel, H., and Brand, M. (2013). Comparative aspects of adult neural stem cell activity in vertebrates. *Dev. Genes Evol.* 223, 131–147. doi: 10.1007/s00427-012-0425-5

Grandel, H., Kaslin, J., Ganz, J., Wenzel, I., and Brand, M. (2006). Neural stem cells and neurogenesis in the adult zebrafish brain: origin, proliferation dynamics, migration and cell fate. *Dev. Biol.* 295, 263–277. doi: 10.1016/j.ydbio.2006.03.040

Guo, H. F., and Vander Kooi, C. W. (2015). Neuropilin functions as an essential cell surface receptor. *J. Biol. Chem.* 290, 29120–29126. doi: 10.1074/jbc.R115.687327

Hayashi, T., Mizuno, N., and Kondoh, H. (2008). Determinative roles of FGF and Wnt signals in iris-derived lens regeneration in newt eye. *Dev. Growth Differ.* 50, 279–287. doi: 10.1111/j.1440-169X.2008.01005.x

Herzog, C., Pons Garcia, L., Keatinge, M., Greenald, D., Moritz, C., Peri, F., et al. (2019). Rapid clearance of cellular debris by microglia limits secondary neuronal cell death after brain injury in vivo. *Development* 146:dev174698. doi: 10.1242/dev.174698

Hirose, K., Shiomi, T., Hozumi, S., and Kikuchi, Y. (2014). Mechanistic target of rapamycin complex 1 signaling regulates cell proliferation, cell survival, and differentiation in regenerating zebrafish fins. *BMC Dev. Biol.* 14:42. doi: 10.1186/s12861-014-0042-9

Huang da, W., Sherman, B. T., and Lempicki, R. A. (2009). Systematic and integrative analysis of large gene lists using DAVID bioinformatics resources. *Nat. Protoc.* 4, 44–57. doi: 10.1038/nprot.2008.211

Hwang, I. K., Park, J. H., Lee, T. K., Kim, D. W., Yoo, K. Y., Ahn, J. H., et al. (2017). CD74-immunoreactive activated M1 microglia are shown late in the gerbil hippocampal CA1 region following transient cerebral ischemia. *Mol. Med. Rep.* 15, 4148–4154. doi: 10.3892/mmr.2017.6525

Ito, M., Yang, Z., Andl, T., Cui, C., Kim, N., Millar, S. E., et al. (2007). Wnt-dependent de novo hair follicle regeneration in adult mouse skin after wounding. *Nature* 447, 316–320. doi: 10.1038/nature05766

Kanehisa, M., and Goto, S. (2000). KEGG: kyoto encyclopedia of genes and genomes. *Nucleic Acids Res.* 28, 27–30. doi: 10.1093/nar/28.1.27

Karra, R., Knecht, A. K., Kikuchi, K., and Poss, K. D. (2015). Myocardial NF-kappaB activation is essential for zebrafish heart regeneration. *Proc. Natl. Acad. Sci. U.S.A.* 112, 13255–13260. doi: 10.1073/pnas.1511209112

Kaslin, J., Ganz, J., and Brand, M. (2008). Proliferation, neurogenesis and regeneration in the non-mammalian vertebrate brain. *Philos. Trans. R. Soc. Lond. B Biol. Sci.* 363, 101–122. doi: 10.1098/rstb.2006.2015

Kaslin, J., Kroehne, V., Ganz, J., Hans, S., and Brand, M. (2017). Distinct roles of neuroepithelial-like and radial glia-like progenitor cells in cerebellar regeneration. *Development* 144, 1462–1471. doi: 10.1242/dev.144907

Kempermann, G., Wiskott, L., and Gage, F. H. (2004). Functional significance of adult neurogenesis. *Curr. Opin. Neurobiol.* 14, 186–191. doi: 10.1016/j.conb.2004.03.001

Kim, D., Langmead, B., and Salzberg, S. L. (2015). HISAT: a fast spliced aligner with low memory requirements. *Nat. Methods* 12, 357–360. doi: 10.1038/nmeth.3317

Kizil, C., Dudczig, S., Kyritsis, N., Machate, A., Blaesche, J., Kroehne, V., et al. (2012a). The chemokine receptor cxcr5 regulates the regenerative neurogenesis response in the adult zebrafish brain. *Neural Dev.* 7:27. doi: 10.1186/1749-8104-7-27

Kizil, C., Kaslin, J., Kroehne, V., and Brand, M. (2012b). Adult neurogenesis and brain regeneration in zebrafish. *Dev. Neurobiol.* 72, 429–461. doi: 10.1002/dneu.20918

Kizil, C., Kyritsis, N., Dudczig, S., Kroehne, V., Freudenreich, D., Kaslin, J., et al. (2012c). Regenerative neurogenesis from neural progenitor cells requires injury-induced expression of Gata3. *Dev. Cell* 23, 1230–1237. doi: 10.1016/j.devcel.2012.10.014

Klaus, A., Saga, Y., Taketo, M. M., Tzahor, E., and Birchmeier, W. (2007). Distinct roles of Wnt/beta-catenin and Bmp signaling during early cardiogenesis. *Proc. Natl. Acad. Sci. U.S.A.* 104, 18531–18536. doi: 10.1073/pnas.0703113104

Kreckel, J., Anany, M. A., Siegmund, D., and Wajant, H. (2019). TRAF2 controls death receptor-induced caspase-8 processing and facilitates proinflammatory signaling. *Front. Immunol.* 10:2024. doi: 10.3389/fimmu.2019.02024

Kriegstein, A., and Alvarez-Buylla, A. (2009). The glial nature of embryonic and adult neural stem cells. *Annu. Rev. Neurosci.* 32, 149–184. doi: 10.1146/annurev.neuro.051508.135600

Kroehne, V., Freudenreich, D., Hans, S., Kaslin, J., and Brand, M. (2011). Regeneration of the adult zebrafish brain from neurogenic radial glia-type progenitors. *Development* 138, 4831–4841. doi: 10.1242/dev.072587

Kyritsis, N., Kizil, C., Zocher, S., Kroehne, V., Kaslin, J., Freudenreich, D., et al. (2012). Acute inflammation initiates the regenerative response in the adult zebrafish brain. *Science* 338, 1353–1356. doi: 10.1126/science.1228773

Lam, C. S., Marz, M., and Strahle, U. (2009). gfap and nestin reporter lines reveal characteristics of neural progenitors in the adult zebrafish brain. *Dev. Dyn.* 238, 475–486. doi: 10.1002/dvdy.21853

Lange, C., Rost, F., Machate, A., Reinhardt, S., Lesche, M., Weber, A., et al. (2020). Single cell sequencing of radial glia progeny reveals the diversity of newborn neurons in the adult zebrafish brain. *Development* 147:dev185595. doi: 10.1242/dev.185595

Lee, J. S., Ray, R., and Chien, C. B. (2001). Cloning and expression of three zebrafish roundabout homologs suggest roles in axon guidance and cell migration. *Dev. Dyn.* 221, 216–230. doi: 10.1002/dvdy.1136

Li, F., Huang, Q., Chen, J., Peng, Y., Roop, D. R., Bedford, J. S., et al. (2010). Apoptotic cells activate the "phoenix rising" pathway to promote wound healing and tissue regeneration. *Sci. Signal.* 3:ra13. doi: 10.1126/scisignal.2000634

Lindsey, B. W., Aitken, G. E., Tang, J. K., Khabooshan, M., Douek, A. M., Vandestadt, C., et al. (2019). Midbrain tectal stem cells display diverse regenerative capacities in zebrafish. *Sci. Rep.* 9:4420. doi: 10.1038/s41598-019-40734-z

Lindsey, B. W., Douek, A. M., Loosli, F., and Kaslin, J. (2017). A whole brain staining, embedding, and clearing pipeline for adult zebrafish to visualize cell proliferation and morphology in 3-dimensions. *Front. Neurosci.* 11:750. doi: 10.3389/fnins.2017.00750

Lindsey, B. W., and Tropepe, V. (2006). A comparative framework for understanding the biological principles of adult neurogenesis. *Prog. Neurobiol.* 80, 281–307. doi: 10.1016/j.pneurobio.2006.11.007

Liu, W., Wang, X., Liu, Z., Wang, Y., Yin, B., Yu, P., et al. (2017). SGK1 inhibition induces autophagy-dependent apoptosis via the mTOR-Foxo3a pathway. *Br. J. Cancer* 117, 1139–1153. doi: 10.1038/bjc.2017.293

Liu, Z., Zhong, Y., Chen, Y. J., and Chen, H. (2019). SOX11 regulates apoptosis and cell cycle in hepatocellular carcinoma via Wnt/beta-catenin signaling pathway. *Biotechnol. Appl. Biochem.* 66, 240–246. doi: 10.1002/bab.1718

Love, M. I., Huber, W., and Anders, S. (2014). Moderated estimation of fold change and dispersion for RNA-seq data with DESeq2. *Genome Biol.* 15:550. doi: 10.1186/s13059-014-0550-8

Lowe, V., Wisniewski, L., Sayers, J., Evans, I., Frankel, P., Mercader-Huber, N., et al. (2019). Neuropilin 1 mediates epicardial activation and revascularization in the regenerating zebrafish heart. *Development* 146:dev174482. doi: 10.1242/dev.174482

Lund-Ricard, Y., Cormier, P., Morales, J., and Boutet, A. (2020). mTOR signaling at the crossroad between metazoan regeneration and human diseases. *Int. J. Mol. Sci.* 21:2718. doi: 10.3390/ijms21082718

Maiese, K. (2015). FoxO transcription factors and regenerative pathways in diabetes mellitus. *Curr. Neurovasc. Res.* 12, 404–413. doi: 10.2174/1567202612666150807112524

Marin-Juez, R., Marass, M., Gauvrit, S., Rossi, A., Lai, S. L., Materna, S. C., et al. (2016). Fast revascularization of the injured area is essential to support zebrafish heart regeneration. *Proc. Natl. Acad. Sci. U.S.A.* 113, 11237–11242. doi: 10.1073/pnas.1605431113

Martowicz, A., Trusohamn, M., Jensen, N., Wisniewska-Kruk, J., Corada, M., Ning, F. C., et al. (2019). Endothelial beta-catenin signaling supports postnatal brain and retinal angiogenesis by promoting sprouting, tip cell formation, and VEGFR (vascular endothelial growth factor receptor) 2 expression. *Arterioscler. Thromb. Vasc. Biol.* 39, 2273–2288. doi: 10.1161/ATVBAHA.119.312749

Marz, M., Chapouton, P., Diotel, N., Vaillant, C., Hesl, B., Takamiya, M., et al. (2010). Heterogeneity in progenitor cell subtypes in the ventricular zone of the zebrafish adult telencephalon. *Glia* 58, 870–888. doi: 10.1002/glia.20971

Marz, M., Schmidt, R., Rastegar, S., and Strahle, U. (2011). Regenerative response following stab injury in the adult zebrafish telencephalon. *Dev. Dyn.* 240, 2221–2231. doi: 10.1002/dvdy.22710

Ming, G. L., and Song, H. (2011). Adult neurogenesis in the mammalian brain: significant answers and significant questions. *Neuron* 70, 687–702. doi: 10.1016/j.neuron.2011.05.001

Mitchell, D. M., Sun, C., Hunter, S. S., New, D. D., and Stenkamp, D. L. (2019). Regeneration associated transcriptional signature of retinal microglia and macrophages. *Sci. Rep.* 9:4768. doi: 10.1038/s41598-019-41298-8

Monga, S. P., Pediaditakis, P., Mule, K., Stolz, D. B., and Michalopoulos, G. K. (2001). Changes in WNT/beta-catenin pathway during regulated growth in rat liver regeneration. *Hepatology* 33, 1098–1109. doi: 10.1053/jhep.2001.23786

Morales, R. A., and Allende, M. L. (2019). Peripheral macrophages promote tissue regeneration in zebrafish by fine-tuning the inflammatory response. *Front. Immunol.* 10:253. doi: 10.3389/fimmu.2019.00253

Moro, E., Ozhan-Kizil, G., Mongera, A., Beis, D., Wierzbicki, C., Young, R. M., et al. (2012). In vivo Wnt signaling tracing through a transgenic biosensor fish reveals novel activity domains. *Dev. Biol.* 366, 327–340. doi: 10.1016/j.ydbio.2012.03.023

Naito, A. T., Shiojima, I., Akazawa, H., Hidaka, K., Morisaki, T., Kikuchi, A., et al. (2006). Developmental stage-specific biphasic roles of Wnt/beta-catenin signaling in cardiomyogenesis and hematopoiesis. *Proc. Natl. Acad. Sci. U.S.A.* 103, 19812–19817. doi: 10.1073/pnas.0605768103

Noctor, S. C., Flint, A. C., Weissman, T. A., Dammerman, R. S., and Kriegstein, A. R. (2001). Neurons derived from radial glial cells establish radial units in neocortex. *Nature* 409, 714–720. doi: 10.1038/35055553

Oosterhof, N., Holtman, I. R., Kuil, L. E., van der Linde, H. C., Boddeke, E. W., Eggen, B. J., et al. (2017). Identification of a conserved and acute neurodegeneration-specific microglial transcriptome in the zebrafish. *Glia* 65, 138–149. doi: 10.1002/glia.23083

Opal, S. M., and DePalo, V. A. (2000). Anti-inflammatory cytokines. *Chest* 117, 1162–1172. doi: 10.1378/chest.117.4.1162

Ozhan, G., and Weidinger, G. (2014). "Restoring tissue homeostasis: wnt signaling in tissue regeneration after acute injury," in *Wnt Signalling in Development and Disease: Molecular Mechanisms and Biological Functions*, eds S. P. Hoppler, and R. T. Moon (Hoboken, NJ: Wiley-Blackwell), 339–356.

Paredes, R., Ishibashi, S., Borrill, R., Robert, J., and Amaya, E. (2015). Xenopus: an in vivo model for imaging the inflammatory response following injury and bacterial infection. *Dev. Biol.* 408, 213–228. doi: 10.1016/j.ydbio.2015.03.008

Patel, A. K., Park, K. K., and Hackam, A. S. (2017). Wnt signaling promotes axonal regeneration following optic nerve injury in the mouse. *Neuroscience* 343, 372–383. doi: 10.1016/j.neuroscience.2016.12.020

Pearson, B. J., and Sanchez Alvarado, A. (2008). Regeneration, stem cells, and the evolution of tumor suppression. *Cold Spring Harb. Symp. Quant. Biol.* 73, 565–572. doi: 10.1101/sqb.2008.73.045

Pellegrini, E., Mouriec, K., Anglade, I., Menuet, A., Le Page, Y., Gueguen, M. M., et al. (2007). Identification of aromatase-positive radial glial cells as progenitor cells in the ventricular layer of the forebrain in zebrafish. *J. Comp. Neurol.* 501, 150–167. doi: 10.1002/cne.21222

Peng, W. M., Yu, L. L., Bao, C. Y., Liao, F., Li, X. S., and Zuo, M. X. (2002). Transplanted neuronal precursors migrate and differentiate in the developing mouse brain. *Cell Res.* 12, 223–228. doi: 10.1038/sj.cr.7290128

Peng, X., Yang, L., Chang, H., Dai, G., Wang, F., Duan, X., et al. (2014). Wnt/beta-catenin signaling regulates the proliferation and differentiation of mesenchymal progenitor cells through the p53 pathway. *PLoS One* 9:e97283. doi: 10.1371/journal.pone.0097283

Peterson, S. L., Nguyen, H. X., Mendez, O. A., and Anderson, A. J. (2015). Complement protein C1q modulates neurite outgrowth in vitro and spinal cord axon regeneration in vivo. *J. Neurosci.* 35, 4332–4349. doi: 10.1523/JNEUROSCI.4473-12.2015

Petrie, T. A., Strand, N. S., Yang, C. T., Rabinowitz, J. S., and Moon, R. T. (2014). Macrophages modulate adult zebrafish tail fin regeneration. *Development* 141, 2581–2591. doi: 10.1242/dev.098459

Piya, S., Kim, J. Y., Bae, J., Seol, D. W., Moon, A. R., and Kim, T. H. (2012). DUSP6 is a novel transcriptional target of p53 and regulates p53-mediated apoptosis by modulating expression levels of Bcl-2 family proteins. *FEBS Lett.* 586, 4233–4240. doi: 10.1016/j.febslet.2012.10.031

Placke, T., Kopp, H. G., and Salih, H. R. (2010). Glucocorticoid-induced TNFR-related (GITR) protein and its ligand in antitumor immunity: functional role and therapeutic modulation. *Clin. Dev. Immunol.* 2010:239083. doi: 10.1155/2010/239083

Rakic, P. (2002). Neurogenesis in adult primate neocortex: an evaluation of the evidence. *Nat. Rev. Neurosci.* 3, 65–71. doi: 10.1038/nrn700

Rolls, A., Shechter, R., and Schwartz, M. (2009). The bright side of the glial scar in CNS repair. *Nat. Rev. Neurosci.* 10, 235–241. doi: 10.1038/nrn2591

Ruiz de Almodovar, C., Lambrechts, D., Mazzone, M., and Carmeliet, P. (2009). Role and therapeutic potential of VEGF in the nervous system. *Physiol. Rev.* 89, 607–648. doi: 10.1152/physrev.00031.2008

Satoh, A., and Makanae, A. (2014). Conservation of position-specific gene expression in axolotl limb skin. *Zoolog. Sci.* 31, 6–13. doi: 10.2108/zsj.31.6

Schlomann, U., Rathke-Hartlieb, S., Yamamoto, S., Jockusch, H., and Bartsch, J. W. (2000). Tumor necrosis factor alpha induces a metalloprotease-disintegrin, ADAM8 (CD 156): implications for neuron-glia interactions during neurodegeneration. *J. Neurosci.* 20, 7964–7971. doi: 10.1523/jneurosci.20-21-07964.2000

Schweitzer, J., Becker, T., Lefebvre, J., Granato, M., Schachner, M., and Becker, C. G. (2005). Tenascin-C is involved in motor axon outgrowth in the trunk of developing zebrafish. *Dev. Dyn.* 234, 550–566. doi: 10.1002/dvdy.20525

Sebastianelli, L., Saltuari, L., and Nardone, R. (2017). How the brain can rewire itself after an injury: the lesson from hemispherectomy. *Neural Regen. Res.* 12, 1426–1427. doi: 10.4103/1673-5374.215247

Seri, B., Garcia-Verdugo, J. M., McEwen, B. S., and Alvarez-Buylla, A. (2001). Astrocytes give rise to new neurons in the adult mammalian hippocampus. *J. Neurosci.* 21, 7153–7160. doi: 10.1523/jneurosci.21-18-07153.2001

Shannon, P., Markiel, A., Ozier, O., Baliga, N. S., Wang, J. T., Ramage, D., et al. (2003). Cytoscape: a software environment for integrated models of biomolecular interaction networks. *Genome Res.* 13, 2498–2504. doi: 10.1101/gr.1239303

Shi, W., Fang, Z., Li, L., and Luo, L. (2015). Using zebrafish as the model organism to understand organ regeneration. *Sci. China Life Sci.* 58, 343–351. doi: 10.1007/s11427-015-4838-z

Shihabuddin, L. S., Horner, P. J., Ray, J., and Gage, F. H. (2000). Adult spinal cord stem cells generate neurons after transplantation in the adult dentate gyrus. *J. Neurosci.* 20, 8727–8735. doi: 10.1523/jneurosci.20-23-08727.2000

Shimizu, N., Kawakami, K., and Ishitani, T. (2012). Visualization and exploration of Tcf/Lef function using a highly responsive Wnt/beta-catenin signaling-reporter transgenic zebrafish. *Dev. Biol.* 370, 71–85. doi: 10.1016/j.ydbio.2012.07.016

Shimizu, Y., Ueda, Y., and Ohshima, T. (2018). Wnt signaling regulates proliferation and differentiation of radial glia in regenerative processes after stab injury in the optic tectum of adult zebrafish. *Glia* 66, 1382–1394. doi: 10.1002/glia.23311

Shitasako, S., Ito, Y., Ito, R., Ueda, Y., Shimizu, Y., and Ohshima, T. (2017). Wnt and Shh signals regulate neural stem cell proliferation and differentiation in the optic tectum of adult zebrafish. *Dev. Neurobiol.* 77, 1206–1220. doi: 10.1002/dneu.22509

Singh, B. N., Weaver, C. V., Garry, M. G., and Garry, D. J. (2018). Hedgehog and Wnt signaling pathways regulate tail regeneration. *Stem Cells Dev.* 27, 1426–1437. doi: 10.1089/scd.2018.0049

Smith, P. D., Sun, F., Park, K. K., Cai, B., Wang, C., Kuwako, K., et al. (2009). SOCS3 deletion promotes optic nerve regeneration in vivo. *Neuron* 64, 617–623. doi: 10.1016/j.neuron.2009.11.021

Sobecki, M., Mrouj, K., Colinge, J., Gerbe, F., Jay, P., Krasinska, L., et al. (2017). Cell-cycle regulation accounts for variability in Ki-67 expression levels. *Cancer Res.* 77, 2722–2734. doi: 10.1158/0008-5472.CAN-16-0707

Spittau, B., and Krieglstein, K. (2012). Klf10 and Klf11 as mediators of TGF-beta superfamily signaling. *Cell Tissue Res.* 347, 65–72. doi: 10.1007/s00441-011-1186-6

Stoick-Cooper, C. L., Weidinger, G., Riehle, K. J., Hubbert, C., Major, M. B., Fausto, N., et al. (2007). Distinct Wnt signaling pathways have opposing roles in appendage regeneration. *Development* 134, 479–489. doi: 10.1242/dev.001123

Strand, N. S., Hoi, K. K., Phan, T. M. T., Ray, C. A., Berndt, J. D., and Moon, R. T. (2016). Wnt/beta-catenin signaling promotes regeneration after adult zebrafish spinal cord injury. *Biochem. Biophys. Res. Commun.* 477, 952–956. doi: 10.1016/j.bbrc.2016.07.006

Tanaka, E. M., and Ferretti, P. (2009). Considering the evolution of regeneration in the central nervous system. *Nat. Rev. Neurosci.* 10, 713–723. doi: 10.1038/nrn2707

Tang, J., Yu, Y., Zheng, H., Yin, L., Sun, M., Wang, W., et al. (2017). ITRAQ-based quantitative proteomic analysis of *Cynops orientalis* limb regeneration. *BMC Genomics* 18:750. doi: 10.1186/s12864-017-4125-4

Tsarouchas, T. M., Wehner, D., Cavone, L., Munir, T., Keatinge, M., Lambertus, M., et al. (2018). Dynamic control of proinflammatory cytokines Il-1beta and Tnf-alpha by macrophages in zebrafish spinal cord regeneration. *Nat. Commun.* 9:4670. doi: 10.1038/s41467-018-07036-w

Tseng, A. S., Adams, D. S., Qiu, D., Koustubhan, P., and Levin, M. (2007). Apoptosis is required during early stages of tail regeneration in *Xenopus laevis*. *Dev. Biol.* 301, 62–69. doi: 10.1016/j.ydbio.2006.10.048

Tsujioka, H., Kunieda, T., Katou, Y., Shirahige, K., Fukazawa, T., and Kubo, T. (2017). *interleukin-11* induces and maintains progenitors of different cell lineages during *Xenopus* tadpole tail regeneration. *Nat. Commun.* 8:495. doi: 10.1038/s41467-017-00594-5

Ueno, S., Weidinger, G., Osugi, T., Kohn, A. D., Golob, J. L., Pabon, L., et al. (2007). Biphasic role for Wnt/beta-catenin signaling in cardiac specification in zebrafish and embryonic stem cells. *Proc. Natl. Acad. Sci. U.S.A.* 104, 9685–9690. doi: 10.1073/pnas.0702859104

Veldman, M. B., Bemben, M. A., Thompson, R. C., and Goldman, D. (2007). Gene expression analysis of zebrafish retinal ganglion cells during optic nerve regeneration identifies KLF6a and KLF7a as important regulators of axon regeneration. *Dev. Biol.* 312, 596–612. doi: 10.1016/j.ydbio.2007.09.019

Walter, W., Sanchez-Cabo, F., and Ricote, M. (2015). GOplot: an R package for visually combining expression data with functional analysis. *Bioinformatics* 31, 2912–2914. doi: 10.1093/bioinformatics/btv300

Wang, Y. H., Keenan, S. R., Lynn, J., McEwan, J. C., and Beck, C. W. (2015). Gremlin1 induces anterior-posterior limb bifurcations in developing Xenopus limbs but does not enhance limb regeneration. *Mech. Dev.* 138(Pt 3), 256–267. doi: 10.1016/j.mod.2015.10.003

Wang, Z., Gerstein, M., and Snyder, M. (2009). RNA-Seq: a revolutionary tool for transcriptomics. *Nat. Rev. Genet.* 10, 57–63. doi: 10.1038/nrg2484

Wehner, D., Tsarouchas, T. M., Michael, A., Haase, C., Weidinger, G., Reimer, M. M., et al. (2017). Wnt signaling controls pro-regenerative collagen XII in functional spinal cord regeneration in zebrafish. *Nat. Commun.* 8:126. doi: 10.1038/s41467-017-00143-0

Whyte, J. L., Smith, A. A., and Helms, J. A. (2012). Wnt signaling and injury repair. *Cold Spring Harb. Perspect. Biol.* 4:a008078. doi: 10.1101/cshperspect.a008078

Wickham, H. (2016). *Ggplot2: Elegant Graphics for Data Analysis*. New York, NY: Springer-Verlag.

Wilson, S. E., Chaurasia, S. S., and Medeiros, F. W. (2007). Apoptosis in the initiation, modulation and termination of the corneal wound healing response. *Exp. Eye Res.* 85, 305–311. doi: 10.1016/j.exer.2007.06.009

Wu, Y. S., and Chen, S. N. (2014). Apoptotic cell: linkage of inflammation and wound healing. *Front. Pharmacol.* 5:1. doi: 10.3389/fphar.2014.00001

Yu, L., Dawson, L. A., Yan, M., Zimmel, K., Lin, Y. L., Dolan, C. P., et al. (2019). BMP9 stimulates joint regeneration at digit amputation wounds in mice. *Nat. Commun.* 10:424. doi: 10.1038/s41467-018-08278-4

Zaman, G., Sunters, A., Galea, G. L., Javaheri, B., Saxon, L. K., Moustafa, A., et al. (2012). Loading-related regulation of transcription factor EGR2/Krox-20 in bone cells is ERK1/2 protein-mediated and prostaglandin, Wnt signaling pathway-, and insulin-like growth factor-I axis-dependent. *J. Biol. Chem.* 287, 3946–3962. doi: 10.1074/jbc.M111.252742

Zambusi, A., and Ninkovic, J. (2020). Regeneration of the central nervous system-principles from brain regeneration in adult zebrafish. *World J. Stem Cells* 12, 8–24. doi: 10.4252/wjsc.v12.i1.8

Zhang, Y., Pizzute, T., and Pei, M. (2014). A review of crosstalk between MAPK and Wnt signals and its impact on cartilage regeneration. *Cell Tissue Res.* 358, 633–649. doi: 10.1007/s00441-014-2010-x

Zhao, L., Jin, Y., Donahue, K., Tsui, M., Fish, M., Logan, C. Y., et al. (2019). Tissue repair in the mouse liver following acute carbon tetrachloride depends on injury-induced Wnt/beta-Catenin signaling. *Hepatology* 69, 2623–2635. doi: 10.1002/hep.30563

Zimmerman, Z. F., Kulikauskas, R. M., Bomsztyk, K., Moon, R. T., and Chien, A. J. (2013). Activation of Wnt/beta-catenin signaling increases apoptosis in melanoma cells treated with trail. *PLoS One* 8:e69593. doi: 10.1371/journal.pone.0069593

Conflict of Interest: The authors declare that the research was conducted in the absence of any commercial or financial relationships that could be construed as a potential conflict of interest.

Copyright © 2020 Demirci, Cucun, Poyraz, Mohammed, Heger, Papatheodorou and Ozhan. This is an open-access article distributed under the terms of the Creative Commons Attribution License (CC BY). The use, distribution or reproduction in other forums is permitted, provided the original author(s) and the copyright owner(s) are credited and that the original publication in this journal is cited, in accordance with accepted academic practice. No use, distribution or reproduction is permitted which does not comply with these terms.

Supplementary Text for Demirci, Cucun et al.

Supplementary Figures

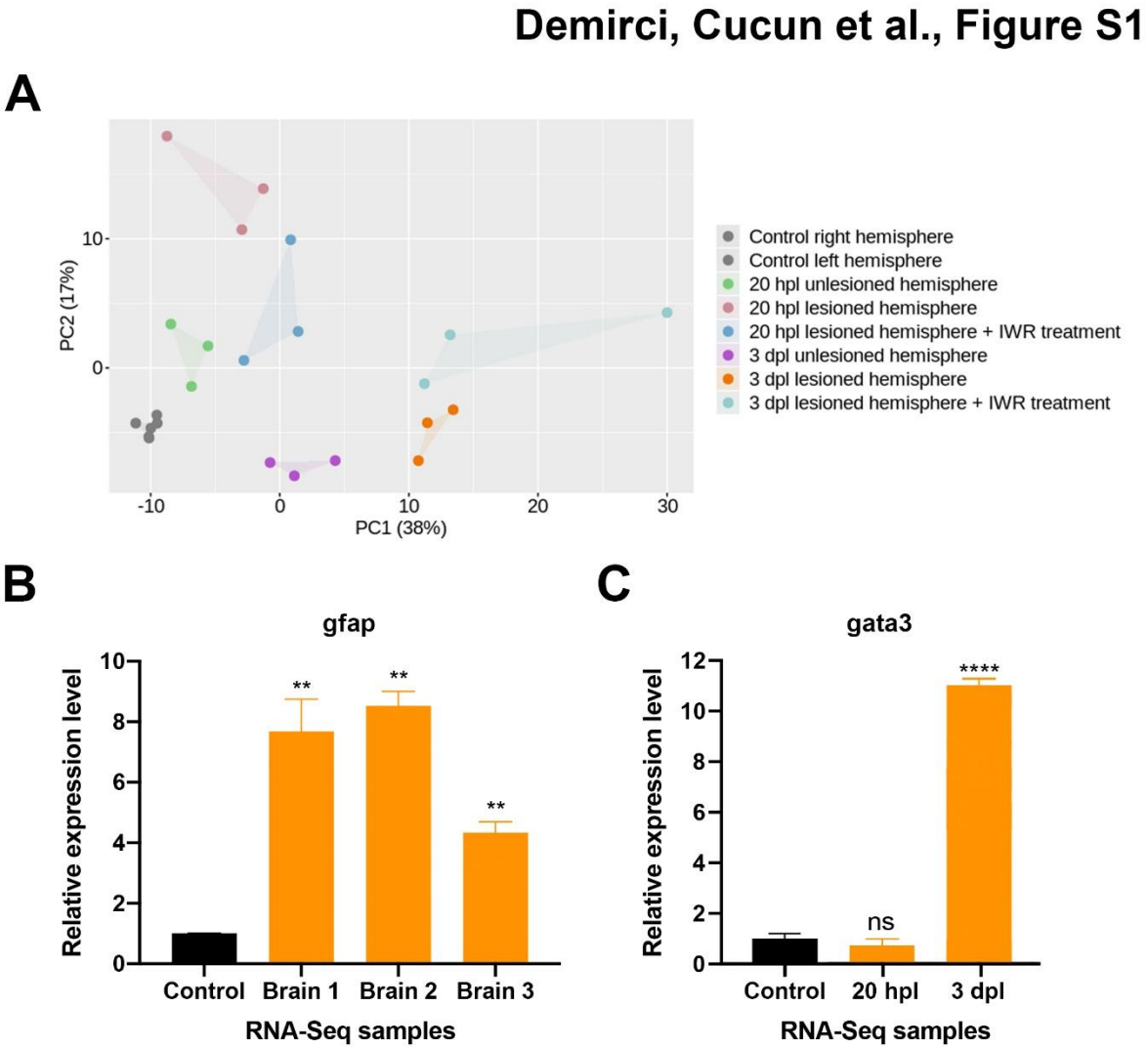

Supplementary Figure 1. Quantitative and qualitative control of RNA samples before and after RNA-seq (A) Principal component analysis (PCA) of all RNA-seq data. The PCA was conducted and plotted using package of "ggplot2". Different colors of circle dots represents the eight groups of samples. Three circle dots with the same color refer to the three replicates of a sample group. Eight sample groups were well separated. Principal Component 1 (PC1, x-axis) represents 38% and PC2 (y-axis) represents 17% of total variation in the data. Relative expression levels of (B) the glia marker gene *gfap* in lesioned hemispheres of three independent telencephalon samples used for RNA-sequencing at 3 dpl and (C) injury-activated gene *gata3* in the pooled three lesioned hemispheres before injury and at 20 hpl and 3 dpl. Statistical significance was evaluated using

unpaired t-test. **p<0.01 and ***p<0.001. Error bars represent ± standard error of mean (SEM, n=3). hpl: hours post-lesion, dpl: days post-lesion, gfap: glial fibrillary acidic protein.

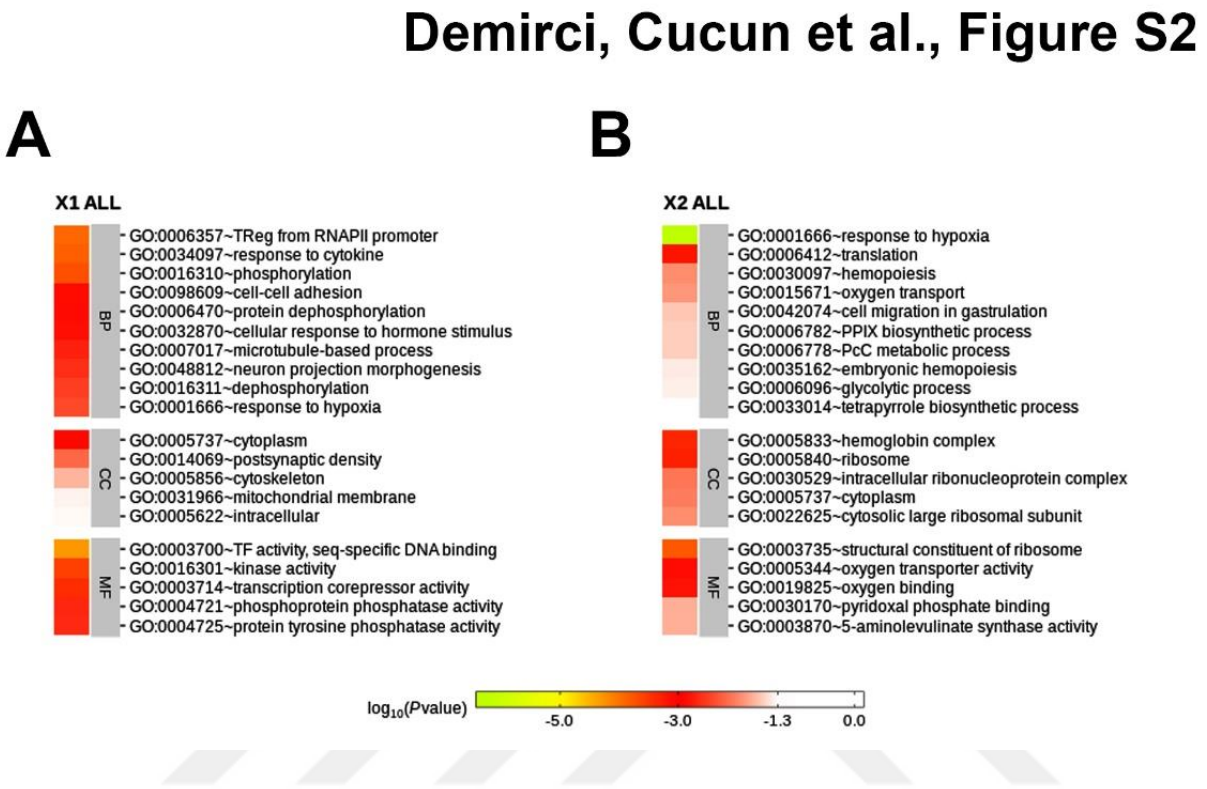

Supplementary Figure 2. GO terms altered in the lesioned and unlesioned hemispheres at the early wound healing stage of brain regeneration by using all significantly changed genes DAVID bioinformatics tool was used to show the most significantly enriched GO terms based on the transcriptional changes in (A) X1 and (B) X2 comparisons. All DEGs (X1 1472, X2 211) were used. The heatmap scale shows the $\log_{10}$ of the EASE P value for the most significantly enriched GO terms. DAVID: Database for Annotation, Visualization and Integrated Discovery, GO: Gene Ontology, BP: Biological Process, CC: Cellular Component, MF: Molecular Function. See Materials and Methods for definition of DEGs covered in X1 and X2.

Demirci, Cucun et al., Figure S3

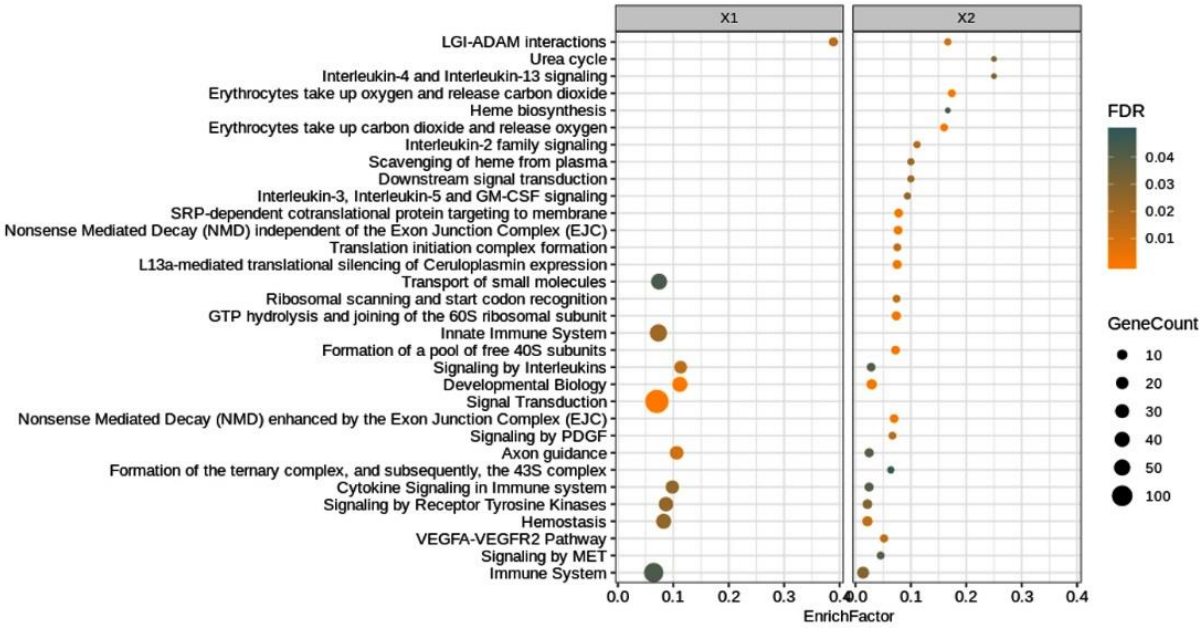

Supplementary Figure 3. Reactome pathways altered in lesioned and unlesioned hemispheres at the early wound healing stage of brain regeneration by using all significantly changed genes STRING bioinformatics tool was used to show the most significantly enriched Reactome pathways based on the transcriptional changes in X1 and X2. Dot plot represents Reactome pathways enriched in X1 and X2 by using all significantly changed genes (X1 1472, X2 211) in these comparisons based on FDR and EnrichFactor. STRING: Search Tool for the Retrieval of Interacting Genes/Proteins, FDR: false discovery rate. See Materials and Methods for definition of DEGs covered in X1 and X2.

Demirci, Cucun et al., Figure S4

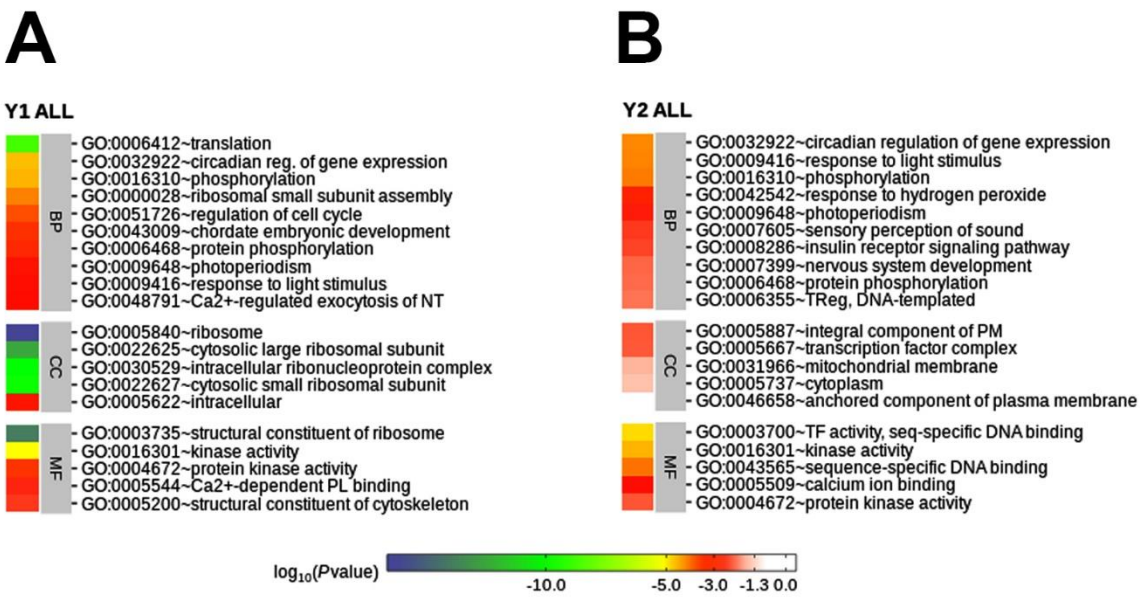

Supplementary Figure 4. GO terms altered in the lesioned and unlesioned hemispheres at the proliferative stage of brain regeneration by using all significantly changed genes DAVID bioinformatics tool was used to show the most significantly enriched GO terms based on the transcriptional changes in (A) Y1 and (B) Y2 comparisons. All DEGs (Y1 1707, X2 1215) were used. The heatmap scale shows the $\log_{10}$ of the EASE P value for the most significantly enriched GO terms. DAVID: Database for Annotation, Visualization and Integrated Discovery, GO: Gene Ontology, BP: Biological Process, CC: Cellular Component, MF: Molecular Function. See Materials and Methods for definition of DEGs covered in Y1 and Y2.

Demirci, Cucun et al., Figure S5

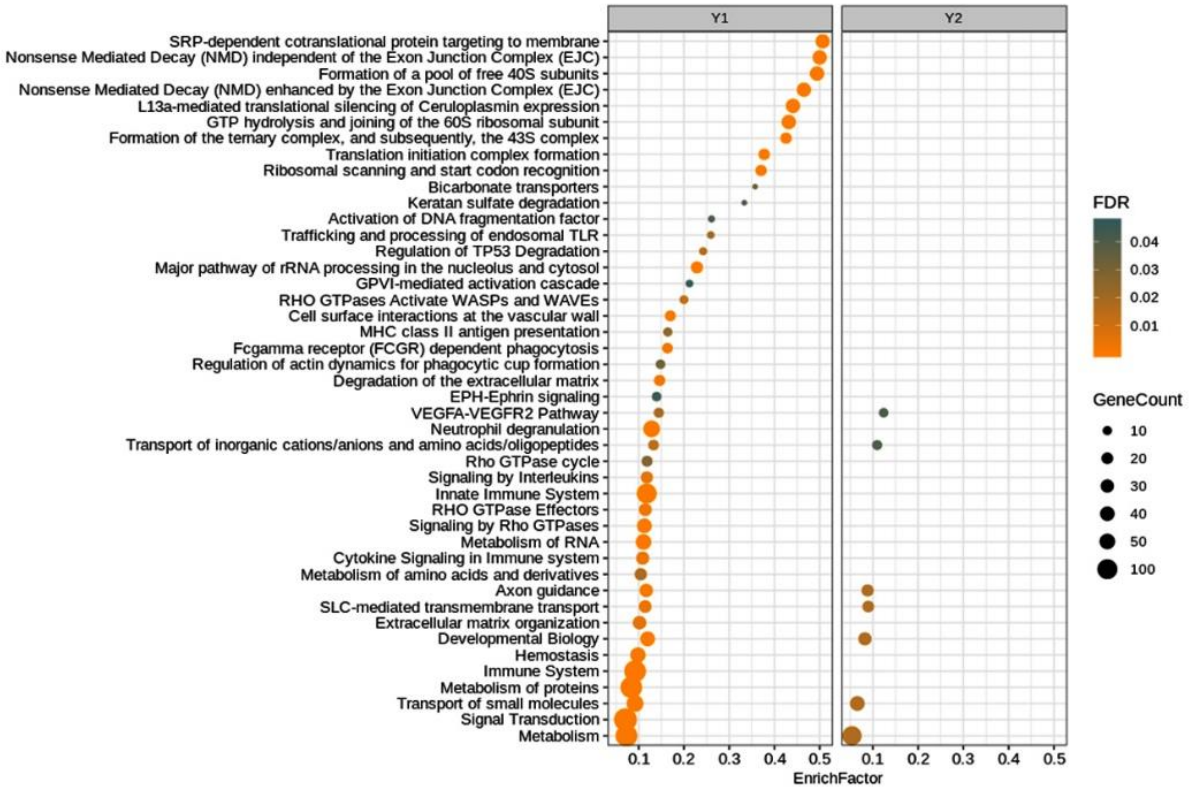

Supplementary Figure 5. Reactome pathways altered in lesioned and unlesioned hemispheres at the proliferative stage of brain regeneration by using all significantly changed genes STRING bioinformatics tool was used to show the most significantly enriched Reactome pathways based on the transcriptional changes in Y1 and Y2. Dot plot represents Reactome pathways enriched in Y1 and Y2 by using all significantly changed genes (Y1 1707, Y2 1215) in these comparisons based on FDR and EnrichFactor. STRING: Search Tool for the Retrieval of Interacting Genes/Proteins, FDR: false discovery rate. See Materials and Methods for definition of DEGs covered in Y1 and Y2 comparisons.

Demirci, Cucun et al., Figure S6

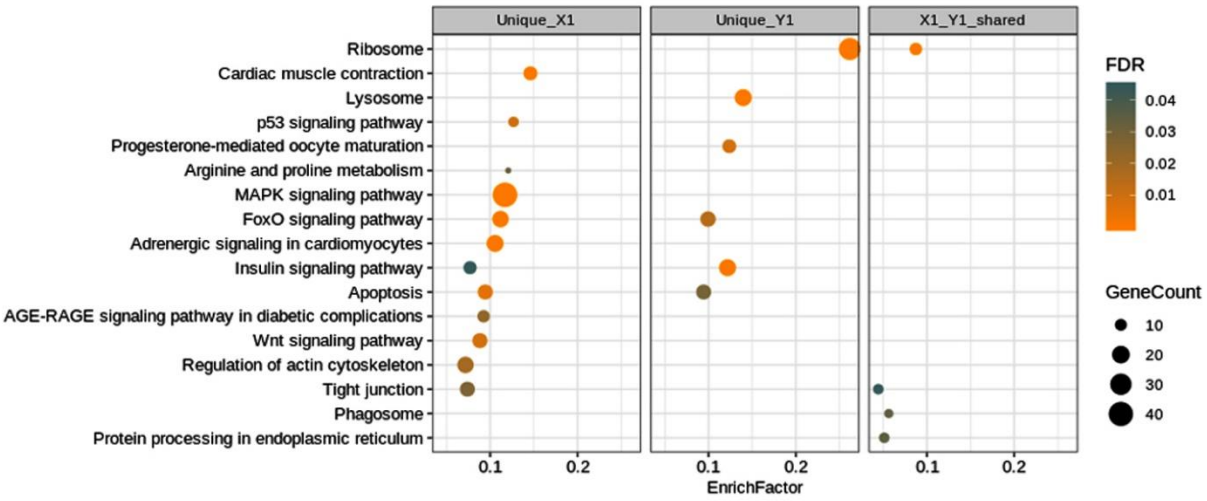

Supplementary Figure 6. KEGG pathways altered in lesioned and unlesioned hemispheres at the early wound healing and proliferative stages of brain regeneration by using shared and uniquely expressed genes STRING bioinformatics tool was used to show the most significantly enriched KEGG pathways based on the transcriptional changes in (A) genes unique to X1 and (B) genes unique to Y1 and (C) genes shared between X1 and Y1. 1015, 1250 and 457 DEGs were used for X1, Y1 and X1&Y1, respectively. Dot plot represents KEGG pathways enriched in X1 and Y1 comparisons based on FDR and EnrichFactor. STRING: Search Tool for the Retrieval of Interacting Genes/Proteins, KEGG: Kyoto Encyclopedia of Genes and Genomes, FDR: false discovery rate. See Materials and Methods for definition of DEGs covered in X and Y comparisons.

Demirci, Cucun et al., Figure S7

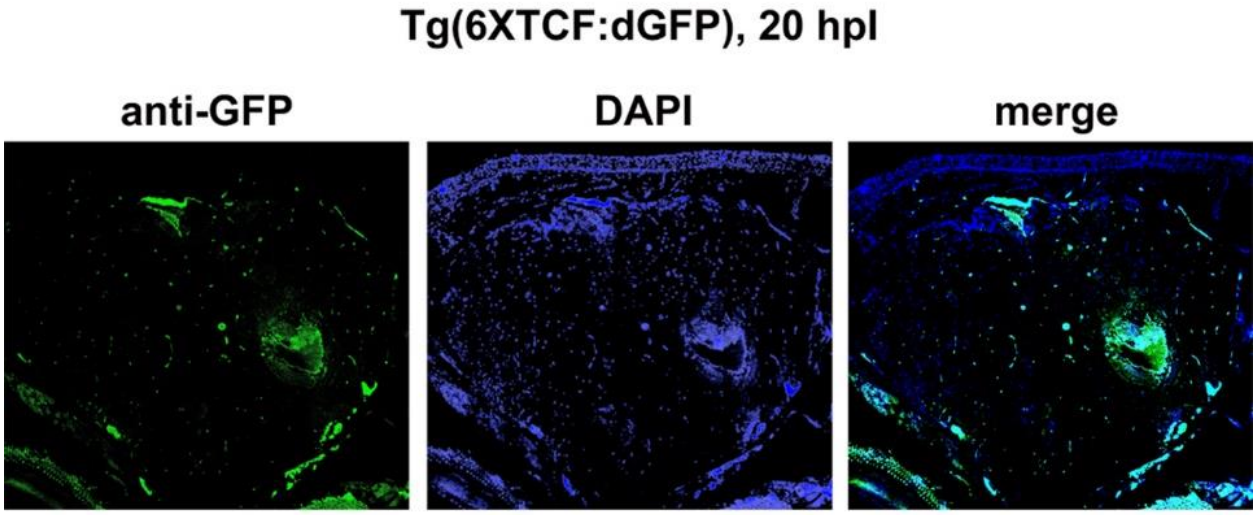

Supplementary Figure 7: Immunofluorescence staining for anti-GFP in Tg(6XTCF:dGFP) transgenic zebrafish reporter of Tcf/Lef-mediated transcription at 20 hpl. GFP expression is visible around the lesioned area, most likely in the endothelial and blood cells of the brain.

Demirci, Cucun et al., Figure S8

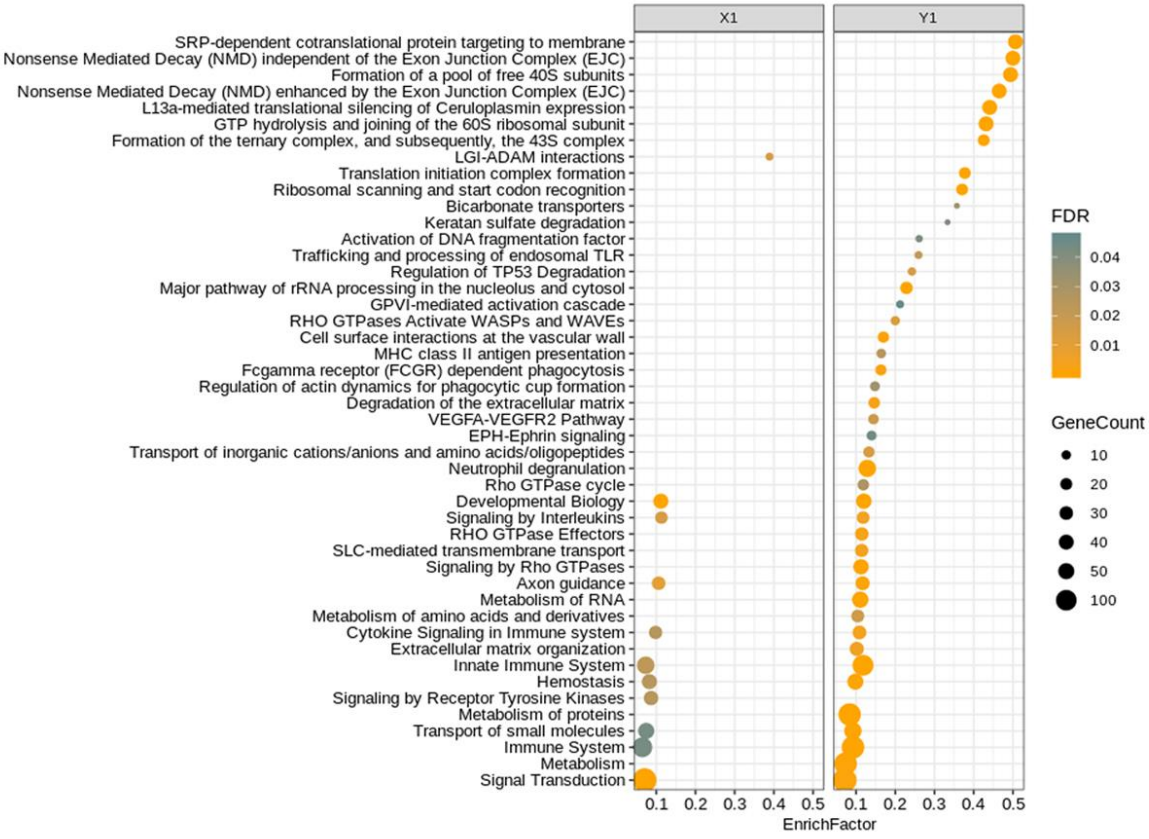

Supplementary Figure 8. Reactome pathways altered in lesioned and unlesioned hemispheres at the early wound healing and proliferative stages of brain regeneration by using all significantly changed genes STRING bioinformatics tool was used to show the most significantly enriched Reactome pathways based on the transcriptional changes in X1 and Y1. Dot plot represents Reactome pathways enriched in Y1 and Y2 by using all significantly changed genes (X1 1472, Y1 1707) in these comparisons based on FDR and EnrichFactor. STRING: Search Tool for the Retrieval of Interacting Genes/Proteins, FDR: false discovery rate. See Materials and Methods for definition of DEGs covered in X and Y comparisons.

Demirci, Cucun et al., Figure S9

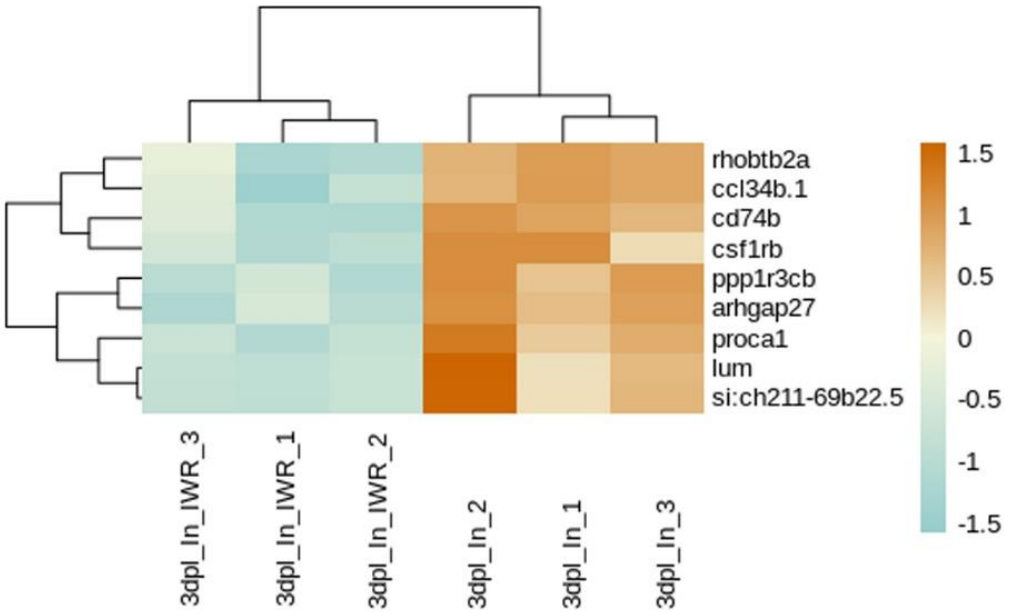

Supplementary Figure 9. The Wnt targetome in the proliferative stage of brain regeneration Intersection heatmap shows Wnt target genes that are Up in Y1 and Down in Y3. Each column represents a single hemisphere from a single telencephalon and each row shows a single gene. The scale bar shows Z-scores for the heatmaps from high to low expression, represented by a color gradient from orange to green, respectively.

Demirci, Cucun et al., Figure S10

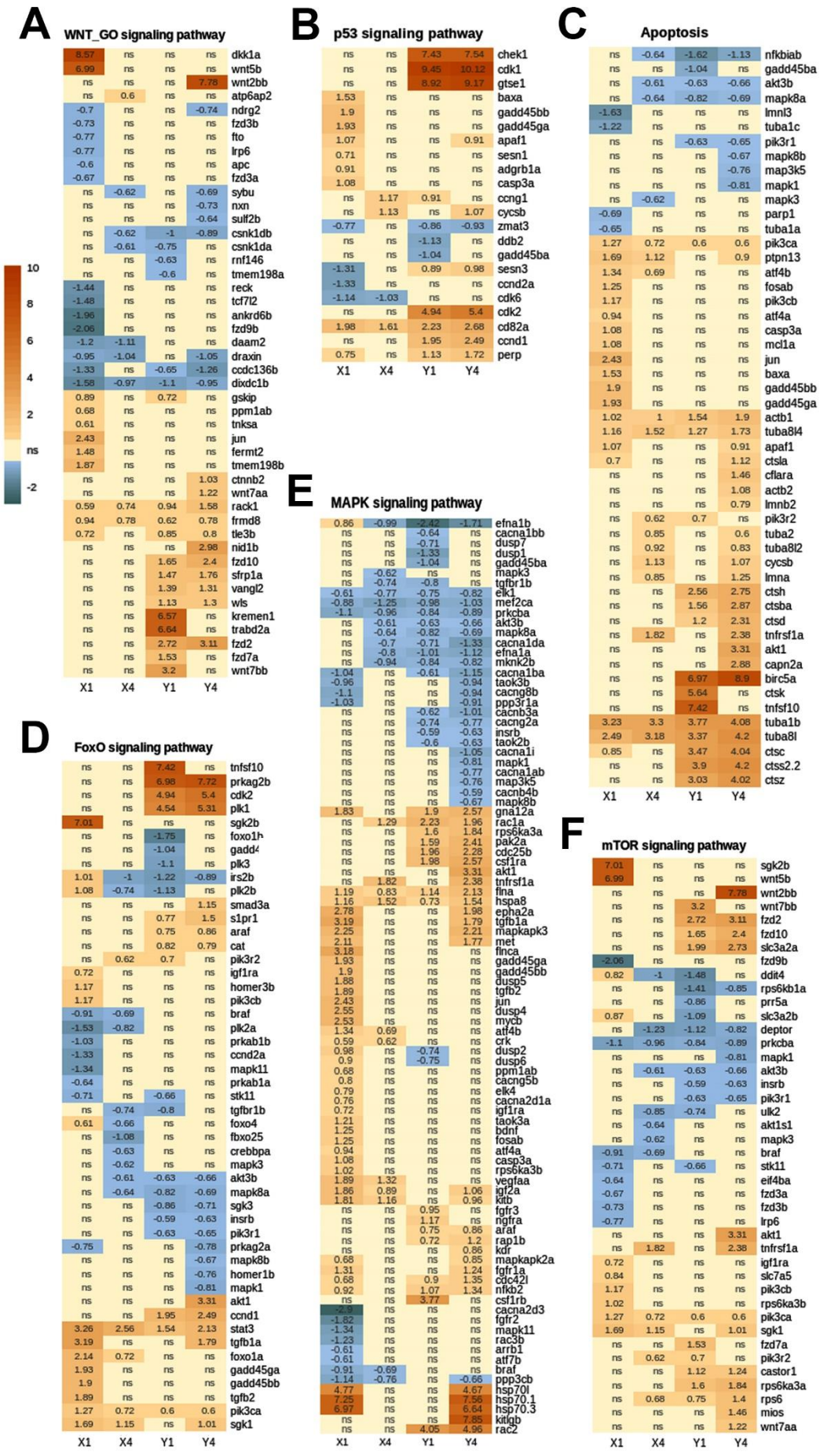

Supplementary Figure 10. Various KEGG pathways are transcriptionally altered during early wound healing and proliferative stages of brain regeneration in response to inhibition of Wnt/β-catenin signaling Heatmap representation of uniquely changed genes in (A) WNT GO term, (B) p53 signaling pathway, (C) apoptosis pathway, (D) FoxO signaling pathway, (E) MAPK signaling pathway and (F) mTOR signaling pathway in X1, X4, Y1 and Y4 comparisons. Each column represents a comparison according to DESeq2 results and each row shows a single gene. The scale bar shows $\log_2$ of the fold change values for the heatmaps from high to low expression, represented by a color gradient from orange to blue, respectively. Statistical significance was evaluated using the Wald test. ns: non-significant. See Materials and Methods for definition of DEGs covered in X and Y comparisons.

Supplementary Results and Discussion

Transcriptome profiling of the telencephalon during early wound healing stage of regeneration

Based on GO term analysis of Up and Down genes separately, DEGs in X1 were enriched in a total of 95 terms in group BP, 21 in group CC and 79 in group MF, while DEGs in X2 were enriched in 17 terms in group BP, 8 in group CC and 15 in group MF (Table S4). The top 40 GO terms in X1 (10 Down and 10 Up in BP, 5 Down and 5 Up in CC and 5 Down and 5 Up in MF) and top 26 GO terms in X2 (10 Down and 2 Up in BP, 2 Down and 5 Up in CC and 5 Down and 2 Up in MF) showed no overlap, parallel to the low number of genes shared between X1 and X2 (Figure 2D-E). We also identified the Reactome pathways significantly enriched in X1 and X2, which showed markedly lower gene counts as compared to X1 (Figure S3, Table S5).

Transcriptome profiling of the telencephalon during early proliferative stage of regeneration

GO term enrichment analysis of Up and Down genes separately revealed that DEGs in Y1 were enriched in 110 terms in group BP, 32 in group CC and 63 in group MF, while DEGs in Y2 were enriched in 58 terms in group BP, 15 in group CC and 42 in group MF (Table S4). The top 40 GO terms in Y1 and Y2 (10 Down and 10 Up in BP, 5 Down and 5 Up in CC and 5 Down and 5 Up in MF) overlapped by 25% (Figure 3D-E). GO terms were also defined for all significantly changed DEGs in Y1 and Y2 groups (Figure S4, Table S4). Although there was no KEGG pathway enriched in Y2, we determined 15 KEGG pathways significantly enriched in Y1 (Figure 3F, Table S5). We found 44 and 7 Reactome pathways to be enriched in Y1 and Y2, respectively (Figure S5, Table S5).

Early wound healing and proliferative stages of brain regeneration are more different than similar

DEGs unique to X1 were enriched in a total of 83 GO terms (50 BP, 5 CC and 28 MF) while DEGs in group 2 were enriched in 58 GO terms (40 BP, 12 CC and 23 MF) (Table S4). These GO terms were only enriched

for DEGs that are unique to X1, but not for DEGs that are unique to Y1 or DEGs shared between X1 and Y1. We found 11 and 44 Reactome pathways that were enriched in X1 and Y1, respectively (Figure S8, Table S5). Interestingly, none of the DEGs we detected at either early wound healing or proliferative stage were regulated oppositely in the two hemispheres, i.e. these genes were either upregulated or downregulated in both halves. At 20 hpl, the number of DEGs in the lesioned hemisphere (X1) is far higher than that of the unlesioned one (X2), whereas at 3 dpl, the number of DEGs in the corresponding halves (Y1 and Y2) both increases and converges. However, the higher number of DEGs at 3 dpl is not reflected in the number of KEGG pathways enriched at this stage, that is the number of KEGG pathways in Y1:Y2 (15:0) was fewer than in X1:X2 (20:4) (see Figures 2F, 3F). Strikingly, the number of DEGs that are shared between X1 and X2 is far fewer than between Y1 and Y2, which shared half of their DEGs including the most strongly downregulated five genes in both groups. This finding is further supported by the low number of DEGs shared between X1 and Y1.

A noteworthy point is that some of the very strongly altered DEGs are shared between the lesioned and unlesioned hemispheres even at different stages of telencephalon regeneration. *en1a*, encoding for the homeobox transcription factor Engrailed-1a, stands out as a notable example of one of the most strongly downregulated genes in X1, Y1 and Y2 (see Table S2). The mouse ortholog *En1* is involved in development and maintenance of the monoaminergic structures such as dopaminergic and serotonergic circuitries in the mid- and hindbrain (Fox and Deneris, 2012; Kouwenhoven et al., 2016). More interestingly, the latter work has described an additional role for En1 as suppressor of Wnt1 and canonical Wnt-signaling in the hindbrain (Kouwenhoven et al., 2016). Thus, strong suppression of *en1a* may indicate loss of ventral dopaminergic neurons, leading to elevation of Wnt/β-catenin signaling. *entpd2b* gene, which is strongly upregulated at 20 hpl and 3 dpl, has been shown to be also upregulated after hepatocellular injury (Feldbrugge et al., 2018), suggesting that it undertakes regeneration-promoting roles in different cellular contexts.

Inhibition of Wnt/β-catenin signaling during early wound stage results in a marked alteration of gene expression profiles represented in KEGG pathway enrichment The genes we obtained from KEGG database included 189 genes involved in Wnt signaling pathway, 371 in MAPK signaling pathway, 167 in Apoptosis, 187 in mTOR signaling pathway, 79 in p53 signaling pathway and 167 in FoxO signaling pathway (Table S8). Besides, GO term enrichment analysis using AmiGO database revealed 275 genes related to Wnt signaling (Table S8). The number of significantly altered genes in X1 decreased dramatically after IWR treatment in X4 as follows: Wnt 21→6, Wnt-GO 25→9, p53 13→4, apoptosis 23→17, FoxO 23→16, MAPK 56→22 and

mTOR 18→13 (Figures 7A, 7C-D, S10 compare the total number of brown and blue shaded boxes in X1 and X4; Table S8). 11/13 DEGs detected in p53 signaling, 16/23 in apoptosis, 17/23 in FoxO signaling, 44/56 in MAPK pathway and 14/18 in mTOR signaling were not any more differentially expressed or regulated in the opposite direction, indicating a regulatory role for Wnt/β-catenin signaling in the early stage of brain regeneration (Figures S10B-F). On the contrary, the number of altered genes in Y1 either did not change much or even increased in Y4 as follows: Wnt 17→20, Wnt-GO 19→20, p53 12→11, apoptosis 20→32, FoxO 23→23, MAPK 37→52 and mTOR 21→20 (Figures 7A, S10 compare the total number of brown and blue shaded boxes in Y1 and Y4; Table S8). The weak response to Wnt pathway in the early proliferative stage of regeneration is further supported by the fact that there was no change in gene expression pattern of 9/12 DEGs detected in p53 signaling, 16/20 in apoptosis, 15/23 in FoxO signaling, 27/37 in MAPK pathway and 13/21 in mTOR pathway after IWR treatment in Y4 (Figure S10B-F).

Since canonical Wnt activity returned to control levels at the proliferative phase of regeneration, RGC proliferation appears to be regulated via another signaling pathway such as Notch, whose inhibition has been shown to cause a reduction in the number of RGCs in the lesioned hemisphere of the telencephalon (Chapouton et al., 2010; Kishimoto et al., 2012; de Oliveira-Carlos et al., 2013). Such a regulatory role in proliferative response is strongly supported by our findings showing that *notch2*, *notch3*, *notch1b* are exclusively upregulated in the lesioned half of the telencephalon at 3 dpl.

Supplementary References

Chapouton, P., Skupien, P., Hesl, B., Coolen, M., Moore, J.C., Madelaine, R., et al. (2010). Notch activity levels control the balance between quiescence and recruitment of adult neural stem cells. *J Neurosci* 30(23)**,** 7961-7974. doi: 10.1523/JNEUROSCI.6170-09.2010.

de Oliveira-Carlos, V., Ganz, J., Hans, S., Kaslin, J., and Brand, M. (2013). Notch receptor expression in neurogenic regions of the adult zebrafish brain. *PLoS One* 8(9)**,** e73384. doi: 10.1371/journal.pone.0073384.

Feldbrugge, L., Jiang, Z.G., Csizmadia, E., Mitsuhashi, S., Tran, S., Yee, E.U., et al. (2018). Distinct roles of ecto-nucleoside triphosphate diphosphohydrolase-2 (NTPDase2) in liver regeneration and fibrosis. *Purinergic Signal* 14(1)**,** 37-46. doi: 10.1007/s11302-017-9590-3.

Fox, S.R., and Deneris, E.S. (2012). Engrailed is required in maturing serotonin neurons to regulate the cytoarchitecture and survival of the dorsal raphe nucleus. *J Neurosci* 32(23)**,** 7832-7842. doi: 10.1523/JNEUROSCI.5829-11.2012.

Kishimoto, N., Shimizu, K., and Sawamoto, K. (2012). Neuronal regeneration in a zebrafish model of adult brain injury. *Dis Model Mech* 5(2)**,** 200-209. doi: 10.1242/dmm.007336.

Kouwenhoven, W.M., Veenvliet, J.V., van Hooft, J.A., van der Heide, L.P., and Smidt, M.P. (2016). Engrailed 1 shapes the dopaminergic and serotonergic landscape through proper isthmic organizer maintenance and function. *Biol Open* 5(3)**,** 279-288. doi: 10.1242/bio.015032.